Design, test and biological validation of microfluidic systems for blood plasma separation

Maïwenn Kersaudy-Kerhoas

A dissertation submitted for the degree of Doctor of Philosophy

Heriot-Watt University

School of Engineering and Physical Sciences

June 2010

Abstract

Sample preparation has been described as the weak link in microfluidics. In particular, plasma has to be extracted from whole blood for many analysis including protein analysis, cell-free DNA detection for prenatal diagnosis and transplant monitoring. The lack of suitable devices to perform the separation at the microscale means that Lab On Chip (LOC) modules cannot be fully operated without sample preparation in a full-scale laboratory. In order to address this issue, blood flow in microchannels has been studied, and red blood cells behaviours in different geometrical environments have been classified. Several designs have been subsequently proposed to exploit some natural properties of blood flow and extract pure plasma without disturbing the cells. Furthermore, a high-level modelling method was developed to predict the behaviour of passive microfluidic networks. Additionally, the technique proposed provides useful guidance over the use of systems in more complex external environments. Experimental results have shown that plasma could be separated from undiluted whole blood in 10μm width microchannels at a flow rate of 2mL/hr. Using slightly larger structures (20μm) suitable for mass-manufacturing, diluted blood can be separated with 100% purity efficiency at high flow rate. An extensive biological validation of the extracted plasma was carried out to demonstrate its quality. To this effect Polymerase Chain Reaction (PCR) was performed to amplify targeted human genomic sequence from cell-free DNA present in the plasma. Furthermore, the influence of the sample dilution and separation efficiency on the amplification was characterised. It was shown that the sample dilution does have an influence on the amplification of house-keeping gene, but that amplification can be achieved even on high diluted samples. Additionally amplification can also be obtained on plasma samples with a range of separation efficiencies from 100% to 84%. In particular, two main points have been demonstrated (i) the extraction of plasma using combination of constrictions and bifurcations, (ii) the biological validation of the extracted plasma.

Acknowledgements

Declaration statement

Table of contents

List of publications by the candidate

Peer-reviewed journal publications

- Maïwenn Kersaudy-Kerhoas, Resham S. Dhariwal, and Marc P.Y. Desmulliez, *System-level simulation of a microfluidic network for passive bifurcation-based blood separation*, (in preparation)

- Maïwenn Kersaudy-Kerhoas, Deirdre M. Kavanagh, Resham S. Dhariwal, Colin J. Campbellb and Marc P.Y. Desmulliez, *Validation of a blood plasma separation system by biomarker detection*, Lab On Chip, **10**, 1587–1595, (2010)

- Deirdre M. Kavanagh, Maïwenn Kersaudy-Kerhoas, Resham S. Dhariwal and Marc P.Y. Desmulliez, *Current and emerging techniques of fetal cell separation from maternal blood*. Journal of Chromatography B, In Press, Accepted manuscript, Available online 27 May 2010.

- M. Kersaudy-Kerhoas, R. Dhariwal, M.P.Y. Desmulliez, and L. Jouvet *Hydrodynamic blood plasma separation in microfluidic channels*, Microfluidics and Nanofluidics, **8**, 2010.

- Maïwenn Kersaudy-Kerhoas, Resham S. Dhariwal and Marc P.Y. Desmulliez, *Recent advances in microparticle continuous separation*, IET Nanobiotechnology, **2**, p. 1-13, 2008.

Peer-reviewed conference publications

- Deirdre. M.Kavanagh, Maïwenn. Kersaudy-Kerhoas, Sumanth. K. Pavuluri, Resham. S. Dhariwal and Marc. P. Y. Desmulliez, *Fabrication and Testing of Microfluidic Devices for Blood Cell Separation*, 2nd Micro and Nano Flows Conference, MNF09, Brunel, UK, 2009

- Maïwenn Kersaudy-Kerhoas, Xiangdong. Dong, Mayur. Patel, Deirdre. M. Kavanagh, Resham. S. Dhariwal and Marc. P. Y. Desmulliez, *Integrated Biomedical Device For Blood Preparation*, ESTC 2008, 2nd Electronics and Systems-Integration Technology Conference, Greenwich, UK, September 2008.

- Maïwenn Kersaudy-Kerhoas, Resham.S. Dhariwal, Marc.P.Y. Desmulliez, Lionel. Jouvet, *Blood flow separation in microfluidic channels*, Proceedings of the 1st European Conference in Microfluidics, Bologna, 1-10, December 2008.

- Maïwenn Kersaudy-Kerhoas, Lionel Jouvet and Marc Desmulliez, *Design, Manufacturing and Test of a Microfluidic System for Continuous Blood-Plasma Separation*, MSB 2008, 22nd International Symposium on Microscale bioseparations and methods for systems biology, Berlin, Germany , March, 2008,

- Maïwenn Kersaudy-Kerhoas, Jens G. Kaufmann, Usama M. Attia, Silvia Marson, David Allen, Anthony Douglas, William O'Neill, Philip Summersgill, Timothy Ryan and Marc Desmulliez, *Evaluation of manufacturing techniques for a minifluidics demonstrator system*, ICRM 2007, 4th International Conference on Responsive Manufacturing Nottingham, UK, September 2007.

Non-peer reviewed conference publications:

- Maïwenn Kersaudy-Kerhoas, Deirdre M. Kavanagh, Resham S. Dhariwal and Marc P.Y. Desmulliez, *A changing world for women: prenatal diagnosis in point-of-care Technology* – 14th International Conference of Women Engineers and Scientists, Lille, France, July 2008.

- Maïwenn Kersaudy-Kerhoas, Farid. Amalou , Deirdre. Kavanagh , Silvia. Marson , Usama. M. Attia , Phillip. Summersgill , Tim. Ryan and Marc P.Y. Desmulliez, *Design, Manufacturing and Test of Disposable Microfluidic System for Blood-Plasma Separation* – Poster EP10396, published on www.eposters.net, Lab-on-a-Chip World Congress, Edinburgh, UK, May 2007.

Patent application:

- Br. Pat., IPO 310809, 2009.

Chapter 1: Introduction

1.1 A revolution in point of care medicine ?

In the 1990s was born a new field derived from microelectronics fabrication techniques, analytical chemistry and biological analysis. A number of scientists from all horizons joined this new and exciting route and contributed to establish the field to a strong hold in the scientific advances of the end of the 20th century and the beginning of the 21st. The name of this field is Micro Total Analysis Sytem (µTAS). This field, derived or linked to MicroElectroMechanical System (MEMS), is also called BioMEMS or Lab-on-Chip (LOC). Although all these denominations might bear slight differences in the orientation of their science, the core of this activity deals with the miniaturisation of the analytical and diagnostic techniques. The application field is large. From core biological science to clinical diagnostic routine, pharmaceutical industry, analytical chemistry, cosmetics and on-site agricultural care, everyday human activity could potentially benefit from it. Toner and Irimia, for example, claimed in 2005 that "*bringing complete labs for blood analysis to the bedside [...] is poised to reshape the delivery of health care*" [1.1]. Although this assumption still remains true, Mariella asks three years later "why has it not progressed further?" [1.2].

20 years on the field of µTAS has produced numerous prototypes for point-of-care or point-of-use devices. However, few of these prototypes have been commercialised yet. These devices are still expensive, sometimes complicated to run, or not handy enough [1.2]. Several reviews consider the *"world-to-chip"* interfacing as one of the major hurdles [1.2, 1.3, 1.4]. Still, some specific consumer applications have emerged early on and are now used all over the world. One could cite the insulin pump and the cardiac diagnostic kit. Nevertheless the revolution promised has not happened so far. Most probably it will never happen as such. It will most likely replace some obsolete conventional techniques, here and there, find its place in niche market and finally convince practioners of its good merits.

1.2 A success story

The insulin pump and glucose meter provide two excellent examples of the miniaturisation of diagnostics or monitoring techniques. Due to the fatal nature of diabetic disease, on-site monitoring techniques had to be developed: the glucose meter was born [1.5]. The first example of portable glucose meter dates back to the 60s with the use of urine strips that turn blue when the sugar levels were normal and orange when the levels were positive. In the late 60s, more accurate glucose metres were commercialised. They were portable, and miniaturised compared to a full laboratory procedure but still were quite bulky. In 1978 a new glucose reading was invented based on the monitoring of hematocrit. From then on, it was commonly accepted that rigorous glucose measurements were of utmost importance. Following this medical breakthrough, dedication to enhance the portability of glucose meter rose. From backpack size, it was transformed to thick credit-card size. Following closely this development, the miniaturisation of insulin pump has been at the forefront of bioMEMS development in the early 70s. The first pumps were syringe pumps that could deliver precise levels of insulin in the hospital bed-side use. By integrating silicon piezo-electric micropump, the insulin delivery was soon truly miniaturised in 1980 to the same extent as the glucose reader [8.6]. In 2007 the nanopump from Debiotech and STM was commercialised, a device which makes use of the latest MEMS technologies. Another new advance in the field was the creation of implantable insulin pumps. 30 years of effort from chemists, doctors and engineers was necessary to create a truly POC solution to diabetes.

1.3 Establishment of the lab-on-chip field in industry and business

The factors which led to the establishment of the academic lab on chip field are as follow. First of all, the need to miniaturise has driven many projects, followed by the need to improve performance and decrease the cost of devices [1.7]. The benefits of miniaturization are also helping to offer smaller response time and the ability to process many samples in parallel.

Novel, more flexible, microfabrication techniques, such as soft lithography have helped researchers to lower the cost of prototype development and offered cheap, disposable

components. Along these new techniques came new developments in biocompatible polymer materials such as Polymdymethylsiloxane (PDMS) and SU8 [1.8] which offered great value to miniaturization. Figure 1.1 presents the breakdown of different materials used in the microfluidics system fabrication in the current market. As can be seem from this diagram, polymer is the material predominantly used in the field of interest in this study: Point of care devices and Clinical and veterinary diagnostics.
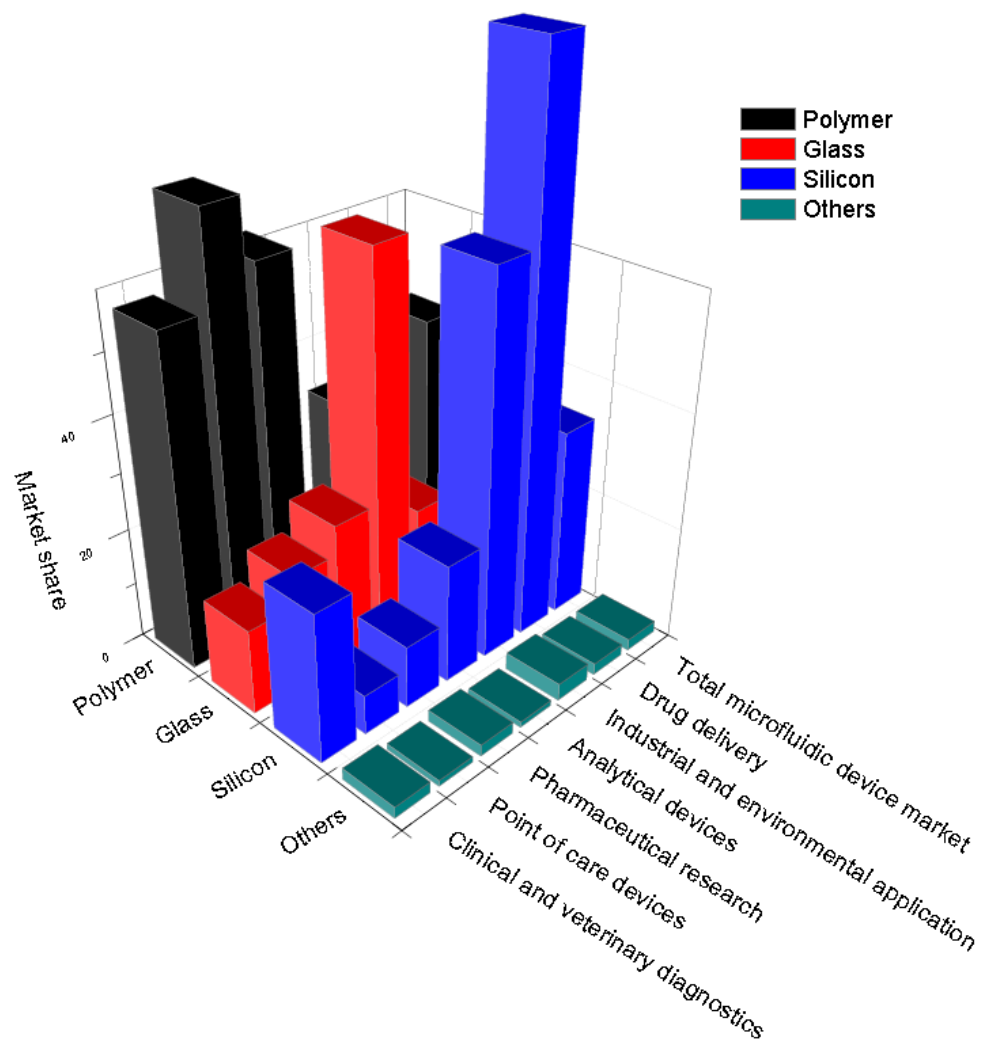
Figure 1. 1: Material breakdown of microfluidic devices in the current market Adapted from [1.9]

Breakthroughs in biology have triggered new routes for miniaturisation in a variety of fields. For example, the discovery of Polymerase Chain Reaction (PCR), cardiac markers or the Acquired Immuno Defficiency Syndrome (AIDS) has carried along the need for portable, miniaturized techniques to provide automated POC diagnosis and treatment. Social factors such the increase of the ageing population in developed countries and the subsequent increased cost of healthcare are also contributing to the fast

establishment of the lab on chip field. A trend towards personalized medicine and the appealing idea of self-diagnostics are driving research and industry to develop new smart tools.

Microfluidic techniques for life-science is a *fast-paced* field and an *emerging* market. Microfluidic supply chains are beginning to be structured and the market of microfluidic devices exceeded 1 billion dollars in 2009 [1.9]. A regular growth has been observed in the last years (2005-2008). Moreover, as suggested by the graph in Figure 1.2, the field is expected to grow up to $3 billion in 2014. Point of care applications represent today 15% of this market and is the one showing the largest growth.
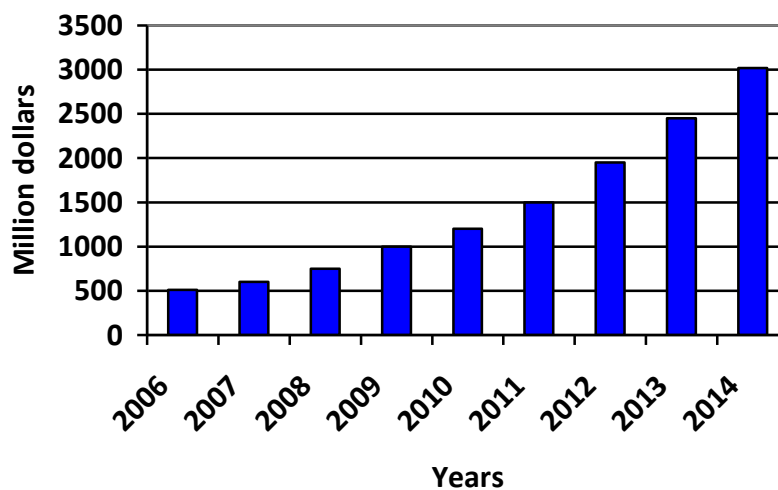
Figure 1. 2: Microfluidic market in M$ adapted from Yole development August 2009 [1.9]

The microfluidic market is a rapidly moving field, and despite the growth predicted in microfluidic devices applications, some challenges remain in the commercialization route. The lack of metrics and standards is a serious obstacle to the development of new industries [1.7]. Manufacturing costs stay high for the moment as few devices are produced in high quantities [1.9]. In the same fashion, the conflicts between different manufacturing approaches (silicon *vs* polymer) and the lack of standardized micropackaging solutions hinders a faster growth in this field [1.7]. Most importantly, in the development of microfluidic systems, the sample preparation steps are often omitted in the development of products, making a "lab on chip" a "chip in the lab". Finally microfluidics addresses important challenges to the healthcare system in terms of acceptance criteria and performance assessment. This step, as well as getting

practitioners and healthcare staff used to these new technologies, might take more time than the development of the systems themselves.

1.4 The weak link: sample preparation

Despite all the advances made in lab on chip, a major technical hurdle lies in the path of large scale commercialization and public access to point of care devices: sample preparation. With very few exceptions such as the pregnancy test kits for example, sample preparation comes with any diagnostic or analysis. It has been branded "the weak link in microfluidics-based biodetection" in [1.2]. Mariella gives several reasons for the lack of interest into sample preparation on-chip. The first reason is economical, Mariella believes that the emerging microfluidic has not triggered enough real commercial possibilities for sample preparation to be developed. Another financial reason is that the microfluidic technologies do not yet compete technically and cost-effectively with the existing techniques. A social reason to explain the low number of sample preparation microtechniques is the "inertia" of the current techniques and the lack of will for trained staff to change the traditional way to prepare samples. Finally, and not the least, the integration of sample preparation technique is another issue, along with the use of disparate material, leakage problems, lack of generic solutions which explain the relative small interest for sample preparation.

In two other reviews [1.3, 1.1] the challenges of "real" sample preparation, and in particular, of blood samples, were discussed. The complexity of the blood matrix is generally pointed out as the major hurdle towards on-chip blood preparation. The requirement for diverse blood sample pre-treatment is seen as one of the major hurdles towards miniaturization. It is observed that a significant part of the blood preparation is still handled manually in such conditions that may impair the collection of analytes of interest [1.1]. The need for low-cost systems reducing the time from blood collection to analysis is recognized.

Blood plasma separation holds a strategic place in sample preparation, as most steps in biological analysis require analytes from the plasma portion or the cellular portion. Figure 1.3 summarizes the various elements of interest to be found in whole blood.
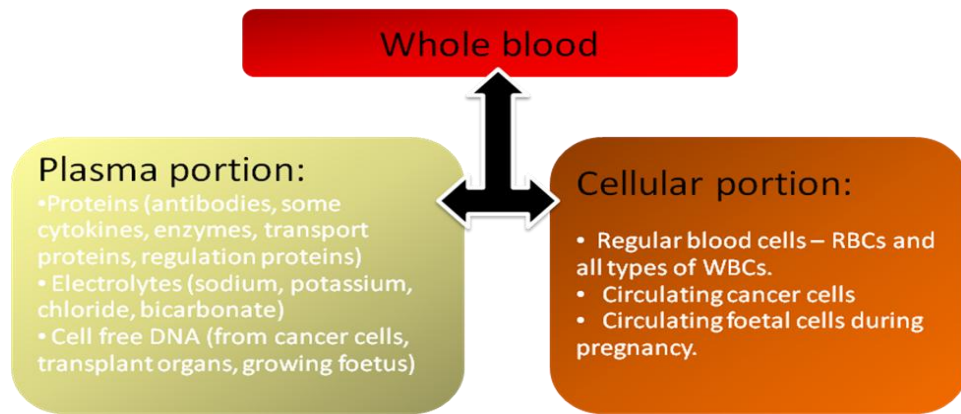
Figure 1. 3: Plasma and cellular portions found in whole blood, courtesy of Deirdre Kavanagh, Heriot-Watt University

1.5 Non-invasive Prenatal Diagnosis

This study is part of a larger project developed within the 3DMintegration Grand challenge. Prenatal diagnosis to determine the outcome of pregnancies and detect conditions that may affect future pregnancies has risen as another big issue among the broad public. Conventional prenatal tests are using invasive techniques, such as amniocentesis or chorionic villus sampling, which can result in abortion or growth abnormalities. Non-invasive prenatal diagnosis can be performed by separating rare foetal cells or cell-free foetal DNA from maternal blood, consequently avoiding the potential risk of amniocentesis. This project focuses on developing a Lab-on-chip device able to diagnose diverse prenatal pathologies within an hour at the doctor's office. The concept of this idea is presented in figure 1.4. A star highlights the specific module developed in this work.

1.6 Aim and scope of this thesis

This thesis aims at addressing the lack of lab-on-chip modules for sample preparation by proposing a blood plasma separator based on hydrodynamic principles only. The system presented here has a high throughput and a high efficiency and resulted in the application for a British patent [1.10]. Our approach is truly continuous meaning that both separated collections, blood cells and plasma, can be recovered at the same time.

Moreover, the material of the system was chosen carefully to ensure the bio-compatibility, the ability to mass-manufacture, the disposability (ideally single-use to
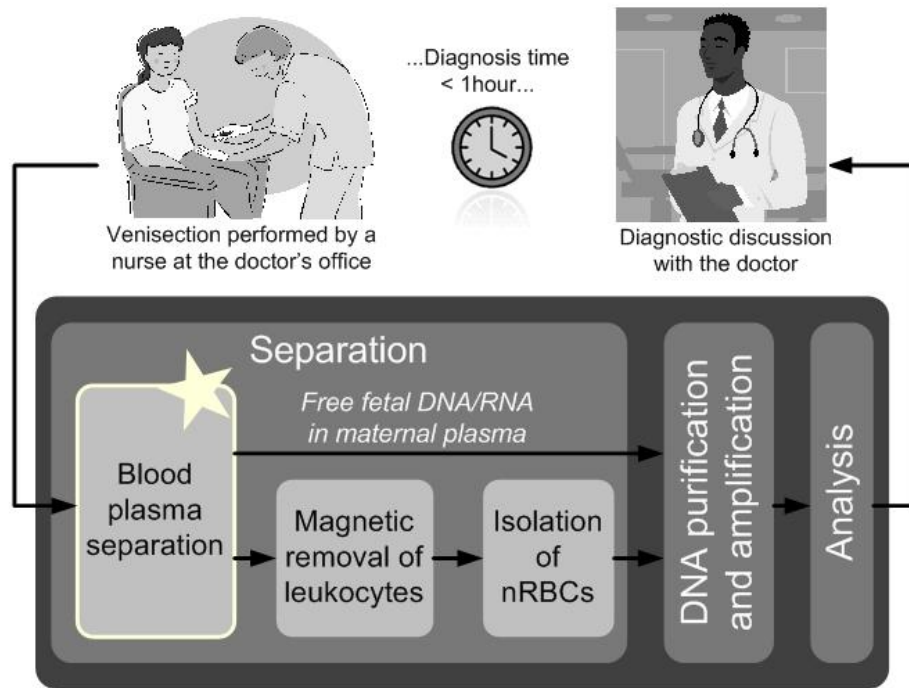
Figure 1. 4: Concept of the lab-on-chip device for the diagnosis of prenatal pathologies at the doctor's office. The star highlights the module developed in this thesis.

avoid contamination issues) and the low cost of the system. Additionally, another benefit of this microfluidic system is to have only one pressure source which eliminates the need for complex control systems. Unlike other microfluidic systems, this device can handle large (1-3mL) and complex (e.g. whole blood) samples.

An extensive physical and biological characterization of the device is presented in this thesis. To biologically characterize the system, state-of-the-art and conventional biological techniques were used, such as flow cytometry, polymerase chain reaction and real time polymerase chain reaction. For the first time a PCR on cfDNA from on-chip extracted plasma was performed without the need for further purification [1.11]. Most importantly, it was shown that the gentle separation of this system avoids RBCs lysis that would otherwise inhibit the PCR.

All the experimental findings indicate that this continuous microfluidic separation system may be used as a preliminary module for a lab on-chip system.

1.7 Thesis organization

Chapter two presents an extensive literature survey on particle separation at the microscale. The techniques specific to blood preparation before analysis are highlighted and polymer based passive separation techniques are found to be the best techniques to separate plasma from blood. In Chapter three the theory and design of a blood plasma separator is presented. The novel device will associate constrictions and bifurcations for enhanced yield and efficiency. Two generations of devices are presented. Chapter 4 is concerned with high-level simulation of the microfluidic separation network. It is found that the external connection might influence the internal separation of cells and plasma. Results are linked to the second generation device design. The rapid prototyping and fabrication routes for the microfluidic devices are presented in Chapter five alongside the experimental protocols developed for the testing of the blood plasma devices. In Chapter six, a hydrodynamic study of the biological samples is carried on the results obtained and the different effects of flow rate and entrance hematocrit levels on the system behavior are described. The results of two flow cytometric studies give detailed account on the separation characteristics. Molecular validation of the extracted plasma is presented in Chapter 7; this study is the first of its kind on non-purified cfDNA in plasma extracted on-chip. Influence of the separation efficiency and dilution levels on the polymerase chain reaction are discussed in this section. Chapter 8 presents the main conclusions and gives the future outlook of this research study.

A diagram linking all chapters of this thesis is presented in Figure 1.5.
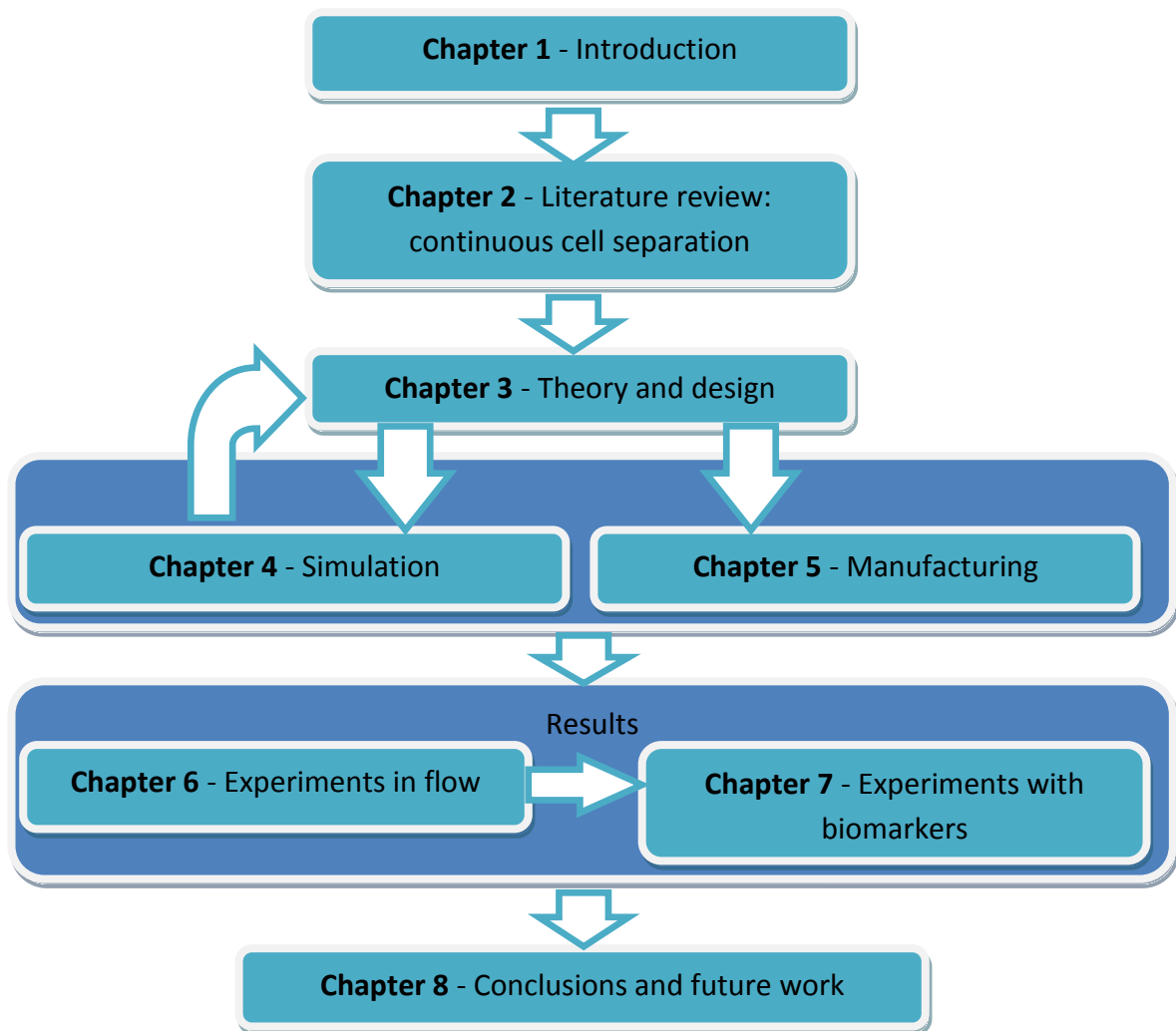
Figure 1. 5: Functional diagram of the thesis

1.8 References

[1.1] M. Toner and D. Irmia, *Blood-on-a-chip*, Annual Review of Biomedical engineering, **7**, 77-103 (2005)

[1.2] R. Mariella, *Sample preparation: the weak link in microfluidics-based biodetection*, Biomedical microdevices, **10**, 777-784 (2008)

[1.3] A.G. Crevillen, M Hervas, M.A. Lopez, M.C. Gonzales and A. Escarpa, Real sample analysis on microfluidic devices, Talanta, 74, 342-357 (2007)

[1.4] H. Becker, *Mind the gap!*, Lab on Chip, **10**, 271 – 273 (2010)

[1.5] M. Sattley, *The History of Diabetes,* Diabetes Health (1996)

[1.6] A. Nisar, N. Afzulpurkar, B. Mahaisavariya, A. Tuantranont , *MEMS-based micropumps in drug delivery and biomedical applications*, Sensors and Actuators B, **130**, 917–942 (2008)

[1.7] R. Mehalso, TIME MSc lecture notes, Heriot-Watt University, 2008

[1.8] E.Renard, G. Costalat, J. Bringer, *De la pompe externe à la pompe implantable, la fermeture de la boucle est-elle possible?* Diabetes & Metab (paris), **28**, 2s19-2s25 (2002)

[1.9] Yole Publication, Micronews, November 2009

[1.10] British Patent, IPO 310809 (2009)

[1.11] M. Kersaudy-Kerhoas, D. M. Kavanagh, R.S. Dhariwal, C. J. Campbell, and M. P. Y. Desmulliez, *Validation of a blood plasma separation system by biomarker detection*, Lab Chip, **10**, 1587–1595 (2010)

Chapter 2: Literature review of continuous microscale separation techniques

2.1 Introduction

Recent techniques of micron-sized particle separation within microsystems are described with emphasis on five different categories: optical, magnetic, fluidic-only, electrical and other, minor separation methods. Examples from the growing literature are explained with insights into separation efficiency and microengineering challenges. Current applications of the techniques are discussed.

Over the last ten years, point-of-use microreactors or point-of-care diagnostic tools have helped to reduce the need for intensive macrochemical plants or long diagnostic procedures. These so-called 'lab-on-chip' devices are built out of several different modules, each of them often achieving similar process functions as a macrochemical plant or a laboratory. Among these modules, the 'separation module', selectively sorts different kinds of particles, often immediately after synthesis or before analysis processes.

Applications of separation techniques at the microscale are broad and versatile. Particle separation is a necessary preparation step in most biological microassays and common in microchemical processing. In the biomedical field, separation techniques are used for fundamental cell studies where the isolation of pure cell types is essential. Separation is a key activity of diagnostic and analysis tools.

The aim of this chapter is to provide a critical review of the current technologies available for continuous microparticle separation within microchannels. Because of the growing rate of publications in the field, this review focuses mainly on advances in the last five years. This chapter describes radical new ways to separate particles, improvement of older methods and novel, cost-effective manufacturing methods. In comparison to recent reviews on particle separation, the emphasis given here is on continuous flow techniques. Although techniques such as electrical, optical or

magnetic separations are used in non-continuous flow, the main advantages of continuous-flow devices lie in profitability, minimum residence time under harmful conditions for separated particles, flexibility and integration of downstream functions. Special attention is given to a parallel, simultaneous separation of many subpopulations, providing potential high-throughput and high-recovery processes. This review focuses particularly on the passive separation of particles, not involving external decision making, and does not treat single-cell separation or trapping. Single-cell separation or trapping is more relevant to an in-depth biological study of some specific cells rather than a bulk separation for a clinical diagnostic device.

Different separation methods are highlighted and illustrated by relevant examples: (i) optical separation, (ii) magnetic separation, (iii) hydrodynamic separation, (iv) electrical separation and (v) other types of separation.

This section describes different kinds of separation techniques within microchannels currently developed as prototypes or already commercially available. A chart summarising the techniques presented in this review is shown in Figure 2.1.
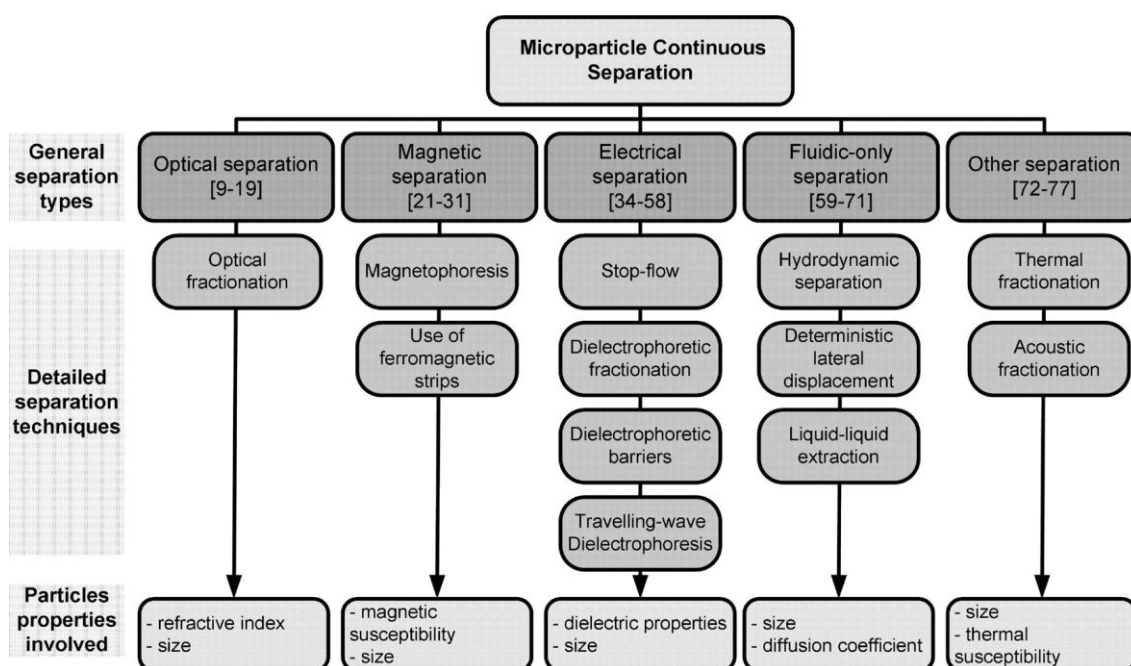
Figure 2. 1: Chart summarising the different microparticle continuous separation techniques.

2.2 Optical separation

A type of optical separation technique attracting attention is the new field of optical fractionation. Dholakia and coworkers [2.1,2] and Grier and coworkers [2.3,4,5] gave proof of the concept of optical fractionation. This method uses the recent advances in manipulation of optical tweezers. Optical tweezers is a manipulation tool developed by Ashkin, where a tightly focused single laser beam is used to trap a single particle [2.6,7]. Optical tweezers have been widely used since then to trap single particles in microfluidic systems. Advances in optical manipulation allowed the creation of three-dimensional arrays of light traps (optical lattices) using holographic optical tweezers, generalised phase contrast or diffractive optical element and multi-beam interferences for example. In optical fractionation, these methods allow the generation of an optical gradient force called potential energy landscape, which can deflect particles from their natural pathway according to their size or intrinsic properties. Particles experiencing sufficient optical force are kinetically locked in arrays of optical tweezers, whereas other particles flow along the natural stream, as shown in Figure 2.2. Dholakia's team reported with this method a sorting efficiency of up to 95% [2.1]. It was shown in [2.8,9] that flashing lattices, realised by amplitude modulation of the laser, can help to reduce the congestion of particles during the separation process. Optical fractionation is patented and yet commercially available from BioRyx200 by Arrys Inc [2.3]. In optical fractionation, the light patterns can easily be tuned making this method very flexible and responsive to new environments. On the other hand, the systems described are able to separate only one species from a mixture. In [2.10], however, separation of four different colloidal species is demonstrated using an optical lattice created with an acousto-optic deflector (AOD). An AOD is used to spatially control laser light and produce a complex potential energy landscape. In this experiment, a mixture of particles with four different diameters (2.3, 3.0, 5.17 and 6.84 mm), pumped through a microchannel is first focused into a single particle stream by an optical funnel. A following exit ramp with decreasing intensity releases the particles at different heights depending on their size. The smaller particles, which experience the weaker optical trapping force, leave the ramp first. Therefore a continuous parallel separation of four subpopulations is achieved. This method shows a near 100% pure sorting efficiency (all particles retrieved in their own specific group) and a throughput of 40 particles per

second. Although this throughput does not reach the throughput of conventional fluorescence-activated cell sorters (FACS), it is claimed that optical fractionation has the potential for higher throughput and might find niche application areas [2.11]. FACS is a common separation technique where particles are optically interrogated one by one and directed into different outlets depending on the interrogation result. However, FACS requires very expensive apparatus and fluorescence labelling.

Optical separation presents for the most part major advantages in terms of sensitivity, selectivity as well as versatility and permits the sorting of particles in a continuous flow. However, the need for laser sources hinders the easy portability of such systems although the integration of vertical cavity surface emitting laser arrays offers real opportunity [2.12]. A real need for miniaturisation of the apparatus is necessary in this field. The scale up of such optical and fluidics microsystems is also a major issue.
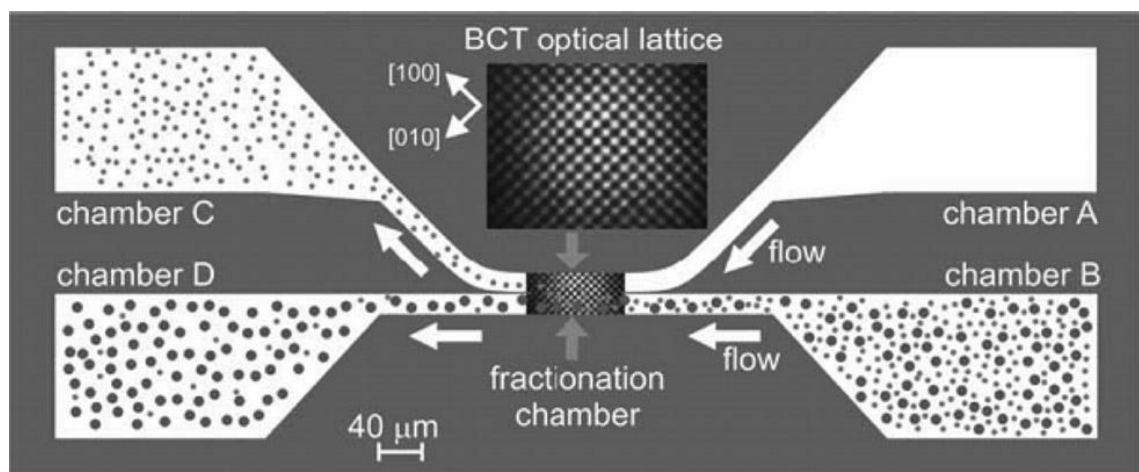
Figure 2. 2: Optical fractionation concept 3D optical lattice is introduced in the shared part of the chambers A, B, C and D allowing the separation of species according to their size or optical properties 3D optical lattice is reconfigurable which allows an easy updating of the selection criteria Scale bar is 40 mm long Reproduced with permission from [2.1]

2.3 Magnetic separation

2.3.1 Magnetophoresis

Magnetism has many uses in biological and chemical assays such as in drug labelling and targeting, transport, mixing and also separation [2.13,14]. In the magnetic separation method, sorted particles have either intrinsic magnetic properties or are

labelled with magnetic beads. In the case of an immunological separation, coated antibodies bind specifically with antigens of the targeted cells in an operation called labelling. The concept of a conventional magnetic separation device is a straightforward and long-established process: a magnet is placed in the vicinity of a column containing the cells to be separated. Magnetically labelled cells are retained in the column, whereas non-labelled cells will be flushed with the buffer allowing the immunological separation of species. The column is removed from the magnet in a second step and flushed to allow the collection of the sorted particles. This kind of separation is termed magnetic-activated cell sorting (MACS). MACS is also a method patented by Miltenyi Biotec but is widely available commercially under other names from manufacturers such as Dexter or StemCell [2.15,16]. The efficiency rate of the protocol is often better than 95% [2.17] and is used with success to isolate rare foetal cells [2.18]. The concept of MACS has been demonstrated at the microscale in order to reduce the volume of the apparatus and add other functions downstream. Benefits and drawbacks arise from the miniaturisation. Miniaturised magnets allow stronger and more precise magnetic fields because of the vicinity of magnets to the microchannels. On the other hand, the fabrication of integrated micromagnets requires numerous and expensive manufacturing steps [2.14,19]. The use of permanent magnets allows for portable (no electric connection) and autonomous devices; however, if the separation is not fully continuous, the removal of the magnet to flush the channel can cause difficulties. Electromagnets have the advantage to be easily switched on and off; however, their fabrication is more complicated and hampers the energetic autonomy of the system. An example of integrated microMACS was presented by Deng et al. [2.20], in which arrays of posts were manufactured on the bottom of a microchannel to trap magnetic particles. This device showed more efficiency compared with its macroequivalent. However, MACS is a batch process and might slow down further downstream analysis and limit the collection yield. Some attempts have been made to fabricate continuous flow magnetic separation devices. A technique called 'on-chip free-flow magnetophoresis' was demonstrated by Pamme et al. [2.21,22]. In this example, a mixture of different magnetic particles and non-magnetic particles is aligned along the wall of a microchannel. A micromagnet placed upon the channel provides a non-homogeneous magnetic field gradient transverse to the laminar flow. Depending on their size and magnetic properties, particles are

deflected more or less from their path. The addition of spacers allows the collection of particles in separated outlets as shown in Figure 2.3. A continuous-flow, magnetic separation device for the enrichment of foetal cells from maternal blood has been described in a patent by Blankenstein [2.23]. This device uses the same working principles as the previous example although the cells require to be labelled.
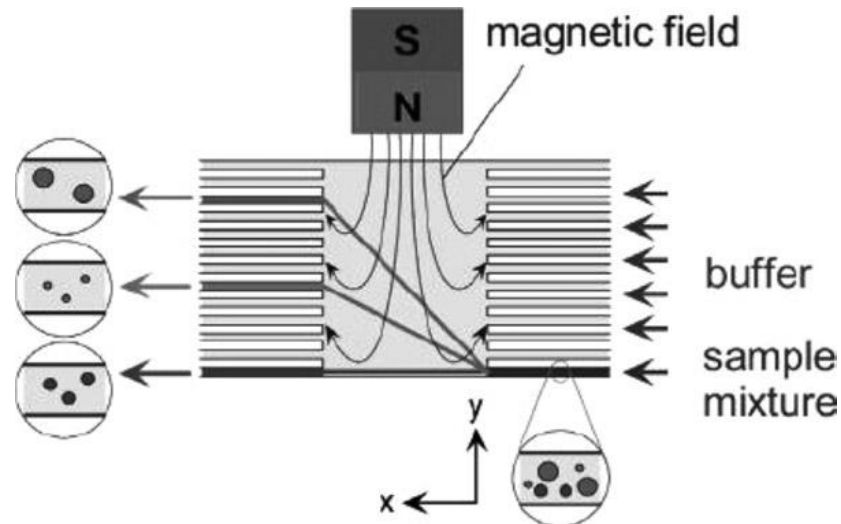
Figure 2. 3: Magnetic separation principle within a microchannel Mixture of different magnetic and non-magnetic particles is injected in a microchannel Depending on their size and magnetic properties the particles will be more or less deflected from their natural path due to the magnetic field Non-magnetic particles will not be deflected Addition of spacers permits the independent recollection of different species [2.21]
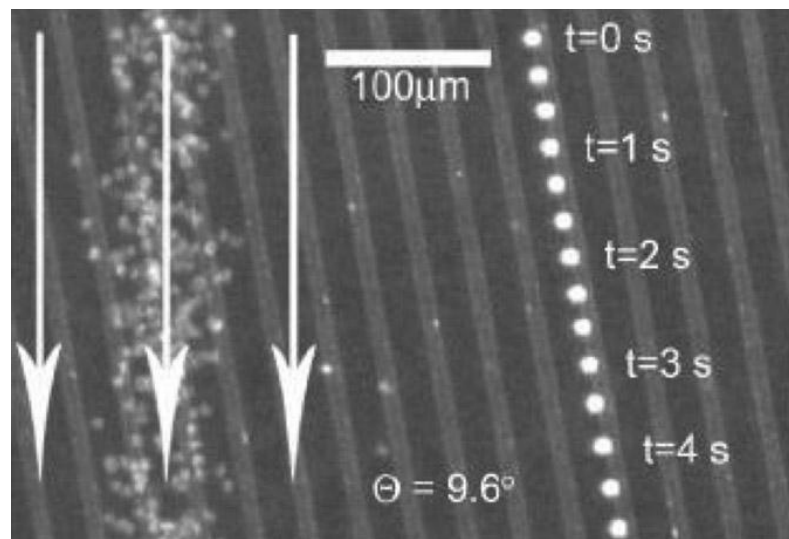
Figure 2. 4: Separation of red blood cells from white blood cells with magnetic strips Superposed images showing the separation of a tagged leucocyte from untagged red blood cells using magnetic stripes Reproduced with permission from reference [2.24]

2.3.2 Magnetic strips

Another type of continuous magnetic separation was demonstrated by Inglis et al. [2.24]. In this example, some ferromagnetic strips fabricated in a microchannel provide an array-like magnetic field pattern at a given angle to flow direction. Cells selectively tagged with magnetic nanoparticles deflect from the flow path to follow the strips. This technique convincingly demonstrates the separation of white blood cells (WBCs) from human blood as shown in Figure 2.4. In another example, Han and Frazier [2.25] used an external magnetic field to activate a ferromagnetic wire integrated to a microchannel as shown in Figure 2.5. Depending on their internal properties, particles will be repelled or attracted by the wire and thus collected at different outlets.
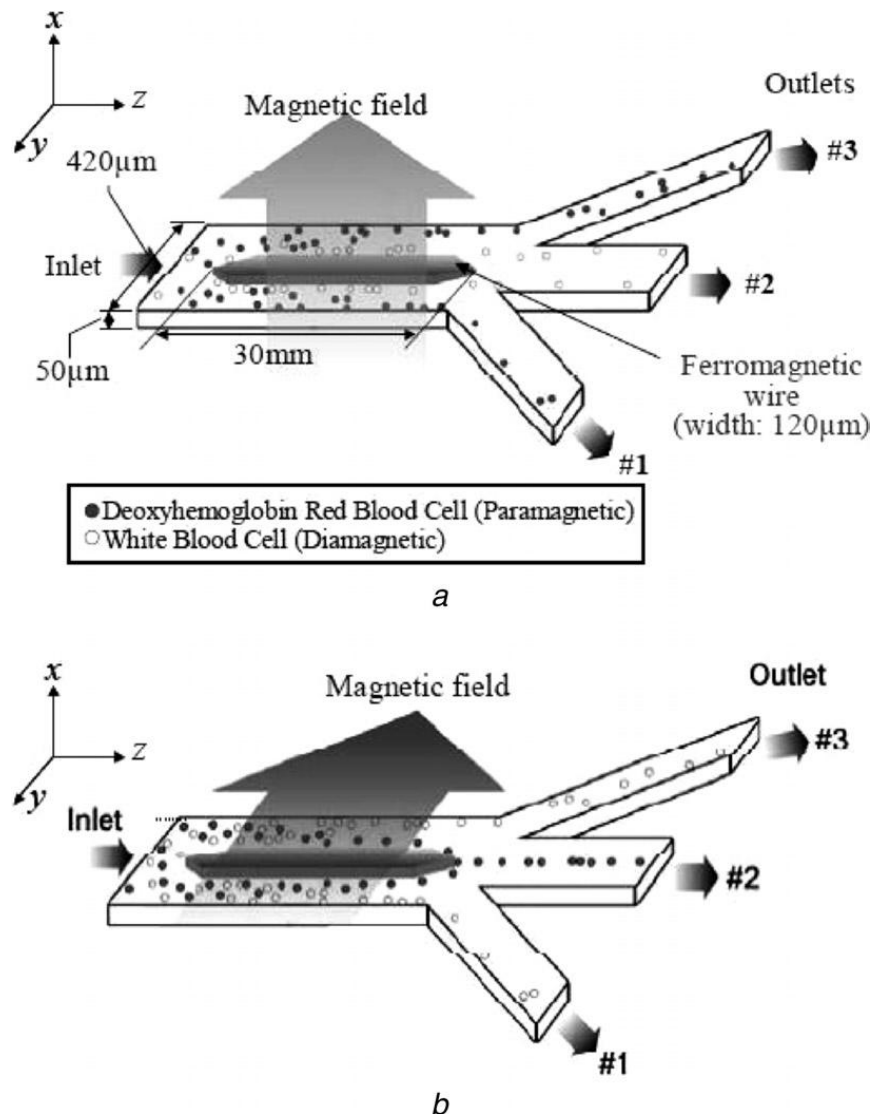
Figure 2. 5: Separation of red blood cells from white blood cells with a ferromagnetic wire Illustration of a magnetophoretic separator Ferromagnetic wire is incorporated along the length of the microchannel In the diamagnetic capture mode, an external magnetic field is applied normal to the x-axis of the

microchannel In this case the red blood cells will be deflected from the ferromagnetic wire and will flow through the outlets 1 and 3 In the paramagnetic mode, the external magnetic field is applied normal to the y-direction of the microchannel, which forces the white blood cells to be deflected at this time from the ferromagnetic wire.

In one publication a magnetic blood plasma separation system was presented. However the system should be further miniaturized to be accepted as a microsystem [2.26].

Magnetic separation is very interesting in terms of portability and autonomy. Magnetic fields have never been reported to damage biological particles and therefore allow the gentle sorting of cells, especially between white blood cells and red blood cells. However, the manufacturability of the magnetic-activated separation mechanism can hamper the development of such devices.

2.4 Electrical separation

2.4.1 Dielectrophoresis and castellated electrodes

Originally, most of the first separation techniques for microparticles used electrical forces. Indeed, electric-field-based manipulation is well suited at the microscale because of the ease with which high electric fields can be produced with micron size gaps and voltage of several volts only. Furthermore, in the last ten years, the diversification of micro-electromechanical systems into areas such as chemistry and biology has increased the tendency to combine electrical microsystems within microchannels. There are two main types of electric field-based manipulation, depending on the properties of the particles to be sorted. Electrophoresis, the movement of charged particles in a uniform electric field, is a very well known technique to separate and transport different kinds of charged particles. Detailed reviews on electrophoresis can be found in recent literature [2.27]. Dielectrophoresis, often confused with electrophoresis, is described by Pohl as 'the translational motion of neutral matter caused by polarisation effects in a non-uniform electric field' [2.28]. This technique has attracted scientific attention because of its ability to manipulate neutral–but polarisable–particles. Dielectrophoresis has first been applied to separate cells according to their size or dielectric properties. A number of early articles report the separation or the enrichment of particles using castellated or interdigitated planar

electrodes providing an inhomogeneous electric field [2.29,30]. These techniques, sometimes referred as stop-flow techniques, often relate to binary separation where a mixture is split into two subpopulations, one usually retained in the channel [2.31]. Sometimes particles approaching DEP affinities and size are difficult or impossible to separate. To overcome this limitation, Yang et al. [2.32] coupled an antibody recognition and a dielectrophoretic stop-flow technique. In this example, antibodies specific to the targeted bacterial cells are coated above interdigitated DEP arrays, isolated by a thin layer of SiO_2. The mixture of bacterial cells is injected into the channel. When the DEP is actuated, all the cells are concentrated above the electrodes against the flow. During this time, the targeted cells bind themselves with the antibodies. When the DEP is deactivated, the unbound cells flow away, leaving the targeted cells separated in the channel. These techniques report high efficiencies, close to pure recollection of each type of particle and are adopted for high product value and low volume application. Some drawbacks can nevertheless be reported. First, cells are often trapped with positive dielectrophoresis (pDEP) and without careful control of the applied voltage and frequency, might experience very high electric fields, which can damage or destroy them. A guide to the values of frequencies and applied electric fields affecting the viability of the cells is given in [2.33]. In [2.32], the cells trapped by pDEP stay viable, but an anomalous protein production is reported. Secondly, in general, only one subpopulation can be extracted from a heterogeneous mixture. Finally, even though fluid is continuously drawn through the chip, voltages often have to be turned on and off to collect the separated subpopulations, which can hamper the continuality of the process. Hydrodynamic forces have been coupled to dielectrophoresis to produce continuous particle separation. This technique uses electrodes to levitate particles to different heights depending on their dielectric properties. The addition of a parabolic flow allows the particles to be dragged away at different velocities. Separation of erythrocytes and latex beads was performed by Rousselet et al. [2.34]. The team of Gascoyne reported separation of different types of leucocytes with purity after separation up to 98% [2.35]. This technique uses negative dielectrophoresis to levitate particles above the electrodes and thus protects vulnerable biological particles from high electric fields. However, it has limitations in separation performance. Cells of one type can contaminate the cell population of another type [2.35].

2.4.2 Isomotive electrode arrangements

Other kinds of electrode arrangements have been successfully tested. Choi and Park [2.36] proposed a trapezoidal planar electrode array providing a specific electric field geometry in a microchannel. Particles focused on one side of the channel are deflected more or less by the electric field depending on their properties. At the end of the microchannel, the addition of spacers helps to collect different particles. Li and Kaler [2.37] reported an ingenious 'isomotive' electrode arrangement for continuous-flow separation. Isomotive refers to a specific electric field where a particle experiences a constant dielectrophoretic force everywhere in the field, a configuration described by Pohl and Pethig [2.38]. This geometry provides a better separation of species, based only on their dielectric properties.
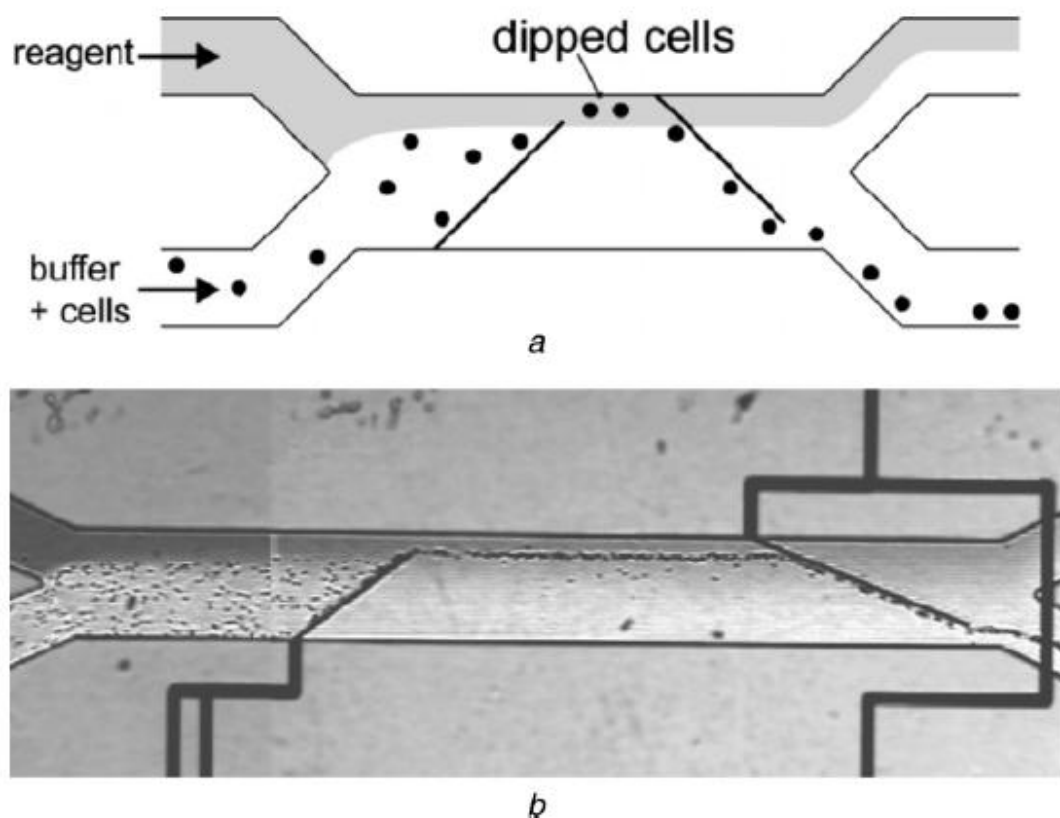
Figure 2. 6: DEP barriers used for cell dipping a Schematic diagram illustrating the concept of cell dipping Electrodes are mounted at the top and bottom of the microchannel Population of cells is introduced in one of the inlets Electrodes, once activated, divert cells from their natural path Cells are guided to the reagent and from the reagent back to the buffer b Photograph of the experiment Transit time in the reagent is 0.3 s [2.39]

2.4.3 Dielectrophoresis barriers

The use of dielectrophoretic barriers has also been widely and successfully demonstrated. A dielectrophoretic barrier refers to electrodes mounted at the top and bottom in a microchannel. This configuration creates an electrical field barrier which deflects particles from the direction of fluid flow. To separate two different species, the frequency and magnitude of the voltage is set such that one species exhibits dielectrophoretic forces and can be deflected, whereas the other species go through the electrical field barrier without experiencing any force. Fuhr and coworkers [2.40] were the first team to report such an arrangement in 1998 with serial and parallel non-contact manipulation at high velocity. From 1998, several patents and articles have been published by the same team in collaboration with the German company Evotec Technologies and includes treatment, separating, sorting or confinement of diverse kinds of biological or synthetic particles [2.41,42,43]. In a publication by Schnelle, a particle separation is reported using dielectrophoretic forces engendered with curved electrodes and hydrodynamic forces [2.44]. In [2.45], a detailed experimental and theoretical study of DEP barriers shows a strong dependency between the channel height and the threshold velocity above which particles may penetrate the barrier. Decreasing the channel height leads to better separation efficiency. In [2.46], a system named NanoVirDetect is described. This versatile module uses standardised biochips packaging and has individually tunable functions such as focusing, separation, holding of micron or submicron-sized particles and thus can be adaptable to a large number of different particles. Electrodes are made out of nanoporous materials to increase the electrode capacitance. This not only expands the frequency range of dielectrophoretic deflection but also allows the system to be used with higher conductivity medium which is of high interest especially with biological samples often flowing in relatively high conductivity liquids. Other teams report also the successful implementation of dielectrophoretic sorters, using improved DEP barriers [2.47,48,49]. Although the new configurations double the maximum flow speed compared to a classical strip-like electrode, plane electrodes show more temperature rise than the classical geometry, which is a major drawback for sensitive biological or chemical applications. A focusing device has been fabricated by Morgan et al. using a quadrupolar electrode arrangement [2.50]. In [2.51], a tripolar electrode arrangement for separation

purposes is demonstrated. In this application, two tripolar strip-like electrode arrangements are embedded on each side of the bottom of the channel. Thus, particles experiencing positive DEP are expected to flow near the electrodes, whereas particles with negative DEP affinity are focused along the central axis of the channel. This simple geometry might not be so proper for continuous flow, as particles with positive DEP will probably stick to the electrodes if the flow is too slow, hampering the collection of the species. A high speed cell-dipping system is proposed in [2.52] and shown in Figure 2.6. A classic pair of strip-like electrodes is mounted at the top and bottom of a 20 mm high microchannel. A large amount of particles is transferred from one reagent to the other in less than 0.5 s at a flow speed of 300 mm.s^{-1}. A large diffusion of the dye shown as the second flow stream can be noticed after the first barrier and might be because of some electrokinetic forces or a perturbation in the flow caused by the accumulation of particles on the tip of the barrier. The addition of a spacer between the two streams, as stated in Fuhr's patent, can help to avoid this perturbation [2.42].

2.4.4 Improvements in dielectrophoretic barriers

In recent years, new ideas have been developed to enhance performance of DEP separations systems. A different channel geometry for dielectrophoretic focusing of particles is presented by Leu et al.[2.39]. In this device, a mixture of particles is separated in a single particle stream with a combination of DEP forces and hydrodynamic forces in a funnel-like channel. Although the result is obviously useful in term of particles analysis, the electrodes need to be embedded on the channel side walls, which is a laborious fabrication step. An interesting insight to improve separation is proposed by the team of Hu [2.53]. In this approach, labelling of cells with particles that differ in polarisation response enhances the sorting activity. A flow speed of 300 mm.s^{-1} in a 20 mm high channel can be obtained. However, this process requires a supplementary step of labelling. Park et al. [2.54] reported a fan-shaped like electrode geometry creating a unique asymmetric electric field gradient. In this concept, the applied fiel[2.39]d is continuously varied because of a half-circular type of microchannel and this geometry increases the discrimination power of the device. However, this approach leads to a higher temperature rise. The use of so-called electrodeless DEP was reported. In this method a homogeneous electric field is created

within a microchannel by introducing electrodes at the inlet and outlet. Insulating obstacles are placed within the channel rendering the electric field non-uniform, which leads to the creation of a dielectrophoretic force. Electrodeless DEP prevents electrode fouling and electrode destruction sometimes reported in DEP manipulation. Originally this principle was applied with arrays of insulating posts in a microchannel [2.55,56]. In this kind of arrangement, particles sensitive to DEP are trapped between posts, whereas others flow along. This results in a non-continuous system as the voltage has to be turned down to recollect the trapped particle. Using the same concept, Barbulovic-Nad et al. realised an original device incorporating an oil droplet at one point of the side wall of a microchannel. Particles approach the base of the droplet in the same fashion and are diverted more or less at the top of the bubble in the highest electric field zone. This allows the parallel collection of different particles [2.57]. The separation can be tuned by changing the size of the droplet. Renaud and coworkers [2.58] proposed recently a device embedding large electrodes insulated from the main microchannel by 5 thin, dead-end channels. These effective methods nevertheless require high voltages and create relatively high electric fields, sometimes exceeding the threshold of safe cell manipulation.

2.4.5 Traveling wave dielectrophoresis

Another kind of electrical separation, known as travelling-wave dielectrophoresis (TW-DEP), has been demonstrated. In TW-DEP, particles are transported across arrays of interdigitated electrodes being energised with sinusoidal electric signals [2.31]. A travelling electric field, produced by phase shifting of the signals, induces a dipole moving in a direction perpendicular to the direction of the electrodes array. As the speed and direction of the motion depends on the particle's dielectric properties, separation of different species can be achieved. Recently, Pethig et al. [2.59] demonstrated the separation of T-cells from monocytes with a superposition of TW-DEP signals. The technique of signal superposition leads to a reduction in the length of the electrode array needed to achieve separation.

To summarise, the use of an electric field for particle separation is a relatively old, established technique. Among the different kinds of microdevices using electric field-based separation in continuous flow, examples include DEP fractionation, DEP barriers

and TW-DEP. Many different electrode arrangements related to these reliable and efficient techniques can be found in the literature. Moreover, it has been demonstrated that dielectrophoretic barriers have the potential for greater exploitation. Nevertheless, the use of electrodes introduces an important fabrication step which increases the cost of the microdevice and might hamper mass-manufacturability. One publication reports on the use of electric field for blood plasma separation in a 10µL drop of diluted blood, however, no result is presented in this study [2.60].

2.5 Fluidic-only separation

2.5.1 Hydrodynamic separation

To tackle the problem of outer force field requirement in separation devices, researchers proposed recently some techniques which can be termed 'fluidic-only' separation. In these separation methods, particles are sorted exclusively by size, often using only the geometries of microchannels and hydrodynamic forces. These techniques are particularly suitable for blood plasma separation as they can be developed using cheap disposable polymer-type of material. Moreover they are often gentle to cells (no electrical field for example), and do not require any outer field.

2.5.1.1 Microcentrifugation

Conventional techniques for blood plasma separation in traditional laboratories include centrifugation and filtration. Both methods are time-consuming, relatively expensive and might damage cells if not used carefully [2.61]. In the light of the disadvantages outlined above and the benefits that microscale techniques can provide in terms of volume of blood extracted, response time and portability, it is therefore unsurprising that the alternative blood-plasma separation on-chip has gained increasing interest over the last few years.

In that respect, several broad avenues of research have been implemented that try to replicate the benefits of traditional centrifugation methods. The miniaturization of centrifugation has been the topic of many research groups. Ducrée and Madou, for example, have utilised centrifugal forces developed through the rotation of their lab-on-CD devices to separate red blood cells from plasma [2.62,63]. Figure 2.7 illustrates

the concept of the lab-on-CD and a blood plasma separation using this tool. Among the advantages of the lab-on-CD platform is the lack of clogging effect that might reduce the efficiency of separation in other devices. Centrifugation is often considered as "non-continuous", however on Lab-on-CD devices, the samples might be processed in-line after the separation or other functions.
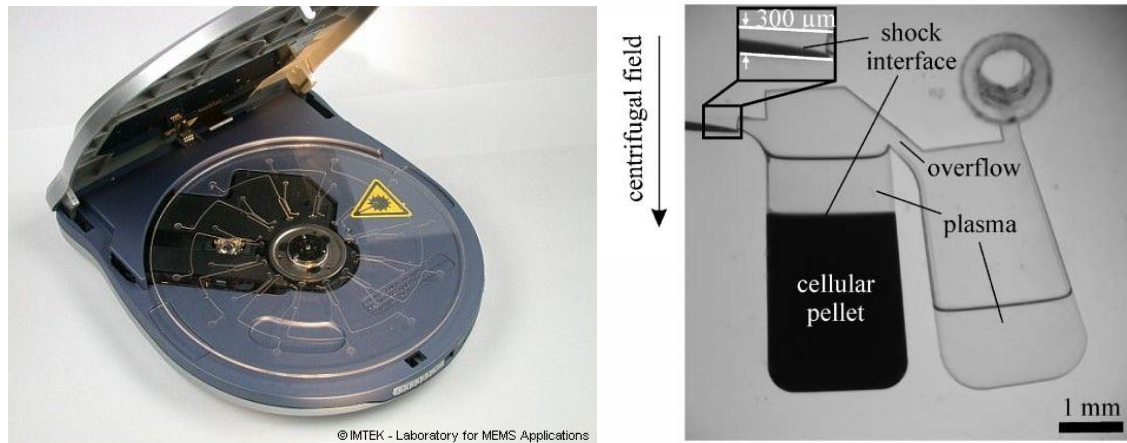
Figure 2. 7: (a) Illustration of the concept of the "biodisk". Courtesy of IMTEC (b) Blood plasma separation in the lab-CD

Using a mini-centrifugal effect, Blattert et al. proposed a bend structure to increase the plasma-free layer existing naturally in microchannels and extract plasma [2.64], in that way the blood plasma separation is fully continuous. This device is shown in Figure 2.8a. More recently, an original centrifugation device using a spiral design was proposed in [2.65] for blood plasma separation. A spiralling channel with a cross-section of 200µm x200µm and 12cm long as shown in Figure 2.8b was used in an attempt to create high centrifuge acceleration. However, due to Dean vortices the efficiency of the system was limited. A 180 bend device was subsequently designed to reduce this side effect. Although this device was more efficient than the first one, significant haemolysis was observed.

2.5.1.2 Filtration

Filtration is another conventional method to separate plasma from whole blood, and has also been miniaturized. Moorthy et al presented a device with an integrated membrane, or porous plug, allowing the filtration of cells greater than 3µm, however the device is easily clogged [2.66]. Cross-flow filtration has been implemented with more success by Vandelinder et al. and Chen et al. in Polydimethyloxane (PDMS)
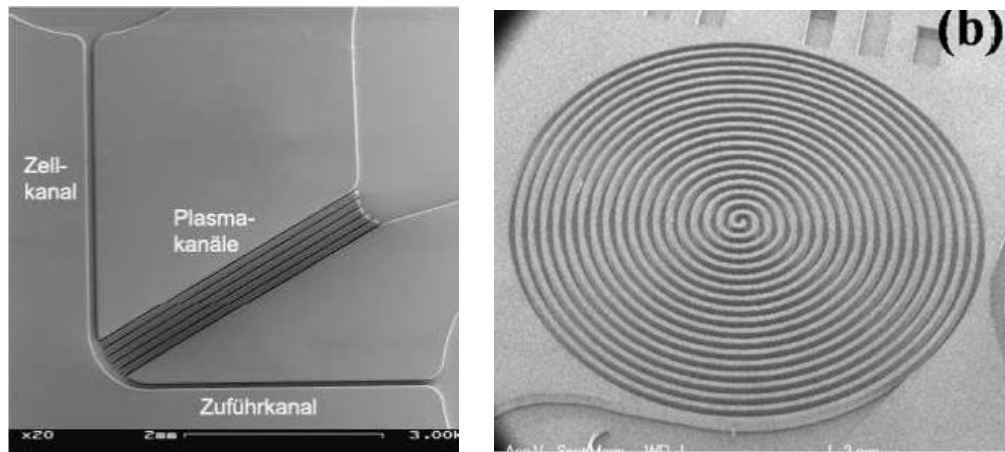
Figure 2. 8: Development of centrifugal effects on-chip [2.64] (a) Bent channel and bifurcations (b) Spiral design[2.65]

devices [2.67,68]. However, as pointed out by Becker, results obtained in PDMS devices are hardly reproducible on commercial chip applications [2.69]. Additionally, two original filtering geometries were proposed by Sollier et al [2.65]. A U-filter and Snake design (serpentine like) were manufactured to test the efficiency of hard beads and RBCs separation. These devices proved to have relatively good separation efficiency, at the expense of a small operation time, due to rapid clogging of the pores.

2.5.1.3 Lateral displacement

Some researchers have focused on the development of more continuous separation methods applicable to blood plasma separation using hydrodynamic forces. These methods, alongside centrifugal and filtration techniques, are sometimes labelled as "passive", as they do not require any external force field but the force induced by the pumping of the fluid itself [2.65].

In 2004, the team of Yamada and Seki proposed a pinched-flow separation device [2.70]. The concept is shown in Figure 2.9. A mixture of different-sized particles is injected into a buffer. With the help of another fluid, particles are aligned to a sidewall of a pinched segment, which is subsequently broadened; at this point, hydrodynamic forces act differently on particles, deflecting the small ones away from the big ones. Flow rates of the two inlets and the angle between the two segments are determining factors to sort the different sizes of particles. In 2005, Yamada et al. proposed a two-step technique called 'hydrodynamic filtration' to get rid of the need of a second buffer to control the separation; concentration and classification are performed at the

same time [2.71]. A fluid containing particles is injected in the main microchannel having multiple branch points and side channels. Particles do not enter the subchannels when the relative flow rates at the branch point are low. This permits in a first step the withdrawal of the liquid and the concentration of the cells. Increasing stepwise the relative flow rates at each branch point allows the collection of firstly small particles and secondly large particles. The size limit of the sorted particles is determined by a precise distribution of the flow rate at each branch. This technique was proven by the enrichment of WBCs. Although, RBCs remain present in the fraction of interest, the relative concentration of WBCs in relation to RBCs was increased by 29 times.
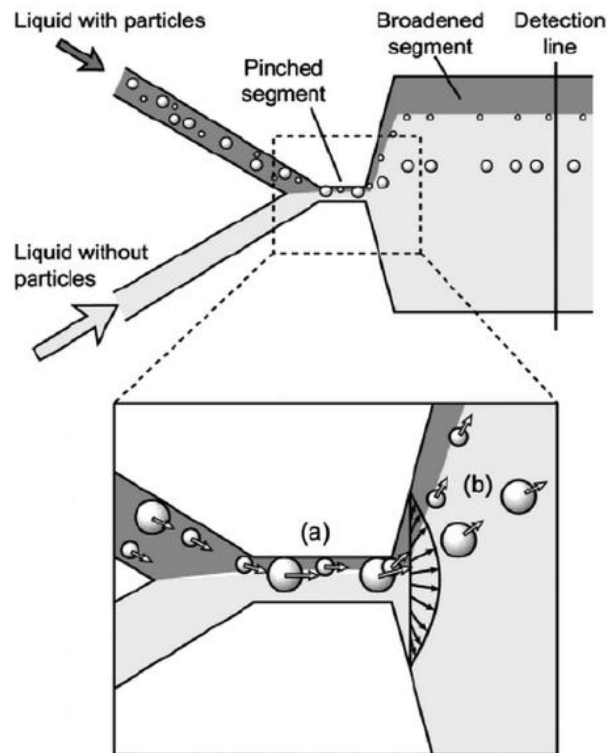
Figure 2. 9: Separation of different-size particles in a pinched segment Schematic diagram illustrating the principle of pinched-flow fractionation a In the pinched segment, particles are aligned to one sidewall regardless of their sizes by controlling the flow rates from two inlets b Particles are separated according to their sizes by the spreading flow profile at the boundary of the pinched and the broadened segments [2.70] Copyright 2004 American Chemical Society

Other fluidic-only separation techniques emerged from preliminary work on microcirculation [2.72]. These techniques are particularly relevant in the case of blood plasma separation, where the axial migration of blood cells in microchannels below 300µm is used for sorting [2.64,73,74]. A number of studies have been published by

27

different groups in the literature. Pharmaceuticals companies like Roche have published reports on the integration possibilities of such preliminary modules [2.75]. An example of blood plasma separation module manufactured by Roche is presented in Figure 2.10a. Faivre has used constrictions integrated before a bifurcation, as shown in Figure 2.10b, to increase the natural cell-free layer of blood flow at low Reynolds number using lateral migration [2.76]. A constriction integrated in a microchannel was demonstrated to enhance the cell free-layer up to 1 cm downstream. The addition of spacers near the channels walls allows the pure collection of plasma. Yang's team presented a microfluidic network of T-channels to retrieve pure plasma with a series of 10μm bifurcations in a 15μm main channel (Figure 2.10c) [2.74]. The same principle was used by Fan et al to extract plasma for protein analysis [2.77]. Effenhauser et al presented a 3D structure taking advantage of a high-aspect ratio with a single bifurcation to produce a better plasma yield [2.78]. Sollier et al, demonstrated recently a series of original structures to enhance the cell-free layer using constrictions and bifurcations (Figure 2.10.c) or ear-cavities and bifurcations and allowing up to 2x increase in extraction yield for 100% pure plasma [2.65,79]

Lateral migration has also been demonstrated to extract plasma at higher Reynolds number and large flow rate by DiCarlo [2.81]. More recently, Rodríguez-Villarreal et al. have demonstrated a high flow rate blood plasma separation device using one constriction and one bifurcation [2.82]. The biological validation of the resulting extracted plasma in terms of contamination was however not presented in this article. An exhaustive comparison of passive blood plasma separation techniques has been presented by Sollier et al.[2.65].

2.5.2 Deterministic lateral displacement

Another technique called deterministic lateral displacement was set up and tested by Huang et al. [2.83]. In this method, microposts are placed in rows within a microchannel. Each row of posts is shifted from the other by a distance which partly sets the critical separating size. The asymmetric bifurcation of laminar flow around obstacles leads particle to choose their path deterministically on the basis of their size. A small particle will have a zigzag displacement path, whereas a large particle will tend to flow straight. After a number of rows, the particles can be collected separately. This
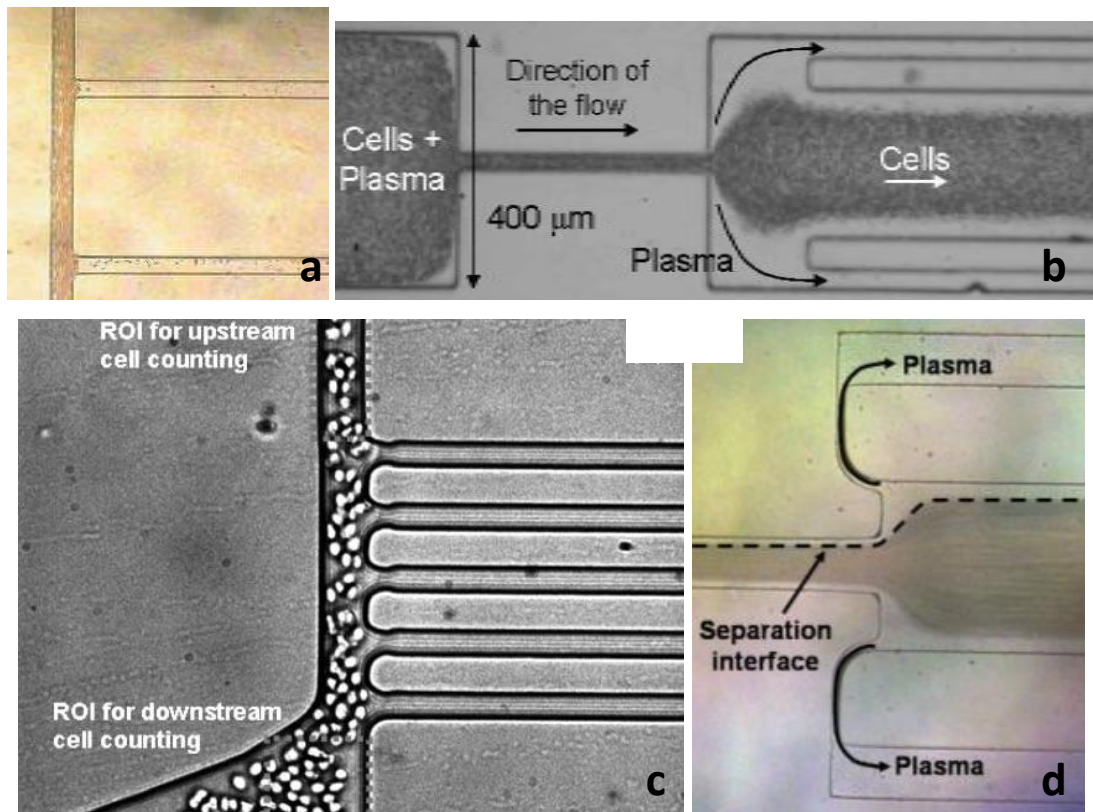
Figure 2. 10: Lateral displacement devices (a) Simple channel for the extraction of plasma from blood [2.75]. (b) Use of a constriction to enhance the natural cell-free layer in RBC flow [2.76]. (c) A more complex microfluidic network [2.74] (d) An example of enhancement of the cell free layer with the use of optimised constriction and bifurcations [2.80].

method is cost effective and can separate in parallel a large number of different-sized particles with a precision of up to 10 nm. The method was successfully tested for the separation of WBCs and RBCs [2.84]. However, because of a high risk of clogging because of the numbers of posts employed and the narrow gaps between them, Huang and coworkers [2.85] presented later an optimised device including additional regions alongside the active sorting arrays. These additional regions collect the larger particles that have been sorted. Although these regions also contain pillars to maintain the same pressure drop across the system, the gaps between the pillars are made larger to avoid clogging. This device removed all the particles larger than 1 mm from whole blood, allowing the collection of pure undiluted plasma. The latest technique is patented in [2.86]. Recently Li et al. labelled CD4p T helper lymphocytes with 25 mm polystyrene beads in a mixture of WBCs injected in a lateral displacement system [2.87]. Up to 91% of the specific lymphocytes were therefore separated from the other kind of WBCs. This article demonstrates the possibility of cell subtype sorting with the continuous-flow lateral displacement method.

29

2.5.3 Density based extraction

Density based extraction, also known as 'liquid–liquid extraction' is another fluidic-only separation technique widely used in the chemical and biological industries. The concept exploits the preferential affinity or differential diffusion coefficients of solid compounds in a laminar flow of two liquid streams. H-filters developed by Yager et al. [2.88] have used this technique to extract molecular analytes from whole blood. Nam et al [2.89] proposed a microsystem incorporating this technique. In this device, the injection of cells in a thin stream between two phases allows the cells to partition in the preferred solvent. The sorting efficiency of the microdevice was reported to be 97% which is higher than its macroscale counterpart. However, it is not a versatile technique, as only two types of particles can be sorted at the same time using sometimes very specific solvents. Liquid–liquid extraction is particularly adapted to chemical extraction, such as extraction of hydrocarbons from oil in the petrochemical industry or extraction of organic compounds from extraterrestrial dissolved minerals in space exploration [2.90,91]. In conclusion, these fluidic-only separation techniques have the great advantage of not requiring any outer field. Therefore the manufacturing of these devices relies only on microchannel networks. Manufacturing of these channels can be achieved via hot-embossing or microinjection moulding. This holds the potential for cheap and mass- manufacturable devices, which is particularly relevant in the case of point-of-care devices. However fluidic-only separation devices, with the exception of the last example, can separate particles by size only.

2.6 Other types of separation

2.6.1 Thermal separation

A system using an outer thermal field is described in [2.92]. In this device, a temperature difference is applied across the microchannel. A separation between particles occurs because of the difference of thermal diffusion coefficient. In such a system, particles can react to a temperature gradient and will be displaced more or less rapidly, depending on their physical properties towards the cold wall of the microchannel across the flow. This technique does not have large separation efficiency and particles are not easily collectable from different outlets. However, it has been

recently observed that temperature modifies the separation parameters of cells in [2.82] and therefore might be applied in the future to enhance hydrodynamic blood plasma separation in some specific cases.

2.6.2 Acoustic separation

Acoustic separation can also be found in the literature [2.93,94,95]. The last reference demonstrates a separation efficiency near 100% which is comparable with conventional blood cell separation by centrifugation. The three-stage separation device is shown in Figure 2.11.
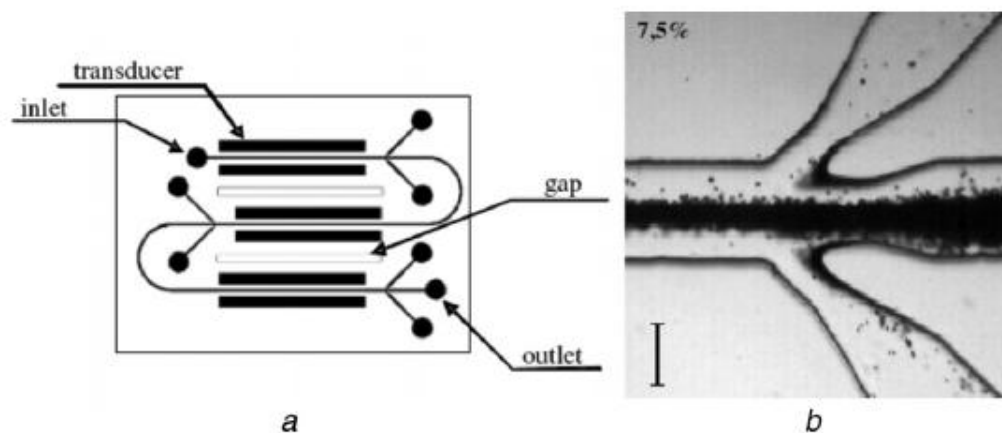
Figure 2. 11: Sorting using ultrasonic field a Schematic of a three-stage microdevice Particle separation here occurs on each stage of the separator On each stage, most of the particles in the solution being affected by the ultrasonic standing waves are directed to the side channels of the flow splitter, whereas the diluted solution flows via the central channel and passes to the second stage for further dilution and separation b Photograph of the experiment in a one-stage microchannel Particle concentration is 7.5% in volume Scale bar is 100 mm.[2.91]

In another study, a transversal excitation was applied to an 8 branch system in order to separate cells from plasma [2.94]. The blood was undiluted, but four systems were needed to end up with a final contamination of the plasma inferior to 1%. The quality of the plasma was studied in a separate publication [2.93].

Acoustic separation techniques can offer continuous sorting of particles and is especially well adapted to blood plasma extraction as its best capability is a particle/medium type of separation.

2.6.3 Hybrid techniques

Acoustic techniques can be adapted with other techniques to form hybrid systems. Indeed, Wiklund et al. [2.96] presented recently a device combining short-range DEP manipulation with long-range ultrasonic wave (USW) manipulation. In this device, a DEP force is induced by an electric field between co-planar electrodes at the bottom of the microchannel. A transducer made of a piezoceramic element and a polymethylmethacrylate (PMMA) refractive edge is placed on the glass cover of the chip. The two combined forces permit particle trapping, sorting, concentration and separation with selectivity up to 90%. This method had been previously described to some extent in a patent [2.97]. In the latter work, USW was also proposed as a means for transportation of particles. The DEP/USW manipulation looks promising for high-throughput (because of the use of long-range USW forces) and high precision (because of the use of short-range DEP forces) applications.

2.7 Applications of cell separation

2.7.1 Blood plasma separation

Blood separation is a strategic preliminary step in preparation for biological analysis on-chip. Polymerase Chain Reaction (PCR) can be performed on whole blood but the reaction is inhibited by components of blood such as haemoglobin (cellular portion) and IgG (plasma portion); therefore, by separating blood into its basic components of plasma and cells, the reaction can be optimised for better results [2.98,99].

Blood plasma separation is particularly relevant in the field of theranostics, the new driver for bed-size diagnostic and treatment. Theranostics is defined as the combination of the diagnostics and therapeutic fields, whereby a disease could be screened daily such that the correct dose of medicine is administered to the patient as in the treatment of HIV [2.100]. Therefore it is necessary to get blood samples from patients once or several times on a daily basis. Microfluidics is particularly helpful in that respect, as it permits the analysis of few microlitres of biological samples, and avoids the painful blood extraction of several dozens of millilitres. Blood microsamples,

once extracted, are separated in most cases for downstream analysis. Theranostics is to grow by 20% until 2010 to reach a market estimated at 3.5 billions Euros [2.101].

For point-of care diagnostics, it is well known that the sample preparation step is a serious bottleneck in microfluidics. The development of miniaturised modules capable of de-skilled blood separation would aid in the translation of this new technology.

Optimum on-chip blood plasma separation techniques should have a large throughput, a high plasma yield and purity, with minimum cellular damage in order to prevent contamination of the plasma with cellular DNA and haemoglobin. Plasma yield is defined as the volume percentage of plasma that can be extracted from the device over the total volume of plasma in the blood.

Blood plasma separation can however be applied to a variety of other fields, such as environmental pollution monitoring. Indeed, evidence shows that various sea shells and fishes indicate perturbed physiology in polluted areas [2.102,103]. The analysis of toxic compounds such as heavy metals in mussel haemolymph can potentially provide valuable environmental monitoring [2.104].

2.7.2 Cell separation for HIV management

The management of HIV disease in patients is a typical example of theranostics. Although HIV diagnostic relies on the separation of specific human T-lymphocytes from whole blood, its treatment is also adapted in function of the advancement of the disease. Therefore separation is continually needed through the length of the disease [2.100].

2.7.3 Prenatal diagnosis

Prenatal diagnosis to determine the outcome of pregnancies and detect conditions that may affect future pregnancies has risen as a big issue among the broad public. Conventional prenatal tests are using invasive techniques, such as amniocentesis or Chorionic Villus Sampling (CVS), which can result in abortion or growth abnormalities in up to 2% of the cases.

Non-invasive prenatal diagnosis can be performed by separating rare foetal cells from maternal blood, consequently avoiding the potential risk of amniocentesis and CVS [2.18,105]. Fetal target cells comprise: lymphocytes, nucleated erythrocytes and trophoblasts. Among the challenges identified in this field are the lack of gender-independent fetal markers, the rarity of fetal cells, the reproducibility of results and the technology [2.18]. Although fetal cell recovery is still in its infancy and has to be greatly improved to meet clinical standards, this route has the potential for non-invasive for early prenatal diagnosis.

Circulating cell-free DNA in plasma and serum was first reported by Mandel and Metais in 1947. The correlation between levels of cfDNA and different pathologies was made three decades later with observations on cancer patients [2.106]. With new molecular technologies being developed, it resulted in an increasing interest in the detection and analysis of cfDNA [2.107,108,109,110]. However, it was not until 1997 that cell free foetal DNA, cffDNA, was detected in circulating maternal blood and arose as a mean to perform non invasive prenatal diagnosis [2.113]. cffDNA is not only used today to diagnose gender-linked conditions or foetal rhesus D status [2.114,115] but cffDNA is also employed as an indicator for pregnancy associated diseases such as pre-eclampsia and preterm labour [2.116]. The separation of plasma or serum from whole blood is a prerequisite to the analysis of cfDNA. Usually, purification is mostly required to remove the major inhibitors of the Polymerase Chain Reaction (PCR). These inhibitors include natural components such as heme and immunoglobulin G and exogenous components such as anticoagulants [2.117]. Furthermore, a plasma free of cells, reduces the contamination of the plasma with cellular DNA which can interfere with the accuracy of the DNA analysis. Traditionally plasma is separated from blood by centrifugation or filtration.

Fetal RNA, like cfDNA, can be detected from the maternal plasma and necessitate the separation of plasma from whole blood. RNA has been found to be very stable at room temperature for up to 24h after the venipuncture, which makes it an ideal target [2.18]. Moreover it is thought that RNA might provide more information than cfDNA.

2.7.4 Cancer cell detection

Microseparation techniques are also needed for the detection of cancer cells or the accumulation and counting of various types of cells and bacteria. As a particular example, testicular stem cell transplantation is a potential solution for the recovery of fertility in testicular cancer survivors [2.118]. However, the effectiveness of the transplantation is based on the number of stem cells transplanted. Testicular stem cells represent a very small fraction of testicular cells collected for this operation (0.03% in the mouse). Enrichment of stem cells is therefore highly desirable. Moreover, there is a risk of contamination by carcinogenic cells in a testicular cell suspension leading to a malignant relapse in the treated patient. Cell sorting is a solution to circumvent the contamination. Tournaye et al. show that the currently available macrotechniques do not allow the total depletion of malignant cells and subsequently illustrates the need for a finer gentle separation of cells [2.119]. Additionally, cfDNA detection allows the diagnosis and prognosis of various malignancies [2.107,108,110,111].

2.7.5 Plasma viscometry

Plasma viscometry is another application for cell separation from whole blood. Plasma viscometry is a technique competing with the more well-known ESR technique (Erythrocytes Sedimentation Rate). Plasma viscometry is a non-specific diagnostic test for a range of disorders. Patient plasma viscosity gives indication of several pathologies as indicated in Table 2.1. Plasma viscometry is used as a diagnostic tool in more than 90% of myeloma cases. Additionally PV is also used to detect haematological cancers and cardiovascular diseases.

2.7.6 Industrial applications

For agrochemical, cosmetic and pharmaceutical companies, these techniques permit, the separation, at production level, of solid products for post-treatment. In the food industry, potentially harmful bacterial activity is carefully monitored. Separation and enrichment of bacteria is necessary preliminary to analysis [2.32]. Monitoring of biological weapons is an important activity in the defence sector. In this field, separation is required to detect threatening agents such as anthrax [2.120]. All these

examples account for the tremendous need of portable, low-cost separation microdevices in a wide range of fields.

Plasma viscosity range	Associated Pathology
<1.40	Found in infants under 3 years old and patients with low immunoglobulin or fibrinogen levels.
1.40-1.75	*None*
1.75-2	Chronic disorders e.g. infection, malignancy, vascular disease. Autoimmune such as rheumatic diseases.
2.01-3	Suggestive of myeloma. IgG-paraproteins. High concentration of asymmetric paraproteins
>3	Suggestive of Waldenstrom's macroglobulinaemia. Grossly raised IgM-paraproteins.

Table 2.1: Associated pathologies versus plasma viscosities range. Adapted from www.benson viscometers.com

2.8 Conclusions

Recent advances in continuous microparticle separation have been presented in this chapter. The extensive literature in the field as well as the wide range of applications, illustrates the tremendous interest drawn by continuous microparticle separation. Separation is an important activity in the biological, medical and defence fields, to name but a few. Microparticle separation illustrates well the joined effort of different scientific communities that characterises the route towards integrated lab-on-a-chip devices. High throughput and high efficiency characterise optical fractionation in continuous flow. Magnetic separation is a gentle separation technique providing potential autonomy for a portable device if used with a permanent magnet. DEP separation is a well-established, robust and reliable technique applicable to a wide range of applications, not only separation but also focusing or dipping. Fluidic-only techniques are gentle, label-free techniques easily mass manufacturable. Other separation techniques such as thermal or acoustic separation can prove useful when coupled with other techniques to form hybrid systems which can manage a wide range of functions.

All techniques presented in this review have the potential for immunological separation. The possibility to label cells with various kind of beads (magnetic,

polystyrene) using antibody recognition, opens up the future of immunological separation within microchannels. Some of these techniques already have commercial applications, whereas some of the others will undoubtedly find new applications. In general, lab-on-a-chip modules will not always replace conventional laboratories but might find niche markets. In this chapter, we have also highlighted new manufacturing trends such as the integration of optical components on a chip and development of cheap, highly mass-manufacturable components. The future of separation techniques may lie in hybrid techniques combining different methods for better accuracy, efficiency and versatility. Reducing the size of the apparatus surrounding the chip remains by itself a challenge to be overcome for separation applications to be commercially viable.

In this study, we chose to tackle the issue of sample preparation in microfluidic system and in particular of blood plasma separation. Among the techniques presented in this review only one type allows a straightforward and cheap manufacturing process: hydrodynamic separation. Among others, this technique was chosen for its small footprint which increases its integrability in a more complex microsystem. The approach presented in this study differs from existing ones as it combines two separation mechanisms previously used separately, namely a constriction effect and a series of bifurcations. These mechanisms will be detailed in the next section.

2.8 References

[2.1] M. P. MacDonald, S. Neale, L. Paterson, A. Richies, K. Dholakia, and G. C. Spalding, *Cell cytometry with a light touch: Sorting microscopic matter with an optical lattice*, Journal of Biological Regulators and Homeostatic Agents **18** (2), 200–205 (2004).

[2.2] M. P. MacDonald, G. C. Spalding, and K. Dholakia, *Microfluidic sorting in an optical lattice*, Nature **426** (6965), 421–424 (2003).

[2.3] Lewis; Gruber, Kenneth; Bradley, Ward; Lopes, Robert W.; Lancelot, Joseph S.; Plewa, and David G.; Grier, United States Patent No. 7241988 (2007).

[2.4] K. Ladavac, K. Kasza, and D. G. Grier, *Sorting mesoscopic objects with periodic potential landscapes: Optical fractionation*, Physical Review E **70** (1), 010901 (2004).

[2.5] M. Pelton, K. Ladavac, and D. G. Grier, *Transport and fractionation in periodic potential-energy landscapes*, Physical Review E **70** (3), 031108 (2004).

[2.6] A. Ashkin, *Acceleration and Trapping of Particles by Radiation Pressure*, Physical Review Letters **24** (4), 156–159 (1970).

[2.7] A. Ashkin, J. M. Dziedzic, J. E. Bjorkholm, and S. Chu, *Observation of a Single-Beam Gradient Force Optical Trap for Dielectric Particles*, Optics Letters **11** (5), 288–290 (1986).

[2.8] A. Libal, C. Reichhardt, B. Janko, and C. J. O. Reichhardt, *Dynamics, rectification, and fractionation for colloids on flashing substrates*, Physical Review Letters **96** (18), 188301 (2006).

[2.9] Ryan L Smith, A G C Spalding, A K Dholakia, and M. P. MacDonald, *Colloidal sorting in dynamic optical lattices*, Journal of Optics A: Pure and Applied Optics, 134–138 (2007).

[2.10] G. Milne, D. Rhodes, M. MacDonald, and K. Dholakia, *Fractionation of polydisperse colloid with acousto-optically generated potential energy landscapes*, Optics Letters **32** (9), 1144–1146 (2007).

[2.11] D. McGloin, *Optical tweezers: 20 years on*, Philosophical Transactions of the Royal Society a-Mathematical Physical and Engineering Sciences **364** (1849), 3521–3537 (2006).

[2.12] C. J. Chang-Hasnain, *Tunable VCSEL*, Ieee Journal of Selected Topics in Quantum Electronics **6** (6), 978–987 (2000).

[2.13]   M. A. M. Gijs, *Magnetic bead handling on-chip: new opportunities for analytical applications*, Microfluidics and Nanofluidics **1** (1), 22–40 (2004).

[2.14]   N. Pamme, *Magnetism and microfluidics*, Lab on a Chip **6** (1), 24-38 (2006).

[2.15]   S. Miltenyi, W. Muller, W. Weichel, and A. Radbruch, *High-Gradient Magnetic Cell-Separation with Macs*, Cytometry **11** (2), 231–238 (1990).

[2.16]   Stefan Miltenyi, Andreas Radbruch, Walter Weichel, Werner Muller, Christoph Gottlinger, and Klaus L   Meyer, United States Patent No. 5,385,707 (1995).

[2.17]   M. Radisic, R.K. Iyer, and S.K. Murthy, *Micro- and nanotechnology in cell separation* International Journal of Nanomedicine **1** (1), 3–14 (2006).

[2.18]   D. W. Bianchi and J. Hanson, *Sharpening the Tools: A summary of a National Institutes of Health workshop on new technologies for detection of fetal cells in maternal blood for early prenatal diagnosis*, Journal of Maternal-Fetal & Neonatal Medicine **19** (4), 199–207 (2006).

[2.19]   H. Andersson and A. van den Berg, *Microfluidic devices for cellomics: a review*, Sensors and Actuators B- Chemical **92** (3), 315–325 (2003).

[2.20]   T. Deng, M. Prentiss, and G. M. Whitesides, *Fabrication of magnetic microfiltration systems using soft lithography*, Applied Physics Letters **80** (3), 461–463 (2002).

[2.21]   N. Pamme and A. Manz, *On-chip free-flow magnetophoresis: Continuous flow separation of magnetic particles and agglomerates*, Analytical Chemistry **76** (24), 7250–7256 (2004).

[2.22]   N. Pamme and C. Wilhelm, *Continuous sorting of magnetic cells via on-chip free-flow magnetophoresis*, Lab on a Chip **6** (8), 974–980 (2006).

[2.23]   G. Blankenstein, United States Patent No. 6,432,630 B1 (2002).

[2.24]   D. W. Inglis, R. Riehn, R. H. Austin, and J. C. Sturm, *Continuous microfluidic immunomagnetic cell separation*, Applied Physics Letters **85** (21), 5093–5095 (2004).

[2.25]   K. Han and A. B. Frazier, "Microfluidic system for continuous magnetophoresis separation of suspended cells using their native magnetic properties", in *NSTI Nanotech* (California, USA, May 2005).

[2.26]   D.R. Kelland M. Takayasu, and J.V. Minervini, , *Continuous magnetic separation of blood components from whole blood*, IEEE Trans Appl Superconductivity, **10**, 927-930 (2000).

[2.27] F. Baldessari and J.G. Santiago, *Electrophoresis in nanochannels: brief review and speculation*, Journal of nanobiotechnology **4** (12), 189–195 (2006).

[2.28] H.A. Pohl, *Dielectrophoresis: The behavior of neutral matter in non-uniform electric field*. (Cambridge University Press, 1978).

[2.29] J. A. R. Price, J. P. H. Burt, and R. Pethig, *Applications of a New Optical Technique for Measuring the Dielectrophoretic Behavior of Microorganisms*, Biochimica Et Biophysica Acta **964** (2), 221–230 (1988).

[2.30] M. Washizu, S. Suzuki, O. Kurosawa, T. Nishizaka, and T. Shinohara, *Molecular Dielectrophoresis of Biopolymers*, Ieee Transactions on Industry Applications **30** (4), 835–843 (1994).

[2.31] Michael Pycraft Hughes, *Nanoelectromechanics in Engineering and Biology* (CRC, 2002).

[2.32] L. J. Yang, P. P. Banada, M. R. Chatni, K. S. Lim, A. K. Bhunia, M. Ladisch, and R. Bashir, *A multifunctional micro-fluidic system for dielectrophoretic concentration coupled with immuno-capture of low numbers of Listeria monocytogenes*, Lab on a Chip **6** (7), 896–905 (2006).

[2.33] A. Menachery and R. Pethig, *Controlling cell destruction using dielectrophoretic forces*, IEE Proceedings - Nanobiotechnology **152** (4), 145–149 (2005).

[2.34] J. Rousselet, G. H. Markx, and R. Pethig, *Separation of erythrocytes and latex beads by dielectrophoretic levitation and hyperlayer field-flow fractionation*, Colloids and Surfaces a-Physicochemical and Engineering Aspects **140** (1-3), 209–216 (1998).

[2.35] J. Yang, Y. Huang, X. B. Wang, F. F. Becker, and P. R. C. Gascoyne, *Differential analysis of human leukocytes by dielectrophoretic field-flow-fractionation*, Biophysical Journal **78** (5), 2680–2689 (2000).

[2.36] S. Choi and J. K. Park, *Microfluidic system for dielectrophoretic separation based on a trapezoidal electrode array*, Lab on a Chip **5** (10), 1161–1167 (2005).

[2.37] Y. L. Li and Kvis Kaler, *Dielectrophoretic fluidic cell fractionation system*, Analytica Chimica Acta **507** (1), 151–161 (2004).

[2.38] H. A. Pohl and R. Pethig, *Dielectric Measurements Using Nonuniform Electric-Field (Dielectrophoretic) Effects*, Journal of Physics E-Scientific Instruments **10** (2), 190–193 (1977).

[2.39] T. S. Leu, H. Y. Chen, and F. B. Hsiao, *Studies of particle holding, separating, and focusing using convergent electrodes in microsorters*, Microfluidics and Nanofluidics **1** (4), 328–335 (2005).

[2.40] S. Fiedler, S. G. Shirley, T. Schnelle, and G. Fuhr, *Dielectrophoretic sorting of particles and cells in a microsystem*, Analytical Chemistry **70** (9), 1909–1915 (1998).

[2.41] G. Fuhr, Hagedorn, R., United States Patent No. 6,465,225 B1 (2002).

[2.42] G. Fuhr, Hagedorn, R., Muller, T., Schnelle, T., Gradl, G., United States Patent No. 6,727,451 B1 (2004).

[2.43] G. Fuhr, T. Schnelle, R. Hagedorn, and T. Muller, United States Patent No. 6,749,736 B1 (2004).

[2.44] T. Schnelle, T. Muller, G. Gradl, S. G. Shirley, and G. Fuhr, *Paired microelectrode system: dielectrophoretic particle sorting and force calibration*, Journal of Electrostatics **47** (3), 121–132 (1999).

[2.45] M. Durr, J. Kentsch, T. Muller, T. Schnelle, and M. Stelzle, *Microdevices for manipulation and accumulation of micro- and nanoparticles by dielectrophoresis*, Electrophoresis **24** (4), 722–731 (2003).

[2.46] J. Kentsch, M. Durr, T. Schnelle, G. Gradl, T. Muller, M. Jager, A. Normann, and M. Stelzle, *Microdevices for separation, accumulation, and analysis of biological micro- and nanoparticles*, IEE Proceedings - Nanobiotechnology **150** (2), 82–89 (2003).

[2.47] J. H. Nieuwenhuis, A. Jachimowicz, P. Svasek, and M. J. Vellekoop, *Optimization of microfluidic particle sorters based on dielectrophoresis*, Ieee Sensors Journal **5** (5), 810–816 (2005).

[2.48] J. H. Nieuwenhuis, A. Jachimowicz, P. Svasek, and M. J. Vellekoop, "High-speed integrated particle sorters based on dielectrophoresis", in *IEEE Int Conf. Sensors*, edited by D. Rocha, P. M. Sarro, and M. J. Vellekoop (Ieee, New York, USA, October 2004), pp. 64-67.

[2.49] J. H. Nieuwenhuis and M. J. Vellekoop, "Improved dielectrophoretic particle actuators for microfluidics", in *IEEE Int. Conf. Sensors* (Ieee, New York, USA, October 2003), pp. 573-577.

[2.50] H. Morgan, D. Holmes, and N. G. Green, *3D focusing of nanoparticles in microfluidic channels*, IEE Proceedings - Nanobiotechnology **150** (2), 76–81 (2003).

[2.51] I. Doh, K. S. Seo, and Y. H. Cho, "A continuous cell separation chip using hydrodynamic dielectrophoresis process", in *17th IEEE International Conference on Micro Electro Mechanical Systems* (Ieee, Maastricht, Netherlands, January 2004), pp. 29–32.

[2.52] U. Seger, S. Gawad, R. Johann, A. Bertsch, and P. Renaud, *Cell immersion and cell dipping in microfluidic devices*, Lab on a Chip **4** (2), 148–151 (2004).

[2.53] X. Y. Hu, P. H. Bessette, J. R. Qian, C. D. Meinhart, P. S. Daugherty, and H. T. Soh, *Marker-specific sorting of rare cells using dielectrophoresis*, Proceedings of the National Academy of Sciences of the United States of America **102** (44), 15757–15761 (2005).

[2.54] J. Park, B. Kim, S. K. Choi, S. Hong, S. H. Lee, and K. I. Lee, *An efficient cell separation system using 3D-asymmetric microelectrodes*, Lab on a Chip **5** (11), 1264–1270 (2005).

[2.55] C. F. Chou, J. O. Tegenfeldt, O. Bakajin, S. S. Chan, E. C. Cox, N. Darnton, T. Duke, and R. H. Austin, *Electrodeless dielectrophoresis of single- and double-stranded DNA*, Biophysical Journal **83** (4), 2170–2179 (2002).

[2.56] E. B. Cummings and A. K. Singh, *Dielectrophoresis in microchips containing arrays of insulating posts: Theoretical and experimental results*, Analytical Chemistry **75** (18), 4724–4731 (2003).

[2.57] I. Barbulovic-Nad, X. C. Xuan, J. S. H. Lee, and D. Q. Li, *DC-dielectrophoretic separation of microparticles using an oil droplet obstacle*, Lab on a Chip **6** (2), 274–279 (2006).

[2.58] N. Demierre, T. Braschler, P. Linderholm, U. Seger, H. van Lintel, and P. Renaud, *Characterization and optimization of liquid electrodes for lateral dielectrophoresis*, Lab on a Chip **7** (3), 355–365 (2007).

[2.59] R. Pethig, M. S. Talary, and R. S. Lee, *Enhancing traveling-wave dielectrophoresis with signal superposition*, Ieee Engineering in Medicine and Biology Magazine **22** (6), 43–50 (2003).

[2.60] Y. Nakashima and T. Yasua, *Blood Plasma Extraction from a minute amount of blood using dielectrophoresis* proceedings of the microTAS Paris, France, 2007.

[2.61] A.M. Sallam, *Human Red Blood-cell Hemolysis In A Turbulent Shear-Flow – Contribution of Reynolds Shear Stresses. *, Biorheology, **21,** , 783-797 (1984).

[2.62] M.J. Madou J.V. Zoval, *Centrifuge-based fluidics platform* Proc. IEEE **92**, 140-153 (2004).

[2.63] T. Brenner S. Haeberle, R. Zengerle, J. Ducrée, , *Centrifugal extraction of plasma from whole blood on a rotating disk* Lab Chip **6**, 776-781 (2006).

[2.64] C. Blattert, R. Jurischka, A. Schoth, P. Kerth, and W. Menz, "Separation of blood in microchannel bends", in *25th Ann. Int. Conf. of the IEEE Engineering in Medicine and Biology Society* (Ieee, Cancun, Mexico, September 2003), Vol. 25, pp. 3388-3391.

[2.65] H.Rostaing E. Sollier, P. Pouteau, Y. Fouillet, J.L. Achard, *Passive microfluidic devices for plasma extraction from whole human blood*, Sens. Actuators B, **141**, 1206-1208 (2009).

[2.66] D.J. Beebe J. Moorthy, *In situ fabricated porous filters for microsystems*, Lab Chip **3**, 62-66 (2003).

[2.67] V. Vandelinder and A. Groisman, *Separation of plasma from whole human blood in a continuous cross-flow in a molded microfluidic device*, Anal. Chem., **78,** , 3765-3771 (2006,).

[2.68] D.F. Cu X. Chen, C.C. Liu, H. Li, , *Microfluidic chip for blood cell separation and collection based on crossflow filtration*, Sens. Actuators B **130**, 216–221 (2008).

[2.69] H. Becker, *Collective wisdom* Lab Chip, **10,** , 271 – 273 (2010,).

[2.70] M. Yamada, M. Nakashima, and M. Seki, *Pinched flow fractionation: Continuous size separation of particles utilizing a laminar flow profile in a pinched microchannel*, Analytical Chemistry **76** (18), 5465–5471 (2004).

[2.71] M. Yamada and M. Seki, *Hydrodynamic filtration for on-chip particle concentration and classification utilizing microfluidics*, Lab on a Chip **5** (11), 1233–1239 (2005).

[2.72] Y.C. Fung, *Biomechanics*. (2004), second ed.

[2.73] S. S. Shevkoplyas, T. Yoshida, L. L. Munn, and M. W. Bitensky, *Biomimetic autoseparation of leukocytes from whole blood in a microfluidic device*, Analytical Chemistry **77** (3), 933–937 (2005).

[2.74] S. Yang, A. Undar, and J. D. Zahn, *A microfluidic device for continuous, real time blood plasma separation*, Lab on a Chip **6** (7), 871–880 (2006).

[2.75] F-Hoffmann-La-Roche-Ltd, *Major advances via miniaturisation*, http:// www.roche.com/pages/downloads/company/pdf/rddpenzberg02_02e.pdf 2010

[2.76] M. Faivre, Abkarian, M., Bickraj., Stone, H.A., *Geometrical focusing of cells in a microfluidic device: an approach to separate blood plasma*, biorheology, **43**, 147-159 (2006).

[2.77] Rong Fan, Ophir Vermesh, Alok Srivastava, Brian K. H. Yen, Lidong Qin, Habib Ahmad, Gabriel A. Kwong, Chao-Chao Liu, Juliane Gould, Leroy Hood, and James R. Heath, *Integrated barcode chips for rapid, multiplexed analysis of proteins in microliter quantities of blood*, Nat Biotech **26**, 1373 - 1378 (2008).

[2.78] R. Sandoz R.D. Jaggi, C.S. Effenhauser, *Microfluidic depletion of red blood cells from whole blood in high aspect ratio microchannels*, Microfluid. Nanofluid. **3**, 47-53 (2007).

[2.79] M. Cubizolles E. Sollier, Y. Fouillet, J.L. Achard., *Fast and continuous extraction from whole human blood based on expanding cell-free layer devices*, biomedical microdevices (2010).

[2.80] M. Cubizolles E. Sollier, M.Faivre, Y. Fouillet, J.L.Achard, *A passive microfluidic device for plasma extraction from whole human blood*, proceedings of the IEEE EMBC, Minneapolis, USA, 2009.

[2.81] D. Di Carlo, Irimia, D., Tompkins, R.G., Toner, M., *Continuous inertial focusing ordering and separation of particles in microchannels*, PNAS **104**, 18892-18897 (2007).

[2.82] M. Arundell A. I. Rodríguez-Villarreal, M. Carmona, J. Samitier, *High flow rate microfluidic device for blood plasma separation using a range of temperatures*, Lab Chip **10**, 211 219 (2010).

[2.83] L. R. Huang, E. C. Cox, R. H. Austin, and J. C. Sturm, *Continuous particle separation through deterministic lateral displacement*, Science **304** (5673), 987–990 (2004).

[2.84] S. Y. Zheng, Y. C. Tai, and H. Kasdan, "A micro device for separation of erythrocytes and leukocytes in human blood", in *27th Ann. Int. Conf. of the IEEE EMBS* (Ieee, New York, USA, 2005), pp. 1024-1027.

[2.85] J.A. Davis, D. W. Inglis, K.J. Morton, D.A. Lawrence, L. R. Huang, Y.C. Stephen, J. C. Sturm, and R. H. Austin, *Deterministic hydrodynamics: Taking blood apart*, Proceedings of the National Academy of Sciences of the United States of America **103** (40), 14779–14784 (2006).

[2.86] Lotien Richard; Huang, Thomas A.; Barber, Bruce L.; Carvalho, Ravi; Kapur, Paul; Vernucci, Mehmet; Toner, and Zihua;   Wang, United States Patent No. 20070026381 (2007).

[2.87] Nan Li, Daniel T. Kamei, and Chih-Ming Ho, "On-Chip Continuous Blood Cell Subtype Separation by Deterministic Lateral Displacement", in *2nd IEEE Int. Conf. on Nano/Micro Engineered and Molecular Systems* (Bangkok, Thailand January 2007), pp. 932-936.

[2.88] Paul; Yager, James P.; Brody, Mark R.; Holl, Fred K.; Forster, and Paul C. Galambos, United States Patent No. 5,932,100 (1999).

[2.89] K. H. Nam, W. J. Chang, H. Hong, S. M. Lim, D. I. Kim, and Y. M. Koo, *Continuous-flow fractionation of animal cells in microfluidic device using aqueous two-phase extraction*, Biomedical Microdevices **7** (3), 189–195 (2005).

[2.90] S. A. Bowden, P. B. Monaghan, R. Wilson, J. Parnell, and J. M. Cooper, *The liquid-liquid diffusive extraction of hydrocarbons from a North Sea oil using a microfluidic format*, Lab on a Chip **6** (6), 740-743 (2006).

[2.91] S. A. Bowden, R. Wilson, J. Parnell, and J. M. Cooper, "Liquid-liquid extrcation of included organic compounds from dissolved sulphate minerals performed on a microfluidic format", in *37th Conf. on Lunar and Planetary Science* (League City, USA, March 2006).

[2.92] T. L. Edwards, B. K. Gale, and A. B. Frazier, *A microfabricated thermal field-flow fractionation system*, Analytical Chemistry **74** (6), 1211–1216 (2002).

[2.93] A. Ahmad-Tajudin A. Lenshof, K. Järas, A.M. Swärd-Nilsson, L. Aberg, G. Marko-Varga, J. Malm, H. Lilja, and T. Laurell, , *Acoustic Whole Blood Plasmapheresis Chip for Prostate Specific Antigen Microarray Diagnostics*, Anal. Chem. **81**, 6030-6037 (2009).

[2.94] A. Nilsson, F. Petersson, H. Jonsson, and T. Laurell, *Acoustic control of suspended particles in micro fluidic chips*, Lab on a Chip **4** (2), 131–135 (2004).

[2.95] H. Li and T. Kenny, "High speed particles separation using ultrasound for micro-TAS and lab-on-a-chip application", in *26th Ann. Int. Conf. of the Ieee Engineering in Medicine and Biology Society* (San Francisco, USA, 2004), Vol. 26, pp. 2631-2634.

[2.96] M. Wiklund, C. Gunther, R. Lemor, M. Jager, G. Fuhr, and H. M. Hertz, *Ultrasonic standing wave manipulation technology integrated into a dielectrophoretic chip*, Lab on a Chip **6** (12), 1537–1544 (2006).

[2.97] Gary; Lock, Ronald; Pethig, and Gerardus Hendricus; Markx, United States Patent No. 6,936,151 (2005).

[2.98] WA. Al-Soud, L.J. Jönsson, and P. Rådström, *Identification and characterization of immunoglobulin G in blood as a major inhibitor of diagnostic PCR*, J. Clin. Microbiol **38**, 345-350 (2000).

[2.99] WA Al-Soud and P. Rådström, *Purification and characterization of PCR-inhibitory components in blood cells*, J. Clin. Microbiol **39**, 485-493 (2001).

[2.100] W. R. Rodriguez, N. Christodoulides, P. N. Floriano, S. Graham, S. Mohanty, M. Dixon, M. Hsiang, T. Peter, S. Zavahir, I. Thior, D. Romanovicz, B. Bernard, A. P. Goodey, B. D. Walker, and J. T. McDevitt, *A microchip CD4 counting method for HIV monitoring in resource-poor settings*, Plos Medicine **2** (7), 663–672 (2005).

[2.101] Clinica report, *New trends in Viral Diagnostics*, http://www.pjbpubs.com/, 2001

[2.102] I. Zorita, I. Apraiz, M. Ortiz-Zarragoitia, A. Orbea, I. Cancio, M. Soto, I. Marigomez, and M.P. Cajaraville, *Assessment of biological effects of environmental pollution along the NW Mediterranean Sea using mussels as sentinel organisms*, Env. Poll **148**, 236-250 (2007).

[2.103] I. Zorita, M. Ortiz-Zarragoitiaa, I. Apraiza, I. Cancioa, A. Orbeaa, M. Sotoa, I. Marigómeza, and M.P. Cajaraville, *Assessment of biological effects of environmental pollution along the NW Mediterranean Sea using red mullets as sentinel organisms*, Env. Poll. **153** (1), 157-168 (2008).

[2.104] Kaloyiannia M, Dailianisa MS, Chrisikopouloua E, Zannoua A, Koutsogiannakia S, Alamdarib DH, Koliakosb G, and Dimitriadisc VK, *Oxidative effects of inorganic and organic contaminants on haemolymph of mussels* Comp. Biochem. and Physiol. C.

[2.105] C. Slack, K. Lurix, S. Lewis, and L. Lichten, *Prenatal genetics - The evolution and future directions of screening and diagnosis*, Journal of Perinatal & Neonatal Nursing **20** (1), 93–97 (2006).

[2.106] B. Shapiro S.A. Leon, D.M. Sklaroff and M.J. Yaros, , *Free DNA in the serum of cancer patients and the effect of therapy*, Cancer Res. **37**, 646–650 (1977).

[2.107] C. Alix-Panabières H. Schwarzenbach, I. Müller, N. Letang, J.P. Vendrell, X Rebillard, and K. Pantel, , *Cell-free tumor DNA in blood plasma as a marker for circulating tumor cells in prostate cancer*, Clin Cancer Res. **15**, 1032-1038 (2009).

[2.108] C. Bigosch O. Gautschi, B. Huegli, M. Jermann, A. Marx, E. Chasse, D. Ratschiller, W. Weder, M. Joerger, D.C. Betticher, R.A. Stahel , and A. and Ziegler., *Circulating deoxyribonucleic Acid as prognostic marker in non-small-cell lung cancer patients undergoing chemotherapy* Clin Onc **22**, 4157–4164 (2004).

[2.109] B. Schmidt M. Fleischhacker, *Circulating nucleic acids (CNAs) and cancer: a survey* Biochim Biophys Acta, **1775**, 181 232 (2007).

[2.110] M. Li F. Diehl, D. Dressman, Y. He, D. Shen, S. Szabo, et al., *Detection and quantification of mutations in the plasma of patients with colorectal tumors*, Proc Natl Acad Sci U S A, **102**, 16368 –16373 (2005).

[2.111] M. Chakrabarty B. Shapiro, E.M. Cohn, S.A. Leon, , *Determination of circulating DNA levels in patients with benign or malignant gastrointestinal disease*, Cancer **51**, 2116 (1983).

[2.112] B. Prieto García V. García Moreira, J.M. Baltar Martín, F. Ortega Suárez, F.V. Alvarez, , *Cell-free DNA as a noninvasive acute rejection marker in renal transplantation* Clin. Chem. **55**, 1958 - 1966 (2009).

[2.113] Y.M.D. Lo, *Recent Advances in Fetal Nucleic Acids in Maternal Plasma* J. Histochem. Cytochem **53**, 293 (2005).

[2.114] P. Ernault J.M. Costa, *Automated Assay for Fetal DNA Analysis in Maternal Serum*, Clin Chem. **48**, 679 (2002).

[2.115] P.G. Martin K.M. Finning, P.W. Soothill, N.D. Avent, , *Prediction of fetal D status from maternal plasma: introduction of a new noninvasive fetal RHD genotyping service* Transfusion **42**, 1079 (2002).

[2.116] C. Wright, *Cell-free fetal nucleic acids for non-invasive prenatal diagnosis* http://www.phgfoundation.org/pages/ffdna.html,

[2.117] W. Holzgreve X.Y. Zhong, S. Kahn. , *The Levels of Circulatory Fetal DNA In Maternal Plasma are elevated prior to the onset of preeclampsia*, Hypertens Pregnancy **21**, 77 (2002).

[2.118] M.; Geens, H. V.; de Velde, G.; De Block, E.; Goossens, A.; Van Steirteghem, and H.; Tournaye, *The efficiency of magnetic-activated cell sorting and fluorescence-activated cell sorting in the decontamination of testicular cell suspensions in cancer patients*, Human Reproduction **22** (3), 733–742 (2007).

[2.119] H. Tournaye, E. Goossens, G. Verheyen, V. Frederickx, G. De Block, P. Devroey, and A. Van Steirteghem, *Preserving the reproductive potential of men and boys with cancer: current concepts and future prospects*, Human Reproduction Update **10** (6), 525–532 (2004).

[2.120] H. O. Fatoyinbo, M. P. Hughes, S. P. Martin, P. Pashby, and F. H. Labeed, *Dielectrophoretic separation of Bacillus subtilis spores from environmental diesel particles*, Journal of Environmental Monitoring **9** (1), 87-90 (2007).

Chapter 3: Theory and design

3.1 Introduction

Due to its particulate nature, blood is a complex fluid which can show specific behavior in a number of different situations. Still today, the theory of blood flow in various vessels is incomplete. This chapter presents the main theoretical ideas of blood flow in microvessels in order to explain the different effects involved into blood plasma separation at the microscale. Blood composition and the particular behavior of red blood cells which compose more than 40% of blood particulates are explained. The requirements for blood plasma separation are then detailed along with the delimitation of the study. An original rationale of red blood cells behavior in microchannels is presented in a chart format. The design of two generations of devices for the extraction of plasma are detailed towards the end of the chapter.

3.2 Blood: a complex living fluid

3.2.1 Blood composition

Blood is a bodily fluid composed of several types of cells suspended in a fluid medium known as plasma. The cellular portion of the blood is divided between erythrocytes (red blood cells), leukocytes (white blood cells) and thrombocytes (platelets) as shown in figure 3.1. The normal blood pH range is 7.35-7.45 and the human blood bulk density at rest is around 1060 kg/m^3. Humans are known to have approximately 5 litres of blood which consist of 7% of the total body weight.
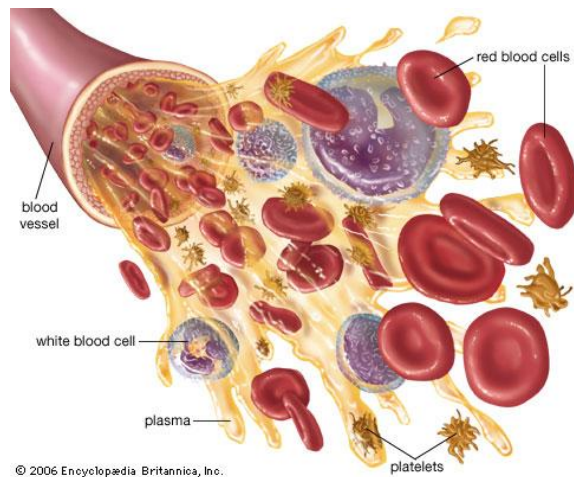
Figure 3. 1: Artist's view of blood composition. Courtesy of Encyclopedia Britannica, Inc.

The primary function of blood is the transport of oxygen which is necessary for the different body tissues. Additionally, blood transports proteins and antibodies. The blood circulation is activated through the organism via heart movement which initiates three distinct circuits:

- the pulmonary circuit transports blood from the heart to the lungs,

- the coronary circulation provides the heart network

- the systemic circulation, is the circulation of blood through all the remaining vessels of the body.

Blood cells originate from the bone marrow which produces stem cells common to all blood cells (pluripotential hematopoietic stem cells). Blood flows through vessels, flexible tubes of different shapes and constructions. Arteries, which branch out of the heart, need to pump a lot of fluid, and therefore can be larger than 10mm in diameter. Arterioles, a smaller kind of vessels branching out of arteries, subdivide into capillaries which can be as thin as diameter as a single cell, ie around 10μm. The thin wall that forms the capillaries is called the endothelium and plays a major role in the absorption of oxygen and proteins delivered to the muscles and organs. The main vessel functions and dimensions are presented in Table 3.1

Name of vessel	Function	Dimensions
arteries	Wide and thick vessels that carry large quantities of blood away from the heart	0.1-20mm
arterioles	Vessels that branch out from arteries	15-100μm
capillaries	Very narrow vessels with thin walls permeable to oxygen and carbon dioxide	5-15μm

Table 3. 1: Main vessels function and dimensions

The volume percentage of Red Blood Cells (RBCs), also called hematocrit, can vary between 35 to 55% depending on the age and sex of the individual. Red blood cells, or erythrocytes, which have a lifespan of around 120 days, are the particles transporting the oxygen to the body tissues from the heart to all limbs.

RBCs get their red colour from the iron present in the hemoglobin molecules. As shown in Figure 3.2, RBCs have no nucleus; their biconcave shape changes depending on the characteristics of the buffer they are immersed in. Blood flow characteristics are dominated by the behaviour of these particles given their high concentration, about 5 millions cells per microlitre of blood.
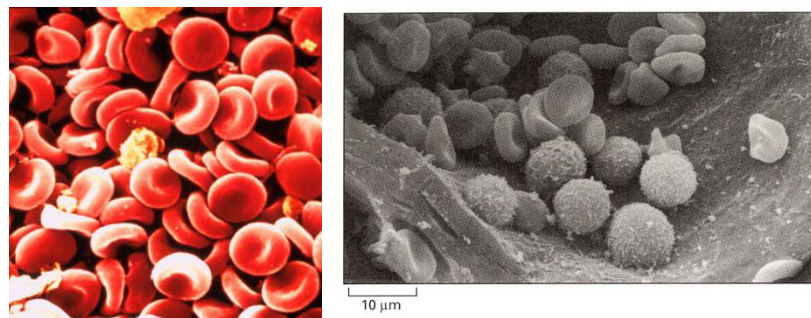
Figure 3. 2: (a) Red blood cells, courtesy of The Science museum (www.sciencemuseum.org.uk) (b) Red blood cells and white blood cells [3.1].

White Blood Cells (WBCs), also called leucocytes, are the primary agents against infections. The number ratio of white blood cells against red blood cells is about 1 to 1000, and the volume ratio is about 1 to 600. Therefore WBCs do not contribute greatly to the blood flow behaviour; although they are the biggest of blood particles (10-40μm), they have little influence on the blood viscosity [3.2]. However it has been suggested that white blood cells may contribute to microvascular network resistance [3.3]. The three main types of white blood cells are the granulocytes, lymphocytes and

monocytes a shown in figure 3.3. Leucocytes are mostly round cells and, in microvessels at low Reynolds number, they roll along the surface before being agglutinated and transported through the membrane during inflammatory response [3.1]. White blood cells have a lifespan ranging from a few days to years.

Platelets, also called thrombocytes,, are the smallest of blood particles (2-3μm). They are responsible for blood clotting, a complex chain of reactions leading to the formation of a clot of blood over a wound. Platelets occupy 1/800 of the cell volume in blood [3.4]. Because of their small size, platelets do not play a considerable role into the blood flow behaviour at microscale. They do have, however, an important role into the blocking of vessels in-vivo and in-vitro. This role will be discussed to some extent in the results chapter. The lifespan of platelets is about 10 days.
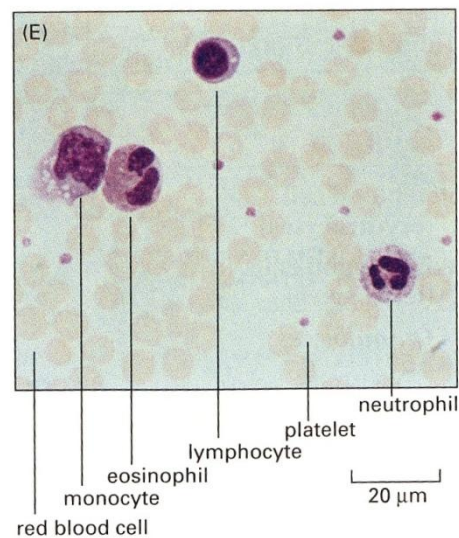
Figure 3. 3: Blood smear with staining showing the different types of white blood cells [3.1]

Plasma is the water-based blood buffer and constitutes more than half of the blood. Plasma hosts many other components such as protein molecules, peptides and metabolites. Protein molecules are important indicators of various diseases and are one of the reasons why separating plasma from blood is of clinical importance.

Proteins play a predominant part in most biological processes. Studying proteins may give clue to the health of cells as evidenced in oncological studies [3.5]. Sampling the blood is the easiest way to detect and monitor cancer without having to subject patients to clinical interventions in order to obtain cancerous tissues as illustrated in Figure 3.4. Instead of studying the tumours themselves, cancer can now be

51

characterized at the molecular level by the analysis of DNA copy number, patterns of gene expressions and changes in serum proteins. For the latter, blood plasma separation is vital as serum is obtained from pure plasma.
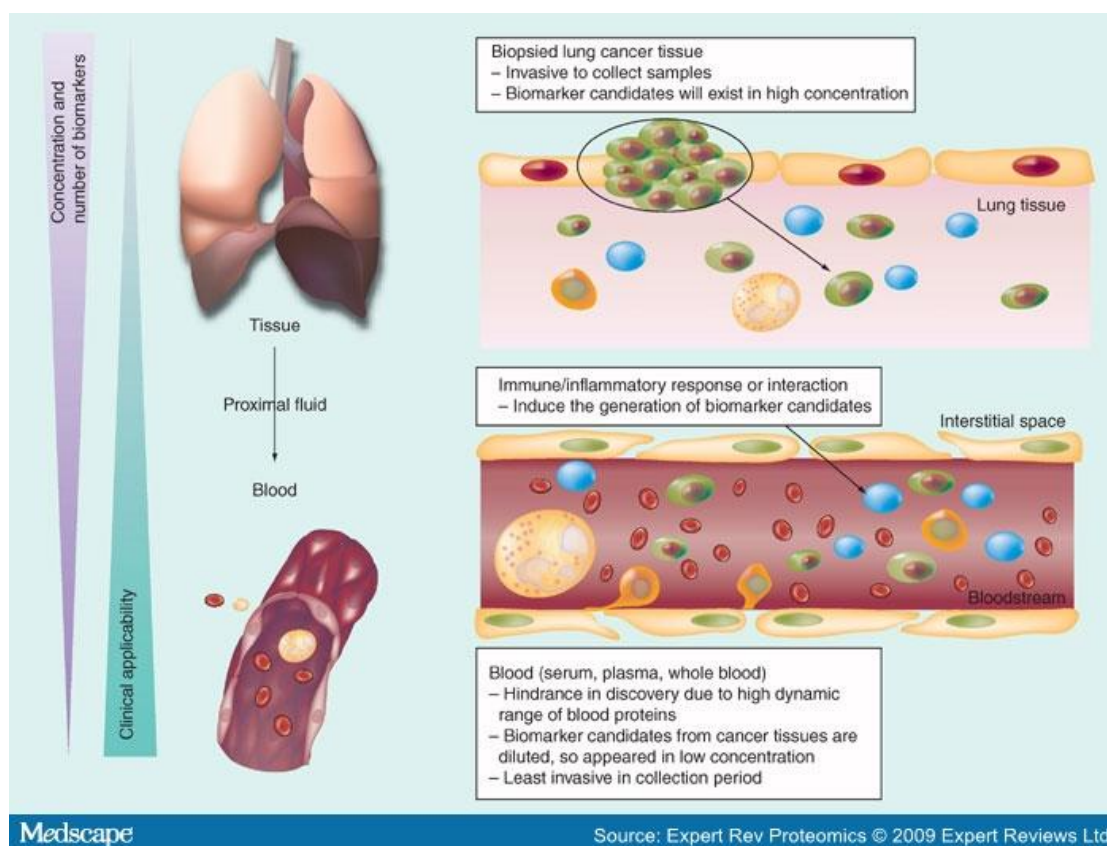
Figure 3. 4: illustration of blood sampling vs tissue sampling, courtesy of Medscape.

Cancer-associated proteins may be used not only to detect cancer tumours at an early stage of development but also to monitor the progression of cancer and the response to therapy [3.6]. Table 3.2 summarizes a list of cancer biomarkers and their location. Many cancer biomarkers approved by the US Food and Drugs Administration are to be found in plasma.

Pregnancy-related biomarkers are present in the plasma of pregnant women. Human Chorionic Gonadotrophin (hCG) protein is a hormone produced during the pregnancy; hCG levels are undetectable in non-pregnant women but double every two days during early pregnancy. A blood hCG test is required to confirm if a woman is pregnant, but hCG levels are also monitored for prenatal diagnosis. A number of other markers including Pregnancy-Associated Plasma Protein A (PAPPA) and pregnancy specific β1-glycoprotein (SP1) are used for prenatal diagnosis, in the latter case the detection of

Trisomy 18, or Edwards Syndrome, a serious chromosomal abnormality. Biomarkers are not necessarily proteins; they can also be Cell-free DNA, or cell-free RNA floating in the plasma. This topic will be discussed in chapter 7.

Biomarker	Type	Source	Cancer type	Clinical use
α-Fetoprotein	Glycoprotein	Serum	Nonseminomatous testicular	Staging
Human chorionic gonadotropin-β	Glycoprotein	Serum	Testicular	Staging
CA19-9	Carbohydrate	Serum	Pancreatic	Monitoring
CA125	Glycoprotein	Serum	Ovarian	Monitoring
Pap smear	Cervical smear	Cervix	Cervical	Screening
CEA	Protein	Serum	Colon	Monitoring
Epidermal growth factor receptor	Protein	Colon	Colon	Selection of therapy
KIT	Protein (IHC)	Gastrointestinal tumour	GIST	Diagnosis and selection of therapy
Thyroglobulin	Protein	Serum	Thyroid	Monitoring
PSA (total)	Protein	Serum	Prostate	Screening and monitoring
PSA (complex)	Protein	Serum	Prostate	Screening and monitoring
PSA (free PSA %)	Protein	Serum	Prostate	Benign prostatic hyperplasia versus cancer diagnosis
CA15-3	Glycoprotein	Serum	Breast	Monitoring
CA27-29	Glycoprotein	Serum	Breast	Monitoring
Cytokeratins	Protein (IHC)	Breast tumour	Breast	Prognosis
Oestrogen receptor and progesterone receptor	Protein (IHC)	Breast tumour	Breast	Selection for hormonal therapy
HER2/NEU	Protein (IHC)	Breast tumour	Breast	Prognosis and selection of therapy
HER2/NEU	Protein	Serum	Breast	Monitoring
HER2/NEU	DNA (FISH)	Breast tumour	Breast	Prognosis and selection of therapy
Chromosomes 3, 7, 9 and 17	DNA (FISH)	Urine	Bladder	Screening and monitoring
NMP22	Protein	Urine	Bladder	Screening and monitoring
Fibrin/FDP	Protein	Urine	Bladder	Monitoring
BTA	Protein	Urine	Bladder	Monitoring
High molecular weight CEA and mucin	Protein (Immunofluorescence)	Urine	Bladder	Monitoring

BTA, bladder tumour-associated antigen; CA, cancer antigen; CEA, carcinoembryonic antigen; FDP, fibrin degradation protein; FISH, fluorescent *in-situ* hybridization; GIST, gastrointestinal stromal tumour; IHC, immunohistochemistry; NMP22, nuclear matrix protein 22; PSA, prostate-specific antigen.

Source: Nat Rev Cancer © 2005 Nature Publishing Group

Table 3. 2: List of cancer biomarkers approved by the US Food and Drugs Administration, courtesy of Medscape (Source: Nature Review Cancer 2005)

3.2.2 Red blood cells characteristics

The highly particular structure of RBCs is the key to understanding the behavior of blood flow. Red blood cells are extremely deformable particles and a precise determination of their geometry is not a straightforward task [3.2]. Additionally, in response to hydrodynamic situations, they can take up different shapes. Their volume also changes depending on the tonicity, the ratio of solutes to solvent, of the buffer solution.

The degree of non-sphericity of particles can be expressed by the shape factor proposed by Wadell [3.7]:

53

$$\Psi = \frac{A_s}{A} \hspace{4cm} (3.1)$$

Where A is the actual surface area and A_s is the surface area of the sphere with the same volume (smallest possible area per unit volume) defined by:

$$A_s = \pi^{\frac{1}{3}}\left(6V\right)^{\frac{2}{3}} \hspace{4cm} (3.2)$$

RBC surface area is approximately 135mm^2 and its volume 94mm^3. In normal situations, the factor of non-sphericity of the red blood cell is around: $\Psi = 0.74$. Figures 3.5a and 3.5b present a normal RBC and a large RBC.
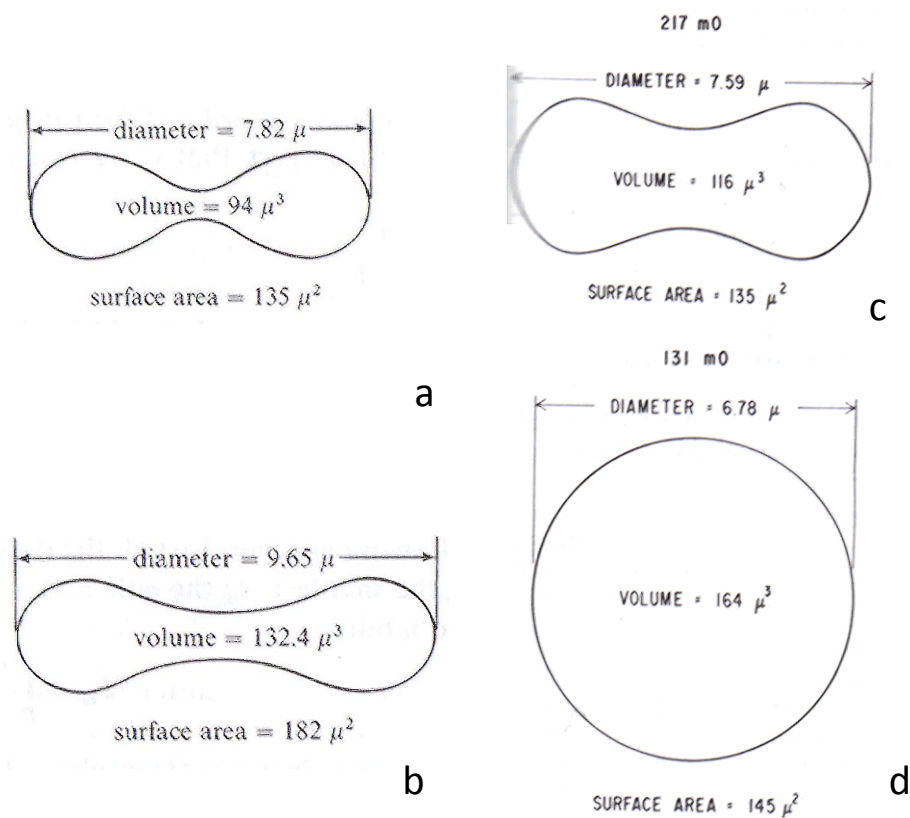
Figure 3. 5: (a) Dimensions of a normal sized RBC at 300mosmol (b) Dimensions of a large sized RBC at 300mosmol. (c) Dimensions of a mean sized cell at 217mosmol (d) Dimensions of a mean sized cell at 131mosmol.

Table 3.3 contains experimental data from Evans and Fung [3.8] which demonstrates that the shape and dimensions of the RBC change with respect to the solution tonicity, the measure of the osmotic pressure[1] between the cell and the solution, here plasma.

---

[1] Osmotic pressure is expressed in osmol or mosmol (=0.001osmol). The osmotic pressure is calculated as the number of moles times the number of solutes present in the solution.

In this case, when the solution is 290-300 mosmol, the solution is isotonic and the net flow of liquid into the RBC equals the net flow out.

When the solution is decreased to 217 mosmol and below, the solution is hypotonic as fewer particles exist in the solution than in the RBCs. The fluid flows into the RBC causing it to expand. At 131 mosmol the RBCs become spherical. The volumes of the RBC in hypotonic case are shown in Figure 3.5a and b.

Tonicity (mosmol)	Diameter (µm)	Minimum Thickness (µm)	Maximum Thickness (µm)	Surface Area (µm²)	Volume (µm³)
300	7.82	0.81	2.58	135	94
217	7.59	2.10	3.30	135	116
131	6.78	*Appears spherical*		145	164

Table 3. 3: Experimental data from Evans and Fung [3.8].

Red blood cells are also extremely deformable when subject to mechanical forces. A shear stress of the order of 0.02mbar can induce a deformation with a stretch ratio of up to 200% on the membrane [3.1]. The cell membrane is elastic and has a finite strength and, due to the absence of a nucleus, a red blood cell can squeeze itself into the smallest of blood vessels. A RBC can flow through microchannels of diameter as small as 2.3µm without hemolysis (death of the cell) [3.9]. This astonishing flexibility makes it the perfect particle to circulate in the entire body to deliver oxygen.

Red blood cell characteristics	Acronyms	Values
Mean Cell Volume	MCV	80-100fL
Mean Corpuscular Hemoglobin Concentration	MCHC	32-36 g/dL
Mean Corpuscular Hemoglobin	MCH	27-31 pg/cell
Red blood cell Distribution Width	RDW	11.5-14.5%

Table 3. 4: Characteristics of common human red blood cells. Values from the US national Libraries of Medecine website [3.10].

The geometrical and chemical parameters of RBCs can be used to detect blood disorders such as anemia and infections. Characteristics of common red blood cells indices include the mean corpuscular volume, which is a measurement of the average size of an RBC, the mean corpuscular hemoglobin which is the calculation of the average amount of oxygen in a RBC, the mean average concentration of hemoglobin

inside a cell and the red cell width distribution which is the variation in the size of RBCs. Such characteristics are shown in Table 3.4 for a normal human being.

3.2.3 Properties of blood flow

With a number density of 5 millions cells per mm^3, red blood cells are found in great number in blood [3.9]. Red blood cells do not always float freely as individual particles in blood, they can form some complex structures called "rouleaux formation" as pictured in Figure 3.6.
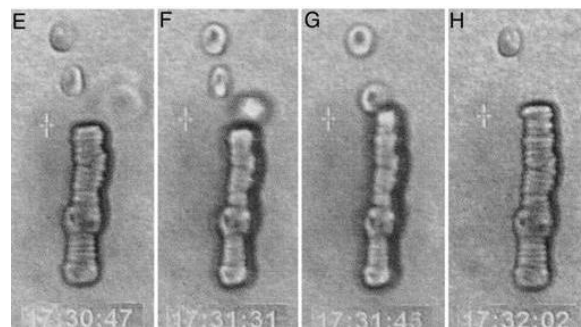
Figure 3. 6: Rouleaux formation, approximately 8 cells tall, three cells can be seen in the background joining the rouleaux formation in (E). (H) Only one cell remains out if the structure [3.11].

These formations are sometimes simply named blood aggregates and arise due to the interactions between individual red blood cells and the action of some plasma proteins like fibrinogen or globulin [3.9]. However this behavior only happens when blood is at rest. Blood aggregates are very sensitive to flow conditions such as increased shear rate [3.9]. The shear rate is defined as the change of velocity of parallel planes in a flowing fluid (shear flow) separated by a distance. Shear stress is the force required to produce the shearing action. This stress acts tangentially on a surface and creates a deformation.

A Newtonian fluid, which has a linear pressure-flow rate curve, obeys the Poiseuille equation and has a unique coefficient of viscosity. However in a non-Newtonian fluid such as blood, polymer or fluid suspensions, there is no unique coefficient of viscosity, as their structure depends on the flow [3.9].
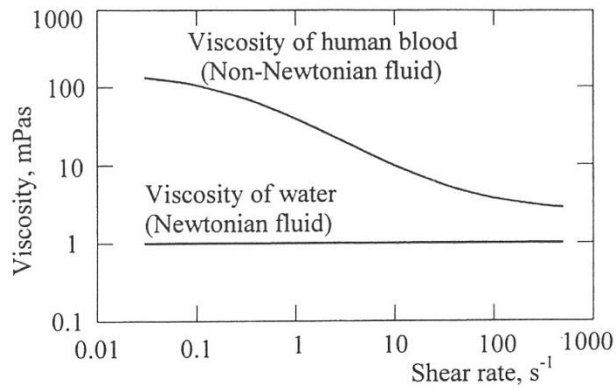
Figure 3. 7: Viscosity-shear rate ratio in Newtonian and non-Newtonian fluid [3.9].

3.2.3.1 Blood flow viscosity

The viscosity of blood is therefore dependant on shear conditions among others. In the case of blood, as shear rate increases, a progressive break-up of red blood cell aggregates is observed; leading to a decrease in viscosity. This behavior is typical of shear-thinning fluid. As shown in Figure 3.8, blood viscosity can change within a factor of 100 [3.9].

Generally, the viscosity in blood depends on:

- Shear rate

- Hematocrit level

- Temperature

- Plasma viscosity[2]

The measure of blood viscosity does not reflect its intrinsic properties but rather a property of the blood/vessel system under specific flow conditions [3.3]. Therefore a relative viscosity can be defined as the ratio of blood viscosity to that of plasma.

A number of rheological equations describe the non-linear relationship of blood viscosity to the shear stress. One of the most well-known is the Casson equation, which is an empirical equation to characterize blood viscosity depending on the shear stress-shear rate relationship. For large values of shear rate the Casson equation should approach the asymptotic viscosity of a Newtonian fluid [3.12].

---

[2] Plasma is a Newtonian fluid and its viscosity is fixed
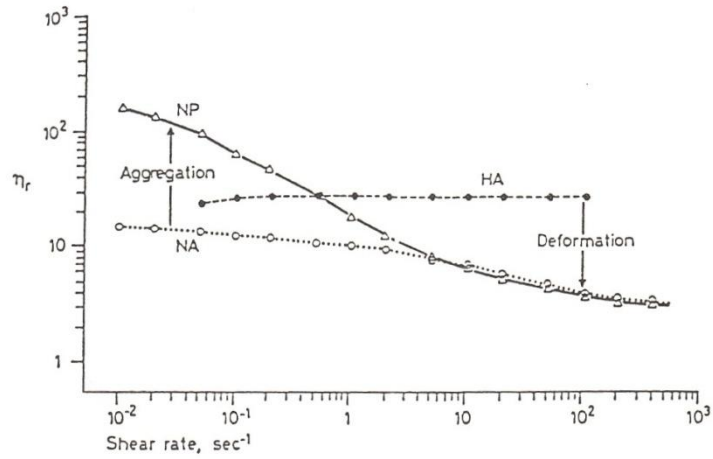
Figure 3. 8: Variation of the relative viscosity in function of shear rate for different suspensions (45% Hct blood, 11% Hct blood, 11% Hct hardened cells) [3.9]

3.2.3.2 Blood flow laws in microvessels

Most of the time, blood is considered to be a non-Newtonian fluid. At high shear rates however, blood can be considered as a Newtonian fluid [3.2]. In large channels it is acceptable to consider blood as a homogenous fluid as the size of the cells is not comparable to the size of the channel. However, for channel diameters of 500μm and below blood should be considered as a two-phase fluid: individual particles immersed in a Newtonian-type plasma.

Fahraeus effect describes the tendency of red blood cells to migrate away from the tube walls, resulting in higher mean velocity of red blood cells compared to plasma.

A related effect, named the Fahraeus-Lindqvist effect, describes the significant decrease in apparent viscosity of blood in channels of diameter less than 500μm. However these hemorheological laws appear at low Reynolds number, Re, defined as the ratio between viscous and inertial forces:

$$Re = \frac{\rho.v.l}{\mu}$$

[3.3]

For an assumed fixed viscosity $\mu=5.10^{-3}$ kg.m^{-1}.s^{-1}, a density $\rho=1057$ kg.m^{-3}, a characteristic length l= 20μm and a flow velocity v = 2.10^{-6} m.s^{-1}, the Reynolds number is 4.3, therefore laminar flow behaviour is expected. Laminar flow is common in most microfluidic system.

3.3 Behaviour of red blood cells in microchannels

The understanding of the movement of a deformable asymmetric particle (such as a blood cell) in a laminar flow is the key to designing an efficient blood plasma separation microdevice. Although extensive studies of the behaviour of RBCs have been carried out over the last 50 years, there are still some unanswered questions about the movement of these cells [3.13,14]. In this section, an explanation of the fundamental mechanisms occurring in blood plasma separation in microchannels, will be given.

3.3.1 Flow of red blood cells flow in straight microchannels

Blood is known to be a non-Newtonian fluid. However, at the scale close to the microvascular network, blood can be considered as a suspension of RBCs in a Newtonian plasma. Plasma flow in a microchannel network of hydraulic diameters ranging from 10 to 500 μm is laminar, but the Reynolds number can vary greatly from 0.01 to 100. RBCs are biconcave disks, reported to be extremely deformable. RBCs are known to exhibit different behaviours and even take different shapes depending on the Reynolds number and the degree of shear force.

Under laminar flow, differentiation between the following cases is possible:

- A rigid spherical particle

- A flexible spherical particle

- A rigid non-spherical particle

- A flexible non-spherical particle.

The red blood cell falls into the last category. At a relatively high Reynolds number, but in the laminar regime, RBCs flip around themselves. This movement is often referred to as tumbling. At lower Reynolds number and higher shear stress however, they follow a tank-treading movement in which the membrane of the cell alone is rotating around its centre of mass. A cell, which tank-treads, maintains a stationary orientation with the flow. Finally a third transitional regime was found by Abkarian et al. and is named swinging [3.14]. In this regime the cell tank-treads but undergoes oscillations around its stationary orientation [3.14].

Tank-treading behaviour arises in the absence of inertia. In the presence of a wall, the asymmetry of the flow surrounding the cell leads to a net force creating a drift that pushes the cell to the centre of the channel. Due to this purely viscous lift force, a thin cell-free layer appears on the wall of the channel [3.15]. Faivre et al demonstrated that this movement depends on the magnitude of the shear force. Thus, the presence of a constriction leads to a local high shear stress zone, pushing the cells even more centrally. Faivre reported a cell free layer of two or three times larger than the straight channel case, the effect of which lasts for up to 1 cm after the constriction. The lift force is dependent on the shape of the particle, deformability of particle, density difference between the particle and the fluid and shear stress. Under these conditions spherical objects do not experience the lift force, although they have been reported to rotate.

Contrary to common belief, inertial forces can overcome the viscous forces in microchannels in the laminar regime [3.16]. In this case, an axial migration effect, sometimes referred to as the tubular pinch effect, also applies to spherical and non-spherical particles. The fact that a non-spherical particle rotates fast and thus exhibits the same mechanical characteristics as a spherical particle can explain that non-spherical particles also experience the tubular pinch effect. The parameters affecting the migration of particles in this regime include the channel diameter-to-particle size ratio, the Reynolds number, the concentration of particles, the shape and deformability of the particle, the density difference between the particle and the fluid, and the presence or absence of particle rotation. In addition, the presence of other forces, such as the Saffman force at relatively high Reynolds number (but still in the laminar regime), acting on the spherical particles cannot be neglected if the rotation speed of the RBC is high enough. A pictorial summary of the different regimes of cell behaviour in microchannels is provided in Table 3.5.
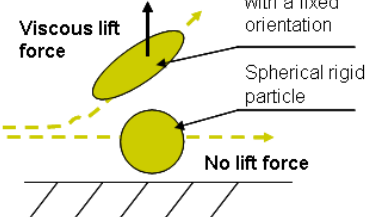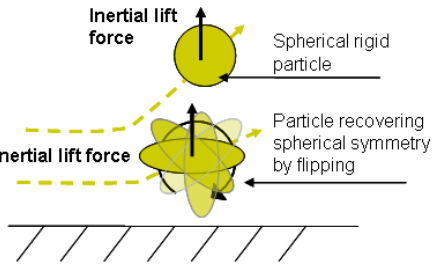
Regime and reference	Reynolds number	Viscosity ratio between inner and outer fluids	Movement of cell	Photographic evidence*	Predominant lateral force	Effect in microchannel
A (tank-treading [3.18])	Very Low (<1)	Low	Tank-treading		Viscous lift force	
B (Swinging [3.14])	Low	Medium	Swinging		*Transition regime*	*The different effects on the cells are not known and therefore no drawing can be provided here.*
C (Tumbling [3.18])	Very low to Low (~1)	High	Tumbling		Inertial lift force	

*Table 3. 5: Different regimes of cell behaviour in a microchannel of diameter less than 300μm. *Photographs of the tank-treading and tumbling cell regimes have been reproduced from reference [3.18], by permission of the Royal Society of Chemistry. Photograph of the swinging regime has been reproduced from reference [3.14] with the authorisation of the authors*

Axial migration is found in the two main regimes. In the absence of inertia, deformable asymmetric particles are pulled towards the centre of the channel, unlike the hard spheres which follow the streamlines. In the presence of inertia, the opposite scenario is more or less happening, although asymmetric particles have also been observed to move towards the centre of the channel. Both effects arise from the presence of a stationary wall and the interaction of a shear gradient on the particle. A transitional regime also exists where both effects may co-exist as discussed in [3.16,17]. The frontier between the two regimes has not been clearly established and this adds to the difficulty of predicting the behaviour of specific particles in microchannels. The cell-free layer observed on the walls at certain conditions depends also on the particle-particle interactions and the particle concentration.

3.3.2 Behaviour of red blood cells at bifurcations

Red blood cells exhibit a specific behaviour at bifurcations. Fung demonstrated empirically that RBCs have a tendency to travel to the highest flow rate daughter channel, providing that (a) the flow rate ratio between the daughter channel and the mother channel after the bifurcation is at least 2.5:1 and (b) the dimensions of the cells are comparable to the channel diameter. This effect is sometimes referred to as the Zweifach-Fung bifurcation law. Its origin is found in the asymmetrical distribution of pressure and shear forces on the cell at the bifurcation, pulling it to the channel with the highest flow as shown in figures 3.9 and 3.10 (left).

Based on this law, a blood-plasma separation unit can be designed such that the daughter channels can maintain the prescribed flow rate ratio. This technique was indeed applied by Yang's team in Pennsylvania and Yamada's team in Japan [3.19,20]. The design can be facilitated by simulating the flow rate using high level behavioural simulation techniques based on lumped elements modeling. This design methodology will be described in the next chapter.

The effect of bifurcations on the performance of the separation of plasma from blood has been discussed thoroughly through literature, but opinions still differ. Fung reports that the geometry of the bifurcation enhances the separation mechanism [3.2]. If the cell keeps a fixed orientation in the tank-treading regime, then it is easier for the cell to enter into a daughter channel as this one has the same orientation as the cell. Roberts

and Olbricht have carried out several experiments on bifurcations, as shown in Figure 3.10 (right), to examine whether the angles made by the mother and daughter channels are influencing the separation. They demonstrated that the magnitude of the separation depends on the bifurcation geometry and the aspect ratio of the channel cross-section [3.21]. On the other hand, Chien et al and Pries et al reported no appreciable effect of the branching angle on the particle distribution at bifurcations [3.3,22]. This contradiction illustrates the difficulty of predicting RBCs movement in microchannels. Microfluidic systems can nevertheless take advantage of RBCs specific behaviour to separate plasma from blood.
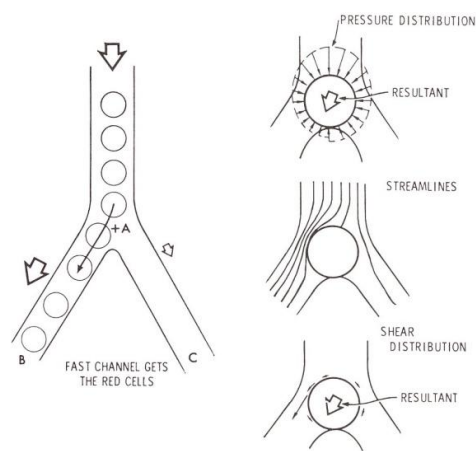
Figure 3. 9: (a) Original illustration of Fung's bifurcation law [3.2]

3.4 Blood plasma separation

Blood separation is a strategic preliminary step in the preparation for biological analysis on-chip. Polymerase Chain Reaction (PCR) can be performed on whole blood but the reaction is inhibited by components of blood such as hemoglobin (cellular portion) and IgG (plasma portion), therefore by separating blood into its basic components of plasma and cells the reaction can be optimised for better results.
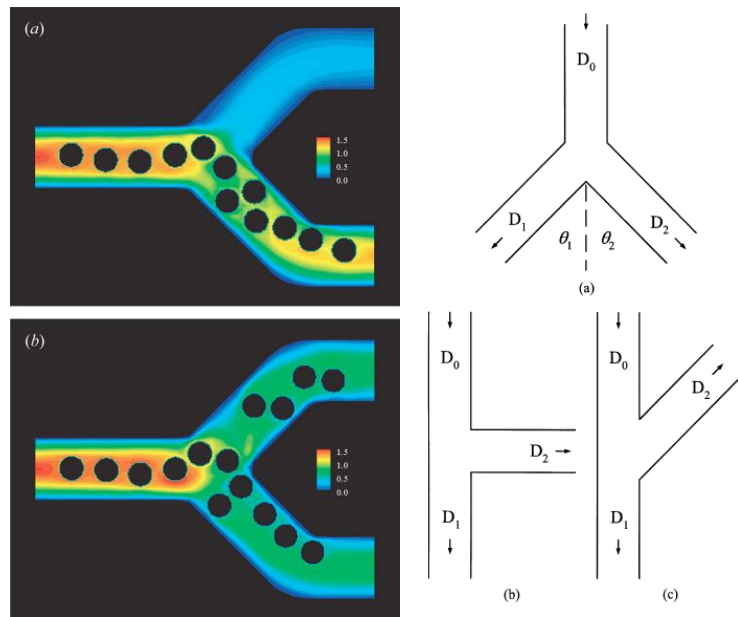
Figure 3. 10: Left, Distributions of RBCs flowing through the bifurcation. RBCs are represented by black dots. In (a) the flow rate ratio is around 1 to 6.6 while in (b) the flow rate ratio is 1 to 2. [3.23]. Different channel geometries studied by Roberts and Olbricht [3.21].

Centrifugation and filtration are the two conventional techniques for blood plasma separation in laboratories. Both methods are time-consuming, relatively expensive and might damage cells if not used carefully.

In the light of the disadvantages outlined above and the benefits that microscale techniques can provide in terms of volume of blood extracted, response time and portability, the alternative blood-plasma separation on-chip has gained increasing interest over the last few years as shown in Chapter 2. Separation techniques using only hydrodynamic forces, channel geometries and bio-physical effects have lately been developed based on preliminary work on microcirculation [3.2]. New technologies like CD-like platform are complex and require expensive instrumentation. The approach chosen in this study uses the latest advances in hydrodynamic blood-plasma separation techniques on-chip, which are passive by nature. The aim is to develop a system with a high plasma yield as well as a low processing time. Plasma yield is defined as the percentage volume of plasma that can be extracted from the device over the total volume of plasma in the blood. To allow mass-manufacturability of the device by high volume manufacturing techniques such as microinjection moulding, channel dimensions greater or equal to 20μm in the first designs were used. The separation method is continuous since no external force field need to be switched

on and off. Moreover the cell and plasma can be continuously collected or directed to in-line processing. The sample injection is kept straightforward and simple, with only one inlet needed for the entire system.

The number of parameters affecting the flow of cells in a microchannel renders difficult the prediction of the behaviour of the RBCs in the separation system. The presence and effects of viscous and inertial lift forces which enable particles to be separated at the microscale has been discussed earlier [3.17].

The designs presented here exploits two main hydrodynamic effects: the Zweifach-Fung bifurcation law and the blood flow focusing effect occurring after a constriction. Although this law was first stated in the context of micro-circulation in the human body, it has also been exploited for in-vitro separation [3.24]. From a few cells in a microvessel, the law was generalised to accommodate the situation where populations of cells flow in microchannels several tens of microns wide. The Zweifach-Fung effect is commonly used in the design of micro-separators to set up a lower limit for flow rate ratio at a bifurcation. However, the physics which underpin the law and its limitations are not clearly understood yet. The second effect is the focusing of particles after a constriction. The design requirements for this device are summarised in Table 3.6.

The overall aim of these systems is to reach maximum purity efficiency, E_p, preferably 100%, defined as:

$$E_p = 1 - \left(\frac{c_p}{c_f} \right)$$

(3.5)

where c_p and c_f are the number of events (or presence of particles) per mL in the plasma collection outlet and in the feed inlet.

In order to meet these requirements, two generations of blood plasma separation devices were designed as presented in Figure 3.7. The first generation devices were developed from two different approaches. The first integrating a single constriction with a series of bifurcations while the second model was integrating four bends with two constrictions. These devices will be presented in greater details in section 3.5. After some initial experiments results, the second module was abandoned because of poor results and especially clogging problems (data not shown in this thesis). Using

Design requirements in terms of:	Solutions
Manufacturing	Cost-effective
Power	None other than power to actuate the flow
Physical forces used	Viscous or inertial forces in flow
Throughput	Relatively high flow rates needed
Separation mode	Continuous

Table 3. 6: Design requirements for the blood plasma separation device

qualitative data from the modelling approach as presented in Chapter 4, and the first experimental results, the second generation device was based on T-channels and constrictions and is presented in section 3.6.
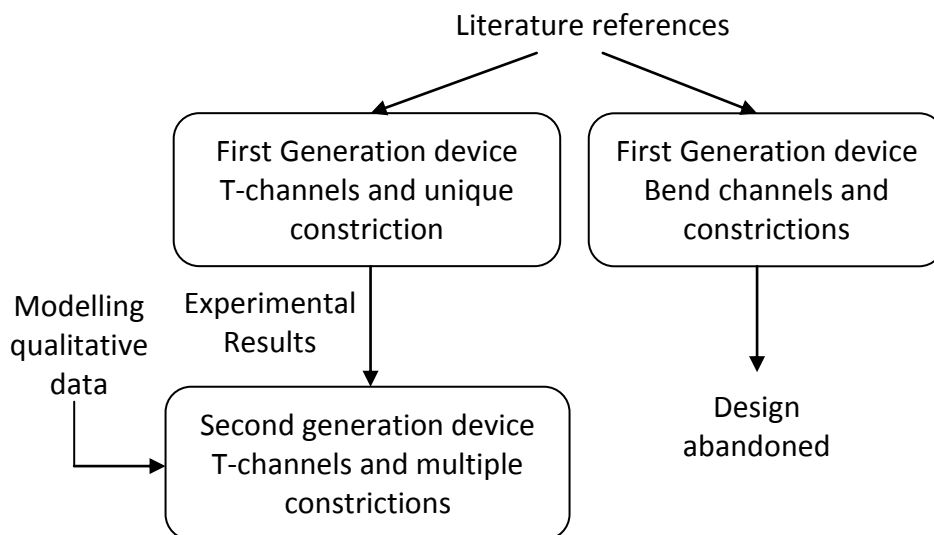
Figure 3. 11: Design approach for the blood plasma separation modules

3.5 First generation devices

In this section, two designs are presented, which use an original combination of the methods previously reported.

3.5.1 T-junction channels and constriction

As RBCs flowing through a bifurcating region of a capillary blood vessel have a tendency to travel into the vessel which has a higher flow rate, Yang et al. proposed a blood plasma separation device based on a T-shape configuration as shown in Figure 2.10c [3.19]. T-channels for blood plasma separation manufactured by Roche are

presented in Figure 2.10b. Finally, Faivre et al reported that constrictions in microchannels increase the natural cell-free layer over a distance of up to 1 cm after the constriction [3.15]. The first design produced in this study, integrates a constriction and a series of bifurcations.

The principle of the microfluidic blood plasma separation module is shown in figure 3.11. This design should theoretically work at both low and medium Reynolds number which is regulated by the flow rate used (respectively 0.01 and 1). The configuration of the separation module is as follows. Firstly, the use of micrometre dimensions ensures laminar flow and the presence of a particle-free layer. Secondly, a constriction in the main channel induces a high-shear stress zone pulling the particles even more centrally. Thirdly, 20 bifurcation channels are placed on each side of the main channel to enhance the plasma yield. In the basic design, the width of the main channel is 100µm and the plasma channels are 20µm wide. The constriction width and length are respectively 25 and 300µm. The height of all channels is 20µm. The drift induced on the cells by the single constriction has been calculated as [3.15]:

$$d \approx 6.\kappa.\frac{L.R^3}{w.h^2} \, , \hspace{4cm} [3.4]$$

Here L, w, h are the length, width and height of the constriction. R is the radius of a sphere having the same radius as a cell and κ is a dimensionless parameter equal to 0.45. Using Eq.(3.4) the drift induced by the constriction is estimated to be around 27.5µm. The constriction width and length, and the main channel width have been used as variable parameters and change from one design to another. The external connection consists of only one inlet to introduce the blood and three outlets. One of these outlets collects the cells and the other two collect the plasma. The length of capillaries connected to the outlets can easily be tuned to change the flow rate ratios at the outlets. The length ratio between the plasma outlet capillaries and the cell outlet capillary will also be used as a variable parameter.

The change of purity efficiency might be achieved by varying the following parameters: main channel width (MCW), buffer type (BT), outlet length ratio (OLR) and flow rate (FR).
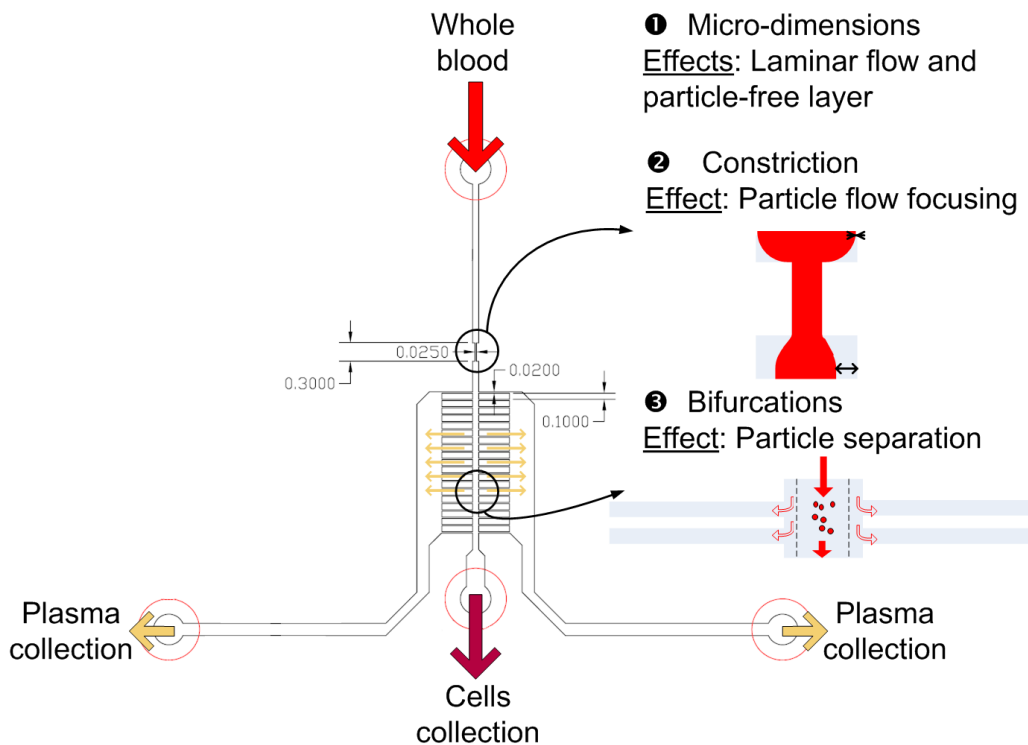
Figure 3. 12: Principles of the hydrodynamic blood plasma separation. The use of laminar flow ensures a particle free layer on the walls of the main channel, a constriction pulls the cells even more centrally. Finally the cells and plasma are separated at the bifurcations using the Zweifach-Fung bifurcation law. Dimensions are given in mm.

3.5.2 Bends and constrictions

Blattert et al introduced a bend structure for blood plasma separation and released optimised devices later on [3.25]. This structure is combining two principles: a centrifugal force field and a "plasma skimming effect". The plasma skimming effect exists naturally in microchannels. An axial accumulation of RBCS has been observed along a microchannel. This has the consequence of leaving a "cell-free layer" or "plasma-rich layer" near the microchannel walls. A bend in the microchannel induces a variation of the flow profile and results in an increased width of the "cell-free layer". A sub-microchannel is placed downstream on the inner wall of the bend to collect the plasma. It was observed that thinner is the sub-microchannel, better is the efficiency. However, a thinner plasma collection channel induces a poor plasma yield. A bend changes the velocity profile in the microchannel with the faster flow layers tending to migrate slightly on the outer wall of the bend. It implies another drift on the blood cells. Blattert found this drift proportional to the density difference of the particle and the medium.

Figure 3.12 shows a "bend" design of the blood plasma separation device. The microsystem is composed of a constriction in each of the two whole blood inlet channels, followed by two bends in each channel, several bifurcating plasma sub-channels and an oulet channel for the blood cells. Geometrical features contributing to the separation are the chosen dimensions of the microchannels, the constrictions, the bends and the bifurcations. The separation of red blood cells from plasma is made possible by the presence of bio-physical effects within the microchannel structure, the Zweifach-Fung bifurcation law and a centrifugal effect.

However, the centrifugal effect has been later found to provide a minimal contribution on the separation process. In the light of the small affect produced by the bends, it was decided to abandon this bend structure and to focus more on the bifurcation and flow rate ratio effect.
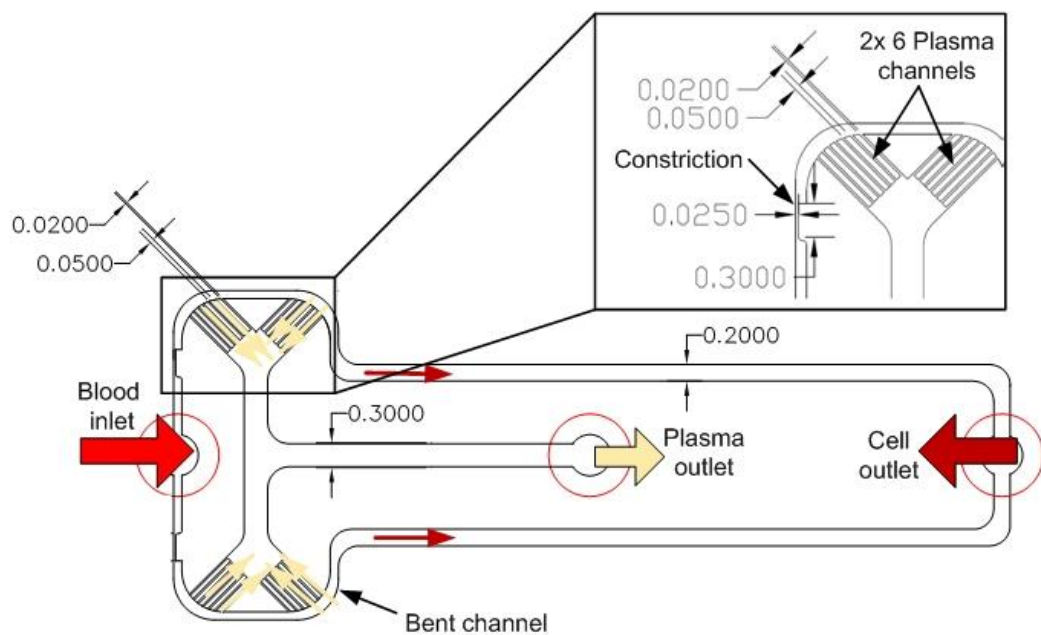
Figure 3. 13: Four bends design

3.6 Second generation device

Subsequently to the simulation results presented in Chapter 4 and the tests performed on the first generation devices and presented in Chapter 6, a second series of device was designed. The aim of this second iteration was to redesign the device in order to

improve the plasma purity, or separation efficiency as defined in Equation (3.5) and reduce the back flow observed in the last channels.

As shown in Figure 3.13, the second generation device has four connections, a single inlet for whole blood, one outlet for the concentrated cells and two outlets for the extracted plasma, as for the first generation T-channel device. Four plasma channels of 5.5mm in length are placed on each side of a 100µm wide main channel at a 45º angle. Meanders are used to minimize the area occupied by the eight plasma channels and keep the footprint of the chip low. A constriction has been placed before each of the plasma channels in order to create a cell-free zone from which the plasma is extracted. A set of chips has 20µm wide plasma channels while another has 10µm wide plasma channels. The depth of the microchannel networks is 20µm for all structures.
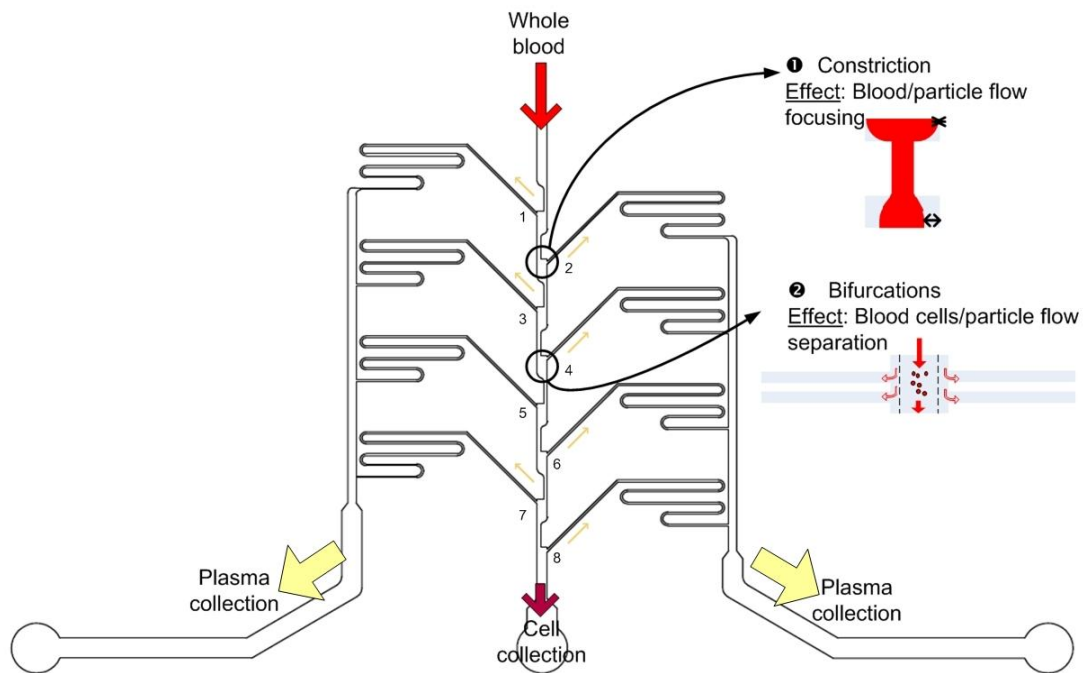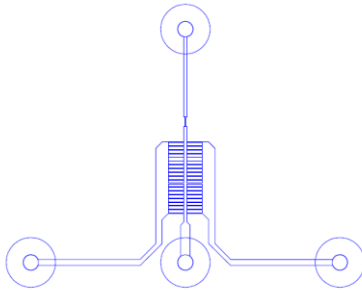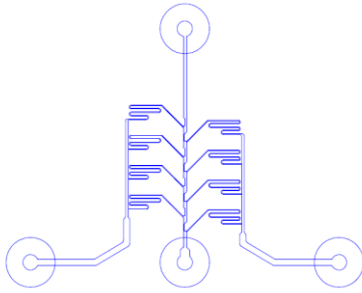
Figure 3. 14: Schematic of a 20µm wide microchannels blood plasma separator. The flow of plasma is indicated by the yellow arrows.

The plasma channels due to their geometrical features (length and width) have a higher fluidic resistance value, whereas the main channel segment, of broader width and shorter length, has lower resistance. This difference in resistance value at each bifurcation is proportional to the flow rate ratio. The value of the fluidic resistance of the main channel decreases after each bifurcation. Since the plasma channels have the same lengths the flow rate ratios are expected to be different at each bifurcation.

The flow rate ratios can be roughly calculated by the Saber$^{(TM)}$ microfluidic applications software (CoventorWare) with the methodology detailed in chapter 4. Flow rate ratios have been calculated as approximately 17.8, 22.6, 31.8 and 55.6 for the left hand side of the chip (bifurcations 1, 3, 5, 7) and 19.2, 25.7, 40.1, and 94.5 for the right hand side of the chip (bifurcations 2, 4, 6, 8) with 20μm plasma channels. The side having the highest flow rate ratios is expected to perform better, this will be verified in Chapter 6. Theoretically, the design should extract 30% of plasma for the 20μm design and 7% for the 10μm design.

3.7 Conclusions

In this chapter, the blood has been presented as a complex living fluid. The theoretical blocks have been assembled allowing the understanding of red blood cells behaviour in microchannels. Two generations of T- junction microdevices for blood plasma separation have been detailed. The main differences between these devices are highlighted in Table 3.7. Chapter 4 will present a simulation model to allow for better control of the system while Chapters 6 and 7 will discuss the results obtained by the two generations of devices.

	First Generation T-channel design	Second Generation T-channel design
Main channel width	100 or 200μm	100μm
Plasma channel width	20μm	10 or 20μm
Plasma channel length	0.5mm	5.5mm
Number of plasma channels	30	8
Geometry	Symmetric	Asymmetric
Overall footprint of the chip	1.8x2.3cm	1.8x2.3cm
Number of constrictions	One single constriction	A constriction before each bifurcation
Constriction dimensions (length x width)	300μm x 25μm	

Table 3. 7: Main physical differences between the two devices chosen for testing.

3.8 References

[3.1]   B. Alberts;, D.Bray;, J.Lewis;, M.Raff;, K.Roberts;, and J.D.Watson;, *Molecular Biology of the Cell, .* (Garland Publishing Inc., , New York 1983).

[3.2]   Y.C. Fung, *Biomechanics*. (2004), second ed.

[3.3]   A.R. Pries, T.W Secomb, and P Gaehtens, *Biophysical aspects of blood flow in the microvasculature*, Cardiovascular Research **36**, 654-667 (1996).

[3.4]   A. S. Popel; and P.C. Jonhnson;, *Microcirculation and Hemorheology*, Annual review of fluid mechanics **37**, 43-69 (2005).

[3.5]   C.L. Sawyers;, *The cancer biomarker problem*, Nature **452**, 548-552 (2008).

[3.6]   S.J. Pitteri and V.M. Faca S.M. Hanash, *Mining the plasma proteome for cancer biomarkers, ,* Nature, **452,** , 571-579 (2008).

[3.7]   Wadell; H., *Volume, Shape and Roundness of Quartz Particles*, Journal of Geology **43**, 250–280 (1935).

[3.8]   Evans; Y.C. E., Fung;, *Improved Measurements of Erythrocyte Geometry*, Microvascular Research **4**, 335-347 (1972).

[3.9]   Stoltz; M Singh; P. J.F., Riha;, *Chapter 2, Hemorheology in Practice*. (IOS Press, Amsterdam, 1999).

[3.10] United States National Library of medicine, www.nlm.nih.gov, 2010

[3.11] J.F. Hoffman; and S. Inoue, *Directly observed reversible shape chages and hemoglobin stratification during centrifugation of human Amphiuma red blood cells*, PNAS **103**, 2971 2976 (2006).

[3.12] R.L. Fournier, *Basic transport phenomena in Bioengineering*. (CRC Press, 2nd edition, 2006).

[3.13] A. Viallat M. Abkarian, *Vesicles and red blood cells in shear flow*, Soft Matter **4**, 653–657 (2008).

[3.14] M.Faivre M. Abkarian, A. Viallat, , *Swinging of red blood cells under shear flow*, Phys Rev Lett **98**, 188-302 (2007).

[3.15] M. Faivre, Abkarian, M., Bickraj., Stone, H.A., *Geometrical focusing of cells in a microfluidic device: an approach to separate blood plasma*, biorheology, **43**, 147-159 (2006).

[3.16] J.F. Edd D. Di Carlo, D. Irimia, R.G. Tompkins, and M. Toner, , *Equilibrium Separation and Filtration of Particles Using Differential Inertial Focusing*, Anal. Chem. **80**, 2204-2211 (2008).

[3.17] R.S. Dhariwal M. Kersaudy-Kerhoas, M.P.Y. Desmulliez and L. Jouvet,, *Hydrodynamic blood plasma separation in microfluidic channels*, Microfluidics and Nanofluidics **8**, 1613-4982 (2010).

[3.18] A. Viallat M. Abkarian, *Dynamics of vesicles in a wall-bounded shear flow. ,* Biophys J **89**, 1055–1066 (2005).

[3.19] S. Yang, A. Undar, and J. D. Zahn, *A microfluidic device for continuous, real time blood plasma separation*, Lab on a Chip **6** (7), 871–880 (2006).

[3.20] M. Yamada and M. Seki, *Hydrodynamic filtration for on-chip particle concentration and classification utilizing microfluidics*, Lab on a Chip **5** (11), 1233–1239 (2005).

[3.21] and W. L. Olbricht B.W. Roberts, *The Distribution of Freely Suspended Particles at Microfluidic Bifurcations*, AIChE J. **52**, 199-206 (2006).

[3.22] C.D. Tvetenstrand S. Chien, M.A.F Epstein, and G.W. Schmidschonbein, , *Model studies on distributions of blood cells at microvascular bifurcations*, Am. J Physiol. **248**, H568-H576 (1985).

[3.23] S.Tominaga T. Hyakutake, T. Matsumoto and S. Yanase, , *Numerical Study on Flows of Red Blood Cells with Liposome-Encapsulated Hemoglobin at Microvascular Bifurcation*, Journal of Biomechanical Engineering -Transactions of the ASME **130**, 011-014 (2008).

[3.24] S. S. Shevkoplyas, T. Yoshida, L. L. Munn, and M. W. Bitensky, *Biomimetic autoseparation of leukocytes from whole blood in a microfluidic device*, Analytical Chemistry **77** (3), 933–937 (2005).

[3.25] C. Blattert, R. Jurischka, A. Schoth, P. Kerth, and W. Menz, "Separation of blood in microchannel bends", in *25th Ann. Int. Conf. of the IEEE Engineering in Medicine and Biology Society* (Ieee, Cancun, Mexico, September 2003), Vol. 25, pp. 3388-3391.

Chapter 4: System-level simulation of microfluidic networks

4.1 Introduction

4.1.1 Motivations

The goal of the present modeling study is to assess the performance of the microfluidic network using a full Newtonian approach, to evaluate the initial design and observe the effects of design variations on the flow rate ratios at each bifurcation.

The chosen simulation approach of the microfluidic device is a system-level simulation, which allows the simulation of not only the critical part of the system where separation takes places, but also the surrounding microchannels which are ancillary to the operation of the system. There are several advantages at taking a holistic approach, as all the resistances in the system are interdependent. System level modeling allows faster design iterations than Computational Fluid Dynamics (CFD) and offers a means to evaluate an initial design and observe the effects of design variations.

The external surroundings of the chip itself, which include the pump, board, plugs and capillary fittings, can play a considerate role on the actual performance of the device in terms of separation efficiency and yield. This influence has to be controlled and integrated into the design not only to avoid perturbation during the test procedures, but also to ensure robustness of performance during device operation.

Although an experimental validation approach was not undertaken, the information determined from the simulation contributed to the development of the second generation device which resulted in a 30% increase in performance.

4.1.2 Blood flow modeling in literature: Computational Fluid Dynamics *vs* System-level modelling

The computational analysis of blood flow in microvessels is a long-sought goal in both (1) clinical research, for the understanding of specific disease such as the presence of stenosis in the circulation and (2) in new biomedical applications, such as the

separation of cells from plasma at the microscale. Blood flow modelling is particularly difficult and computationally expensive due to the unusual contribution of the red blood cells, these highly deformable particles, to the physical model. Apart from RBCs, the rest of the particulates form less than 1% of the total volume. Several strategies have been developed to model blood flow in microvessels. Computational Fluid Dynamic (CFD) is the common tool for modelling microfluidic flow. The meshing requirements for a microfluidic network are very important to obtain results close to experimental data. CFD simulations are computationally expensive, and, without the use of powerful computers, these simulations would be useful only for the determination of the flow at localised points rather than through the entire system. However, biophysical analysis can often be enhanced by CFD modelling. For example, CFD was employed for the study of the flow around a stenosis [5.1]. In other cases, such as in ref [5.2] simple structures have been simulated to predict the relationship between pressure and flow rates in different geometrical situations. In another original study, a flow of RBCs in a straight microchannel, was simulated using a 2D particulate model [5.3]. As shown in Figure 4.1a, the model is composed of 1200 individual RBC, initially organized in 10 rows and 120 columns in a microchannel with a width of 75μm. Each RBC is itself modeled by 100 particles, allowing the model to account for deformability. The flow of multiple RBCs over a length of 200μm in this channel was been successfully simulated as shown in Figure 4.1b, and predicted the aggregation of RBCs at the centre of the channel. This simulation however, required the computational power of 80 processors and 12 hours in real time (960 hours in CPU time).

In another example, Barber et al presents a model for the behaviour of RBCs at microvessel bifurcations, using a two-dimensional, flexible-particle model [5.4]. The model accounts for the effects of flexibility of RBCs and asymmetry of the bifurcations. The model does not incorporate a larger and more complex microfluidic network other than a single bifurcation. Other studies have focused on the behaviour of one or several red blood cells in a straight, bent, constricted microchannel or at bifurcations [5.5].
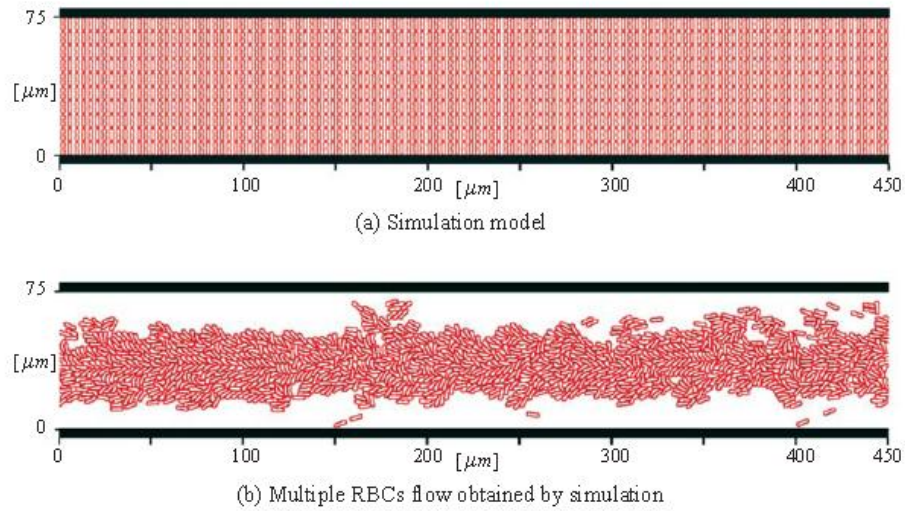
Figure 4. 1: Tsubota's red blood cell flow model resulted in these accurate rendering of blood flow in a channel but necessitate 80 processors to compute just a straight channel segment [5.3].

System-level fluidic modelling is more adapted to the case of microfluidic networks if rapid conclusions need to be made for the manufacturing of such a system. In this approach, also named lumped parameters model, the microfluidic network is broken down into several elements, each having a different function [5.6]. A brief description of the basic building lumped parameters is given below.

Poiseuille flow is known as the steady-state flow of incompressible fluid into microchannels [5.7]. In this case a constant pressure drop, ΔP, results in a constant flow rate, Q. This law is known as the Hagen-Poiseuille law:

$$\Delta P = R_{hyd} Q$$

[4.1]

Where R_{hyd} is the hydraulic resistance. This law is analogous to Ohm's law. The concept exploits the analogy of microfluidic networks to electrical circuits and an equivalent to Kirchhoff laws can be used to compute the response of the system [5.8]. The concept of hydraulic resistance is essential for the characterization of microchannel network as presented in this study [5.7].

Figure 4.2 presents the different models that can be used in microfluidic analysis.
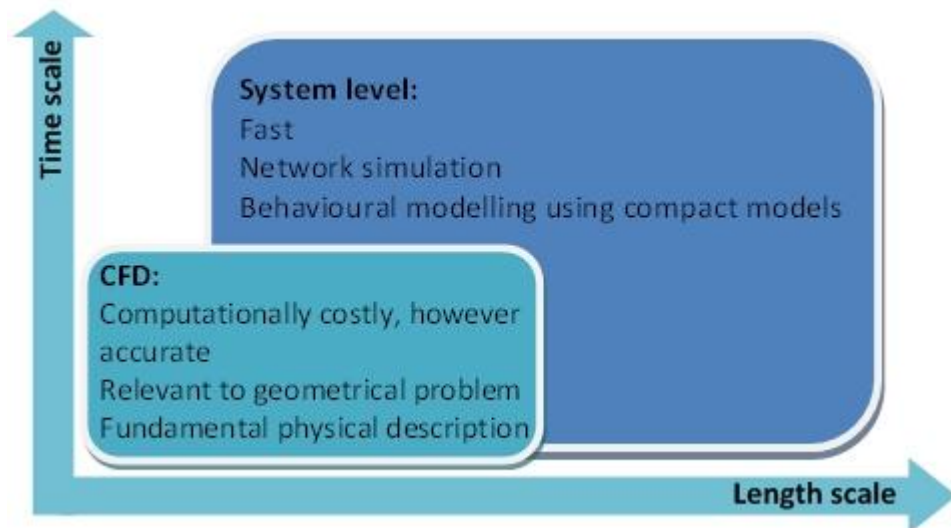
Figure 4. 2: Comparison between CFD and system-level modeling, adapted from [5.9].

The aim of this study is to find solutions for an efficient design of microfluidic networks for the passive separation of plasma from blood using the Zweifach-Fung bifurcation law. This chapter demonstrates that, not only the chip itself but also its surroundings can affect the overall performance of the device. This study also aims at examining the validity and usefulness of a system-level approach for general modelling of microfluidic network. Only Newtonian fluids and particle-free fluids have been considered for this study although improvement on the existing model could be carried out at the expense of computational time.

The model presented incorporates the Zweifach-Fung bifurcation law in the simulation of a Microfluidic network. In the first section, the design is presented in detail and the algorithm for the simulation of the microfluidic network is described. The second section introduces the numerical verification of the algorithm using the software package CoventorWare. In the third section we discuss the results and the limitations of the model.

4.2 Separation of plasma from blood

4.2.1 System design

The principle of the microfluidic blood plasma separation module has been presented in Chapter 3 [5.10]. This design can work both at low (around 0.01) and medium (around 1) Reynolds number which is regulated by the flow rate used.

The configuration of the separation module is as follows. Firstly, the use of microscale dimensions ensures laminar flow and the presence of a cell-free layer. Secondly, a constriction in the main channel induces a high-shear stress zone pulling the particles even more centrally [5.11]. Thirdly, in the first generation device, 15 bifurcation channels are placed on each side of the main channel to enhance the plasma yield, as defined in Chapter 3. In the basic design, the width of the main channel is 100µm and the plasma channels are 20µm wide. The constriction width and length are respectively 25 and 300µm. The depth of the entire structure is 20µm. As shown in Figure 4.3, the chip sits on a platform which routes the fluid from the chip to fluid adaptors. Standard microfluidic connectors with capillaries (or tubing) are plugged to the fluid adaptors. The fluid adaptors are shown in green on Figure 4.3, and the capillaries plugged to the holder is presented in Figure 4.4. Capillaries are required to bring the blood from the syringe to the platform itself. In the same way, for the outlets, capillaries bring the blood from the platform to Eppendorf tubes for collection. The length of capillaries connected to the outlets can easily be tuned to change the flow rate ratios at the outlets. The length ratio between the plasma outlet capillaries and the cell outlet capillary will also be used as a variable parameter.

The separation at each bifurcation is based on the Zweifach-Fung principle. In the design figure 3.11, the flow rate ratio cannot be the same at each bifurcation as the flow rate in the main channel reduces after each bifurcation, but the plasma channel length remains the same. This potentially induces different separation efficiency at each bifurcation if the efficiency at the last bifurcation is below 100%. It is of interest to regulate the flow to get the same ratio at each bifurcation in order to avoid either red blood cells entering the plasma channels or the lysis of the cells if the flow rate is too high. Such design iteration can make the system stronger and more reliable. In the
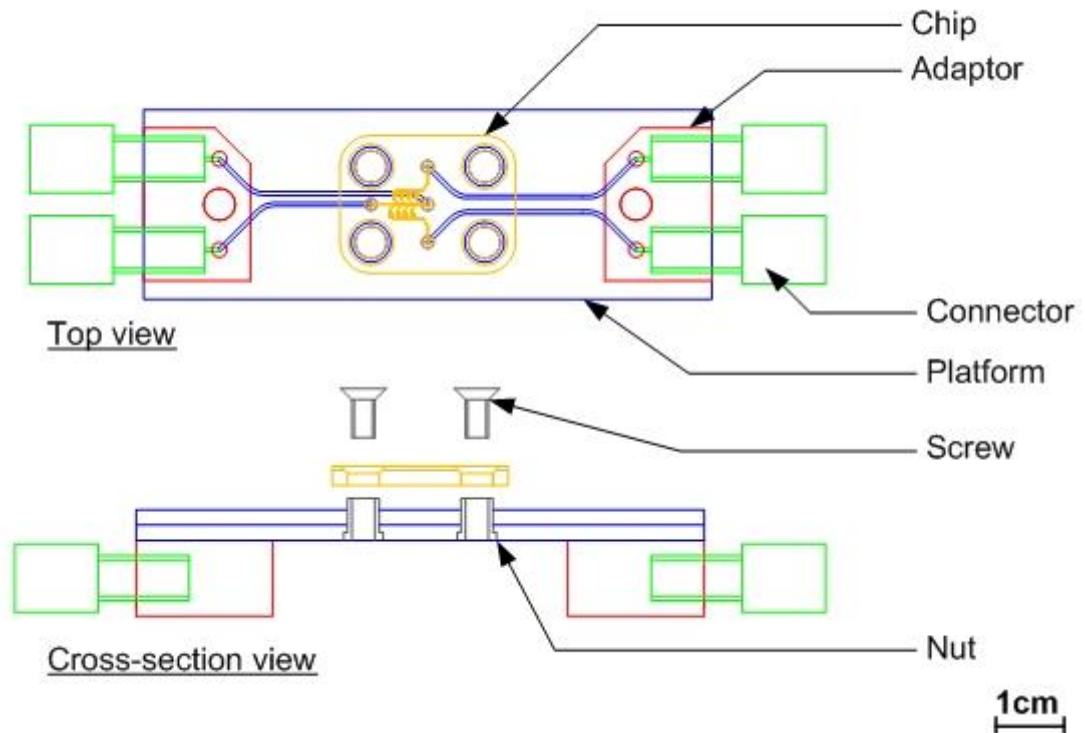
Figure 4. 3: The physical design comprises a bifurcation to focus the flow of red blood cells and 15 bifurcations situated on each side of the main channel to extract the plasma. Platform schematic, courtesy of Epigem Ltd.
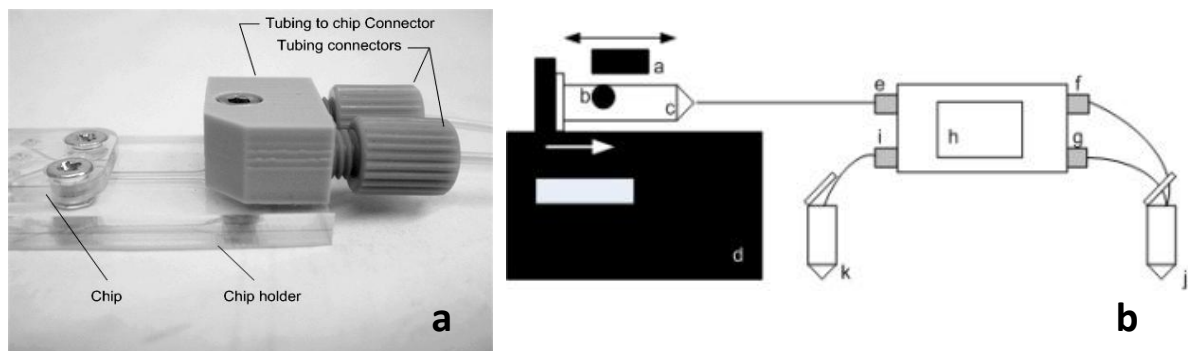
Figure 4. 4: (a) Photograph of the chip on the chip holder, or platform, connected to standard microfluidic capillaries. (b) Schematic of the experimental set-up detailing the chip on the holder and the capillaries connected from the chip to the collecting tubes

context of these simulation, the level of hematocrit used is considered very low (in the order of 3%), which allows us to model the flow of plasma as a Newtonian fluid without any particles.

In this case, there are several advantages at taking a holistic approach, as all the resistances are interdependent. System level modelling allows faster design iterations

than CFD and offers a means to evaluate an initial design and observe the effects of design variations.

4.2.2 Hypothesis and major assumptions

In this model, the liquid is assumed to be driven at a constant flow rate by a syringe pump. The three outlets are connected to hydraulic ground, at a pressure nil.

The microfluidic network designed in this study can be described as an assemblage of straight segments with hydraulic resistances and nodes (or bifurcations) as shown in Figure 4.5. Unlike in some other lumped parameter models, the hydraulic equivalents of capacitance and inductance have been considered as negligible [5.12]. This is a valid assumption as the elastic capacity of the channel and inertia of the flow of blood are small. Each segment of the network is therefore considered as a pure hydraulic resistance.
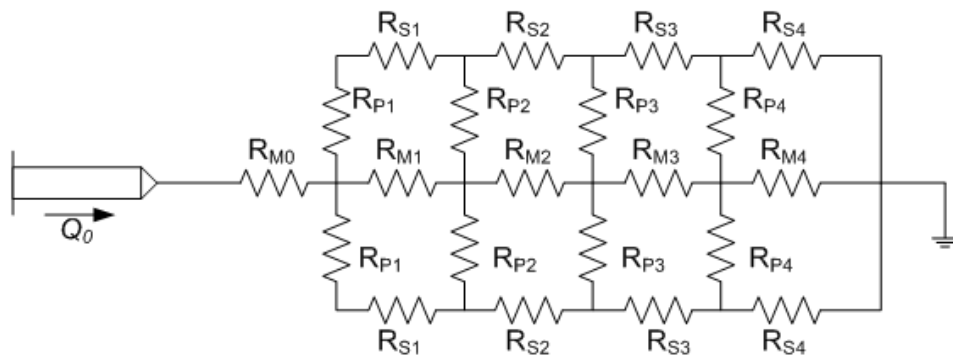
Figure 4. 5: The microfluidic network can be seen as an assembly of straights channels linked by nodes. The inlet is fed with a constant flow rate Q_0. The outlets are connected to the hydraulic ground. In this figure only four plasma branches on each side of the main channel have been considered.

The following assumptions have been made for the development of the analytical equations describing the flow of liquid in each segment:

- The flow is considered Newtonian, incompressible and laminar;

- The flow is considered set and stable at the time of the analysis, meaning that entry and exit effects are neglected;

- The effect constriction is ignored, as the system is flow rate driven;

- Channels have been manufactured using SU8 (epoxy based photoresist) by photolithography and have a rectangular cross-section;

81

- The fluid used in the model is water and

- The system is flow rate driven.

The design requirements to be met by the model are: (i) The flow rate ratio between mother and daughter channel should be equal at each bifurcation (ii) The total depth of the microfluidic channels is 20µm (iii) The plasma channel has a width of 20µm.

The model will calculate the required lengths for plasma channels lengths to get constant flow rate ratios at each bifurcation.

The goal of the present modeling study is to assess the performance of the microfluidic network, evaluate the initial design and observe the effects of design variations.

Figure 4.6 details the flow chart used for the modelling process. A model producing a set of internal and external parameters based on initial conditions is solved analytically. A numerical model is built using the internal and external parameters given by the analytical model as inputs. By comparing the compilation results, the match between the two models is checked. We have now the chip completely designed and ready for the manufacturing and testing. As it is often found, the chip has to be connected to external devices or capillaries for either test purpose of for operation. These changes are not always foreseen during the design step. The second half of the modelling proposes to investigate changes occurring in the flow distribution inside the chip after the manufacturing when changes are impossible.

4.2.3 Algorithm

The algorithm has been constructed that is based on the lumped element model developed by Berthier [5.13].

The algorithm is built using the basic laws of conservation of mass and energy. The first step of the algorithm is the calculation of flow rates; the second step deal with the calculation of the associated resistances. Finally the third step is the extraction of the channel length.

Looking at the first node, let α be the constant flow rate ratio between the flow rate in the plasma channels and the flow rate in the main channel after the bifurcation. At
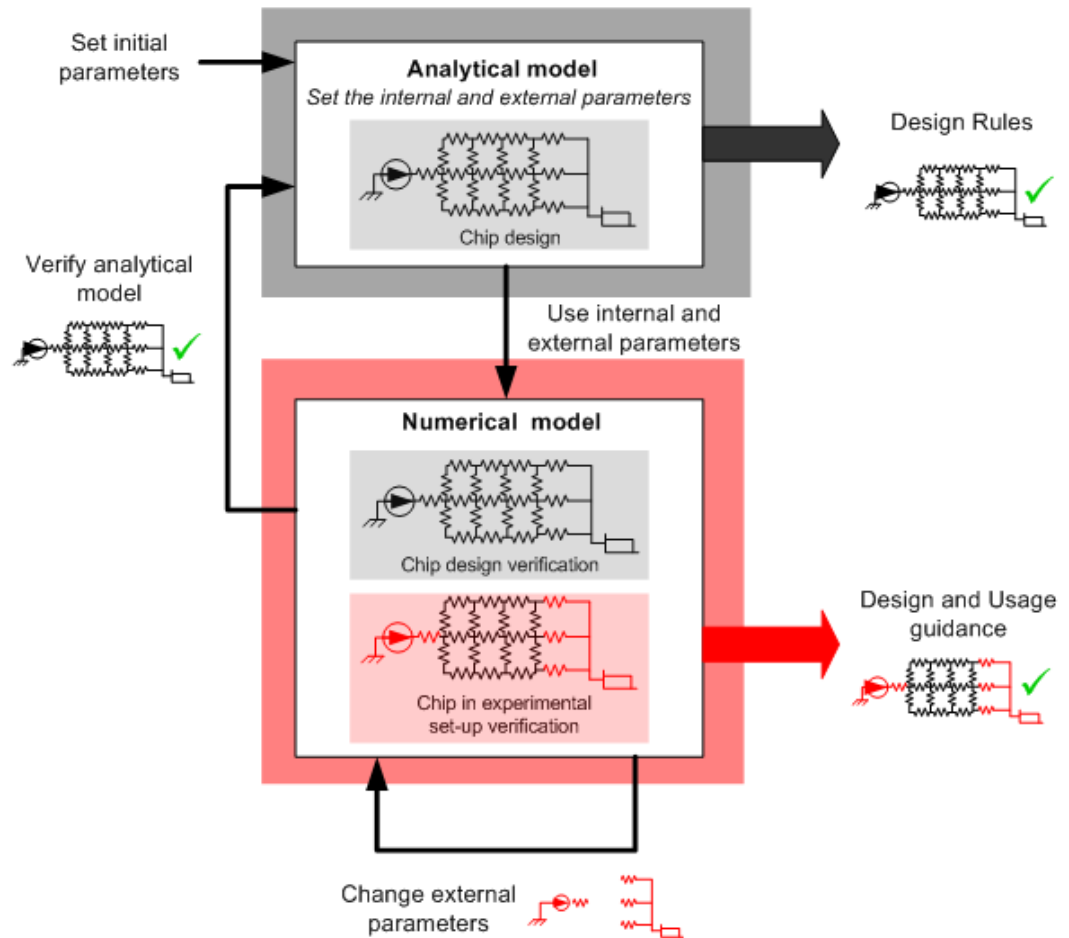
Figure 4. 6: Typical simulation flow chart. This diagram is detailing the relationships between the analytical and numerical model.

the first node, the sum of the flows entering and leaving each node must sum to zero such that:

$$2F_{P1} + F_{M1} = Q_0 \; , \qquad\qquad\qquad [4.2]$$

Where F_{P1} and F_{M1} are the flow rates of the two plasma channels and of the main channel at the first node, respectively. As $\alpha = F_{P1}/F_{M1}$,

$$F_{M1} = \frac{Q_0}{2\alpha + 1}$$
$$F_{P1} = \frac{\alpha Q_0}{2\alpha + 1} \qquad\qquad [4.3]$$

Using a recurrence relationship we obtain, the flow rates at the nth are:

$$F_{Mn} = \frac{Q_0}{(2\alpha + 1)^n}$$

$$F_{Pn} = \frac{\alpha Q_0}{(2\alpha + 1)^n}$$

[4.4]

The continuity equation for an incompressible fluid is directly linked to mass conservation can be checked by verifying the following expression [5.7]:

$$2\sum F_{Pk} = Q_0$$

[4.5]

The plasma channels join together on both side of the main channel to form side channels, or daughter channels. The flow rates for these channels are as follow:

$$F_{S1} = F_{P1} = \frac{\alpha Q_0}{2\alpha + 1}$$

$$F_{S2} = F_{S1} + F_{P2} = \frac{\alpha Q_0}{2\alpha + 1} + \frac{\alpha Q_0}{(2\alpha + 1)^2}$$

$$F_{S3} = F_{S2} + F_{P3} = \frac{\alpha Q_0}{2\alpha + 1}\left[1 + \frac{1}{2\alpha + 1} + \frac{1}{(2\alpha + 1)^2}\right]$$

...

$$F_{Sn} = F_{Sn-1} + F_{Pn} = \frac{\alpha Q_0}{2\alpha + 1}\left[1 + \frac{1}{2\alpha + 1} + \frac{1}{(2\alpha + 1)^2} + ... + \frac{1}{(2\alpha + 1)^{n-1}}\right]$$

$$F_{Sn} = \frac{Q_0}{2}\left[1 - \frac{1}{(2\alpha + 1)^n}\right]$$

[4.6]

The flow resistances can now be calculated by determining all the possible paths that the flow will follow. As the design of the first prototype is symmetric with respect to the main channel, half the system with four branches is considered as shown in Figure 4.7. Five independent paths can be distinguished and are represented by different colours.

Remembering the generic equation [4.1], the microfluidic network can be modeled as a set of linear equations. Each equation uses the generic equation [4.1] for each of the individual paths:
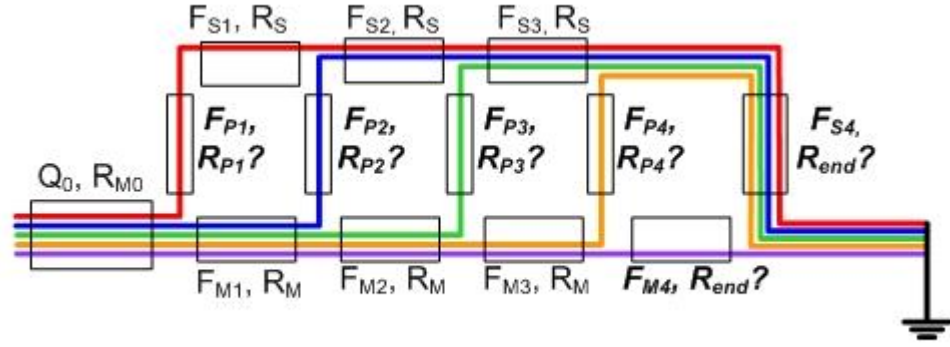
Figure 4. 7: Five independent flow paths, represented by different colours, exist for the half network. The unknowns in the system are highlighted in bold and italic. Compared to Figure 4.4, all the channels branches are identical such that $R_{M1}=R_{M2}=R_{M3}=R_M$. All the side channels are also equal. Here, the flow resistances of the end branches on the cell and plasma sides are equal, ie: $R_{S4}=R_{M4}=R_{end.}$

$$P_i = R_{M0}Q_0 + R_M\left(F_{M1} + F_{M2} + F_{M3}\right) + R_{M4}F_{M4}$$

$$P_i = R_{M0}Q_0 + R_M\left(F_{M1} + F_{M2} + F_{M3}\right) + R_{P4}F_{P4} + R_{S4}F_{S4}$$

$$P_i = R_{M0}Q_0 + R_M\left(F_{M1} + F_{M2}\right) + R_{P3}F_{P3} + R_S F_{S3} + R_{S4}F_{S4}$$

$$P_i = R_{M0}Q_0 + R_M F_{M1} + R_{P2}F_{P2} + R_S\left(F_{S2} + F_{S3}\right) + R_{S4}F_{S4}$$

$$P_i = R_{M0}Q_0 + R_{P1}F_{P1} + R_S\left(F_{S1} + F_{S2} + F_{S3}\right) + R_{S4}F_{S4}$$

[4.7]

Where P_i is the inlet pressure and F_{Mi} is the flow rate in the main channel after the ith bifurcation.

We know the values of R_S and R_{M0}, so:

$$P_i = R_{M0}Q_0 + R_M\left(F_{M1} + F_{M2} + F_{M3}\right) + R_{end}F_{M4}$$

$$P_i = R_{M0}Q_0 + R_M\left(F_{M1} + F_{M2} + F_{M3}\right) + R_{P4}F_{P4} + R_{end}F_{S4}$$

$$P_i = R_{M0}Q_0 + R_M\left(F_{M1} + F_{M2}\right) + R_{P3}F_{P3} + R_S F_{S3} + R_{end}F_{S4}$$

$$P_i = R_{M0}Q_0 + R_M F_{M1} + R_{P2}F_{P2} + R_S\left(F_{S2} + F_{S3}\right) + R_{end}F_{S4}$$

$$P_i = R_{M0}Q_0 + R_{P1}F_{P1} + R_S\left(F_{S1} + F_{S2} + F_{S3}\right) + R_{end}F_{S4}$$

The system can be solved step by step to obtain the hydraulic resistances of the plasma channels as well as the resistance of the end channel:

$$R_{end} = \frac{1}{F_{M4}} \left[P_i - R_{M0}Q_0 - R_M \left(F_{M1} + F_{M2} + F_{M3} \right) \right]$$

$$R_{P4} = \frac{1}{F_{P4}} \left[P_i - R_{M0}Q_0 - R_M \left(F_{M1} + F_{M2} + F_{M3} \right) - \frac{F_{S4}}{F_{M4}} \left[P_i - R_{M0}Q_0 - R \left(F_{M1} + F_{M2} + F_{M3} \right) \right] \right]$$

$$R_{P3} = \frac{1}{F_{P3}} \left[P_i - R_{M0}Q_0 - R_M \left(F_{M1} + F_{M2} \right) - R_S F_{S3} - \frac{F_{S4}}{F_{M4}} \left[P_i - R_{M0}Q_0 - R \left(F_{M1} + F_{M2} + F_{M3} \right) \right] \right]$$

$$R_{P2} = \frac{1}{F_{P2}} \left[P_i - R_{M0}Q_0 - R_M \left(F_{M1} \right) - R_S \left(F_{S2} + F_{S3} \right) - \frac{F_{S4}}{F_{M4}} \left[P_i - R_{M0}Q_0 - R \left(F_{M1} + F_{M2} + F_{M3} \right) \right] \right]$$

$$R_{P1} = \frac{1}{F_{P1}} \left[P_i - R_{M0}Q_0 - R_S \left(F_{S1} + F_{S2} + F_{S3} \right) - \frac{F_{S4}}{F_{M4}} \left[P_i - R_{M0}Q_0 - R \left(F_{M1} + F_{M2} + F_{M3} \right) \right] \right]$$

[4.9]

This algorithm can be implemented and solved using the software package by Matlab[TM]. To get the length of the channels out of their resistance values, the Washburn law and Bahrami's expression are used for the pressure drop in a channel with a rectangular cross-section [5.14]:

$$L = \frac{\Delta P d^2 \varepsilon}{8 \mu U} = R d^3 w \frac{\varepsilon}{8 \mu}$$

[4.10]

With

$$\varepsilon = 2 \left[\frac{1}{3} - \frac{64d}{w \pi^5} \tanh \left(\frac{\pi w}{2d} \right) \right]$$

[4.11]

Where ΔP is the difference of pressure between the entrance and the exit of the channel, w is the width of the channel, d is the depth of the structure, μ is the viscosity of the liquid and U is the mean velocity of the liquid in the channel.

Finally, the length of the last cell channel and the length of the plasma channel are solved by using a set of input parameters. The list of parameters is given in Table 4.1 alongside their symbol, value and dimension.

Parameter	Parameter symbol	Value	Dimension
Pressure at the entrance	P_i	varying	Pa
Flow rate at the entrance	Q_0	$1.6.10^{-7}$	$m^3.s^{-1}$
Depth of the structure	d	20	μm
Length R_{M0}	L_{RM0}	2000	μm
Width R_{M0}	W_{RM0}	100	μm
Length side channel Rs	L_{RS}	varying	μm
Width side channel Rs	W_{RS}	80	μm
Length main channel sections	L_{RM}	varying	μm
Width Main channel section	W_{RM}	100	μm
Width plasma channels	W_{RP}	20	μm
Width end channels	W_{Rend}	100	μm
Viscosity of the fluid	μ	0.0012	Pa.s
Flow rate ratio	α	varying	-

Table 4. 1: List of parameters name, symbol, value and dimensions.

Table 4.1 shows the parameters of the computation. A number of parameters have been varied to study their influence on the length of the channels. The channel lengths resulting from the compilation for three characteristic parameter sets are presented in Table 4.2. In the two first cases, α is set to 0.1 which corresponds to a flow rate ratio ($1/\alpha$) of 10. The length of the main channels has to be greater or equal to 400μm to allow for the future integration of constriction before each bifurcation. The length of the side channel is arbitrarily set to 200μm in case 1 and doubled in case 2. The equality of the length of the side and main channel leads to a reduction in the plasma channel length span. In case 3 the flow rate ratio is set to 20, which results in larger plasma channel lengths as expected. These channel lengths can be manufactured. The end plasma and main channel lengths are set-up to a fixed value (here 1063 μm for α = 0.1).

	Case 1 $L_{Rs}(w)=200\mu m$ $L_{Rm}(w)=400\mu m$ $\alpha = 0.1$ P=11.05 MPa	Case 2 $L_{Rs}(w)=400\mu m$ $L_{Rm}(w)=400\mu m$ $\alpha = 0.1$ P=11.05 MPa	Case 3 $L_{Rs}(w)=200\mu m$ $L_{Rm}(w)=400\mu m$ $\alpha = 0.05$ P=11.05 MPa
L_{RP1}	1124	989	2574
L_{RP2}	912	781	2005
L_{RP3}	695	604	1409
L_{RP4}	478	478	787
L_{Rend}	1063	1063	528

Table 4. 2: This table presents the length of plasma channels and end channel for three different situations. The common parameters used are; Q0=2.77.10^{-9}m^3.s$^-$1; μ=1.2.10^{-3}. All the dimensions of the channel lengths are in microns.

4.3 Optimisation of the algorithm

4.3.1 Microfluidic platform and capillaries

In the results presented in the preceding section, only the structure of the chip has been taken into account for the calculation of the microfluidic performance of the device. The modeling fails to account for the microfluidic connectors linking the chip itself to the outside equipment such as the chip holder, or platform. The chip is indeed plugged to a chip holder. From the same platform, capillaries are branched to direct the fluids from the outlet to collecting Eppendorf tubes. This microfluidic manifold is shown in the schematic, Figure 4.4 and the photograph, Figure 4.5. The length of the fluidic path, which can be calculated by adding the length of each channel, microchannel and capillary section, is now taken into account.

These new parameters are introduced in the model. The algorithm is also slightly changed to set the lengths of the end plasma and main (cell outlet) channels and deduce the required length of the main channel segments (L_{RM}). Table 4.3 presents the new dimensions obtained when taking into account the extra length of the fluidic path off-chip.

		LRM0=6.6cm LRPend=9.6cm LRMend=6.6cm LRs=400 µm α = 0.1 P=341.6.10^6 Pa	LRM0=6.6 cm LRPend=9.6 cm LRMend=6.6 cm LRs=400 µm α = 0.1 P=399.10^6 Pa
L_{Rp1}		14520	85038
L_{Rp2}		14323	84940
L_{Rp3}		14158	84893
L_{Rp4}		14047	84909
L_{RM}		2714	4053

Table 4. 3: For P=341.6.10^6Pa, FRe=5mL/h; µ=1.2.10^{-3}Pa.s; α=0.1; Q_0=1.6.10^{-7}m³.s⁻¹. Channel lengths are expressed in microns.

The differences in the length of the plasma channels to be applied to get the same flow rate ratios at each bifurcation is not as large as in the previous example. In the first example of Table 4.2 with an ideal set-up, the mean size reduction between each channel is approximately 41% from one bifurcation to another. In Table 4.3 the mean size reduction is about 1.13%. Therefore it can be concluded that the external chip board and capillaries significantly attenuate the geometrical differences at each bifurcation.

4.3.2. Asymmetrical design

The same modeling methodology was applied in the case of a new design presented in Figure 4.8. The design cannot be considered as symmetric anymore. A new algorithm is therefore developed.
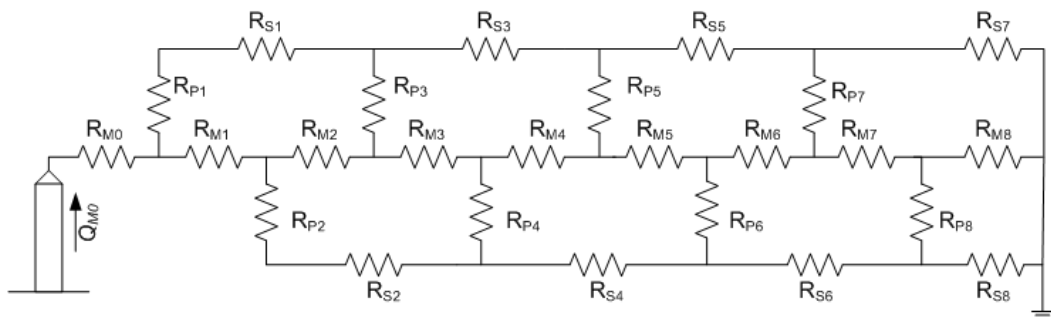
Figure 4. 8: The design comprising asymmetric branches. The number of plasma channels stays the same, but channel are not placed anymore in front of each other alongside the main channel.

At the entrance node the sum of the flow rates is now expressed as:

$$F_{P1} + F_{M1} = Q_0 \tag{4.12}$$

The introduction of α, the flow rate ratio provides the expressions of the main channel and plasma flow rates:

$$F_{M1} = \frac{Q_0}{\alpha + 1}$$

$$F_{P1} = \frac{\alpha Q_0}{\alpha + 1} \tag{4.13}$$

The recurrence relationship becomes:

$$F_{Mn} = \frac{Q_0}{(\alpha + 1)^n}$$

$$F_{Mn} = \frac{\alpha Q_0}{(\alpha + 1)^n} \tag{4.14}$$

The flow rates of the side channels become

$$F_{S1} = F_{P1} = \frac{\alpha Q_0}{\alpha + 1}$$

$$F_{S2} = F_{P2} = \frac{\alpha Q_0}{\alpha + 1} + \frac{\alpha Q_0}{(\alpha + 1)^2}$$

$$F_{S3} = F_{S1} + F_{P3} = \frac{\alpha Q_0}{\alpha + 1}\left[1 + \frac{1}{\alpha + 1} + \frac{1}{(\alpha + 1)^2}\right]$$

$$F_{S4} = F_{S2} + F_{P4} = \frac{\alpha Q_0}{\alpha + 1}\left[1 + \frac{1}{\alpha + 1} + \frac{1}{(\alpha + 1)^2}\right]$$

...

$$F_{Sn} = F_{Sn-1} + F_{Pn} = \frac{\alpha Q_0}{\alpha + 1}\left[1 + \frac{1}{\alpha + 1} + \frac{1}{(\alpha + 1)^2} + ... + \frac{1}{(\alpha + 1)^{n-1}}\right] = \frac{Q_0}{2}\left[1 - \frac{1}{(\alpha + 1)^n}\right] \tag{4.15}$$

There are now 9 different flow paths, resulting in a system of 9 relationships for the 8 different flow resistances of the plasma channels and of the back segments. The former algorithm can be easily adapted to this new configuration. Table 4.4 details the results for two different parameter settings with the new *asymmetric* configuration. To simplify, the external contribution is as follows: at the main entrance and cell outlet, channels are 66mm in length with a width of 100 μm; at the plasma outlet a channel is

90

chosen of 96mm in length with a width of 100μm. The 20μm depth in these channels is the same as in the whole structure. A example of a Matlab code for this part can be found in Appendix A.

In this new model the differences of plasma channel lengths to get a constant flow rate ratio exist but are not large compared to the total length of the channels. One can imagine keeping the same length to simplify the design. This situation will be highlighted in the numerical verification using CoventorWare.

	Case 1	Case 2
	Rs(L,w)=1000μm,80μm $\alpha = 0.1$ P=350MPa	Rs(L,w)=1000μm,80μm $\alpha = 0.05$ P=420MPa
L_{Rp1}	13695	92361
L_{Rp2}	15915	92692
L_{Rp3}	12352	89785
L_{Rp4}	15038	90150
L_{Rp5}	10911	87098
L_{Rp6}	14161	87501
L_{Rp7}	9390	84305
L_{Rp8}	13323	84749
L_{RM}	1949	2914

Table 4. 4: This table presents the length of plasma channels and end channel for three different situations. In every case P=15.104mPa, FRe=5mL/h; μ=10-3Pa.s. Channel lengths are expressed in microns.

4.4 Numerical verification & Network behaviour

4.4.1. Numerical verification

CoventorWare[TM] and in particular, its Architect Parametric Fluidics Library can be used to design and simulate microfluidic networks. Here we use CoventorWare[TM] mainly to

COVENTOR

DEPTH:20u

LENGTH_ENTRANCE:400u
LENGTH_MAIN:400u

LENGTH_COLLECT:400u
LENGTH_BLOOD_OUT:1000u

LENGTH_PLASMA_OUT:3000u
LENGTH_PLASMA_1:1619.6u
LENGTH_PLASMA_2:1457.34u
LENGTH_PLASMA_3:1331.98u
LENGTH_PLASMA_4:1252.54u

WIDTH_MAIN:100u
WIDTH_PLASMA:20u
WIDTH_COLLECT:80u
WIDTH_BLOOD_OUT:100u

WIDTH_PLASMA_OUT:100u

Collection Channel
d:DEPTH
length:LENGTH_COLLECT
width:WIDTH_COLLECT

Collection Channel
d:DEPTH
length:LENGTH_COLLECT
width:WIDTH_COLLECT

Collection Channel
d:DEPTH
length:LENGTH_COLLECT
width:WIDTH_COLLECT

Plasma Out Right
d:DEPTH
length:LENGTH_PLASMA_OUT
width:WIDTH_PLASMA_OUT

Plasma Channel
d:DEPTH
length:LENGTH_PLASMA_1
width:WIDTH_PLASMA

Plasma Channel
d:DEPTH
length:LENGTH_PLASMA_2
width:WIDTH_PLASMA

Plasma Channel
d:DEPTH
length:LENGTH_PLASMA_3
width:WIDTH_PLASMA

Plasma Channel
d:DEPTH
length:LENGTH_PLASMA_4
width:WIDTH_PLASMA

Entrance Channel
d:DEPTH
length:LENGTH_ENTRANCE
width:WIDTH_MAIN

Main Channel
d:DEPTH
length:LENGTH_MAIN
width:WIDTH_MAIN

Main Channel
d:DEPTH
length:LENGTH_MAIN
width:WIDTH_MAIN

Main Channel
d:DEPTH
length:LENGTH_MAIN
width:WIDTH_MAIN

Blood Out
d:DEPTH
length:LENGTH_BLOOD_OUT
width:WIDTH_BLOOD_OUT

flow_dc

dc_value:1.39m

width:WIDTH_PLASMA
length:LENGTH_PLASMA_1
d:DEPTH

Plasma Channel

width:WIDTH_PLASMA
length:LENGTH_PLASMA_2
d:DEPTH

Plasma Channel

width:WIDTH_PLASMA
length:LENGTH_PLASMA_3
d:DEPTH

Plasma Channel

width:WIDTH_PLASMA
length:LENGTH_PLASMA_4
d:DEPTH

Plasma Channel

Reservoir

P = 0

Collection Channel
d:DEPTH
length:LENGTH_COLLECT
width:WIDTH_COLLECT

Collection Channel
d:DEPTH
length:LENGTH_COLLECT
width:WIDTH_COLLECT

Collection Channel
d:DEPTH
length:LENGTH_COLLECT
width:WIDTH_COLLECT

Plasma Out Left
d:DEPTH
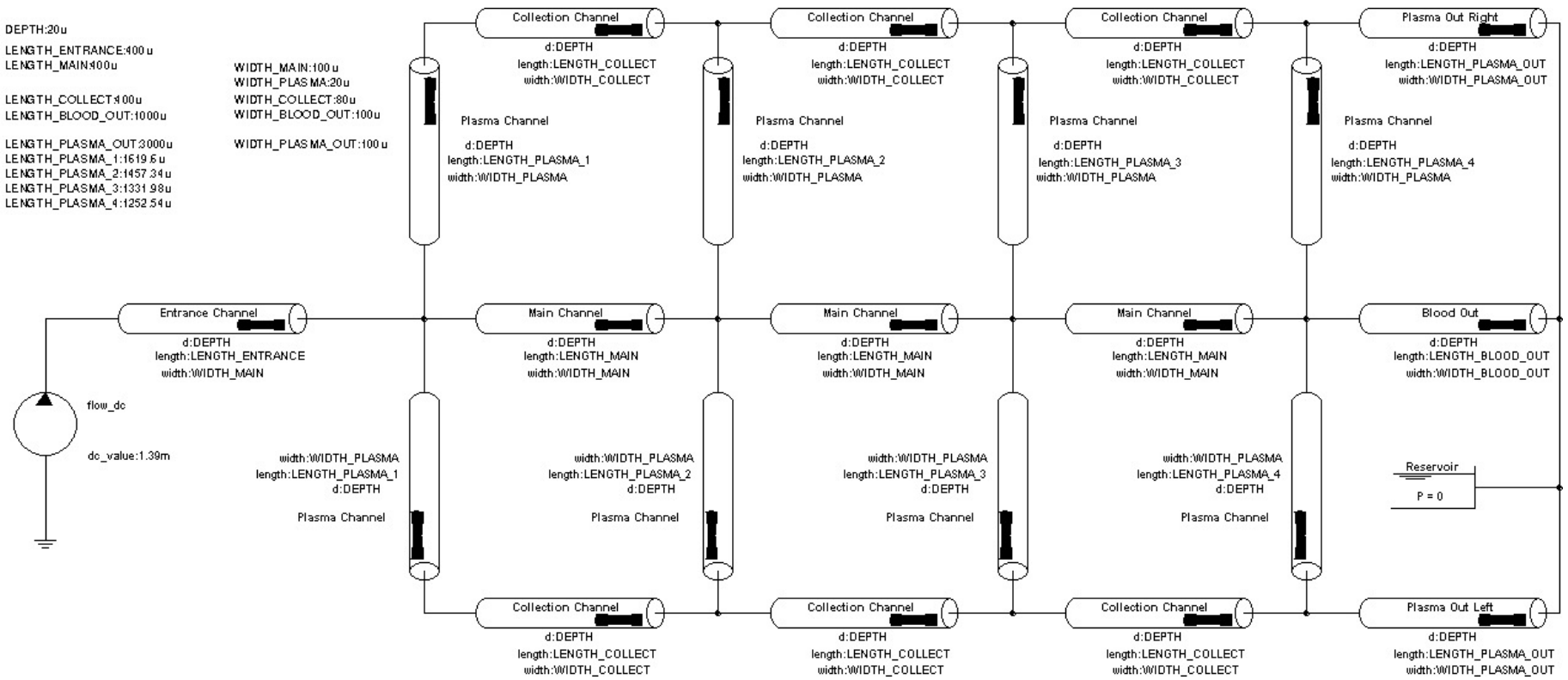length:LENGTH_PLASMA_OUT
width:WIDTH_PLASMA_OUT

Figure 4. 9: CoventorWare™ model for the symmetrical configuration built using the Architect SaberSketch Schematic Editor, with the collaboration of David Bease..

92

verify the analytical solution. The channel lengths, outputs of the analytical solution are used as parameters in the model of the software package.

The circuit is broken down into very simple straight channel elements, as no other passive or active component is present in the network. The network is composed of an assemblage of straight segments. At each bifurcation there is a corresponding node. In this model, to verify the algorithm calculated in Matlab, we consider just 4 channels on each side of the main channel.

The same assumptions have been made for the numerical model in CoventorWare as for the analytical development. The model is a flow-rate driven system. This model is based on the assumption that the outlets wells are at a pressure nil and room temperature. The cross-sections are assumed to have assuming perfectly rectangular shapes with the general etch depth of 20μm throughout the structure.

A schematic is created using the Saber tool of CoventorWare^{TM}. The hydrodynamic source at the start of the network is a constant flow rate source. At the end of the two plasma and the cell branches a hydraulic reservoir with a pressure of zero is set. The rest of the fluidic elements are all passive components. This model is shown in Figure 4.9.

The validity of the analytical approach can be studied by comparing the flow rate obtained at each bifurcation in each case. Figure 4.10 shows a close match between the flow rate obtained through the analytical development and obtained in the numerical analysis. In the same figure, the Bahrami's fluidic resistance equation is compared to the more common Bruus' resistance. Fluidic resistance equation is used to obtain the plasma channel lengths which build the numerical model. The use of the Bahrami's resistance shows a better fit with the analytical model.
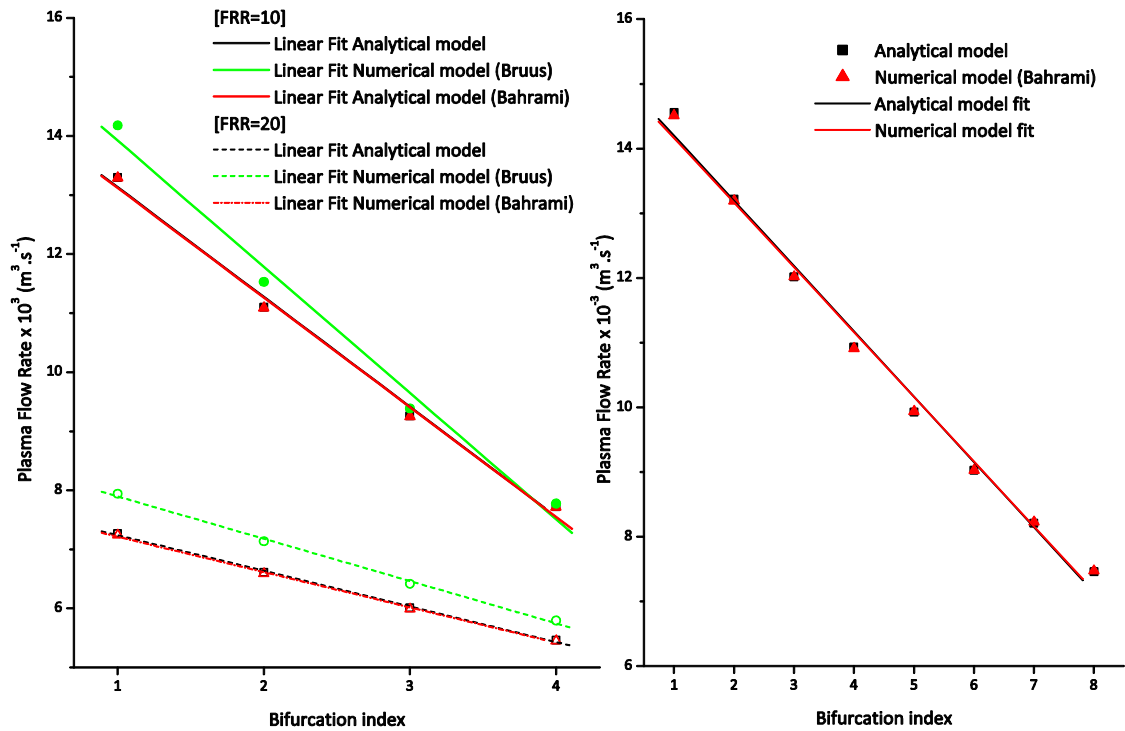
Figure 4. 10: Comparisons between the analytical and numerical computation for the Bahrami and Bruus resistance. The graph shows the flow rate in the plasma channels at each bifurcation versus channel index.

CoventorWare model validates the analytical development and can also be used on its own to optimize a given design.

4.4.2. Network behaviour

Particularities of the network behaviour are investigated using the Coventor model. The influence of the entrance parameters is studied. As expected, flow rate ratios are independent of the entrance flow rate as illustrated in Figure 4.11. More generally flow rate ratios are independent of all entrance parameters such as the width and length of the entrance channel.

Having validated the analytical model, the parameters from this model are used as input parameters for the CoventorWare[TM] model. "External" parameters such as the entrance and outlet channels lengths, or entrance flow rate are then modified. The internal geometry of the chip cannot be changed but external capillaries can be plugged into the inlet and outlets or the entrance flow rate can be changed. Therefore, by varying these external parameters, we can study the *response* of the performance the network, notably, the changes in flow rate ratios at each bifurcation.

Figure 4. 11: Comparison of flow rate ratios for different entrance flow rates (numerical results). This graph shows the flow rates and flow rate ratios of the system for two cases versus the bifurcation index. Flow rate ratio are the same in both cases as shown in the figure on the right.

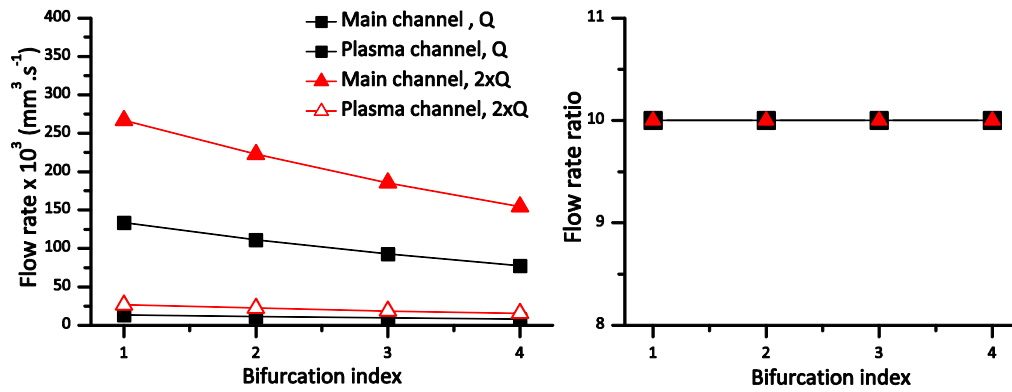To start with, the influence on the cell and plasma outlets, of the lengths of the end channels, in fact, any capillaries plugged to the outlets. These output lengths are doubled and quadrupled onto two different Coventor models for two different values of the initial flow rate ratio, FRR. The first model is the symmetrical, and chip isolated model presented in the first part and the second model more realistic model takes into account the chip board. Figure 4.12 shows the main channels and plasma channels flow rates at each bifurcation as well as the corresponding flow rate ratios (FRR) for two values of an initial FRR of 10 on the chip and platform model and chip only. In every case but the control (normal output length, first network diagram), a rapid decrease of the flow rate ratio is observed. A greater decrease is witnessed in when the chip is isolated. It can be concluded that any capillaries or other devices plugged downstream the system will greatly affect the performance of the chip itself.

The situation worsens with a larger flow rate ratio. Figure 4.13 shows the flow rates and flow rate ratios for an initial FRR of 20. The separation efficiency being theoretically coupled with the flow rate ratio, the system efficiency is therefore dependent on the downstream microfluidic network. The continuous separation system is meant to be part of a modular system that incorporates further microfluidic modules downstream. The strong dependence of the separation efficiency on downstream device eventually means that a downstream system of valves and reservoirs will be needed to restore the initial flow rate ratio.

Figure 4. 12: Influence of the external microfluidic devices on the internal flow rate ratios at an initial FRR=10. These graphs illustrate the flow rates of the main and plasma channels and the corresponding flow rate ratios at each bifurcation. The diagrams are obtained using the parameters given by the analytical computation in the CoventorWare™ model. Two models are used, the first one is the real model with the chip embedded on the board (left column), the second is the ideal chip on its own (right column). For each of these models, the outlet lengths are multiplied by two (in red on second inset diagram) and four (in green on third inset diagram).
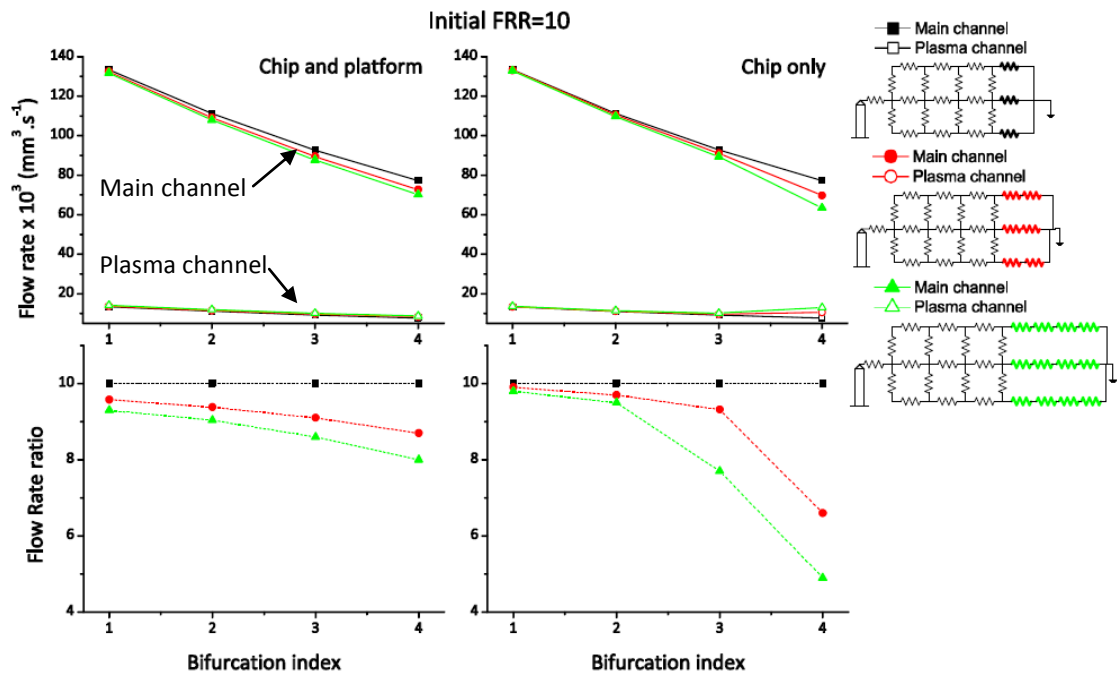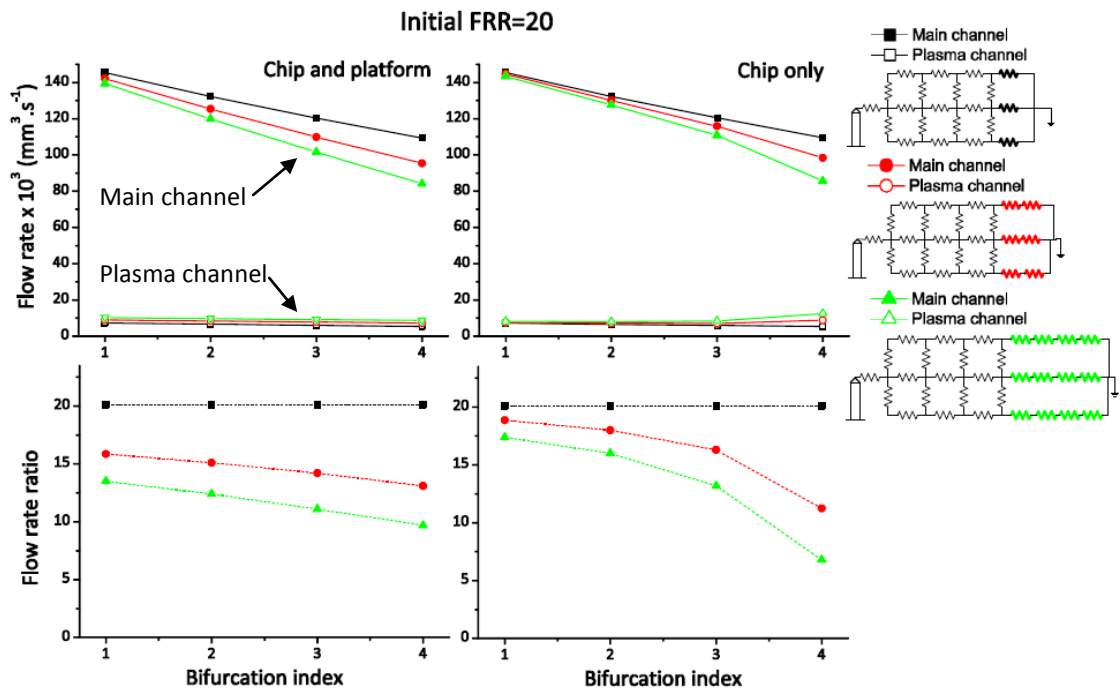

Figure 4. 13: Influence of the external microfluidic circuitry on the internal flow rate ratios at an initial FRR=20. This graph illustrates the flow rates of the main and plasma channels and the corresponding flow rate ratios at each

bifurcation. Two models are used, the first one is real life model with the chip embedded on the board, the second is the ideal chip on its own. For each of these models, the outlet lengths are multiplied by two (red curves) and four (green curves).

Alternatively the flow rate ratios can be tuned by externally adapting the output lengths. We define an Outlet Length Ratio, OLR as :

$$OLR = \frac{L_{RMend}}{L_{RPend}}$$ [4.6]

Where LRMend and LRPend are the lengths of the output lengths on the main channel and plasma channel, respectively. In the optimised symetrical model designed with an initial FRR of 10, the attainement of a FRR of 20 from the first bifurcation necessitates an OLR of at least 10. However an OLR of 10 set-up a back flow in the fourth and last channel (FP4=-0.3123) as illustrated in Table 4.5. Although an OLR of 9 provides a FRR of 19.8 at the first bifurcation, and a positive flow rate in the fourth and last bifurcation the flow rate is really small in the last channels. Clearly from the table, the rise in the FRR is not directly proportional to the rise in the corresponding OLR, it is therefore hard to predict during the experiment the consequence of additional pieces of tubing being plugged to the device. The design methodology outlined above therefoare helps in predicting quickly the performance the overall system when additional microfluidic circuitry is used to complete the microfluidic device.

In conclusion, it is possible to vary the outlet lengths in order to tune the inner flow rate ratio at each bifurcations. However, the technique has its limitations as an increase in the outlet length reduces the flow rate in the last channels.

4.4.3. Pull mode as an alternative strategy to influence the internal flow rate ratio

Using two syringe pumps to pull the fluids out of the outlets instead of injecting the fluid through the single inlet (the push mode operation) is a practical, direct and flexible way to externally manipulate the internal flow rate ratios. This configuration, there onwards defined as the pull mode operation is shown in Table 4.6 (last row). The manipulation of the output length ratio, OLR, finds its limits when the flow rate of the last channels reaches zero and eventually becomes negative creating a back flow. Table 4.6 compares the three methods to influence the flow rate ratios once the chip is

	Main flow rate	Channel flow rate	Flow rate ratio
OLR 1.45	133.4	13.3	10
	111.2	11.1	10
	92.67	9.257	10
	77.23	7.72	10
OLR 2	135.5	12.22	11.1
	115.6	9.955	11.6
	99.62	8.01	12.4
	86.97	6.324	13.8
OLR 9	145.3	7.333	19.8
	135.7	4.801	28.26
	130.9	2.389	54.79
	130.9	0.0181	723.20
OLR 10	145.8	7.077	20.6
	136.8	4.531	30.2
	132.6	2.095	63.3
	133.2	-0.3123	N.A.

Table 4. 5: Comparison of the main channel and plasma channels flow rates, and flow rate ratios at each bifurcation in the optimised symmetrical model for an initial FRR=10.

manufactured: the tuning of (1) the outlet length ratios in the push mode, (2) the outlet widths ratios in the push mode and (3) the external flow rate ratios in the case of the pull mode. The figures of comparison chosen are the rounded values of the ratios at which a backflow is introduced in the system and the values for which the FRR is doubled at the first bifurcation. From Table 4.6, it is impossible with the variation of the OLR to get a doubling of the FRR without having a backflow in the system. When varying the OWR it is possible to go far beyond a doubling of the FRR without having a back flow. The flow rates in the last plasma channels can be very slow however. Finally the last solution provides the easiest solution for the doubling of the FRR at the first bifurcation; the solution is however at the expense of rapidly decaying flow rates in the plasma channels.

Way to externally influence the internal flow rate ratios at each bifurcation	Value from which a backflow is introduced in the system	Value from which the first bifurcation FRR is doubled (from 10 to 20)	Parts of the design which varies
Outlet lengths ratio $$OLR = \frac{L_{RM_{end}}}{L_{RP_{end}}}$$	10	9	
Outlet width ratio $$OWR = \frac{W_{RM_{end}}}{W_{RP_{end}}}$$	6	10	
Pull Mode - External flow rate ratio $$ExtFRR = \frac{F_{M_{end}}}{F_{P_{end}}}$$	5	5	

Table 4. 6: Comparison between the different strategies of externally tuning the internal flow rate ratios in the chip. All the calculations are based on the optimised symmetrical model with an initial FRR=10.

In conclusion, the separation efficiencies, directly linked with the flow rate ratios, are highly dependent on the network downstream in the separation module.

CoventorWare[TM] can be used as a useful tool to model these types of passive microfluidic networks. The software can also directly be used to optimise the performance of the system and provide guidance over the safe usage of the device.

4.5 Discussion

High-level system modelling provides a system-oriented technique which can take into account the operation of complex networks. In this study an algorithm to calculate the geometries of a microfluidic network for passive blood separation has been demonstrated. The model is still incomplete due to the blood particulate behaviour, a feature absent from the modelling. However, the blood to be used in the device may be substantially diluted (up to 1:20). Therefore a Newtonian model may hold in certain cases. A numerical model of this network was subsequently built using the software package CoventorWare to (i) verify the validity of the analytical approach, (ii) and take into account subsequent changes to fluid path appearing during the experimental set-

up and/or device operation after the chip has been manufactured. Nevertheless the model helps setting the correct flow rate ratios at each bifurcation and also allows to assess changes in geometry and behaviour of the entire system.

The model is only valid for the analysis of simplex or complex microfluidic networks operated at low Reynolds number where the Hagen-Poiseuille law can be applied. In this model the viscosity is also independent of the flow rate ratios. The technique developed is simple and versatile. The strategy presented in this article is valid for any number of plasma branches. Zweifach-Fung law states that if a flow rate ratio better than 2.5 is achieved 100% separation can be achieved. However, very little has been written about the kind of geometries used, only that the size of the channel has to be comparable to the size of a cell. Therefore 100% efficiency is not guaranteed by these simulations. Nevertheless, the modeling ensures a precise control of the flow rate within the system and guidance over the limits to which the system can be used.

The flow rate ratios have been shown to be independent of the entrance flow rate and the geometries of the entrance. In general, it was demonstrated that the flow rate ratios (in a push mode) are independent from any entrance parameter. It is worth noting that in this model the viscosity is also independent from the flow rate ratios.

Once the chip has been manufactured, it is still possible to influence the internal flow rate ratios at each bifurcation by careful manipulation of the *external parameters*. It was demonstrated that *back capillaries* decrease the flow rate ratio, at the expense of the separation efficiency. The longer these capillaries are, the more the flow rate ratio decreases. This effect accounts also for the negative backflows found in the last plasma channels. However, back capillaries can also increase the separation ratio if the length of the plasma channel is larger than the length of the cell channel. Holistically, the design of a complete continuous separation system in-line with other modules, will require a separation module that can be operated independently of the further modules downstream independent will have to be developed. This can be achieved by a system of valves and reservoirs. In total, three external means of acting on the internal FRR have been simulated: output length ratios (OLR), Output Widths Ratio (OWR) and the External Flow Rate Ratio (ExtFRR). Amongst these, the last one is the

more direct and practical solution, albeit at the additional cost of additional valves or reservoirs.

No blood damage modeling has been carried out in this present work. Reasonable flow rates (<20mL.h^{-1}) should be used within the system to avoid dangerous shear rates leading to hemolysis.

4.6 Conclusions

In this chapter a modelling methodology to optimise the geometry of a microfluidic network for maximum separation efficiency of plasma from blood has been described. The analytical study permits to define the correct plasma channel lengths to get a constant flow rate ratio at each bifurcation, allowing for a more stable and reliable separation throughout the system. The analytical results were confirmed by the use of a numerical analysis tool, CoventorWare^{TM}. Subsequently, CoventorWare^{TM} was used on its own to highlight the general network behaviour and provide useful guidance over the use of such systems. It was further demonstrated that additional capillaries plugged at the back of the device can have a dramatic impact on the microfluidic chip separation efficiency. Generally, the separation device, as part of a modular system, can only be reliable if independent from downstream modules. Therefore a system of valves and reservoirs will have to be used to isolate this separation module from the rest of the system if a fully lab-on-chip system, as defined in chapter 1 is to be manufactured.

An experimental study will have to confirm the results of the analytical and numerical study. To check for the flow rate in each bifurcating channels, it is suggested that Particle Image Velocimetry (P.I.V.) could be used. Two attempts at developing a PIV study are described in Chapter 8. The method developed in this study is applicable to many other microfluidic systems, sustaining a large range of different activities. Useful future developments include the implementation of a Non-Newtonian approach and a change of the blood viscosity along the network as more and more plasma is being directed to the plasma channels.

4.7 References

[4.1] P. Dantan and M. Faye, *Numerical simulations of Thixotropic Fluids*, Proceedings of the Comsol Users Conference (2006)

[4.2] D, Trebotich W. Chang, and D. Lipemann, *Modelling of blood flow in simple microchannels*, Proc. Modelling and Simulation of Microystems, 218-222 (2001)

[4.3] K. Tsubota, S. Wada, H. Kamada, Y. Kitagawa, R. Lima and T. Yamaguchi, *A Particle Method for Blood Flow Simulation*, Application *to Flowing Red Blood Cells and Platelets*, J. of the Earth Simul., **5**, 2-7 (2006)

[4.4] J.O. Barber, J.P. Alberding, J.M. Restrepo, T.W. Secomb, *Simulated Two-dimensional Red Blood Cell Motion, Deformation, and Partitioning in Microvessel Bifurcations*, Annals of Biomedical Engineering, **36**, 1690-1698 (2008)

[4.5] M. Abkarian and A. Viallat, *Vesicles and red blood cells in shear flow,* Soft Matter, **4**, 653-657 (2008)

[4.6] J. Berthier, P. Silberzan, *Microfluidics for Biotechnology*, Micromechanical systems series, Artech House Publishers (2005)

[4.7] H. Bruus lecture notes, *Theoretical Microfluidics*, Oxford Master Series in Physics, Oxford University Press (2007)

[4.8] A. Ajdari, *Steady flows in networks of microfluidic channels: building on the analogy with electrical circuits*, C. R. Physique, **5** (2004)

[4.9] R. Zengerle and C. Cupelli, *Methods of Microfluidic Design and Analysis I*, lecture notes, www.imtek.de, last accessed, May 2009

[4.10] M. Kersaudy-Kerhoas, R.S. Dhariwal, M.P.Y. Desmulliez, *Blood flow separation in microfluidic channels*, Proceedings of the first European Conference on Microfluidics (2008)

[4.11] M. Faivre, M. Abkarian, K. Bickraj K, *Geometrical focusing of cells in a Microfluidic device: An approach to separate blood plasma*, Biorheology, **43**, 147-159 (2006)

[4.12] Pietrabissa, A lumped parameter model to evaluate the fluid dynamics of different coronary bypasses, Medical Engineering and Physics, **18**, 477-484 (1996)

[4.13] J. Berthier, F. Rivera, P. Caillat and F. Berger, *Dimensioning of a New Micro-Needle for the Dispense of Drugs in Tumors and Cell Clusters*, Technical Proceedings of the NSTI Nanotechnology Conference and Trade Show (2003)

[4.14] M. Bahrami, M.M. Yovanovich, J.R. Culham, *A novel solution for pressure drop in singly connected microchannels of arbitrary cross-section,* International Journal of Heat and Mass Transfer, **50**, 2492–2502 (2007)

Chapter 5: Manufacturing routes and experimental set-ups

5.1 Introduction

The blood plasma separator is a versatile module aimed at producing high-speed and high-efficiency plasma separation to compete with conventional plasma extraction or CD-like platforms. The industrially-oriented product should therefore be manufactured using cheap material and low-cost techniques. To this end, different manufacturing methods have been implemented to decide on the best competitive one.

The performance of the system is governed by the ratios of the channels widths and the length of the constrictions. The different designs present a number of engineering challenges such as tight arrays of relatively small channels and sharp edges. The designs provide a base for testing several manufacturing methods.

The industrially-oriented product should have a set of desirable characteristic features such as: use of cheap biocompatible material and low-cost manufacturing techniques which allow rapid-prototyping. In this respect, different methods have been investigated and experimented upon the designs to determine the best one. The challenge of the microfluidic chips manufacturing lies in the balance between the dimensional accuracy needed and the fast manufacturing response.

The first part of this Chapter presents three different manufacturing routes taken by three different institutions to fabricate the microfluidic blood plasma separation system. Although the actual fabrication of the prototypes was carried out by other institutions, the following discussion and comparison of the results of these three different manufacturing approaches is original.

In the second part the experimental set-up will be discussed in detail with an explanation of the major difficulties experienced.

5.2 Manufacturing routes

5.2.1. Lamination

Lamination is one of the 3D-Mintegration manufacturing philosophies as it permits the creation of truly 3D structures. Manufacturing layer by layer was undertaken with an EnvisioTEC Perfactory[3] [TM] machine at the Cambridge Institute for Manufacturing [5.1]. As in a stereo-photolithographic process, the machine optically cures layers of liquid polymer. However, in the perfactory system the polymer is cured by means of a Digital Light Processing (DLP) projector from underneath the basin while the part is raised above the liquid polymer. The only material compatible with the process at the time was orange methalycrate. Figure 5.1 presents a cross-section view of the Envisotech Perfactory system. The main advantage of this technique is the speed of the process and the small footprint of the machine. The time response from the production of a design to the prototype is approximately one day and depends on the size of the device.
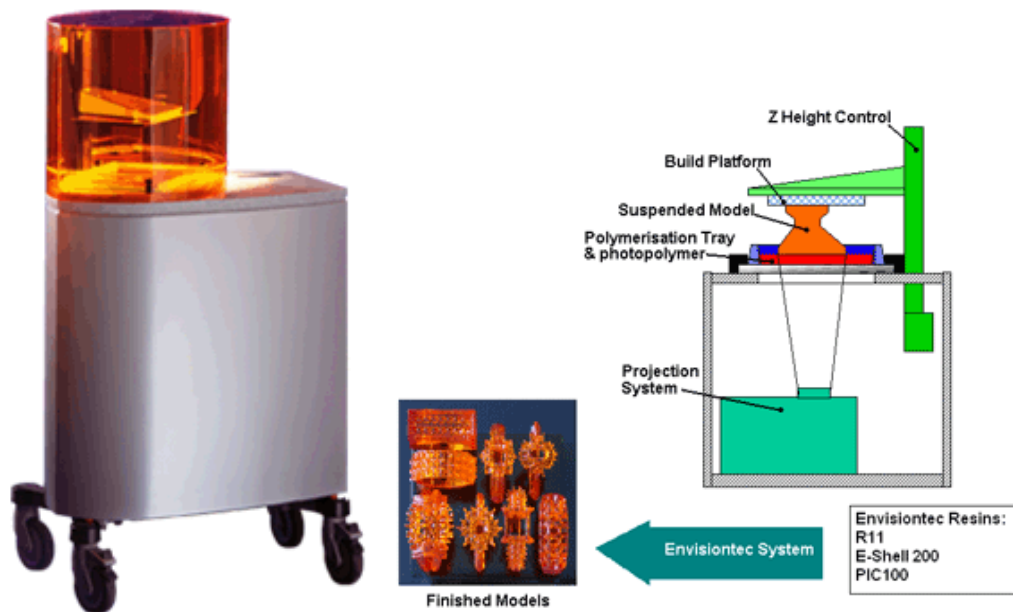

Figure 5. 1: Photograph of an EnvioTEC machine and cross-section view of the workbench [5.1]

A prototype has been manufactured layer by layer in methalycrate by such a machine. A photograph of some prototypes is shown in Figure 5.2. Various fabrication inclinations were tested from horizontal to vertical with angles of 0°, 10° and 20° to test the process capabilities of this manufacturing technology. Detailed scans showed that channels were either of a U- or V-shape. The roughness, Ra, varied from 170 to

570 nm. The horizontal inclination showed the best results. Although all samples showed acceptable shape for the main channels and the constriction, the definition of the plasma channels was poor as shown in Figure 5.3a, In figure 5.3b a section of the channel is shown when viewed with a white light interferometer. The channel widths were in general larger than expected. These prototypes were therefore not considered for testing.
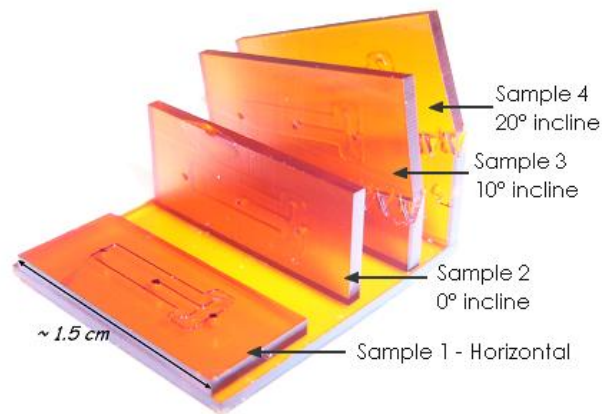
Figure 5. 2: Photograph of four samples with different manufacturing orientations. (Photograph Courtesy of Cambridge University)
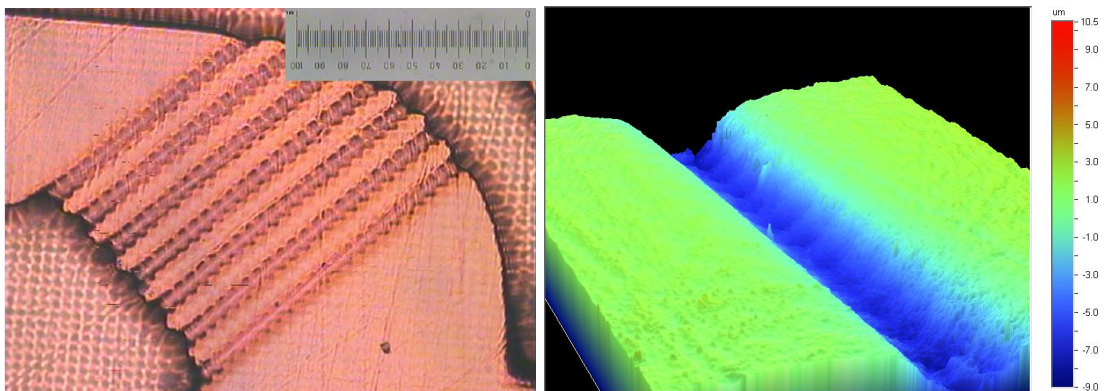
Figure 5. 3: (a)Microscope view of the device (b)White light interferometer view of a main channel. Photographs: Courtesy of Cambridge University

In conclusion, although the lamination fabrication route offers an excellent response time of a day or less, the technique was not applicable to our prototype. Nevertheless, lamination using the EnvisoTEC prototyping machine could be satisfactorily undertaken for a microfluidic device with structures in the x and y directions larger than 100µm.

5.2.2 Micro-injection moulding

Microinjection moulding was considered at Cranfield University on a Battenfeld Microsystem machine to study the mass-manufacturability of the microfluidic system. Microinjection moulding is a fast replication method for the high volume production of polymeric parts. Micron-size features can be easily replicated in polymer and thus the precision depends on the mould itself. This mould has to be micro-milled. This preliminary step can hamper the rapid prototyping of components with this technique. Figure 5.4 presents the different steps involved in the preparation of microinjection moulded plastic parts.
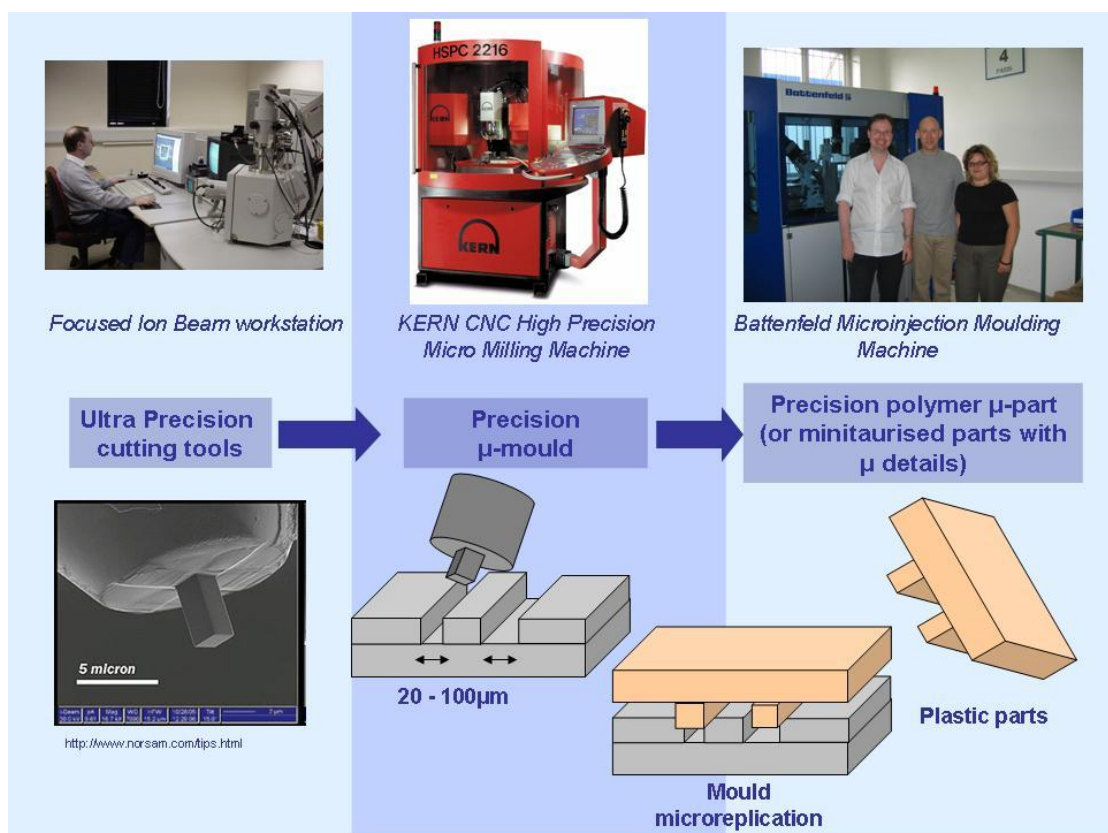
Figure 5. 4: Microinjection moulding process flow. Courtesy of Cranfield University

After a preliminary study, the manufacturing of the prototype using microinjection moulding has been abandoned because of the difficulties in creating a metallic mould for the specific component geometries. Indeed, sharp edges and tight small channel arrays as shown in Figure 5.5 cannot be milled by the currently available tools. Thus, the limits of micromilling have been reached in this particular design. In this example, the use of microinjection moulding is hampered by the preliminary milling step in the mould fabrication.

Figure 5. 5: Schematic of the challenging parts in the design

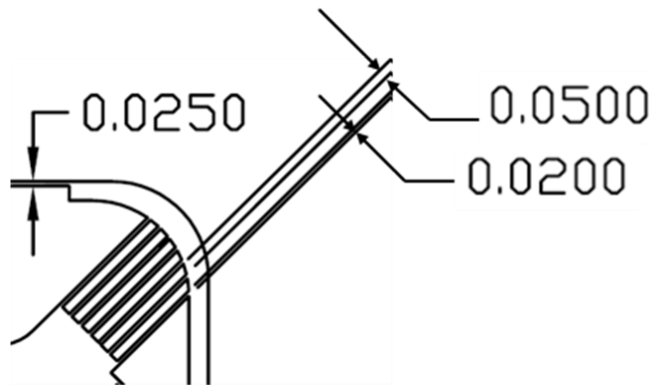| Micromilling	
200-300µm slots	Ok and safe
100µm slots	OK but needs further investigation
20-30µm slots	Under development but not close to application bespoke tools for micromilling

Table 5. 1: Summary of the challenging parts in the design

Microinjection moulding is a powerful high volume microfabrication technique [5.2]. However, due to the lengthy preparation of the tool and mould necessary for the replication, this technique was found to be unsuitable for our prototypes. However microinjection moulding is undoubtedly very useful for the manufacturing microfluidic parts at high production volume given that these parts have been carefully designed such as to accommodate the technique's desirable features.

5.2.3 Industrial photolithographic solution

An industrial collaboration with Epigem Ltd., Redcar, UK lead to the rapid production of microfluidic chips [5.3]. At Epigem, conventional photolithographic technique is a cost-effective technique for the production of low and high numbers of components. The epoxy based negative photoresist SU8 is Epigem's material of choice for the manufacturing of microfluidic chips. Among the reasons to use SU8 are its biocompatibility and the fact that high aspect ratios can be achieved with this material. Polydimethyloxane (PDMS) is another useful and flexible polymer with extremely simple processing capabilities. However, SU8 offers the advantage of highly defined, rigid and non-permeable channels unlike PDMS. Although widely used in microfluidics

prototyping, results using PDMS have been found to be unreliable and therefore not applicable to commercial chips [5.4].
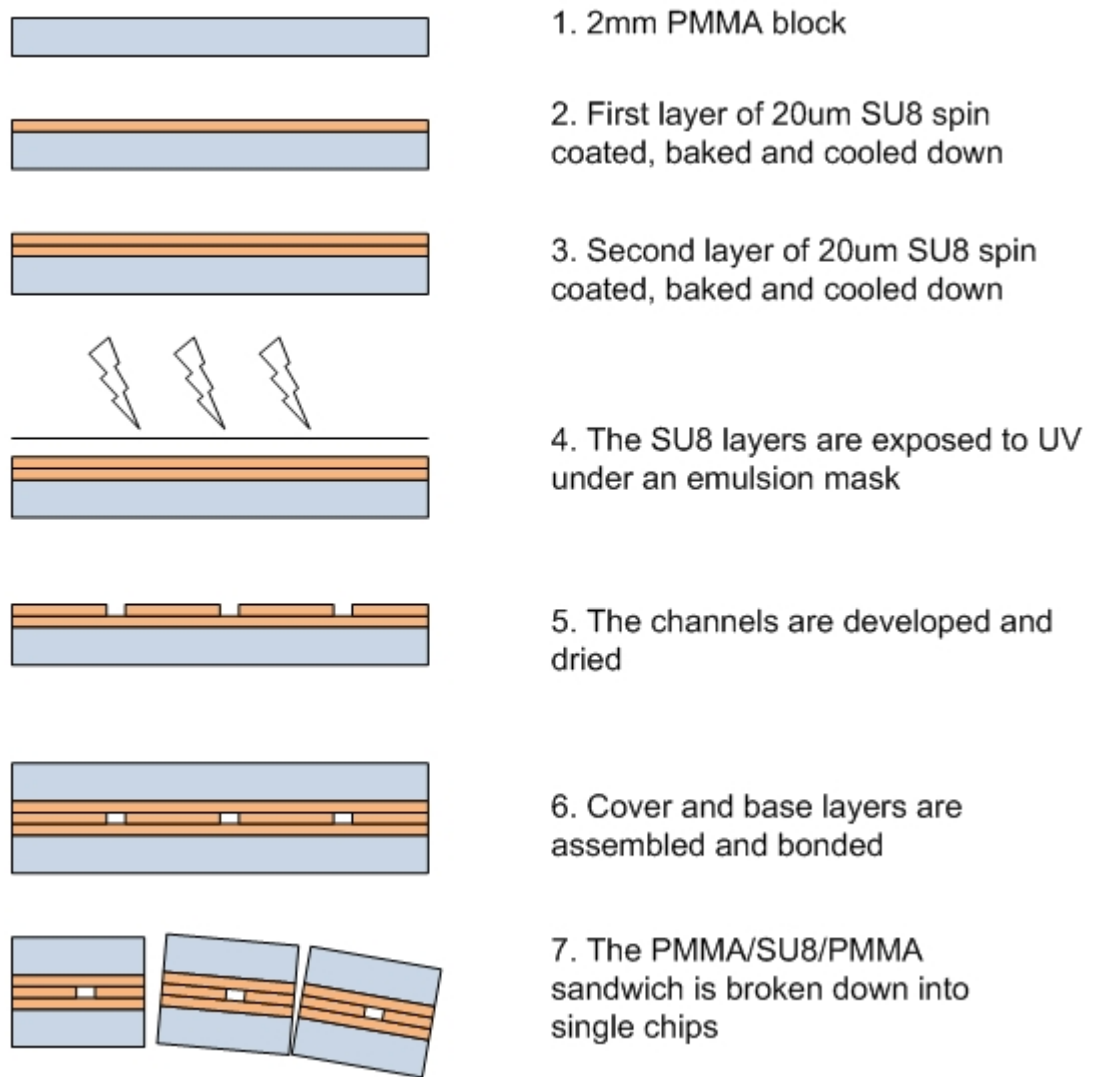
Design of masks for photolithography was carried out using AutoCAD (Autodesk Inc, USA). Electronic files of the masks were directly sent to Epigem in .dxf format. The masks were produced directly on-site at Epigem Ltd.
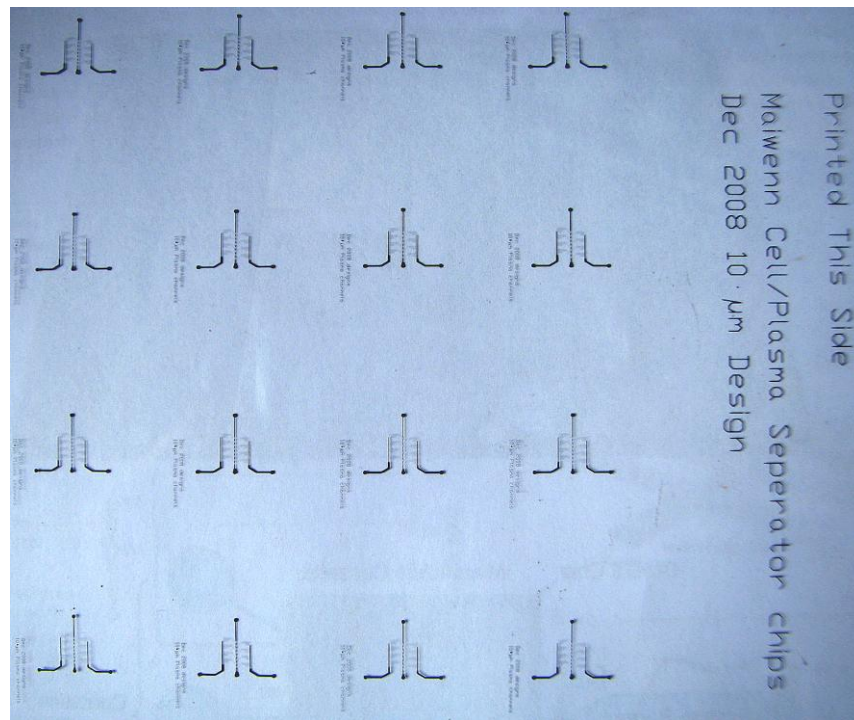
Figure 5. 6: Photograph of the acetate mask used by Epigem to manufacture the blood plasma separation chip.

For this separator device, a lid and base layer are produced in order to create the bonded chip laminate. The lid and the cover layers are composed of PMMA layers and a thin layer of SU8. The channel features are defined by the photolithography of an additional layer of SU8. Since the chips consist of several sandwiched layers of the negative photoresist SU8, thus ensures a "whole SU8" channel network. Having the same material on all four walls, helps to obtain better control and repeatability of the process. Layers are subsequently cleaned and layered together in bonding jigs, loaded and heated for a predetermined time period. The laminate is then chopped up into separate chips.   Figure 5.7 presents the main steps of the fabrication process flow.

1. 2mm PMMA block

2. First layer of 20um SU8 spin coated, baked and cooled down

3. Second layer of 20um SU8 spin coated, baked and cooled down

4. The SU8 layers are exposed to UV under an emulsion mask

5. The channels are developed and dried

6. Cover and base layers are assembled and bonded

7. The PMMA/SU8/PMMA sandwich is broken down into single chips

Figure 5. 7: Fabrication process flow for the microfluidic chips

Since the chip footprint is small (18mm x 23mm) a generic platform using the patented Fluence ferrule system presented in Figure 5.8 was also made from an assembly of PMMA and SU8. This system is used as a holder featuring standard microfluidic connections (Cheminert) as shown in Figure 5.9b.
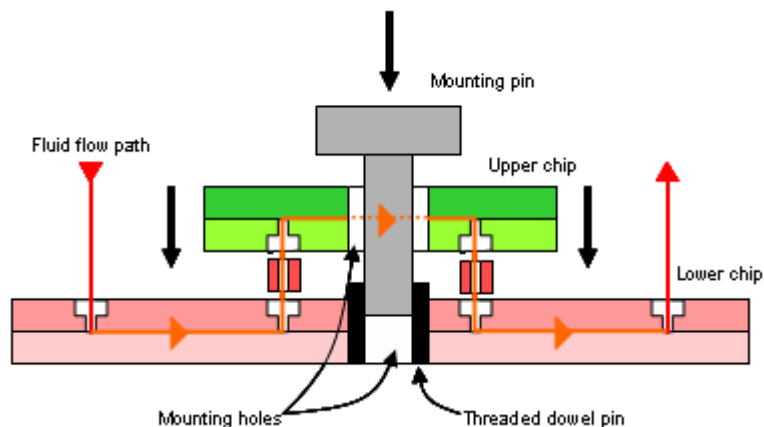
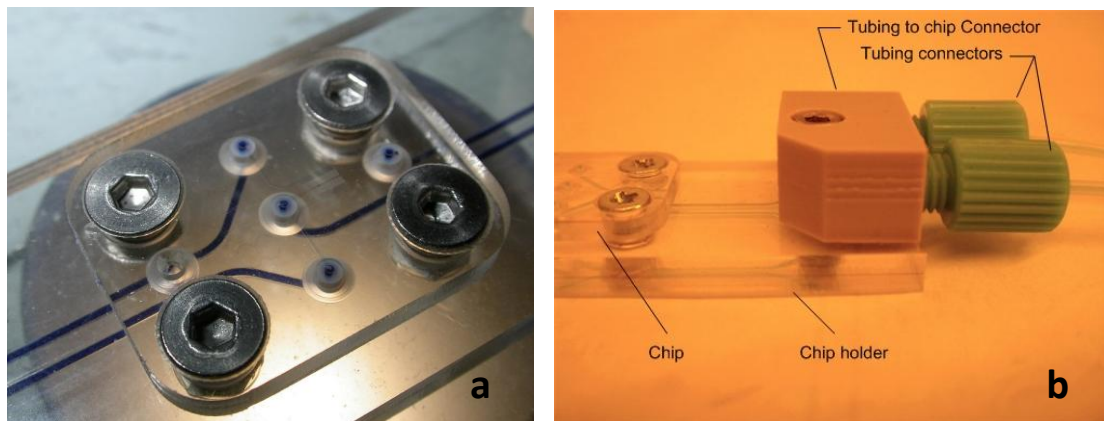*Figure 5. 8: Illustration of the assembly technique of Epigem chip and breadboard, Courtesy of Epigem.*

Figure 5. 9: Photographs of the microfluidic chips manufactured by Epigem. (a) Microfluidic chip filled with blue ink sitting on a chip holder. (b) Close-up view of the thin channels microfluidic network.

For analysis purposes a chip was cut in half along the main channel using a diamond saw. The cross-section obtained was observed and the geometries measured using a USB microscope (DinoLite, big C, USA). As shown in Figure 5.10 (a) and (b), the channels are well-defined and within 5% of the required dimensions (side channels 20x20μm).
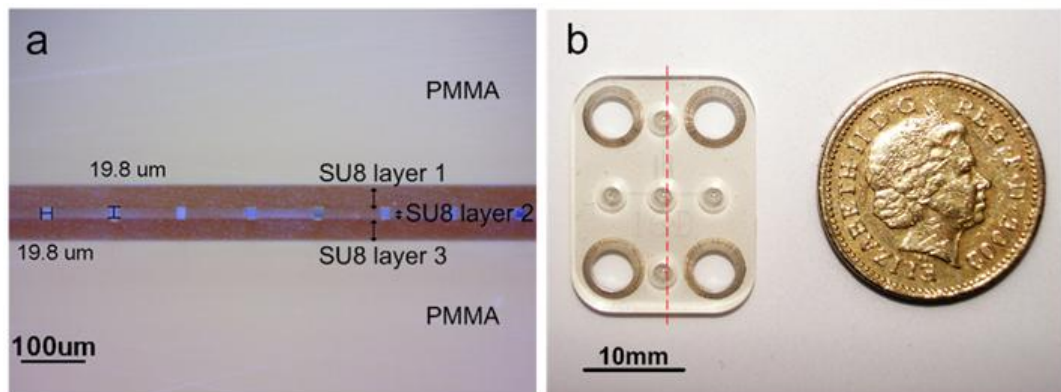
Figure 5. 10: Microfluidic chip. (a)Cross-section view of the chip assembly. (b) Top view of a chip next to a British one pound coin. The red line corresponds to the cross-section in (a)

The manufacturing route followed by Epigem is an established process. Sixteen chips with different geometrical variations were produced and mounted on microfluidic holders for testing. The chips were tested and no leakages were spotted. The channels are well defined and the roughness is very low. As compared to the first lamination technique presented, the manufacturing of the chips requires the fabrication of

photomasks after the design of the prototype. The response delay to changes is estimated at 1 to 2 weeks.

5.2.4 Conclusions

Three different manufacturing techniques for a particular design were tested. In this section, the advantages and drawbacks arising from these techniques are discussed in the form of a summary table.

	Possibility of:				Response time from design to product-ion	Cost for low volume	Cost for high volume
	using bio compatible material	inserting dense arrays	inserting narrow channels (<20 μm)	inserting sharp edges			
Layer by layer manufacturing	yes	medium	low	medium	1 day	low	medium
Microinjection moulding	yes	low	medium	low	1 week	medium	low
Lithographic lamination method	yes	high	high	high	1-2 weeks	low	low

Table 5. 2: Summary of the fabrication methods

Although all the proposed techniques allow the manipulation of cheap and biocompatible material, the photolithographic lamination method is the only manufacturing method able to reach the optimum system performances. The optimum system performances are defined in this case by the presence of dense arrays, narrow channels (<20μm) and sharp edges. The manufacturing response time from design to production of the methods tested was also evaluated. The response time from design to production indicates only a fair performance in that category for the photolithographic lamination.

In this chapter, the designs of a microfluidic chip for blood plasma separation provided the basis for a study on the limits of some rapid prototyping and high volume manufacturing techniques. Back-side stereo-photolithography with the Perfactory machine showed the best response time from design to production of the prototype. However the technique did not prove appropriate for features below 20μm. Micro-

injection moulding is a promising technique for high volume production of microfluidic components, although the tooling for micro-milling of tight structures is not available yet. Other methods such as Fused Deposition Modelling or laser ablation technique have been envisaged but have not been tested yet. Finally, the photolithographic manufacturing route is good although the response time to design changes ought to be improved. 3D-manufacturing techniques are likely to become strong contenders once these techniques become more mature.
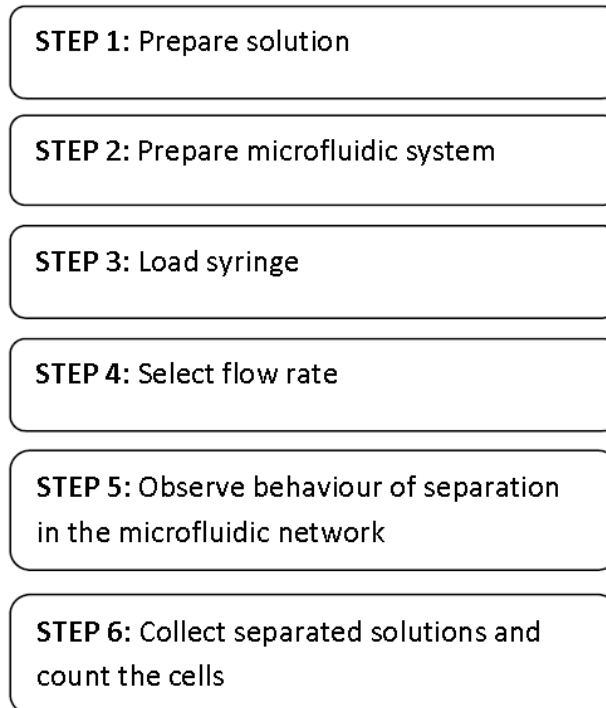
5.3 Experimental approach

The ultimate goal of the experiments presented in chapter 6 is to characterize the efficiency of the plasma extraction, that is to say, how well the plasma is extracted from the blood using the microfluidic approach. Additionally, from these experiments some very useful observations can also be made.

The experimental approach used throughout this study is presented in Figure 5. 11. Firstly, a "solution" or "sample" was prepared with a view to be separated in the microfluidic system. The different "solutions" or "samples" used for experimental purposes will be detailed in this section. Then the system itself was prepared, the chip was mounted onto its platform and capillaries were connected to the inlets and outlets. These capillaries were connected to tubes for the collection of the separated products.

The experimental set-up will be discussed in further detail in the next section. A syringe was loaded and placed onto a syringe pump, this type of pump was chosen for the experiments. A flow rate was selected on the syringe pump which will be the entrance flow rate of the solution in the system. Once the flow rate was selected, the pump was turned on and the observation of the separation behaviour was made possible through a microscope placed above the chip as shown in the experimental set-up. At the end of the separation, the products were collected for cell counting.

Different types of experiments and parameter variations were undertaken with the first and second generation devices in order to fully assess their performance. These parameters are presented in Figure 5. 12. With the first generation devices, streamlines and particle free zones in the devices were observed using milk and latex

beads. These results and observations were used to optimise the second generation devices. Blockages, cell population and cell viability could then be controlled in the second generation devices.

> STEP 1: Prepare solution

> STEP 2: Prepare microfluidic system

> STEP 3: Load syringe

> STEP 4: Select flow rate

> STEP 5: Observe behaviour of separation in the microfluidic network

> STEP 6: Collect separated solutions and count the cells

Figure 5. 11: Overview of the experimental approach in six steps.

The efficiency of separation for different solutions were measured in both generation devices using different tools. The cell-free or particle-free zones are measured in micrometers and the efficiency is measured as a percentage using the following equation:

$$E_p = 1 - \left(\frac{c_p}{c_f} \right)$$

With cp, the concentration of cells in the plasma and cf, the concentration of cells in the inlet solution. In the experiments on the first generation device, the concentration corresponds to the number of "events" measured by the flow cytometer on a volume unit. In the experiments on the second generation device, the concentration corresponds to the number of red blood cells measured by an automatic cell Coulter counter per volume unit.

114

The plasma yield is approximated by calculating the ratio of the volume of plasma extracted to the total volume of plasma. For example, a plasma yield of 40% means that over 1mL of blood with an absolute plasma volume of 55%, 0.22mL of plasma will be extracted.

Throughout the experiments on the devices a range of solutions was used and the necessary information for these is summarised in table 5.3 . The preparation of these solutions is detailed in the next section.

	Usage	Particle size range
Milk	Streamlines observation	2-3µm
Latex beads	Particle free zone observation and experimental determination of Reynolds number range	6.1µm
Mussel haemolymph	Efficiency characterisation	10-50µm
Human blood	Efficiency characterisation	RBCs: 5-7µm WBCs: 10-100µm Platelets < 2µm

Table 5. 3: The different solutions used in the experiments on the first and second generation devices

There are three main experimental variables, on top of the geometrical variables that vary from model to model (eg, plasma channel width):

- The output capillary ratio

- The entrance hematocrit (%)

- The entrance flow rate (mL/hr)

In the experiments on the first generation devices, these three experimental variables are used to produce different results. In the experiments on the second generation devices however, the focus was on the variations of the entrance hematocrit and flow rate as it was considered impractical to vary the output capillary ratio.

	First generation devices (T-junctions)		Second generation devices (T-junctions)	
Observations on flow	Streamlines 6.2.2	*Visual observation latex beads and milk*	Blockages 6.2.4	*Visual observation*
Measurement of cell-free zone			Cell-free zones 6.3	*Visual observation*
Measurement of purity efficiency	Efficiency *Mussel blood* 6.4.1.1	*Flow Cytometry*	Efficiency *Human blood*	*Cell Coulter Counter*
	Efficiency *Human blood* 6.4.1.2	*Flow Cytometry*		
Control of cell population			Cell populations 6.3.2.2	*Flow cytometry*
Control of cell viability			Cell viability 6.3.2.3	*Trypan blue test*

Figure 5. 12: Experimental controls in the two generation devices. Numbers refer to corresponding sections in Chapter 6.

5.4 Experimental set-up

In this section are presented the main components of the experimental set-up for passive blood plasma separation, featuring the pumping system, the microfluidic set-up, the video and image analysis system, particle counting apparatus and finally the sample preparation protocols.

5.4.1 Pumping systems

Although the final device in the prenatal diagnosis system should have an integrated pump, two types of external pumping systems were used for the first prototypes.

A pumping system has to be chosen to inject the liquid into the microfluidic chip. A dual-piston pump system "Flash100" from LabAlliance (Figure 5. 13(a)) was used in the first tests as it was available in the Department.. The "Flash 100" is ideally designed for High Performance Liquid Chromatography and is quite a complex pumping system which includes: a prime purge valve, two pistons, and an outlet filter. The fluid is pumped and filtered through the system and arrives at the front panel of the pump where tubing must be connected to direct the fluid to the microfluidic chip. This results in a relatively long flow path in terms of microfluidic volume and is not suitable for pumping fixed volumes of fluid below 10mL to a chip. Indeed before entering the chip, the 10mL will be dispensed through the tubing of the pump and more fluid will be needed in the primary reservoir at the beginning of the flow path in order not to damage the pump by pumping air into the system. Although primary tests could be performed with the Flash100 pumping systems, a second solution had to be chosen for further tests.

Figure 5. 13: (a) Flash 100 pumping system from LabAlliance (www.laballiance.com) (b) Aladdin syringe pump system from WPI (www.wpi-europe.com)

Due to the inconvenience of the dual HPLC pump system, a second pumping system was chosen. A syringe pump offers a convenient facility for pumping small amounts of fluid to a microfluidic chip. A syringe pump is delivering a set flow rate using a step motor to push on a syringe. The fluid path is much reduced compared to the dual pump system. The selected syringe pump is the "Aladdin" from WPI (Figure 5. 13(b)) in which the syringe volume can range from to 60mL to 1mL. The syringes used are disposable plastic syringes from BD Plastipak. Different tips can be chosen from slip to luer-lock tip. The slip tip is a simple tip while the luer-lock tip offers the possibility to screw on the luer-adapter and therefore minimize leakage or the possibility of the tip coming off.

It has been observed that in the microlitre range, the use of syringe pump might lead to long equilibration times and irreproducibility of the results [5.6]. Existing fluid handling devices are thus often inadequately adapted to the manipulation of small fluid volumes, however in this study the Aladdin syringe pump has been found to cope extremely well with the manipulation of 1mL biological samples at flow rates ranging from 1mL/h up to 30mL/h.

The fast response of liquids to actuation in microchannels is a desirable benefit in Microsystems. For this reason, syringe pumps are suitable for most microfluidic applications. However, due to the various connections and tubing between the syringe and the microchannels, instantaneous flow actuation might be hard to obtain and has been shown to be relatively independent of the settings of the pump [5.6]. However, using the Aladdin syringe pump and semi-rigid tubing, equilibrium time have found to short, of the order of a few seconds, and the pump settings did correspond to the actual flow rate obtained.

Moreover, the control of the pressure or the flow rate control may introduce different velocities in multiphase flows, such as blood [5.7]. Therefore different flow controls will have to be tested on the prototypes in the future.

The tubing 1/16 inches Outer Diameter (OD) and 0,005 inches Internal Diameter (ID) delivered with the Epigem chips set the standard tubing dimensions of the microfluidic systems developed here. In the syringe pump system, the fluid path is reduced to that of the syringe barrel and tip, tubing, and the microfluidic chip, therefore only two

connections are needed. The first connection is linking the syringe luer tip (Slip or lock-luer tip) and the piece of tubing. The connection solution chosen consists of two parts, the P659 and the F-120 from Upchurch. The P-659 is a female luer to female 10-32 adapter shown in Figure 5. 14(a) and the F-120 is a fingertight fitting for 1/16'' OD tubing shown in Figure 5. 14(b).
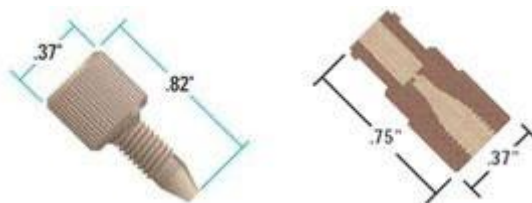
Figure 5. 14: a) F-120 part from Upchurch. 10-32 Fingertight Fittings for 1/16" OD Tubing, b) P-659 Female Luer to Female10-32 Adapters (www.upchurch.com)

5.4.2 Microfluidic set-up

The first part of the tests was performed at Heriot-Watt University. The syringe pump was loaded with a 2.5mL disposable syringe (BD Plastipak). The fluid flow rates used ranged from 1mL/h to 30mL/h, although the chip could sustain a flow rate of up to 100mL/h. The overall assembly of the experimental set-up is presented Figure 5. 15. A bead (b) was inserted in the syringe (c) and a magnet (a) was manually activated to agitate the fluid in the syringe and avoid sedimentation when the syringe was activated at low flow rates. The cellular and plasma samples were collected in eppendorfs via tubing connected at the outlets as shown in Figure 5. 15. In the first part of the tests both plasma samples were collected in the same tube and therefore no differentiation was made between the two samples. The flow was observed using a conventional microscope on which a digital camera could be mounted.

Figure 5. 15: Diagram of the experimental set-up for the tests on the first generation device . a) magnet, b) stainless steel ball, c) syringe, d) syringe

pump, e) holder inlet, f)&g) plasma outlets, h) chip, i) cell outlet, j)&k) eppendorfs for cell and plasma collection.

The second part of the tests, involving the characterisation of the second generation of blood plasma separation chips, was performed at the division of pathway medicine (DPM), 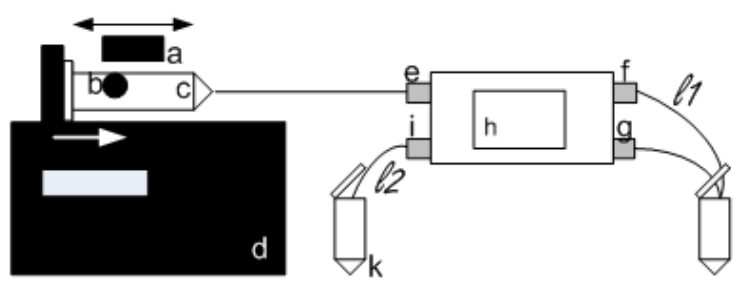University of Edinburgh (Royal Infirmary of Edinburgh, Little France, Edinburgh). The chip was loaded onto the holder with microfluidic connections as shown in Figure 5. 16. The chip and holder assembly was maintained onto a custom made back-light apparatus under a microscope (DinoLite USB microscope, Big C, USA) to observe the flow and detect any obstacle to the flow path during each experiment. The flow was activated at flow rates ranging from 1mL/h to 10mL/hr by a syringe pump (Aladdin, WPI, USA). A syringe (BD Plastipak) with 1mL of blood was loaded for each experiment.

For each single experiment, a 1mL disposable syringe filled with the sample was loaded on a syringe pump (Alladin, World Precision Instruments). The microfluidic devices were prefilled before each experiment with a 1% BSA-PBS buffer for at least 10mins to avoid cell adhesion during the separation process [5.7]. Despite this prevention, the microfluidic network tends to clog up after a number of experiments. However, the device is rarely clogged up during the first experiment. The cheap, plastic device is meant to be single-use and disposable to avoid contamination. However, at the time of the study a limited number of chips were accessible, and therefore chips were sometimes used several times but never more than 10 times. If a blockage was spotted, or if the efficiency of the chip seemed to drop, the chip was discarded and a new one was loaded on the holder. As shown in Figure 5.14, for the tests on the second generation device, the plasma collection was separated into two tubes.
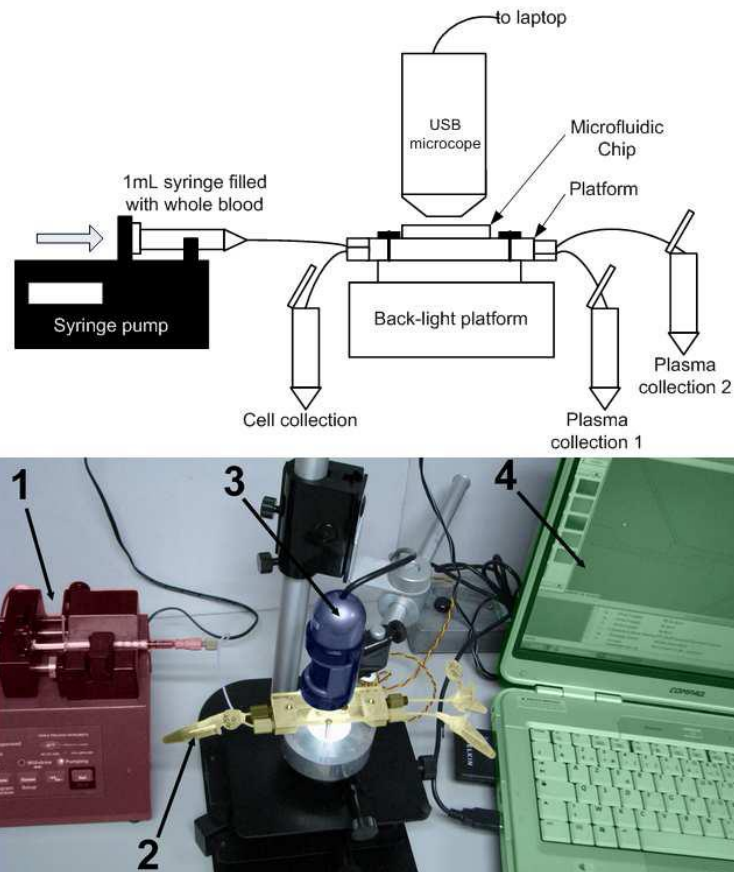
Figure 5. 16: Photo of the experimental set-up at the DPM, University of Edinburgh, Royal Infirmary, for the second part of the tests.

In Figure 5. 17, a close view of the chip is shown during the experimental tests. The flow of red blood cells, can be seen clearly in the main channel. A close-up on the cell free layer is shown.

5.4.3. Video and Analysis

In the first part of the tests a conventional microscope with a mounted digital camera was used for the video setting. For the second part of the tests an apparatus with a back-light system was manufactured in-house.

The chip and holder assembly was mounted onto a custom made back-light apparatus under a microscope (DinoLite USB microscope, Big C, USA) to observe the flow and detect any obstacles to the flow path during each experiment that was carried out.

Some of the experiments required image analysis, for this application the free software package Image J was used. The use of the software will be presented in the next section.

121

Figure 5. 17: The blood plasma separation chip (second generation) in use during experiment . Blood dilution 1:2.

5.4.4 Sample preparation for the first generation device

Experiments have been carried out on milk, mussel blood and human blood. Whole milk is injected into the separator as a blood simulator. Milk is a water-based suspension composed of fat globules. Cow's milk fat globules size range from 1 and

10μm. However after homogenization, fat globules are reduced to a size range from 1 to 2μm. Fat globules are surrounded by a phospholipidic membrane like cells. Altho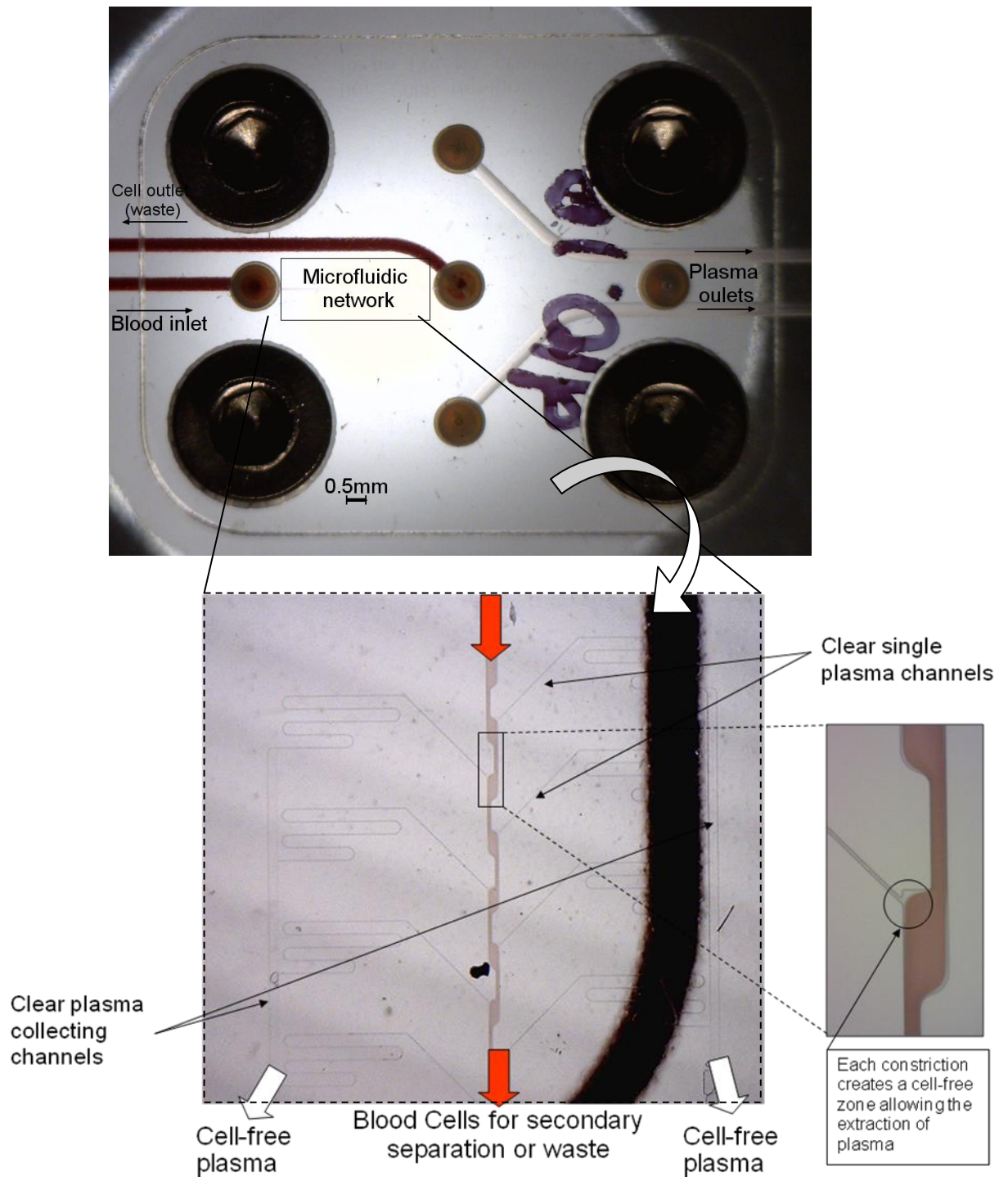ugh a milk skimming effect is observed after the constrictions in both designs, no separation of fat globule from the water base was observed. Several reasons can lead to these results. First of all, the size of the fat globules is much smaller than that of red blood cells. Due to this, fat globules may not be as deformable as RBCs and therefore do not experience a radial drift strong enough which would coerce them into entering into subchannels.

Human blood was collected from healthy donors with a sterile lancet (Accu-check, Roche, Switzerland). The collected blood was suspended in 1mL of anticoagulant solution composed of Phosphate Buffered Saline (PBS) at normal strength and 10μL of ethylene diamine tetraacetic acid trypsin (EDTA-trypsin) (0.05M, Gibco).

The immune cells of the blue mussel, Mytilus edulis, range from 5μm up to 25μm in diameter and were used to investigate the behaviour of larger deformable particles in our system. These immune cells are transparent and have a range of internal complexity. In order to investigate the influence of the buffer type on the purity efficiency, the mussel blood was suspended in two different buffers. The first buffer comprised formaldehyde, known to fix and harden the cells. To keep the cell characteristics as close as possible to the physiological conditions, the second buffer was free of fixing solution. Details of the mussel blood preparation are given in Table 5. 4.

5.4.5 Samples for second generation device

Human blood was obtained in 500mL bags from the Scottish National Blood Transfusion Service, Lauriston Place, Edinburgh. Samples were used with the donors' prior consent and ethical clearance was obtained from the SNBTS Sample Governance Committee. Blood was treated with oxalate and stored at 4°C upon the day of reception. The blood was used within a month. Ideally the blood should be separated on the same day, and the PCR performed within hours after the separation. However, this could not be achieved in the current situation. This delay has been taken into account when interpreting the results. During the length of the study two different blood samples were obtained. The blood samples were subjected to different dilutions

Buffer Preparation	Preparation	Note
With Formaldehyde	5 mussels of 4-5cm in length were bled using 2.5mL syringe filled with 1mL of fixing solution (3.6%formaldehyde in 3x TBS). The haemocyte suspension was centrifuged at 1000rpm for 10 minutes. The cell pellet was re-suspended in 1mL of methanol and 20μL of Wright's stain pure solution. After 2 minutes, 10mL of TBS buffer was added to the suspension and centrifuged at 1000 rpm for 10 minutes. Finally the cell pellet was re-suspended in 10mL of fixation solution and ready for use.	The cell mixture was kept at room temperature before processing and used within two hours after bleeding
Without Formaldehyde	The mussel blood was collected in a saline solution (v:v) composed of 0.45M NaCl, 0.1M glucose, 0.03M Tris-Sodium citrate, 0.1M EDTA, 0.026M citric acid. The pH is adjusted at pH=8 with KOH	The cell suspensions were kept on ice and used within following 2 hours from extraction.

Table 5. 4: Table illustrating the preparation of two different buffers for the mussel blood experiments

using Phosphate Buffered Saline, (PBS, Sigma). The dilution levels ranged from zero to 1:20. Dilution levels on different blood samples are biased by the intrinsic hematocrit of the blood donor at the time of the collection. Therefore, only resulting hematocrit levels truly reflect the different dilutions performed. Hematocrit level measurements and a full cell count were performed using a Beckmann Coulter Counter before each run.

Around 50μL aliquots of each blood samples were placed in individual eppendorfs tubes for hematocrit level verification using a Beckmann Coulter Counter.

The samples were loaded at entrance flow rate in the 2-10mL/h range. Once the blood samples filled the main channel, the separation process occurred at each bifurcation and the plasma flowed through the individual plasma channels and collection channel.

The cell-enriched mixture and the extracted plasma were collected in three individual eppendorf tubes and stored at 4°C until further processing.

5.4.6 Particle counting

After the first stage of collecting suspensions from the different outlets, the particles or cells contained in the different outlets must be counted to determine the efficiency of the separation. This section details the different techniques used to count the cells, their advantages and disadvantages of each method are explained.

Disposable haemacytometer

After the first stage of collecting suspensions from the different outlets, 10µL are pipetted from each of the collection beaker (cell and plasma). The 10µL are then inserted into a disposable haemacytometer from Labtech as shown in Figure 5.16. The so called "C-chip" is normally used for manual cell counting under a microscope. It consists of two surface-patterned enclosed chambers with two ports for sample injection. A standard grid pattern is used for counting the cells (Figure 5. 18(b)). Counting cells using a manual haemacytometer is very tedious, and time-consuming, and due to human eyes fatigue, can have a high error rate.
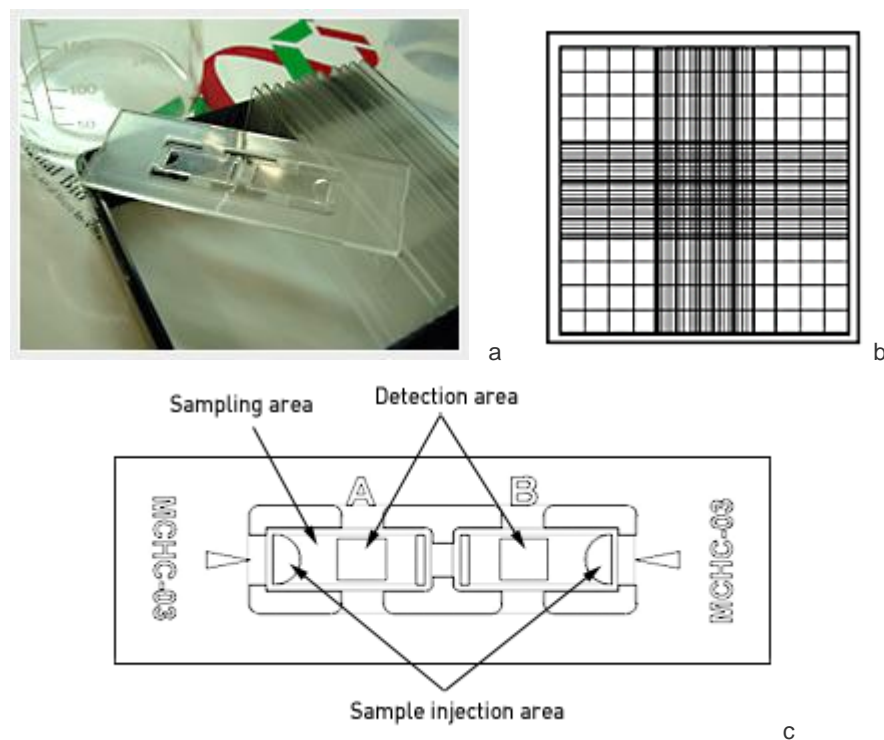
Figure 5. 18: Haemacytometer principles, Labtech website (www.labtech.com). (a) Photograph of a C-chip; (b) Neubauer pattern grid used for conventional cell counting; (c) haemacytometer diagram.

Cell collection (diluted)   Plasma collection
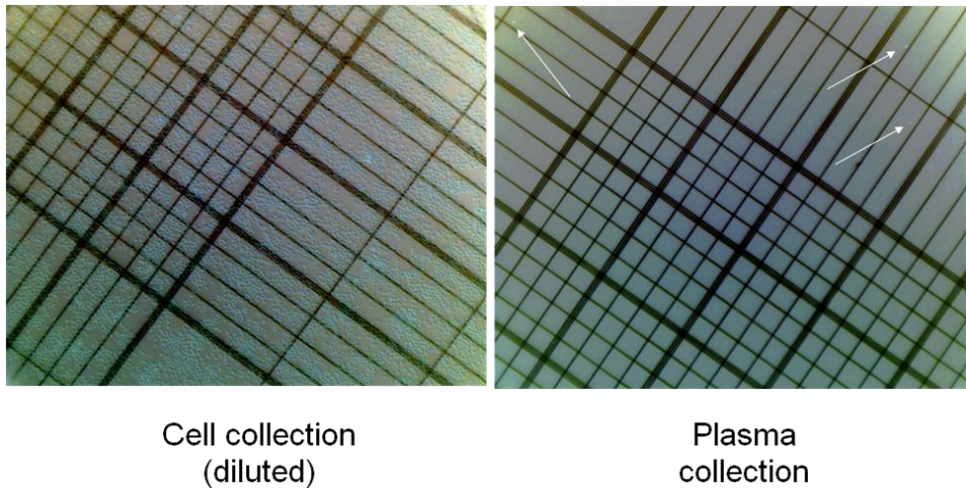
Figure 5. 19: Photographs of hemacytometer counting grid

Image processing

Instead of counting the cells by eye, a photograph of the cells in the C-chip is processed with the free image analysis software known as ImageJ. In **Figure 5. 20**, the diagram shows the path of image processing to obtain a cell count from an image of the haemacytometer taken through a microscope.
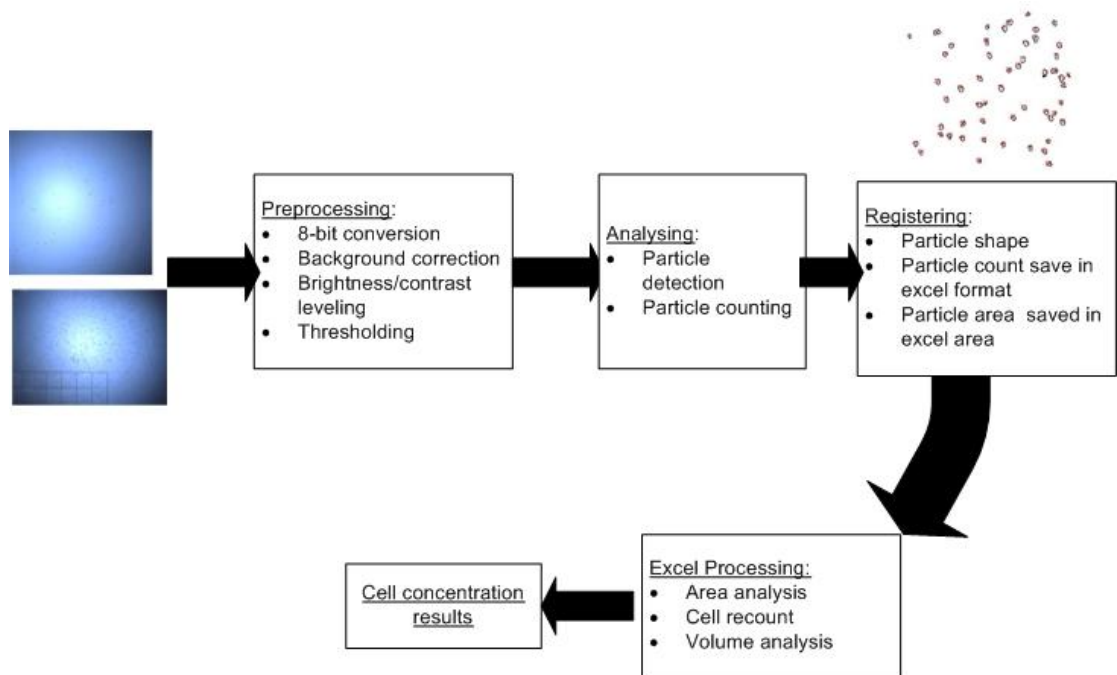
Figure 5. 20: Image processing flow to extract the cell count from a photograph of a cellular sample.

Automated cell coulter counter

A Coulter counter is an automated apparatus to count cells. Fluid passes through a small aperture and the machine uses variations of the electrical conductance to calculate the number of cells passing through the tube. The concept which created a small revolution in the analysis of microparticles, was invented in 1947 by Wallace H.Coulter.

Cell counting using a Beckmann Coulter counter was performed at the cardiovascular unit, at the Queen's Medical Research Institute (QMRI) at the University of Edinburgh, Royal Infirmary. This apparatus is visible on Figure 5. 21(a). The external interface consists of metallic tip (Figure 5. 21 (b)) and a touch screen (Figure 5. 22). The metallic tip is directly placed in the tube prepared for cell counting as shown in Figure 5. 21(b) and the results are read on the touch screen (Figure 5. 22). This Coulter counter not only allows the reading of the population of red blood cells but also counts the white blood cells, platelets, haemoglobin level and other parameters.
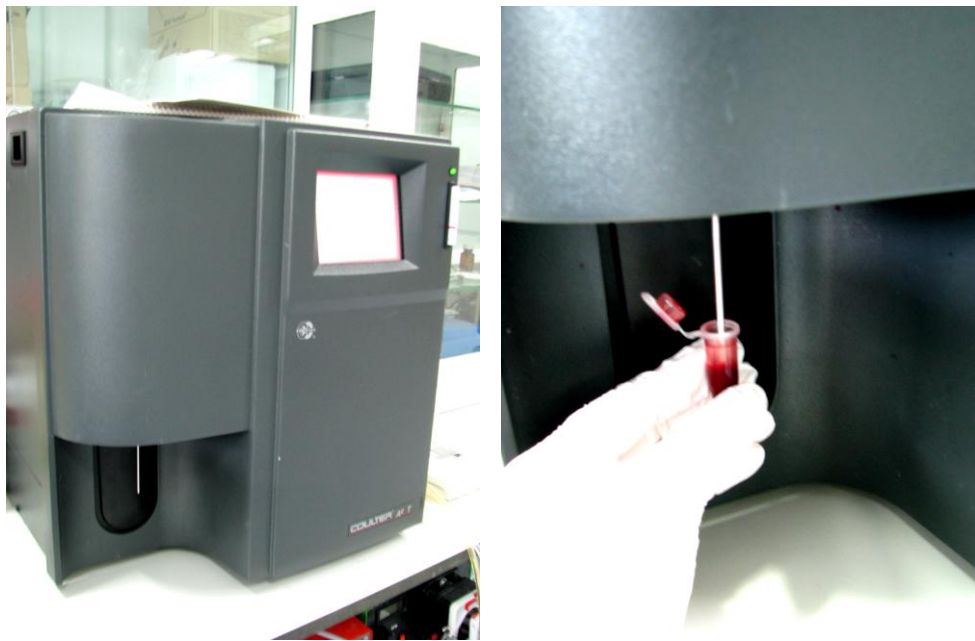
Figure 5. 21: Automated cell counting (a) Beckman Cell coulter counter (b) Blood sampling on the cell counter.
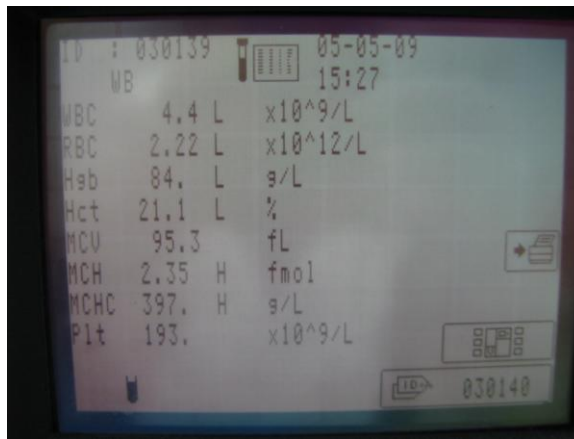
Figure 5. 22: Screenshot of the Beckman Cell coulter counter. WBC: White Blood Cells, RBC, HgB: Hemoglobin level, Hct: Hematocrit level, MCV: Mean Corpuscular Volume, MCH, MCHC, Plt: Platelets concentration.

Flow cytometry

A flow cytometric study was performed on several samples to get an in-depth knowledge of the separation of plasma from blood. Flow cytometry allows a very precise counting of particles in a fluid and, in this case, provides information on the cell population, such as cell lysis that may be caused by the high shear rates in the microchannels. Flow cytometry offers a higher level of sensitivity than can be achieved with a Coulter Counter.

Flow cytometry was invented in the late 60s and is based on the principle that as different cells pass individually in front of a laser beam on an individual basis, they reflect back differently some of the light which can be analysed using a photodetector [5.10]. This technique, shown in Figure 5. 23, is also known as Fluorescence Activated Cells Sorting, (FACS). Although having inherent fluorescence, cells are often labelled using fluorescent tags for sorting purposes.

Flow cytometry offers a higher level of sensitivity (error <1%) than can be achieved with a Coulter Counter (error >3-5%). As the ultimate goal of the plasma separation is to detect cfDNA in the plasma, it is crucial to prove that the cells are not damaged or destroyed during separation. Damaging the cells and causing lysis leads to more contamination of the plasma. In order to give useful biomedical information, the cfDNA detected in the plasma should be present in the blood prior to extraction and should not come from cell lysis as a result of sample preparation.
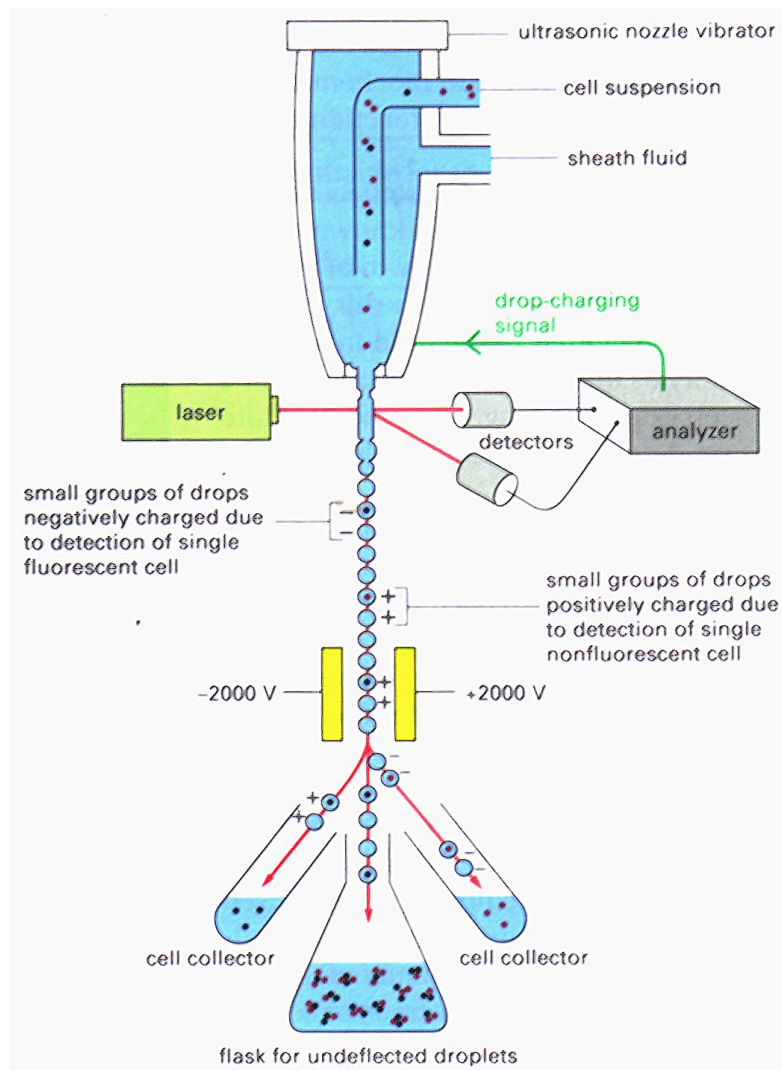
Figure 5. 23: Diagram of the Flow cytometry concept [5.8]

The flow cytometer focuses individually the cells in a laminar flow of ultrapure water. The cells pass through a 488nm wavelength blue laser and 5 characteristics are measured: the relative size of the particles, their internal complexity (or granularity), and fluorescence at the three most common wavelengths (520nm, 590nm, 620nm).

Two different flow cytometers were used. In the first part of the tests, mussel blood was analysed using a Partec Cyflow cytometer in the marine biology unit at Heriot-Watt University. In the second part of the tests, counting was performed using a FACS scan instrument from the flow analysis department Flow Laboratory, Queen's Medical Research Institute, Edinburgh. The next two sections present in detail the experimental set up for each of the flow cytometers.

Partec Cyflow

200µL of the sample collections (cell and plasma) were screened using a flow cytometer (FC) (Partec CyFlow® SL, Germany). A lower limit has been set up to exclude the particles smaller than 2- 3µm; this filtering allows the reduction of the size of the files stored on the computer. The flow cytometry data was acquired with the *Partec FloMax® FCM* software and analysed with the freeware *WinMDI Version 2.9*. For direct control of the cell content in the collection samples, 10µL of the cell and plasma collections were inserted into independent chambers of a disposable hemocytometer (C-Chip, Labtech International, UK) and manually inspected through a microscope.

FACS Scan

Staining of the blood sample was performed to label leukocytes and platelets. The R-phycoerythrin (R-PE)-conjugated monoclonal antibody CD45 (PE Mouse Anti- Human, BD Biosciences) was used for leukocytes surface staining. The fluorescein isothiocyanate (FITC)-conjugated CD42 antibodies stained the platelets. Using these markers we were able to identify the leukocytes and platelets population. The RBCs were identified by being non-stained. Blood cell population analysis was carried out on a *FACS Scan* instrument (BD Biosciences, San Jose, USA) and results were analysed using *Flow Jo* software v7.5.3 (Tree Star, Ashland, OR, USA). Determination of the absolute cell count was achieved by the use of flow cytometric beads Flow-Check Fluorospheres (Beckman Coulter). 50µL of well-mixed beads mixture was added to the 200µL of sample and mixed thoroughly. The flow cytometer was then calibrated to count a specific number of beads allowing a precise absolute count of the cells.

Comparison of the different counting techniques used

Four techniques have been presented for counting particles in the resulting collection after blood plasma separation. Advantages and disadvantages of each method are given in Table 5.5.

Counting technique	Accuracy	Advantages	Disadvantages
Disposable hemacytometer (eye count)	+/- 20%	Cost-effective	Low accuracy, slow, tiring
Disposable hemacytometer (digital count)	+/- 10%	Additional accuracy/repeatability compared to eye count	Fairly long processing time
Automated cell coulter counter	+/- 5%	Rapid, accurate, easy to use	Fairly expensive to run (washing reagents)
Flow cytometry	+/- 1%	Highly accurate	Processing needed, Training needed, apparatus expensive to run

Table 5. 5: Comparison of four cell counting techniques

In conclusion, although the flow cytometer offers the best accuracy, the automated cell Coulter counter was found to be the best solution to rapidly and accurately count cell populations in the resulting collection and was used in the second part of the tests presented in Chapter6.

5.5 References

[5.1] EnvisioTEC website, http://www.envisiontec.de/02hperfa.htm, last accessed April 2010

[5.2] U. M. Attia, S. Marson and J. R. Alcock, *Micro-Injection Moulding of Polymer Microfluidic Devices*, Microfluidics and Nanofluidics, 7, 1-28 (2009)

[5.3] Epigem website, www.epigem.co.uk, last accessed April 2010

[5.4] H. Becker, *Mind the gap!*, Lab on Chip, **10**, 271 – 273 (2010)

[5.5] Fluigent

, http://www.fluigent.com/index.php?option=com_content&view=article&id=17, last accessed May 2010.

[5.6] M. Faivre, Thesis, University of Grenoble, France (2006)

[5.7] R. Fan, O. Vermesh, A. Srivastava, B.K.H Yen, L. Qin, H. Ahmad, G.A. Kwong, C.Liu, J. Gould, L. Hood & J. R Heath, *Integrated barcode chips for rapid, multiplexed analysis of proteins in microliter quantities of blood*, Nature Biotechnology, Nat Biotech **26**, 1373 - 1378 (2008).

[5.8] B. Alberts, D.Bray, J.Lewis, M.Raff, K.Roberts, and J.D.Watson, *Molecular Biology of the Cell,* Garland Publishing Inc., New York (1983)

Chapter 6: Experimental results on flows and separation efficiencies

6.1 Introduction

This chapter presents the results obtained with the first and second generation microfluidic separators. On the one hand, the study focuses on the characterisation of the flow at the constrictions and bifurcations, and sheds lights on the different behaviour of biological particles in such microfluidic networks. On the other hand, separation efficiencies are extensively characterised as a function of a number of parameters including entrance hematocrit levels and flow rates. It is demonstrated that the forces acting upon the cells are of inertial origin and therefore linked to the flow speed. The two generations of devices are shown in Figure 6.1. From one design to another, the mean separation efficiency is increased by 30% approximately. The more efficient design was found to be the second generation design with the 10um width plasma channels, which gives purity efficiency of 99% with 45% entrance hematocrit level. However, this design also gives the lowest yield (<7%), while the second generation design with the 20 μm width plasma channels gave a yield of around 30%.

This chapter is divided into two distinct parts. The first part focuses on the observations of the flow in the microfluidic network and investigates the reason for blockage in the system. The second part looks into the separation efficiencies on the two generation systems. Two independent flow cytometric studies are presented.

Both generation devices have one outlet for the whole blood, two outlets for the plasma and one outlet for the cell collection. The first generation device, as shown on Figure 6.1 (a), features 15 plasma channels (also named daughter channels) which are 20 μm in width, symmetrically arranged along the main channel. The main channel is 100 or 200μm depending on the model and the entire structure has a depth of 20μm. A constriction (20μm by 100μm) is placed in the main channel before the separating network. In the second generation device, shown in Figure 6.1 (b), there are only four channels, 10 or 20μm in width and 1.4cm in length arranged asymmetrically on each

side of a main channel. In this device the main channel is 100µm in width and constrictions are arranged before each bifurcation.
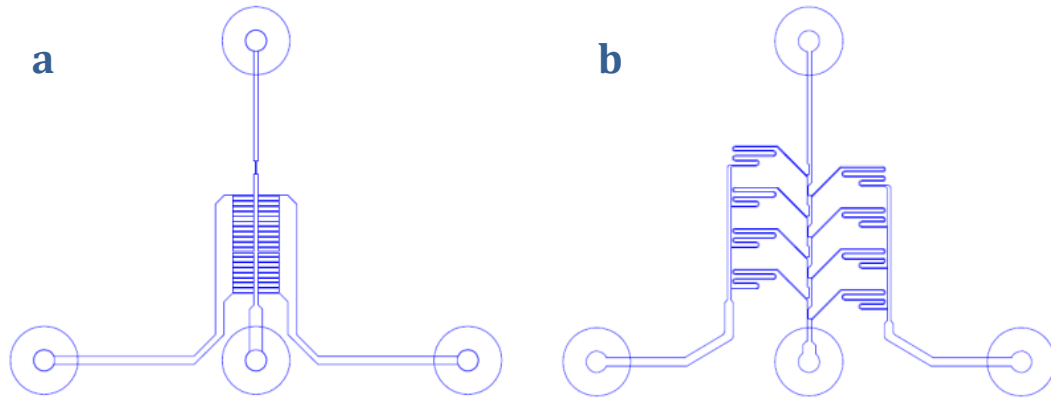
Figure 6. 1: First (a) and second generation (b) of blood plasma separation systems

6.2 Controls and observations on flows

6.2.1 Discussion about the Reynolds number and the forces acting upon the cells.

Although the results of the experiments are satisfactory in terms of purity efficiency as reported in the next section, the separation mechanisms happening at the cell level are not as yet fully quantified. In order to gain a better understanding of these mechanisms, it is of interest to present experimental observations of cell flow and compare them with work from other groups. To do so we define the dimensionless channel Reynolds number by R_c:

$$R_c = \frac{\rho . V . D_h}{\mu}$$

(6.1)

Where ρ is the density of the liquid, μ the viscosity, V the mean velocity across the channel and D_h the hydraulic diameter. Faivre et al showed that, in their system, rigid spheres did not encounter an axial migration; in other words, the viscous forces overcame the inertial forces [6.1]. Indeed, the Reynolds number in Faivre was found to be 0.01. In [6.2] Yang et al the Reynolds number is less than 0.01, which also indicates that the system is in the tank-treading regime. In [6.3] however, Jaggi et al mention a higher Reynolds number of up to 5, and yet separation is observed. In these papers the assumption of a fully laminar regime dominated by viscous forces is made. In our case,

for typical flow conditions of 10mL/h, the channel Reynolds number was found to be 0.69 (blood viscosity, of 4.10^{-2} Pa.s; width, 100μm; depth, 20μm; density of 10^{3} kg.m^{-2}). The flow pattern in the system can be easily identified using a milk mixture (data not shown). The regime is laminar but recirculating eddies appear after the constriction. Recirculation eddies are not turbulences but secondary laminar flows due to the back facing step. Recirculations have also been observed in [6.4] in the same circumstances and might have further extraction power when used carefully. Although the channel Reynolds number was found to be close to 1, it was observed that the constriction did not focus the cells as much as expected. This can be explained by the fact that the bifurcations create a force on the cells pulling them again towards the main channel walls. In order to compare the behaviour of deformable asymmetric particles with non-deformable spherical ones, a mixture of 6.6μm latex spheres was dispensed into the system at varied flow rates. Particles were observed when they passed through the constriction using a microscope and videos were recorded. As shown in Figure 6.2, at a flow rate of 10mL/hr, the particle-free layer is more important with the latex spheres mixture than with the blood. This proves that the inertial forces are dominating the viscous forces. With flow rates around 20mL/h, the latex beads followed however closely the streamlines. At these flow rates the blood cells are expected to focus well, however we observed only a slight focus much smaller than the 27.5μm predicted by Equation [3.4].

The reason for this behaviour might be the effect of the plasma channels placed 500μm downstream which act on the flow forcing the cells to travel closer to the channel wall. However, as spherical beads cannot experience a lateral force at low Reynolds number, it is therefore proved that inertial forces create this lateral drift [6.5], it is more likely that the inertial forces are present in the microchannel and overcome the viscous forces. It is a common mistake to state that inertial forces do not exist in microchannels [6.6], and blood plasma separation has been achieved both by using inertial separation [6.6] and viscous forces [6.1].
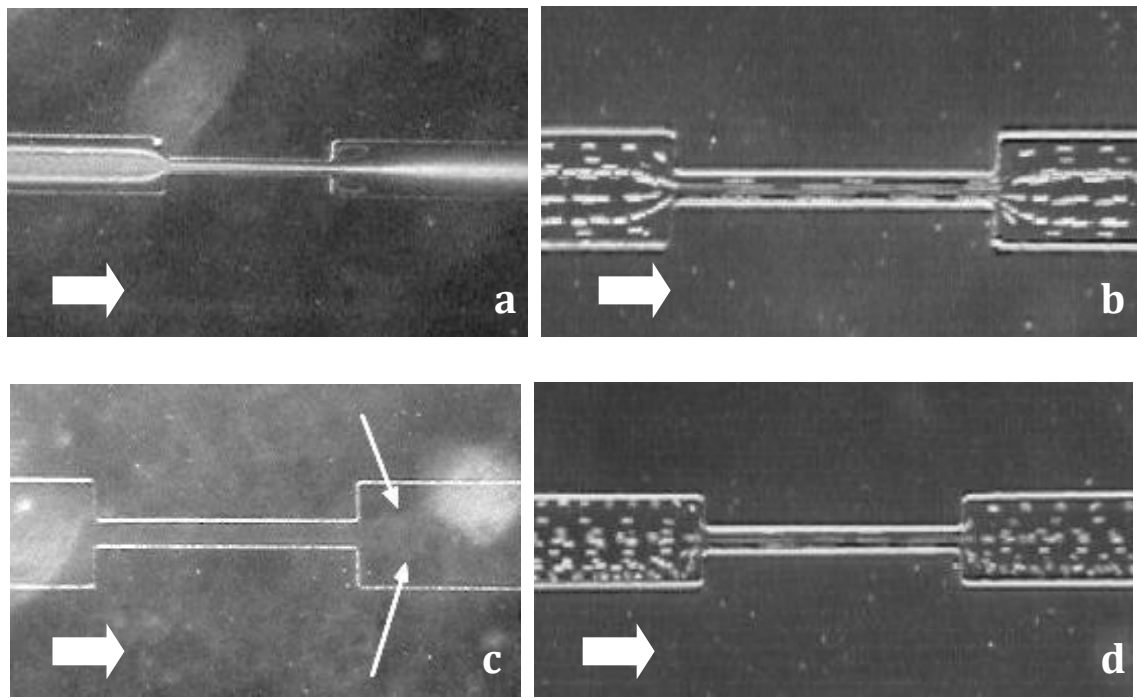
Figure 6. 2: (a) A photograph of 6.6 μm latex spheres passing through the constriction (25x300μm). The flow rate is 20mL/h. The flow is from left to right in all photographs. The focus is very visible at the end of the constriction (b). Superposition of photographs of 6.6 μm latex beads at a flow rate of 5μL/hr. Each sphere is following a flow streamline. (c) A photograph of red blood cells passing at 20mL/h in the constriction. The focus is less accentuated than in (a) and the cells retrieve their position near the walls only 150μm after the constriction. (d) Superposition of photographs of red blood cells passing through the constriction at a flow rate of 5μL/h. Here a focus of a few microns is visible after the constriction.

In conclusion, depending on the flow rate used in this type of system, the potential exists to achieve two modes of separation. One mode would be better at separating hard spheres using the inertial lift force; while the other one would separate soft deformable particle using a viscous lift force. Consequently, the use of a lower flow rate for the full viscous mode would significantly reduce the plasma yield. In the rest of the present study, high flow rates (ranging from 2 to 10 mL/h) were used.

6.2.2 Patterns and backflow problems in the microfluidic system

Milk is a cheap and safe testing material alternative to blood. The solid and liquid phases of milk can be separated at high shear rate. Milk can be useful to observe the patterns and streamlines in the microfluidic network and rapidly detect backflow or other fluidic problems. In Figure 6.3, dyed whole milk was flowed into the first generation chip to observe the changes in patterns at low and high flow rates.
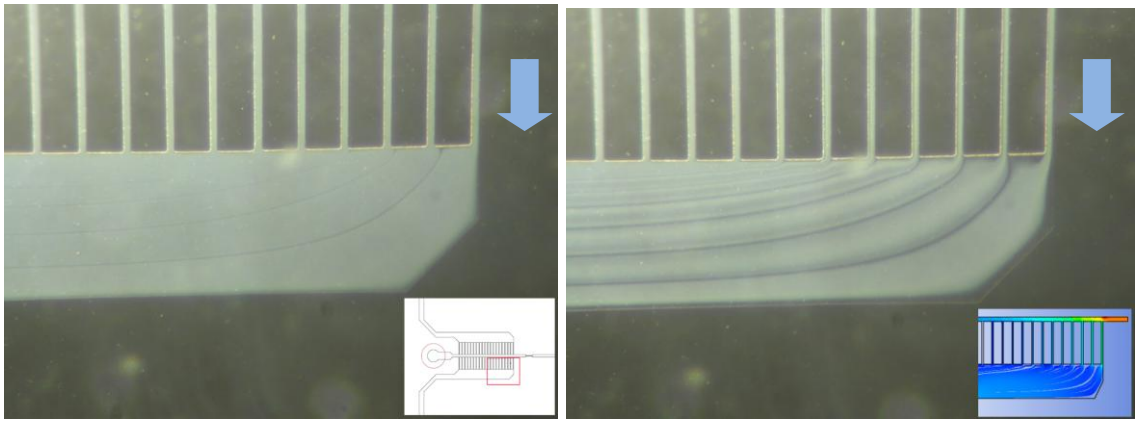
Figure 6. 3: Patterns in the milk stream in the plasma channels of the microfluidic structures. The flow is from right to left. The flow rate is raised from the first to the second picture. First picture, icon: zone of interest in the system. Second picture, icon: simulation of streamlines in the system are showing the same kind of patterns.

In the first generation separator some backflows were observed in the system at high flow rates as indicated in Figure 6.4. The resistance in the collecting channel is higher than the resistance in the three last plasma channels, therefore a part of the fluid escapes back through the plasma channel to the main channel. In the second generation system no back-flow was observed. Backflows were avoided by the use of a high-level modeling, described in Chapter 5, to predict flow behaviour in the system.
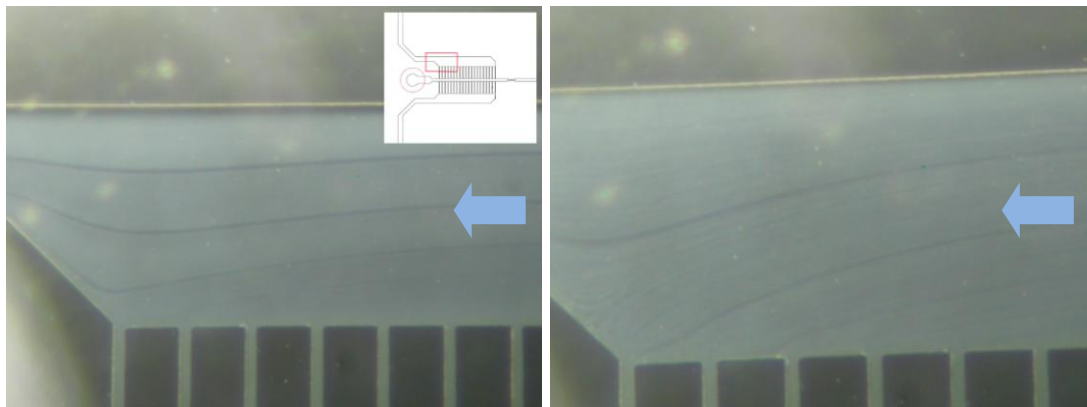
Figure 6. 4: Milk stream patterns in the plasma channels of the microfluidic structures. The flow is from right to left.

6.2.3 Blockages in the microfluidic network

Blockage of the microchannels by dust particles or air bubbles is a common problem in Microfluidics. In these experiments, the syringe was loaded and carefully connected to the system to ensure minimum air bubbles. After priming, the air bubbles were easily removed from the microchannel separation network. Nevertheless it did not deter other particles to enter and block the channels. Dust particles are the primary first reason for channel blockage in the system. Figure 6.10 (a) illustrates a dust particle blocking the entrance of a constriction in the network. RBCs are still able to flow through the channel, but the dust particle creates a high shear stress zone which will encourage platelets aggregation.

Platelets aggregation, as shown in Figure 6.10 (b) is the second most common reason for channel blockage in this system.

These blockages can create serious disturbance to the normal operation of the system. Figure 6.11 (a) shows that platelets aggregation blocking the cell collection outlet. Figure 6.11 (b) illustrates a case where the combination of dust and platelet aggregation block the flow of RBCs in the main channel. The flow of RBCs is diverted to a plasma channel and pollutes the plasma collection.

The system has originally been developed to allow plasma extraction as well as the recovery of cells for further analysis. If the recovery of intact cells is not necessary, a pillar structure upstream from the separation network could potentially reduce the occurrence of blockages.
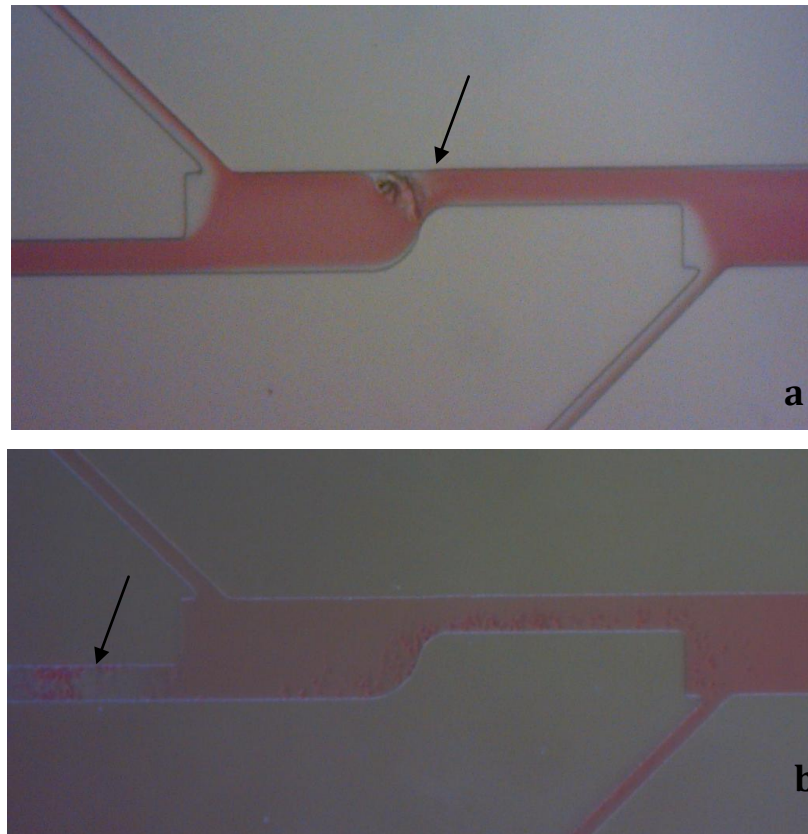
Figure 6. 5: (a) Photograph illustrating the blockage of the main channel by dust. Platelets are aggregating easily around the dust particle blocking the channel. (b) Photograph illustrating another case of blockage in a 20μm channel. Some entire cells are visible, while the channels are tainted with red. The high shear stress has resulted in the breakdown of a lot of cells, releasing thereby hemoglobin in the channels.
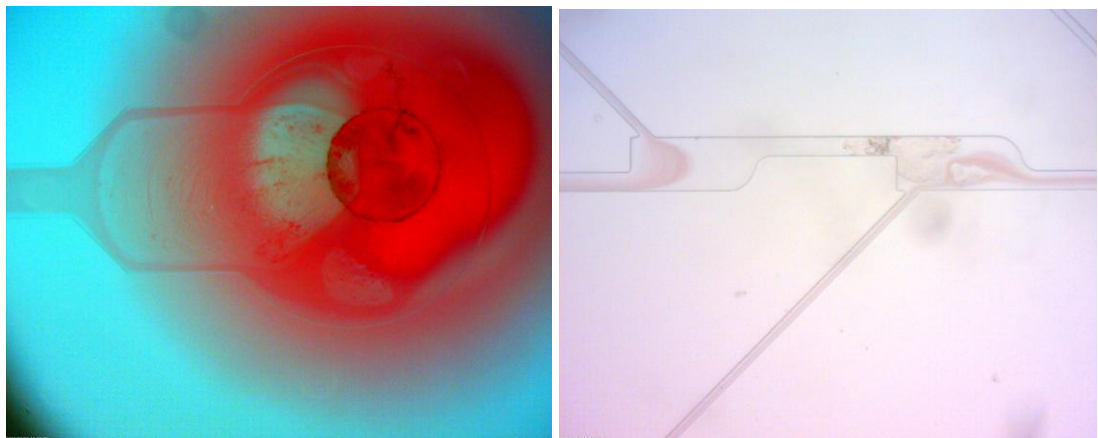
Figure 6. 6: (a) Photograph illustrating platelets aggregation (white shape) at the cell outlet. Some red blood cells are trapped in the platelets aggregate. (b) Photograph showing a large disruption of the blood flow due to a platelet aggregate blocking the main channel.

6.2.4 Formation of platelets aggregates under shear flow

The formation of platelet aggregates was observed and is reported in this section. Although these observations were not studied systematically, links were made with existing theory and experimental observation, which allowed the understanding of the formation of platelets aggregates under specific circumstances.

In vivo, the formation of platelet aggregates is triggered by a range of parameters, however, in vitro, as in these separation channels, aggregates are mainly due to the shear stress. Although aggregate formation is a problem in this system, it is still a fascinating event, and a subject of many studies. In this short section an account is given of our findings and compared with existing studies on the subject.

Several biological mechanisms induce platelets aggregation in-vivo and in-vitro. A local zone of shear acceleration is one of them. Platelet aggregates formation in this system occurred mainly in the main channel before the first constriction. A small aggregate firstly forms of the vertical wall on the channel and is gradually expanded by the accumulation of platelets and red blood cells in its "tail" as shown in Figure 6.11.a. The tail could also be made out of fibrin clots. Yoshimura et al noticed that, despite large amount of heparin in blood, fibrin clots could still be formed in a microchannel and hinder the normal blood flow [6.7]. Figure 6.12.b presents a model for platelet aggregation in local shear flow. When comparing Figure 6.12 (a) and (b), we can hypothetically assume that part (1) creates the shear microgradient in the microchannel, part (2) is composed of discoid platelets and part (3) consists of platelets with restructured tethers.
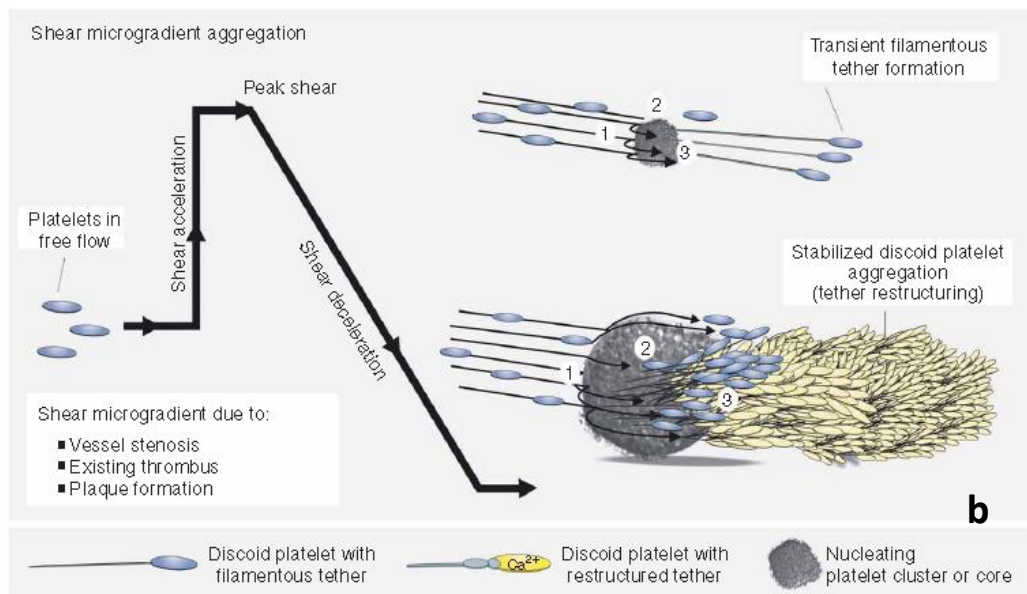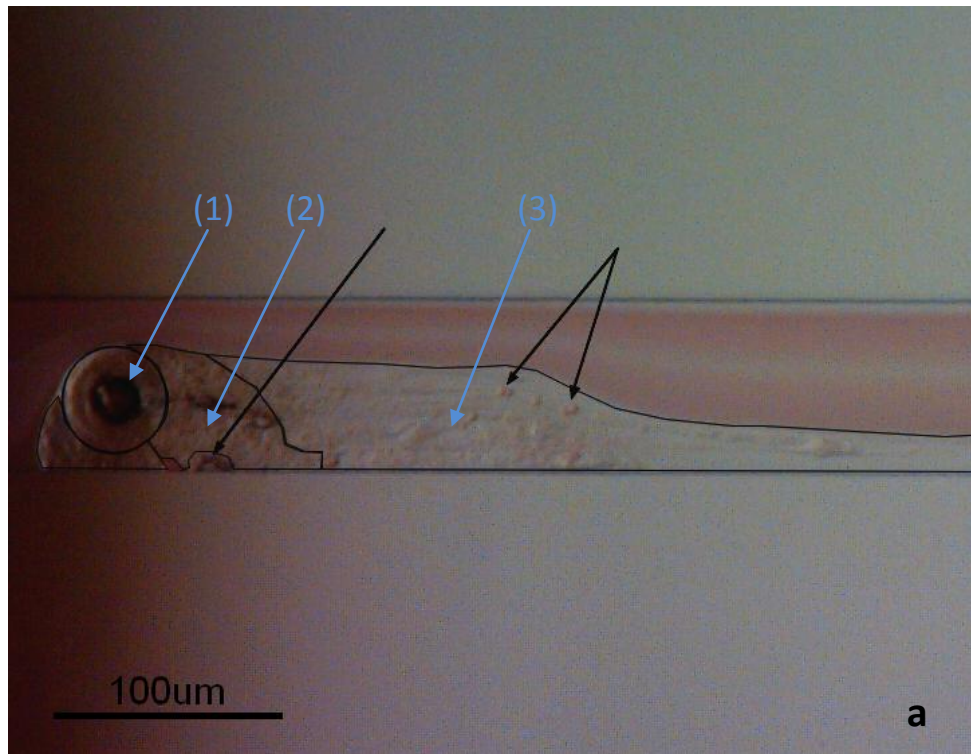
Figure 6. 7: (a) Observed platelets aggregation in the main channel. Black arrows indicate red blood cells trapped in the platelet aggregate (b) Diagram explaining the platelet aggregation mechanisms under local shear stress [6.8]

Figure 6.13 presents the movement of a platelet aggregate in the main channel for duration over 12 seconds. As explained earlier tethers may restructure on the "tail" of the platelet aggregate. This is characterised by free movement of the platelets around a fixed anchor point [6.8].
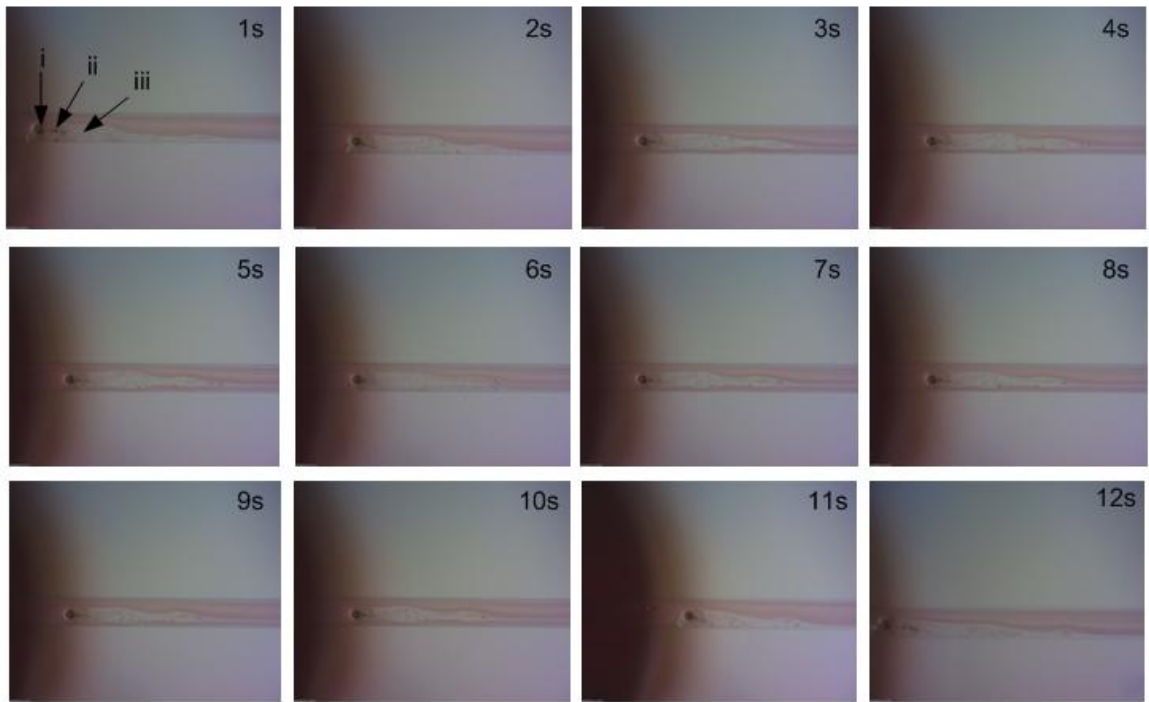
Figure 6. 8: Movement of platelets aggregate in channel over 12 seconds. (i) Core forming a local shear stress (ii) Platelet aggregation, possible tether formation (iii) Platelet aggregation, possible tether restructuring.

6.3 Controls and measurements of the cell-free zones

6.3.1 Cell-free layer and cell free zone observation

A cell-free layer is created by the inertial forces pushing the cells centrally. In Figure 6.5, a cell-free layer can be seen to the right of the first bifurcation. This layer is just a few microns wide, comparable to the naturally occurring cell-free layer in blood vessels smaller than 300µm.

As illustrated in Figure 6.6 (a) and (b), the lateral force can be more or less strong depending on the flow rate applied at the inlet and on the entrance hematocrit level. In Figure 6.6 (b) a cell-free layer larger than the layer of RBCs can be observed. This occurs with a high flow rate and low entrance hematocrit. As suggested in [6.1,4], at low hematocrit levels the interactions between the red blood cells are becoming minimal and does not prevent the lateral force acting on the cells.

In the next section the influence of the flow rate and entrance hematocrit level on the cell-free zone will be detailed.
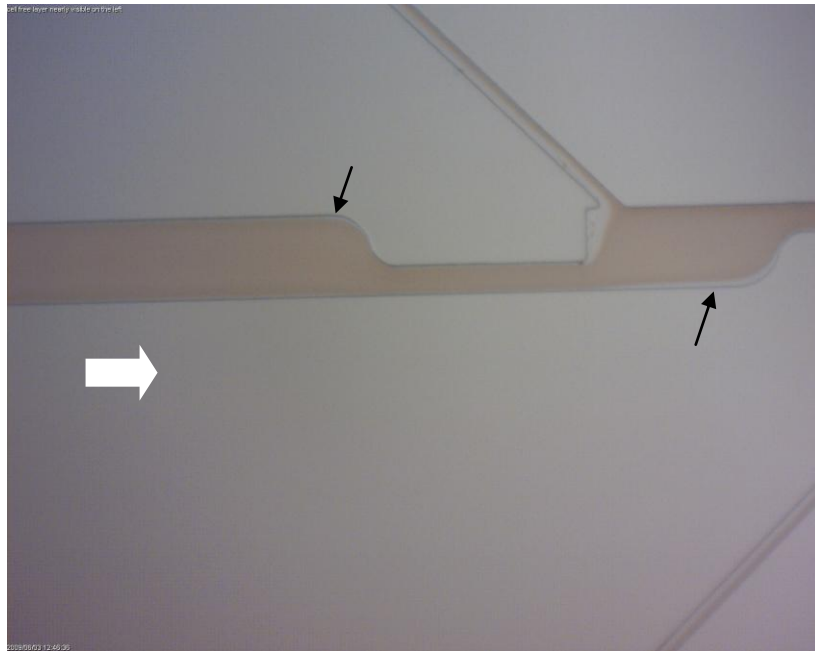
Figure 6. 9: Cell-free layer of a few microns as indicated by the black arrows. The chip has 20µm plasma channel, flow rate: 5mL/h, the blood is undiluted (Hct 33.3%). The white arrow indicates the flow direction.
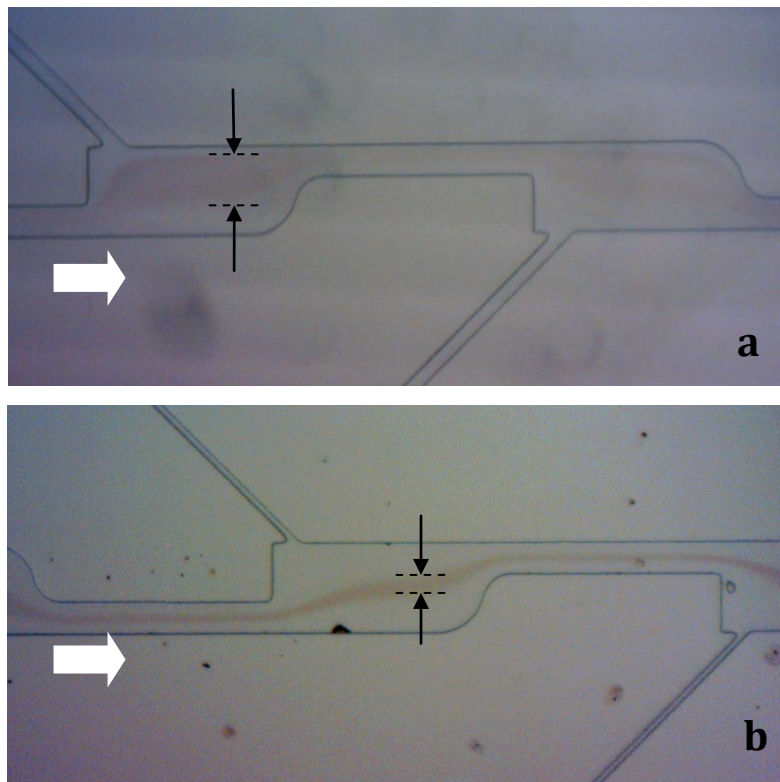
Figure 6. 10: (a) shows a very large lateral force for a chip with $20\,\mu m$ channels. Chip 20µm, Hct 1.8%, 2mL/hr (b) Photographic evidence of high lateral force acting of the RBCs for a chip with $10\,\mu m$ channel. The RBCs are clearly forced into the middle of the main channel and a large cell-free zone is created after the constriction.

6.3.2 Hematocrit and the cell-free zones

The influence of the hematocrit on the cell-free zone at each bifurcation was observed independently of the flow rate. Figure 6.7 (a, b, c) shows the difference at bifurcation number 7 of the cell-free zone depending on the hematocrit level. The lower the entrance hematocrit level, the larger is the cell free zone. For low hematocrit levels (8.3% and 3.3%) and a relatively high flow rate (here 10mL/hr) a recirculation forms just after the constriction, while no recirculation is observed for a level of 16.8%. The lower the hematocrit level, the larger the recirculation will be. The recirculation doesn't affect the separation, nor does it indicate the presence of turbulences.
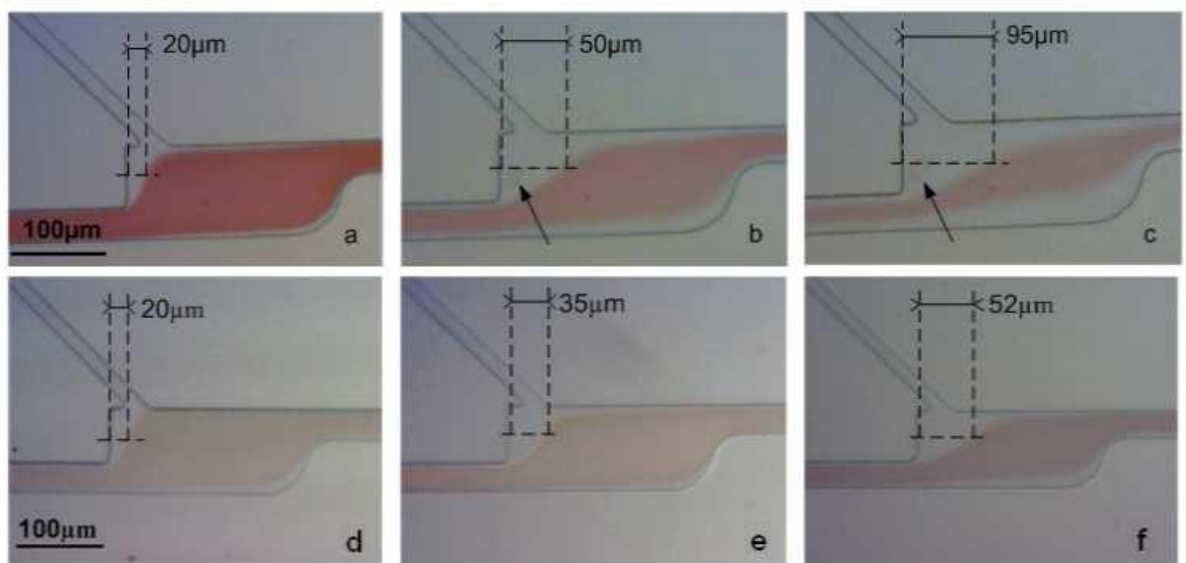
Figure 6. 11: First row: Effect of the entrance hematocrit level at bifurcation 7, constant flow rate 10mL/hr, (a) eHCT=16.8% (b) eHCT=8.3% (c) eHCT=3.3%. Second row: Effect of the flow rate at constant hematocrit level, 8.3% (d) 2mL/hr (e) 5mL/hr (f) 10mL/hr.

6.3.3 Flow rate and the cell-free zones

In the same fashion, an effect of the flow rate on the cell-free zones was observed. As shown in Figure 6.7 (d,e,f), three separation experiments were carried out with the same entrance hematocrit of 8.3%. The flow was varied in each experiment from 2 to 10mL/h. A difference of several tens of microns was observed at the bifurcation between each experiment. A flow rate rise leads to a higher purity at the risk of damaging the cells which encounters greater shear rate forces.

6.3.4 Cell-free zone along the main channel: an account of flow rate ratios

Due to the difference in flow rate ratios, the cell-free zone dimension varies from bifurcation to bifurcation. For high hematocrit levels, this results in different purity efficiencies at each bifurcation. The plasma channels then join a common outlet channel on each side of the main channel. To observe the effect of the different flow rate ratios at each bifurcation, a number of observation windows were set-up as shown in Figure 6.8.
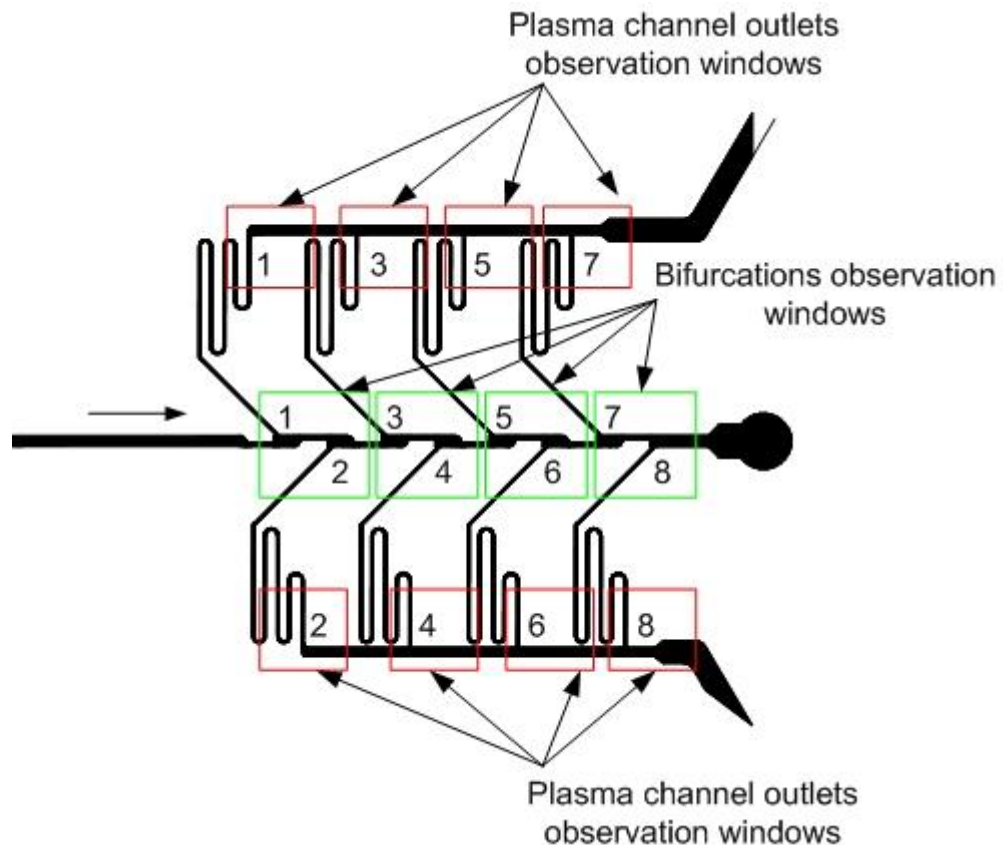
Figure 6. 12: Observation windows on the second generation device

Figure 6.9 illustrates the cell-free zone and the outlets in the main plasma channels corresponding to different bifurcations. In this experiment the hematocrit (Hct) was chosen deliberately high, 22.2%, to illustrate the dramatic changes in separation efficiency at each bifurcation in the 20μm channel device. On (a-1), (b-1), (c-1) and (d-1), the cell-free zone broadens at every bifurcation along the direction of the flow. As flow rate ratios are getting higher and higher in the direction of the flow, the separation efficiency is increasing. In this experiment, red blood cell flow enters all plasma channels except bifurcations 6, 7, and 8. In the other channels, the flow of RBCs is reduced as the flow travels down the main channel. For example the flow of

RBCs is reduced from the plasma outlet 1 (a-2) compared to the plasma outlet 3 (a-3). This experiment demonstrates that the cell-free zone is different at each bifurcation, which in turn results to a different separation efficiency (plasma purity) at each plasma outlet. It could be argued that the change of viscosities along the separation channel is affecting the cell-free zone. However, the flow rate ratio is also changing dramatically, therefore these two effects combined are probably responsible for the difference in separation efficiencies at each bifurcation.
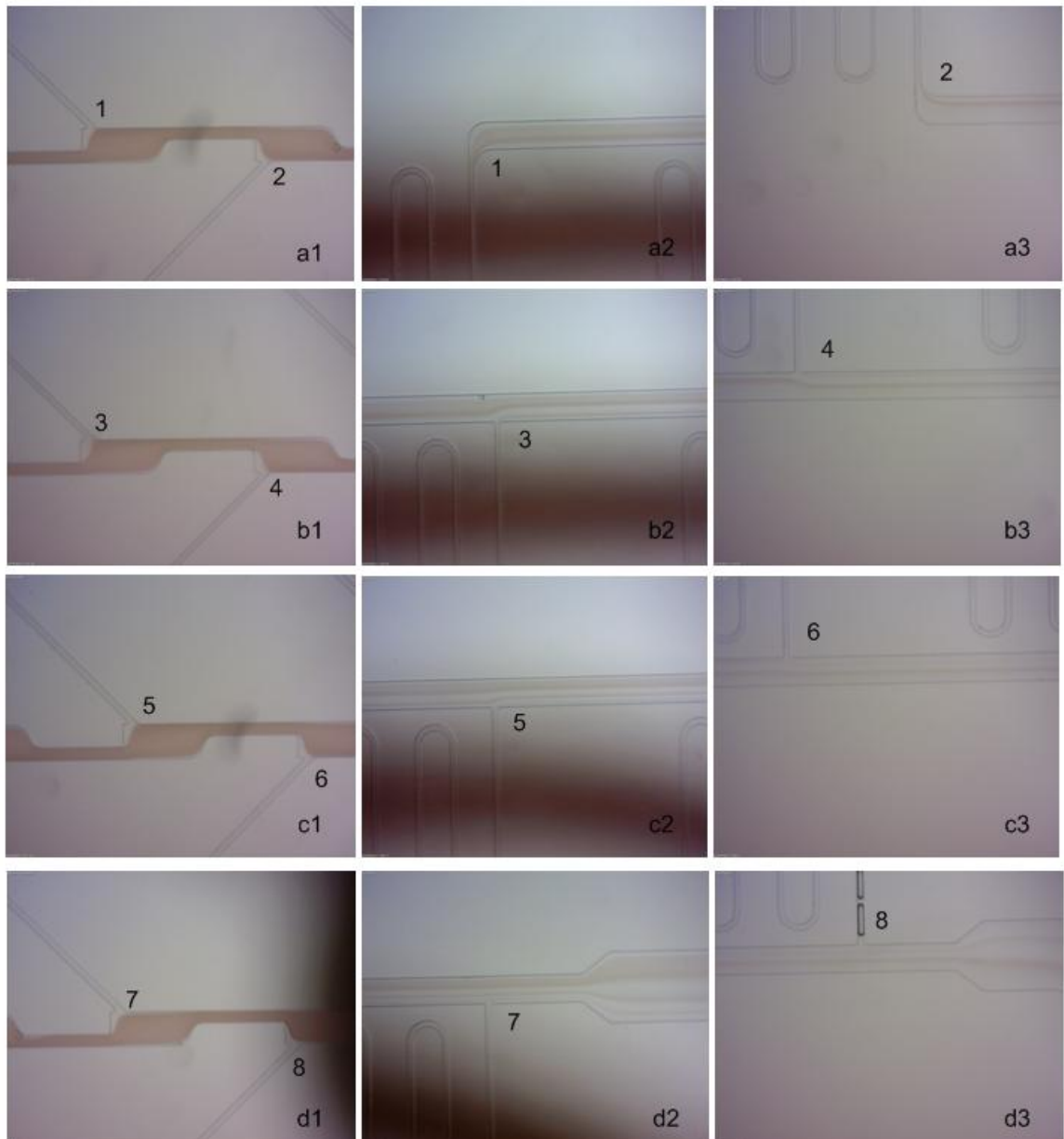
Figure 6. 13: Photographs of a 20 μm blood plasma separation chip using a flow rate of 5ml/hr, at Hct=22.2% (a)First and second bifurcations- bottom second bifurcation (b) third and fourth bifurcations (c) fifth and sixth bifurcations (d) seventh and eighth bifurcations.

Getting identical separation efficiencies at each bifurcation would be possible by setting the length of each plasma channels independently. Plasma channels length can be calculated to set identical flow rate ratios at each bifurcation as proposed in Chapter 4.

6.4 Measurements of separation efficiencies

6.4.1 Separation efficiencies in first generation chips

In this section experimental results and their analysis are presented to understand the influence of the different parameters on the efficiency of the separation system. The first section concerns the results obtained from the mussel blood separation. The second section presents human blood results. All the experiments in this publication have been carried out at large flow rates.

6.4.1.1 Mussel blood plasma separation

The study firstly focused on the influence of the buffer type and chip geometry. In Fig.6.13 the density plots obtained from the flow cytometry results of two separate experiments are given. The X axis corresponds to the forward scatter (laser light passing through the cell, FCS) which is proportional to the size of the cells. The Y axis corresponds to the forward Scatter (laser light being reflected by the cell) which is proportional to the granularity, or complexity of the cell. By placing each event on these two axes, the different populations (namely RBCs, WBCs, platelets) emerge. In this experiment, the cell populations have been depleted in the plasma outlet. The largest cells are the most depleted ones in this outlet. In both experiments, the main channel is 200μm and the flow rate 10mL/h. In Experiment 1, formaldehyde was used in the mussel cells buffer and the outlet length ratio, OLR, was kept to zero. In Experiment 2, however, no formaldehyde was used and the OLR was 4.5. The tuning of these two parameters, deformability of the cells (adjustable through the buffer type) and OLR, produces an enhancement of the separation effect.

The influence of the OLR on the separation efficiency can be studied independently of the other variable parameters. The OLR is varied as 1, 1.8 and 3 in three experiments in which the other parameters are kept the same. Figure .6.14a and Figure .6.14b show the results of these experiments. When the length ratio is increased 3-fold, the particle concentration in the plasma collection is still 70,000 events/mL as indicated in Figure 6.14 (b). An event corresponds to a single particle being detected by the flow cytometer. This particle may be a dust particle, a fragment of cell or a cell. Areas of different cell types (depending on size and granularity) are assigned according to literature on the density plots with WinMDI functions. The percentage of each cell type on the total event count is extracted and compiled into Figure 6.15 (b). In the case of a length ratio of 3, more than 80% of the remaining particles are small particles or cell debris of the order of 3-4µm. The cellular content of the cell and plasma collection samples were also examined in a disposable haemocytometer under a conventional microscope. An eye check at 400x magnification confirmed these results. The purity efficiency of the device for mussel blood is 60% on average.
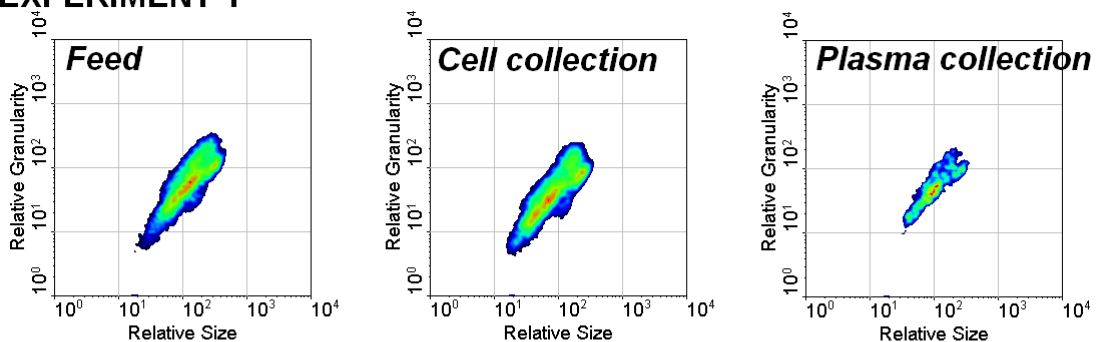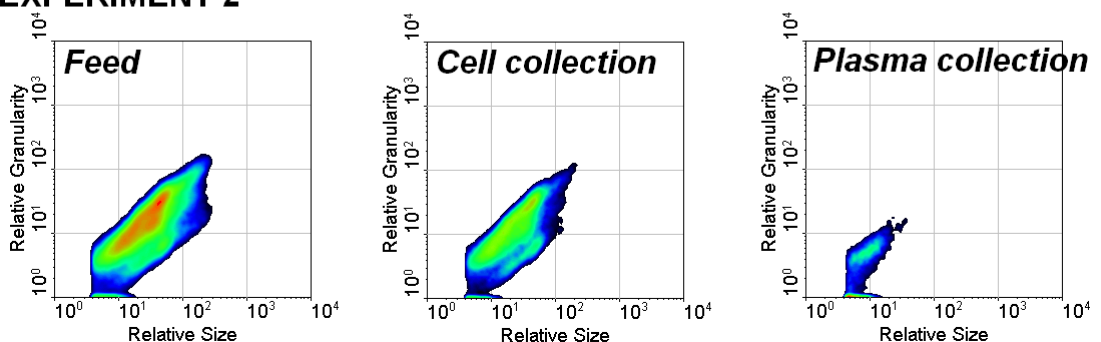
Figure 6. 14: Density plot from the flow cytometry results illustrating the influence of the BT and OLR in two different experiments. In Experiment 1 the main channel width is 200µm, flow rate 10mL/h, BT with formaldehyde, OLR:1. In Experiment 2, the main channel width is 200µm, flow rate 10mL/h BT without formaldehyde, OLR:4.5. The difference in shape of the cellular fraction is due to the difference in buffer solutions.
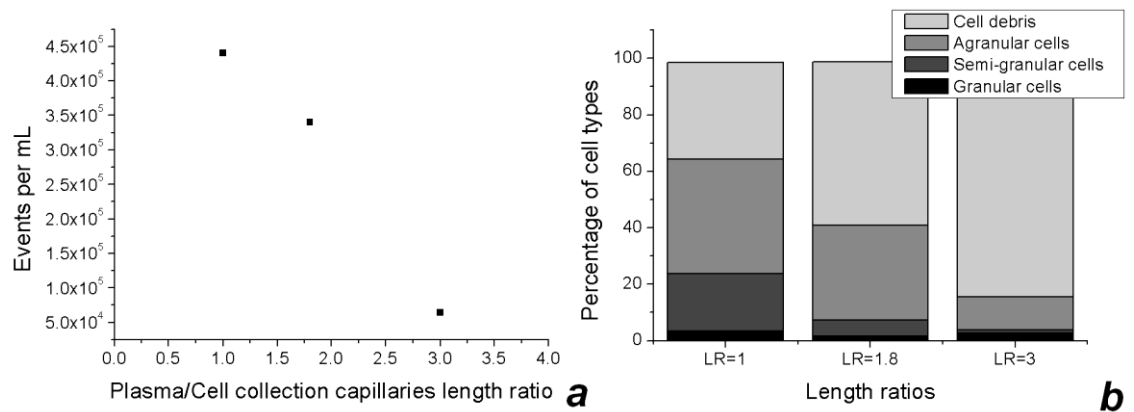
Figure 6. 15: (a) Graph illustrating the influence of the outlet length ratio on the number of events per mL. (b) Graph illustrating the influence of the outlet length ratio on the repartition of event types in the plasma collection.

6.4.1.2 Separation of plasma from **human blood**

The separation efficiency of cells in the plasma collection of human blood experiments is generally inferior to the result obtained with mussel blood. This can be partly explained by the difference in cell size. In the human blood the size of red blood cells is ranging from 7 to 8µm, which is very different from the size of the depth of the channels, and therefore the effect is not as clearly visible as for the larger mussel blood cells.

Table 6.1 presents the results of two experiments to determine the influence of the flow rate. The OLR is 4.5 in both experiments, and the flow rate was varied from 5 to 20mL/h. The results show a modest increase in efficiency of 7.6%.

Experiment number	Outlet length ratio	Flow rate	Number of events (feed) (/mL)	Number of events (plasma coll)	Purity efficiency (%)
N13	4.5	5mL/h	1.9e5	1e5	49
N12	4.5	20mL/h	6.6e5	8.3e4	56.6

Table 6. 1: Table illustrating the influence of the flow rate on the purity efficiency in the human blood experiments.

149

6.4.1.3 Discussion of the results (first generation device)

The results of these experiments have been compared to those published by other research groups. The present experiments have been carried out at an average flow rate of 10ml/h which is at least one order of magnitude higher than previously reported. For reference, the average flow rate in publications [6.1,6.2] is 100μL/h. Plasma yield is approximately 40%, comparable to Ducree's results [6.9], but it is not reaching the 95% of the common centrifugation technique. The purity efficiency is calculated as in Equation (6.1):

$$Ef = 1 - \frac{c_f}{c_p} \tag{6.1}$$

where c_f is the concentration of RBCs in the feed collection and c_p is the concentration of RBCs in the plasma collection.

The purity efficiency found for the mussel blood is 60% on average, which is comparable to other groups. Results of the human blood experiments show an efficiency of 40% on average, which is slightly below the results reached by other groups. Generally, the hematocrit used in these experiments is low (3%) which means that the blood is heavily diluted before the experiments.

6.4.2 Separation efficiencies in the second generation chips

6.4.2.1 Influence of the entrance hematocrit and flow rate on the separation efficiency.

The influence of the hematocrit on the separation efficiency was studied using different dilution levels. For the chip with the 20μm plasma channels, the corresponding hematocrit levels to the dilution levels were comprised between 3.3% and 31%. In the chip with the 10μm plasma channels, higher levels of hematocrit were studied, ranging from 9.4% to 45% (1:10 dilution to no dilution at all). The purity efficiency is given in equation 6.1.

Figure 6.16 shows the different purity efficiencies obtained as a function of the level of hematocrit at the entry for the 20μm model. Some hematocrit levels have several experimental points (two or four). Two points are due to the independent collection of

data from each plasma outlet. Four points are due to two different experiments, each of them having two different experimental points. Two different flow rate were used (2mL/h and 5mL/h) and figure 6.16 also illustrates the influence of flow rate on the separation efficiencies. After the threshold of 9.4% hematocrit, the purity efficiency decreases sharply. The experimental points at 5mL/h and 10mL/h show a slight increase in purity efficiency, confirming the preceding results. The high hemoglobin levels results from the low purity efficiencies after the threshold.
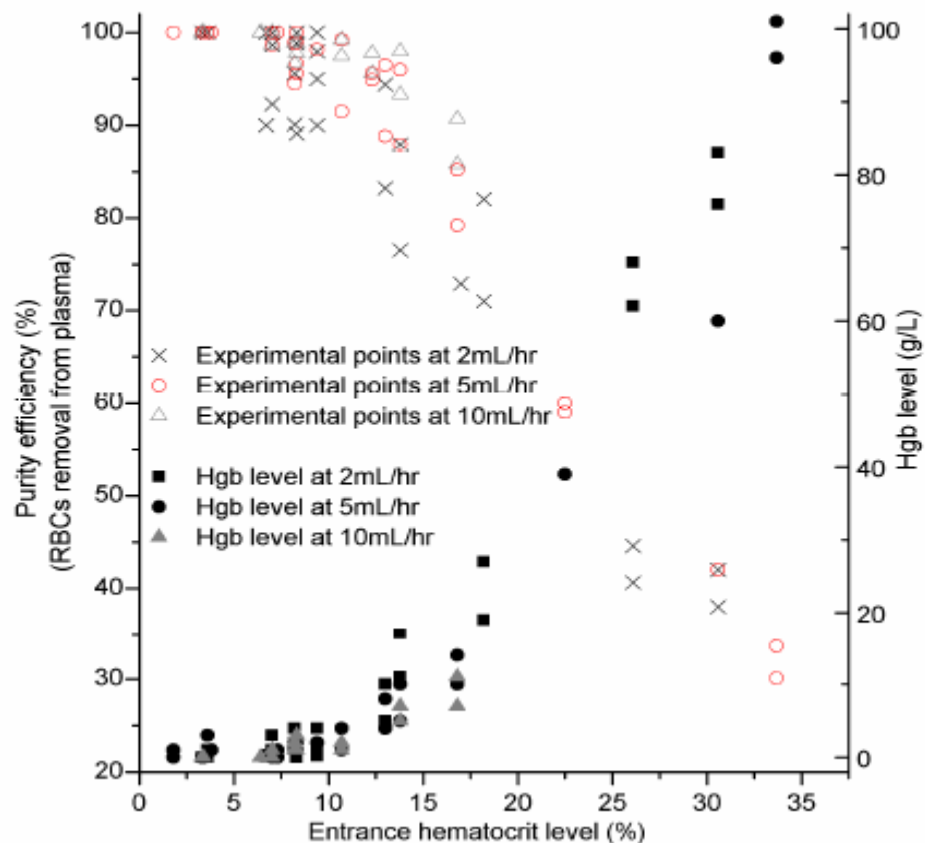
Figure 6. 16: Influence of the flow rate on the purity efficiency of the 20µm microfluidic system

Figure 6.17 details the results of the 10µm plasma channel chips. In these experiments, the only flow rate used was 2mL/h. Hemoglobin levels are indicated here to report on cell destruction, it can be seen that the hemoglobin level are increasing with the hematocrit. However it stays below the level reported to introduce interference in the downstream analysis = 5g/L [6.11]. The purity efficiency decreases very slightly towards hematocrit levels comparable to whole human blood. Generally, the 10µm design showed excellent plasma purity. However, this comes at the expense of low

yield (<7%). Furthermore, the use of non-diluted blood increases the risk of clogging the separation chip within the few minutes of use. Nevertheless, this is an achievement as very few groups have reported the separation of non-diluted blood using passive microfluidic devices.
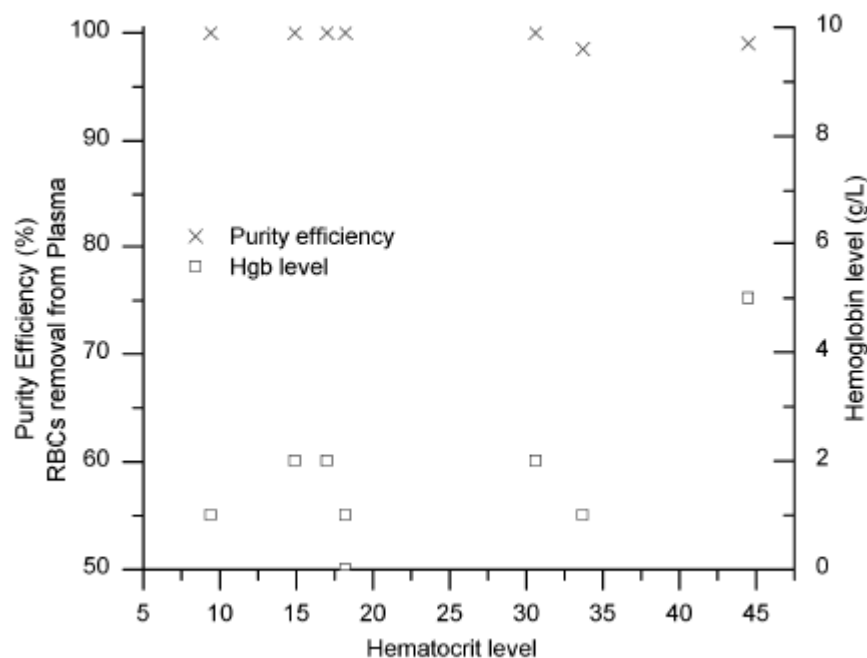
Figure 6. 17: Influence of the flow rate on the purity efficiency of the 10μm microfluidic system

6.4.2.2 Control of cell population: a flow cytometric study

A flow cytometric study was performed on several samples to get an in-depth knowledge of the separation of plasma from blood. As the ultimate goal of the plasma separation is to detect cfDNA in the plasma, it is crucial to prove that the cells are not damaged or destroyed during separation. Damaging the cells and causing lysis lead to more contamination of the plasma. In order to give useful biomedical information, the cfDNA detected in the plasma should be present in the blood prior to extraction and should not come from cell lysis as a result of sample preparation.

Material and Methodology

Staining of the blood sample was performed to label leukocytes and platelets. The R-phycoerythrin (R-PE)-conjugated monoclonal antibody CD45 (PE Mouse Anti- Human, BD Biosciences) was used for leukocytes surface staining. The fluorescein isothiocyanate (FITC)-conjugated CD42 antibodies stained the platelets. Using these

152

markers we were able to identify the leukocytes and platelets population. The RBCs were identified by being non-stained. Blood cell population analysis was carried out on a FACS Scan instrument (BD Biosciences, San Jose, USA) and results were analysed using Flow Jo software v7.5.3 (Tree Star, Ashland, OR, USA). Determination of the absolute cell count was achieved by the use of flow cytometric beads Flow-Check Fluorospheres (Beckman Coulter). 50μL of well-mixed beads mixture was added to the 200μL of sample and mixed thoroughly. The flow cytometer was then calibrated to count a specific number of beads allowing a precise absolute count of the cells.

Three types of samples are analysed with the FACS scan instrument:

- Feed samples (diluted whole blood)

- Cell collection samples (concentrated feed samples)

- Plasma collection samples (cell-depleted samples)

A certain number of controls are necessary to make sure that the antibodies work and will allow the detection of all components. Table 6.2 details the different controls set-up before the study.

Type of sample	Type of control
Diluted WB	Negative control, check background fluorescence
Diluted WB + CD42	Check binding CD42
Diluted WB + CD45	Check binding CD45
Diluted WB + CD 42 + CD45	Antibodies Positive control
Diluted WB + counting beads	Check counting beads
Diluted WB + CD42 + CD45 + counting beads	Entire Positive control

Table 6. 2: Flow cytometric controls using whole blood(WB) samples.

Figure 6.18 shows the results of the flow cytometric data after processing. The horizontal axis represents the size of the cells (Forward scatter, FSC) and the vertical axis represents their granularity (Side Scatter, SSC). In the feed collection the population is mainly constituted of RBCs (95.62%), platelets (4.1%), leucocytes (0.28%), which corresponds to normal physiological conditions. Additionally the counting beads are present in the mixture, as well as the population identified as platelets aggregates and platelets-monocytes aggregates [6.7]. The platelets are located in the bottom-left quadrant of the diagram, as they are the smallest and least granular particles. In this

quadrant a large population of red blood cells is also present; these are either very small RBCs or RBCs debris present in the blood before separation. The presence of these debris can be explained by cell damage caused by the processing, transport and storage of the blood. Other RBCs, counting beads, monocytes and platelets aggregates can be found in the upper right quadrant. Linking these two quadrants is the "tail" of the healthy RBCs population, smaller or damaged RBCs. Little change is observed between the feed collection and the cell collection after separation. The tail does not show signs of growth which means that the cells either have not been through high stress or have resisted the stress. Looking at the plasma collection outlets, the plasma is not entirely devoid of cells, but has been strongly depleted by 250 times compared to the feed sample. Most of the RBCs debris has also been removed, which enhance the overall quality of the plasma. The population of platelets is the less depleted of all cell populations, confirming the results from a previous study by Sollier et al. [6.12]. Additionally, a measurement of the concentration of potassium ions could be used as a marker of cell death to assess global cell damage. This has not been carried out in this study.

In conclusion, the flow cytometric investigation has shown that the cells are not damaged through the system. Additionally, the plasma is not entirely devoid of cells as the cell Coulter counter suggests, but the RBC population in the plasma collection has been reduced 250 times compared to the feed sample. Finally, the system also removes the cell debris, rendering the plasma even purer.

Although cytometric studies have also been carried out by other research groups looking at blood plasma separation, this flow cytometry study has provided the most in-depth analysis so far [6.6].
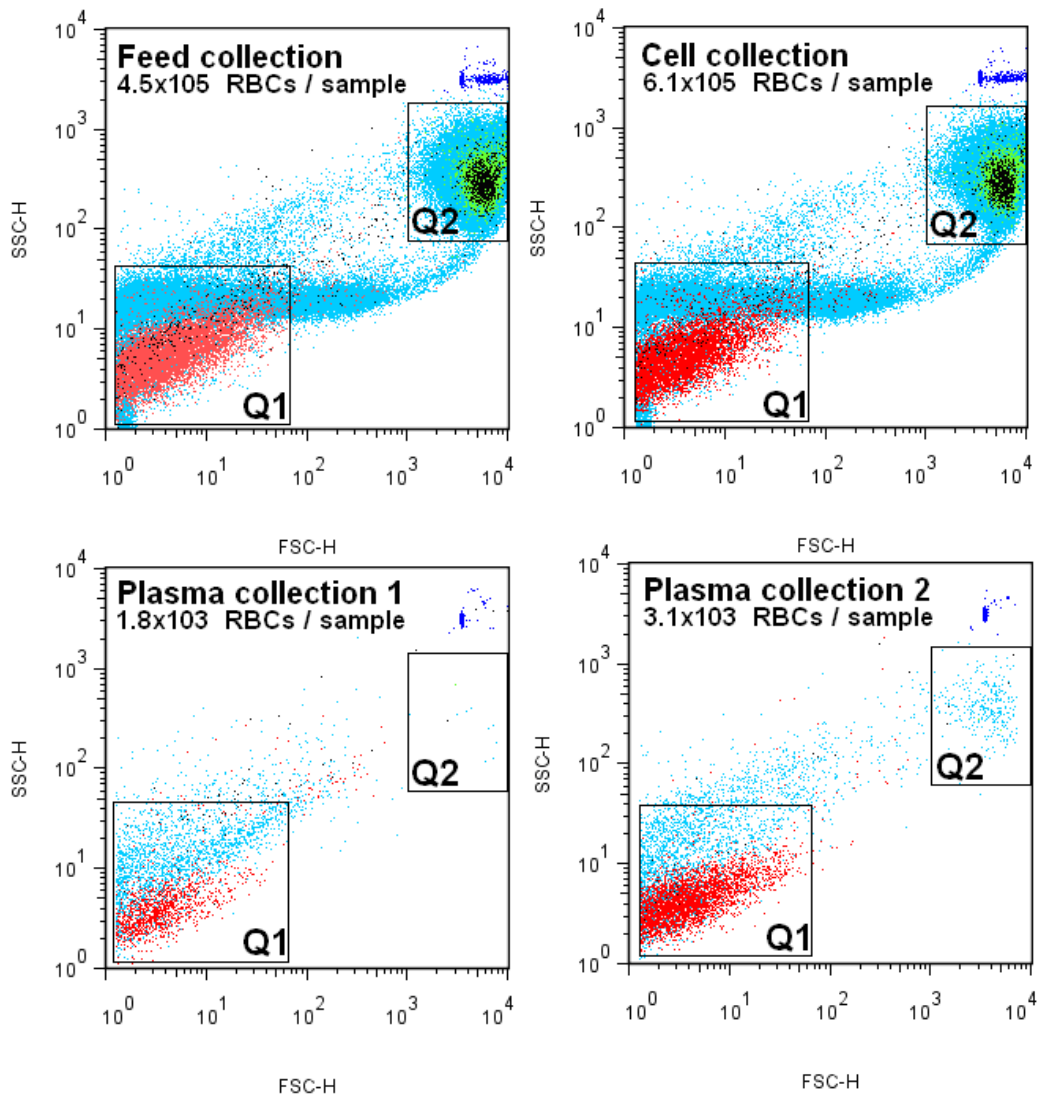
Figure 6. 18: flow cytometer results for each of the four collections. Both plasma collections are largely depleted from red blood cells and white blood cells. No noticeable cell damage by separation method was observed.

6.3.2.3 Control of cell viability

The flow cytometric study does not indicate fully if the cells are dead or not. It only shows the amount of debris and cell population present in the different collections. A flow cytometric study can be completed by a study of the cell viability. Cell viability can be observed using a trypan blue exclusion test.

Trypan blue test is based on the principle that living cells have strong cell membrane impermeable to certain dyes such as Trypan blue. On the other hand, in dead cells the membrane becomes permeable to all sorts of chemicals. [6.13]. Both dead red blood cells and dead white blood cells can be detected in a blood sample using this method.

The white blood cells, which are whitish/transparent of a clear background will appear blueish if they are permeable to the trypan blue. The red blood cells which already have pigmentation due to their iron content, will appear purple.

The trypan blue test is a simple procedure where the sample is diluted about 10 times. A volume of 1 to 4 of 0.4% trypan blue is added to the cell mixture, gently agitated and allowed to stand for 15 minutes at room temperature. A disposable haemacytometer can be used for cell observation. The sample chosen for this test was a sample of the cell solution. Figure 6.19 shows a photograph of the haemacytomter fill with a cell mixture containing trypan blue. The arrow points out to the only blue cell visible in the area.

In conclusion this short cell viability study confirmed the results obtained with the flow cytometry. The process is relatively safe for the cells and it can be envisaged to use the cell from the concentrated outlet for an analytic purpose.

Figure 6. 19: Evidence of cell viability. Cells dyed with Trypan blue. Here only one colored cell is spotted (black arrow). Size of square is 250µmx250µm.

6.4 Conclusions

Table 6.3 gives a summary comparison between the two types of devices that were made for this study and other publications in blood plasma separation. A maximum of 40% improvement in the purity efficiency has been realized from the first device type to the second. This was possible at the expense of the plasma yield.

Separation of plasma out of diluted whole blood in a passive microfluidic device was demonstrated and characterized in this chapter. The mean separation efficiency from the first generation device to the second generation device was found to be better than 30%. Generally the cells were found to be unharmed by the separation, and no cell debris was found to be produced from the separation. This study demonstrates an efficient and disposable way to extract at high flow rate cell-free plasma from whole blood at different dilution levels. The purity efficiency reached 100% even with the use of relatively large channels (20μm) which are suitable for mass manufacturing.

Difficulties related to the processing of large difficult biological samples such as whole blood samples were also presented and the reasons of their presence were proposed.

In the next chapter, biological characterization of the separation will be carried out. Influence of the separation efficiency and of the entrance hematocrit level on polymerase chain reaction will also be studied.

	Ducrée [6.9]	Faivre [6.1]	Jaggi [6.3]	Blattert [6.10]	Yang [6.2]	Common centrifugation	This work First generation	This work Second generation
Flow rate	15µL/min	3,3µL/min	5mL/min	1,2mL/min	0,167µL/min	batch	10mL/h	5mL/hr
Hematocrit	45%	16%	4.5%	5%	<25%	45%	3%	Up to 45%
Counting method	Optical (colour recognition)	NC	Auto cell counter	Auto cell counter	Optical (image analysis)	FC	FC	Auto cell counter
Regime used	Centrifugation on a CD	A	C	Small centrifugal force + C (predominant)	A	Centrifugal force	C	C
Plasma Yield*	40%	18%	2.5%	3%	19%	95%	40%	5 to 30%
Purity Efficiency	99%	100%	30%	90%	100%	99%	60%	Up to 100%

*plasma yield definition varies depending on the research group.

Table 6.3: Table illustrating the comparison between different blood plasma separation microtechniques and the common centrifugation process. The behaviour of the RBCs is also indicated with reference to Table 3.5 in Chapter 3.

6.5 References

[6.1]   M. Faivre, Abkarian, M., Bickraj., Stone, H.A., *Geometrical focusing of cells in a microfluidic device: an approach to separate blood plasma*, biorheology, **43**, 147-159 (2006).

[6.2]   S. Yang, A. Undar, and J. D. Zahn, *A microfluidic device for continuous, real time blood plasma separation*, Lab on a Chip **6** (7), 871–880 (2006).

[6.3]   R. Sandoz R.D. Jaggi, C.S. Effenhauser, *Microfluidic depletion of red blood cells from whole blood in high aspect ratio microchannels*, Microfluid. Nanofluid. **3**, 47-53 (2007).

[6.4]   M. Cubizolles E. Sollier, Y. Fouillet, J.L. Achard., *Fast and continuous extraction from whole human blood based on expanding cell-free layer devices*, biomedical microdevices (2010).

[6.5]   P. Olla, *Simplified model for red cell dynamics in small blood vessels*, Physical Review Letters **82**, 453-456 (1999).

[6.6]   J.F. Edd D. Di Carlo, D. Irimia, R.G. Tompkins, and M. Toner, , *Equilibrium Separation and Filtration of Particles Using Differential Inertial Focusing*, Anal. Chem. **80**, 2204-2211 (2008).

[6.7]   Y. Hiramatsu Y. Yoshimura, Y. Sato, S. Homma, Y. Enomoto, Y. Kikuchi and Y. Sakakibara, , *Activated neutrophils and platelet microaggregates impede blood filterability through microchannels during simulated extracorporeal circulation*, Ann. Thorac. Surg. **75**, 1254–1260 (2003).

[6.8]   E. Westein W. S. Nesbitt, F. J. Tovar-Lopez, E. Tolouei, A. Mitchell, J. Fu, J. Carberry, A. Fouras and S. P Jackson *A shear gradient–dependent platelet aggregation mechanism drives thrombus formation*, Nature Medicine **15**, 665 - 673 (2009).

[6.9]   T. Brenner S. Haeberle, R. Zengerle, J. Ducrée, , *Centrifugal extraction of plasma from whole blood on a rotating disk* Lab Chip **6**, 776-781 (2006).

[6.10] C. Blattert, R. Jurischka, A. Schoth, P. Kerth, and W. Menz, "Separation of blood in microchannel bends", in *25th Ann. Int. Conf. of the IEEE Engineering in Medicine and Biology Society* (Ieee, Cancun, Mexico, September 2003), Vol. 25, pp. 3388-3391.

[6.11] V. Vandelinder and A. Groisman, *Separation of plasma from whole human blood in a continuous cross-flow in a molded microfluidic device*, Anal. Chem., **78,** , 3765-3771 (2006,).

[6.12] M. Cubizolles E. Sollier, M.Faivre, Y. Fouillet, J.L.Achard, *A passive microfluidic device for plasma extraction from whole human blood*, proceedings of the IEEE EMBC, Minneapolis, USA, 2009.

[6.13] R. Freyshney, *Culture of animal cells: a manual of basic technique*. (Alan R Liss Inc, New York, 1987).

Chapter 7: Biological validation of the extracted plasma by biomarkers detection

7.1 Introduction

7.1.1 Motivations

The quality of the plasma has already been assessed by cell counting and flow cytometry as shown in the previous chapter. One other interest in this study is the subsequent recovery of cell-free DNA from the plasma after blood plasma separation on-chip. As seen in Chapter 2, several applications demand the screening of cell-free DNA present in the plasma or serum of the patient. Briefly, this includes the assessment of rejection levels in the monitoring of transplantation and the detection of fetal DNA in the case of prenatal diagnosis.

To truly assess the quality of the plasma extracted on-chip and its use in a common biological reaction, PCR on house-keeping genes (GAPDH, ALU and β-actin) has first been carried out using the product of the separation. The goal of this biological study is to prove that cell-free DNA can be extracted in plasma obtained by the on-chip separation method proposed in this study. It has been suggested that dilution level prior to separation could alter the recovery of biomarkers. In order to answer this question, the influence of the pre-dilution on the PCR efficiency has been studied in this chapter. Additionally to characterise the limits of this separation method, the influence of the separation efficiency on the PCR efficiency has been studied. This study will assess wether 100% pure plasma is required to achieve successful amplification of house-keeping or gender-specific genes. As it is not always easy to extract 100% pure plasma from passive microfluidic device, it is interesting to know if a lesser level of purity would suffice for some types of analysis.

7.1.2 Polymerase Chain Reaction (PCR): a brief introduction

Polymerase Chain Reaction was developed in 1983 by K. Mullis. This powerful technique allows the amplification of DNA strands from a few copies to millions of them.

A number of reagents are necessary in the PCR process:

- *Primers* are oligonucleotides that are complementary to the beginning and end of the targeted DNA strand (forward and reverse primers). These sequences, about 10 to 20 base-long, "prime" the PCR.

- *Polymerase* is the enzyme catalysing the replication of DNA. Under the polymerase activity the complementary bases assemble along the DNA strand. The most common PCR polymerase is Thermus Aquaticus (Taq). The polymerase cannot start the replication of the DNA without primers preliminary binding.

- *Bases,* the bases are the deoxyribonucleotides forming the backbone of DNA. The term dNTPs relates to the four bases, Adenine (A), Guanine (G), Thymine (T) and Cytosine (C).

- *Buffer Solution,* a buffer solution is required to provide a salted solution necessary for the optimisation of the PCR.

- *Magnesium-chloride MgCl$_2$* is used to regulate the number of cations necessary to the reaction, it is usually used at a molar concentration of 3mM.

- *Template nucleic acid*, this is the target of the amplification, the DNA to be amplify. Templates added to the PCR reaction can be in various forms. For example, pure genomic content in water-based solution is used for positive controls. In this case the template are in high concentration and often relatively easy to amplify. In this study, the templates are generally in low concentration, dispersed in unpurified plasma. In the case where there are multiple templates, the PCR is called a *multiplex-PCR*.

As shown in Figure 7.1, the PCR is composed of 5 distinct steps. The first and last steps occur only once in the procedure, whilst the three middle steps are repeated over a number of cycles ranging from 20 to 40 cycles. During the first *initialisation* step, the polymerase is activated by temperature ranging from 90 to 95°C for 10 minutes. During *denaturation*, the first step of the PCR cycle, the double helix is separated into two strands under high temperature. It usually takes place at 94°C step for 20 to 60 seconds. The primers are then bonded to the DNA strands during the *annealing* step which occurs at lower temperature (50-60°C). The polymerase is then attracted to the primer-strand bonding sites and the *extension* step can begin when temperatures is raised to 72°C. The polymerase enzyme travels along the strand to assemble the complementary oligonucleotides. Generally, the cycle of *denaturation-annealing-extension* is performed about 30 times before the efficiency of the polymerase seems to drop. After these cycles a *final extension* is performed for 10 minutes, this step ensures the full extension of the single DNA strands. PCR is an exponential reaction, after n cycles, the number of copies will reach 2^n. In theory, PCR can be achieved from a single DNA copy, however, in practice a more substantial amount of DNA is often necessary to start off the reaction.
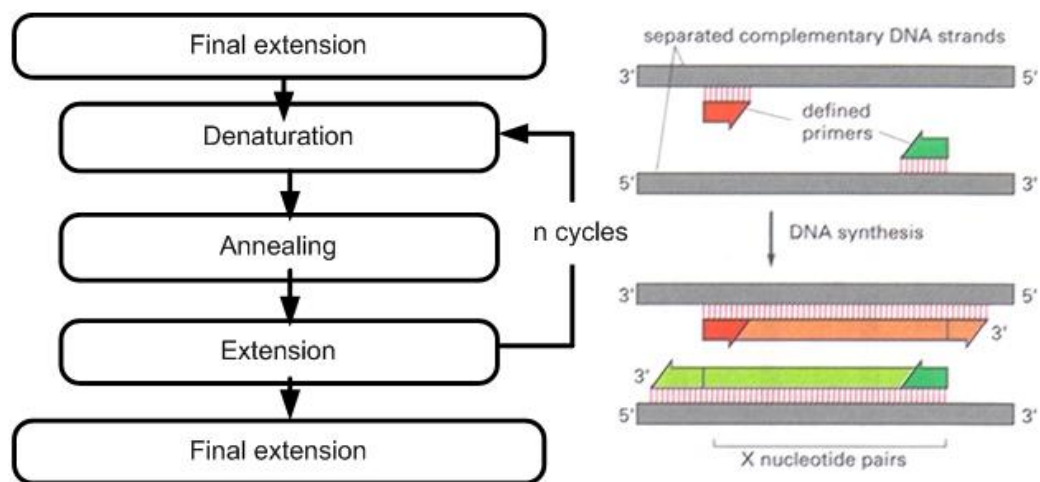

Figure 7. 1: Polymerase Chain Reaction (PCR) steps

In conventional PCR the detection and quantification of the amplified product occurs after the process is finished. Gel electrophoresis is the most common post-PCR analysis. When the PCR is finished the samples may be purified using common QIAGEN PCR purification kit. The sample containing the amplified product is then loaded in an

Agarose gel upon to which is applied a voltage which separates DNA molecules by size. The DNA material has been stained using fluorescent probe such as Ethidium bromide or SYBRsafe. The DNA bands are visualised using UV radiation and analysed. More details on the gel electrophoresis procedure can be found in Appendix B.

PCR analysis can be affected by contamination by volatile nucleic acids present in the laboratory environment. Cross-contamination can also arise between samples [7.3]. Contamination can be relatively severe in the case where house-keeping genes are amplified. In this particular study, anti-contamination measures had to be set-up to prevent contamination. Preparation of the PCR was carried out under laminar flow hood, in a dedicated room. Surfaces, pipettes and gloves were cleaned using DNase-Zap (Ambion) previous to the preparation of the PCR mix. Appendix C summarises the different steps generally taken to avoid contamination.

7.2 Recovery of cell-free DNA by Conventional PCR

Theoretical aspects of PCR has been treated in the previous section. In order to make the entire process faster and in the future outlook of implementing a microPCR module directly downstream from the separation module, the common purification step of the DNA before PCR was omitted. The protocol used is shown in Figure 7.2.

Three house-keeping genes have been chosen in this study. ALU is a very abundant gene (redundant) in the human genome. Its redundancy makes it a gene of choice, for example, in the recovery of human DNA in forensic science [7.4]. However, because of ALU redundancy, a PCR with this gene is more susceptible to contamination. Glyceraldehyde 3-phosphate dehydrogenase (GAPDH) is a gene responsible for the enzyme catalising glucose for energy supply in the cell. β-actin is another house-keeping gene, encoding a cytoskeletal protein. β-actin levels are known to be very stable, and is often used as control measures in diverse biological protocols.
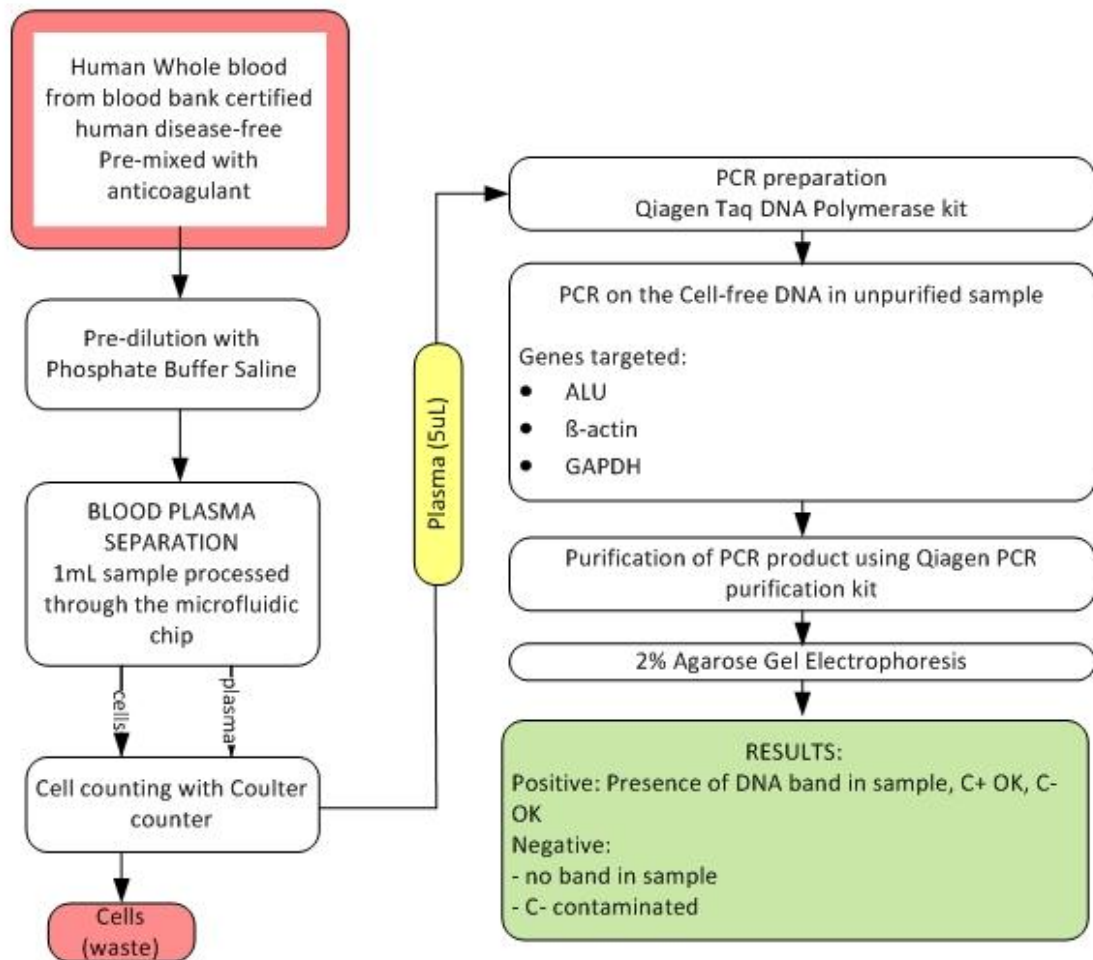
Figure 7. 2: Generic protocol for the extraction of DNA from plasma obtained on-chip.

7.2.1 Amplification of house-keeping genes in the cell-free DNA population present in the serum extracted on-chip.

The amplification primers for the GAPDH gene (Forward primer 5'- GAA GGT GAA GGT CGG AGT CA-3', reverse primer 5' GAC AAG CTT CCC GTT CTC AG) were purchased from Metabion International AG. For the PCR with the GAPDH gene, each reaction aliquot contained 0.4µM forward primer, 0.4µM reverse primer, 0.1µM dNTP (Sigma), 0.1µM dCTP (Sigma), 2.5U Taq DNA polymerase (QIAgen HotStarTaq DNA Polymerase kit), 2.5µL PCR buffer (HotStarTaq DNA Polymerase kit), 4mM MgCl2 (QIAgen HotStarTaq DNA Polymerase kit), 9µL DNA free water. For each reaction, 5µL of serum was added to 20µL of the PCR master mix.

In order to determine whether GAPDH gene could be amplified directly in whole blood a negative control consisting of untreated blood (as received from the blood bank) has

been introduced in the protocol. In the same fashion, to determine if GAPDH gene was present in the buffer solution, a negative control consisting of the 1% BSA PBS solution was used in the PCR on the GAPDH gene (data not shown). ALU primers were also used primarily, however, ALU being a highly repetitive human genomic sequence; it makes the test very sensitive to contamination. It was found, in agreement with ref [7.4] that contamination cannot be avoided, and therefore GAPDH sequence, shorter and less repetitive was more appropriate for the detection tests.

The human genomic control was obtained from Promega in 210ng/µL concentration, and was diluted 10x, 100x and 1000x. 1µL of the dilution was added to the 20µL mastermix, with 4µL of DNA-free water to get a total of 20, 2 and 0.2 ng of DNA per reaction.

Thermal cycling was initiated with a 10min denaturation at 95°C, followed by 40 cycles of 1min denaturation at 94°C, 1min primer annealing at 68°C, 1min extension at 72°C. The final extension step consisted of a further 5min cycle at 72°C and the samples were kept on hold at 10°C until further processing.

The PCR product was purified using the QIAgen PCR purification kit using the procedure specified by the manufacturer. The purified DNA product was eluted in 30µL Elution buffer. 10µL of this product was then stained with 2µL of loading buffer for a gel electrophoresis analysis. The 2% agarose gel was made with 100mL TAE buffer and 2µL of ethidium bromide (10mM/µL). The gel was loaded in the tank and run at 80V for 60min. A gel electrophoresis picture was subsequently taken using a CCD camera in a BioRad UV transluminator and analysed using GelDoc-It^{TM} software.

7.2.2 Influence of the dilution of whole blood previous to on-chip separation

A PCR was performed on the GAPDH gene in the plasma samples extracted on-chip. Samples were isolated after the separation experiment and stored in 1mL eppendorf tubes at 4°C. The separation efficiency was characterised by a Coulter counter as described previously. In order to assess the influence of the pre-dilution of the PCR efficiency, six samples (S1 to S6) with approximately the same separation efficiency but different pre-dilution levels were chosen as shown in Table 7.1. The same separation

efficiency can be achieved through the use of different flow rates and the two chip models (10μm or 20μm width plasma channels).

	Code	Separation efficiency of sample (%)	Entrance hematocrit level (%)
Plasma Samples series 1	S1	100	3.3
	S2	100	6.2
	S3	100	7.0
	S4	100	14.9
	S5	100	17
	S6	100	33.7
Positive controls	G1	Genomic control 1 – 1:10	
	G2	Genomic control 2 – 1:100	
	G3	Genomic control 3 – 1:1000	
Other controls	WB	Whole blood	
	W	Ultrapure Water	
Negative control	C	Plasma sample extracted by gentle centrifugation (3000 rpm, 10 min)	

Table 7. 1: Characteristics of the samples and controls used in the blood dilution influence experiment

Three human DNA controls (G3041, Promega, Madison, WI, USA) were prepared at dilution levels (G1 to G3). Samples of whole blood, ultrapure water and plasma extracted by centrifugation were collected.

PCR and gel electrophoresis were performed on these samples, as shown in Table 7.1, following the protocol presented in the previous section. The on-chip extracted samples were doubled. A 1000bp ladder was used in the first column of the gel.

The amplified products of the plasma samples are shown in Figure 7.3. In all columns but the negatives samples a clear 200bp band is present, showing the amplification of the GAPDH gene fragment. The intensity of the bands varies from sample to sample. Within the duplicates, the intensity does not vary. For the samples series 1, all PCR products show a relatively strong amplification. Interestingly, a gradient in the fluorescent signal can be noted from S1 to S6, excluding S5 which stands out and shows a lower amplification. The presence of a gradient confirms that the PCR

amplification efficiency is depending on sample dilution. Additionally, the presence of an amplification band in the sample with the highest dilution (corresponding hematocrit level 3.3%) demonstrates that PCR can be achieved on diluted samples.

All the other controls, including the negative controls show no amplification. In line WB, and C, the PCR has been inhibited by the presence of Immunoglobulin G present in the whole blood and in the plasma sample extracted by centrifugation.
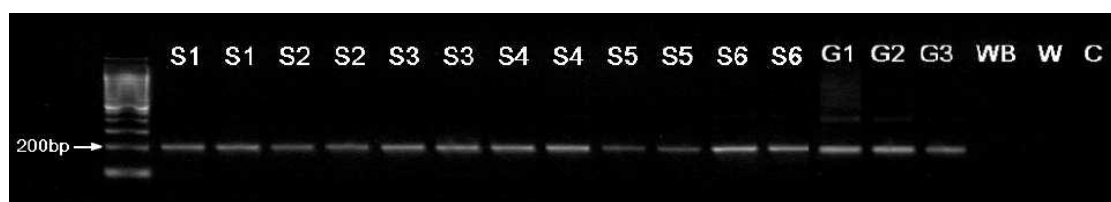
Figure 7. 3: Ethidium bromide-stained agarose gel of PCR products obtained with GAPDH primer and unprepared plasma samples obtained by microfluidic extraction. The first lane is a molecular weight marker (1000-bp ladder).

7.2.3 Influence of the separation efficiency on the PCR efficiency.

As demonstrated by Figure 7.3, PCR can be achieved on cfDNA in plasma extracted on-chip for purity efficiency of 100%. Further study was carried out to assess the limits of the PCR capability on cfDNA in untreated plasma sample. In that respect, plasma aliquots from samples with similar entrance hematocrit levels and with different purity efficiencies were collected after separation and stored at 4°C. The different samples used in this experiment are presented in Table 7.2. The separation efficiency of the samples ranged from 65.1% to 100%. The amplified products of this experiment are shown in ethidium bromide-stained agarose gel in Figure 7.4. A clear gradient of band intensity through samples S1 to S5 can be observed. No PCR product could be amplified from S5 (purity 65.1%), whole blood and water lanes. The band from S4 (purity 84%) is visible but faint.

This experiment demonstrates that the PCR efficiency depends on the separation efficiency, and most importantly shows that at the high separation efficiencies which are standard for our device, PCR can be routinely performed. Moreover these experiments have successfully shown that the plasma extracted on-chip is pure enough to perform amplification without further purification steps as routinely done after centrifugation today, reducing thereby reagent costs, material waste and

processing time. For more difficult cfDNA targets such as cffDNA, this step might still be necessary.

	Code	Separation efficiency (%)	Hematocrit level (%)
Plasma samples	S1	100	14.9
	S2	97.8	12.3
	S3	94.9	12.3
	S4	84	16
	S5	65.1	16
Positive controls	G1	Genomic control 1– 1/10	
	G2	Genomic control 2 – 1/100	
	G3	Genomic control 3 – 1/1000	
Other control	WB	Whole Blood	
Negative control	W	Water	

Table 7. 2: Characteristics of the samples and controls used in the experiment on separation efficiency influence
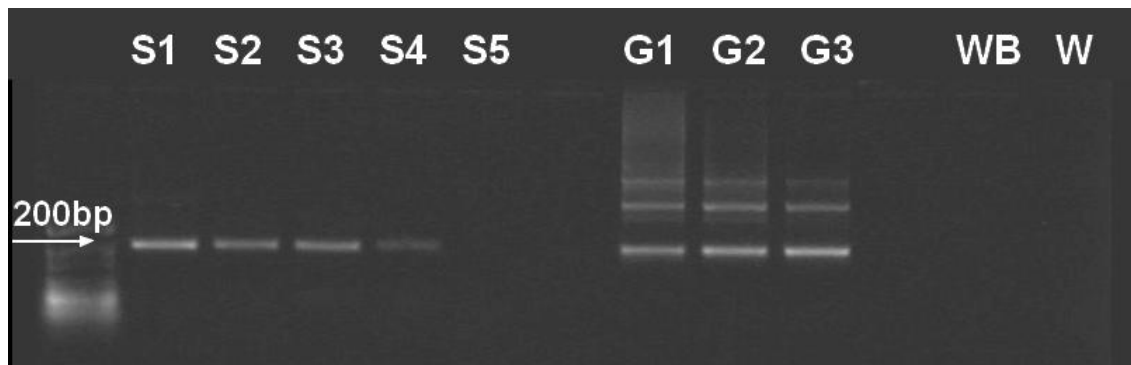

Figure 7. 4: Influence of the separation efficiency on the detection of the GapDH house-keeping gene in the on-chip extracted plasma. The first lane is a molecular weight marker (50bp ladder).

One final and important point to consider is the effect of the time delay between draw and processing of blood which has been shown to be a factor in the quantification of cfDNA. Lysis of intact cells caused by a delay in blood processing would result in increased concentrations of cfDNA (caused by ex-vivo processing) which might lead to misleading results especially if cfDNA is used as a biomarker in cancer, prenatal and post transplant care. Integrating the process of blood plasma separation and PCR analysis onto a single chip will overcome this limitation for the routine use of cfDNA analysis in clinical settings.

7.3 Detection of biomarkers via real-time quantitative PCR (qPCR)

7.3.1 Introduction to qPCR and goal of this study

Real-time quantitative PCR, or qPCR is one of the most powerful techniques in molecular biology. Like PCR it allows the amplification of specific sequences within DNA. However, unlike conventional PCR where the sequences are detected at the end of the PCR process via a purification, staining and gel electrophoresis, qPCR allows the measurement of the amplified product at the end of each cycle via real-time fluorescence monitoring. Therefore by comparison it is possible to determine the initial concentration of product in each sample.

In this study it is particularly interesting to use qPCR to quantify the differences in amplification between the different samples. As shown in the previous part, it is possible to observe these differences on a gel, but difficult to quantify them. Real-time PCR is also attractive to detect low levels of target DNA in samples. Additionally, in qPCR the amplification and the detection are combined which saves manipulation time and prevent post-PCR contamination. Finally qPCR presents advantages for on-chip integration, as it combines amplification and detection at the same time, and therefore greatly reduces the assay time, as well as the possible manual intervention. The realisation of truly integrated qPCR devices has been branded as a "bottleneck" [7.5]. Nevertheless, a number of examples of qPCR integration on microfluidic chip can be found in the literature [7.6]. In the 1990s, many microfluidic PCR examples used silicon as a substrate material [7.5,7]. However in the recent years, PDMS and PMMA have been used to build PCR module.

7.3.2 Materials and methods

Reaction mix and samples

The qPCR was carried out on a Stratagene MX300P. The 25μL reaction contained 12.5 μL of 2X SYBR Green jump start Taq ReadyMix (Sigma), 0.4 μL of 10uM of each primer, 5.5μL distilled H2O, and 5uL of sample containing the input DNA. The parameters used for qPRC on B-actin is given in Table 7.3. The reaction samples were pipetted into microplate (ABgene plate, ThermoScientific) wells and the plate was spun at 1000rpm for 30s prior to the amplification to ensure a homogenous reaction in each well. Both

β-actin and GAPDH genes were used as target DNA in these experiments. The positive controls consisted of human genomic DNA at different concentrations.

	[Start]	[Finish]	Volume per reaction	Master Mix
SYBR Green jump start Taq ReadyMix	2x	1x	12.5µL	150µL
Forward primer	10µM	0.4	1µL	12µL
Reverse Primer	10µM	0.4	1µL	12µL
Water	N/A	N/A	5.5µL	66µL
Sample	N/A	N/A	5µL	N/A
Total Volume			25µL	

Table 7. 3: Mastermix parameters for qPCR on β-actin

Figure 7.5 presents the thermal profile of the qPCR as designed on Stratagene MxPro QPCR software of the Mx3000p qPCR machine (Stratagene). The optimised real-time quantitative PCR temperature consisted of a 10min hot start at 95°C (segment 1, Figure 7.5) followed by 45 cycles of 30s denaturation step at 94°C, 15 seconds of annealing step at 64°C and 30 seconds elongation step at 72°C (Segment 2, Figure 7.5). The annealing step was purposefully set at high temperature and short duration to avoid primer-dimer formation. In the last step the dsDNA present in the wells is denatured once again, then gradually cooled to a "melting temperature" (Tm) (based on the primers Tm value) followed by a last increase in temperature to 95°C (Segment 3, Figure 7.5). This last step produces the dissociation curve or melting curve and is specific to SYBR green qPCR.

7.3.2.2. Plate occupation

A qPCR plate has 64 wells. A plate can be divided into different parts for different tests and be run at different times. It is a cost effective method but may bring cross-contamination if the wells are not carefully closed.

For each run the samples may be run in duplicate to cancel out artefacts. Genomic controls at different dilution levels may be used to produce standard curves. Figure 7.6 shows a typical plate occupation.
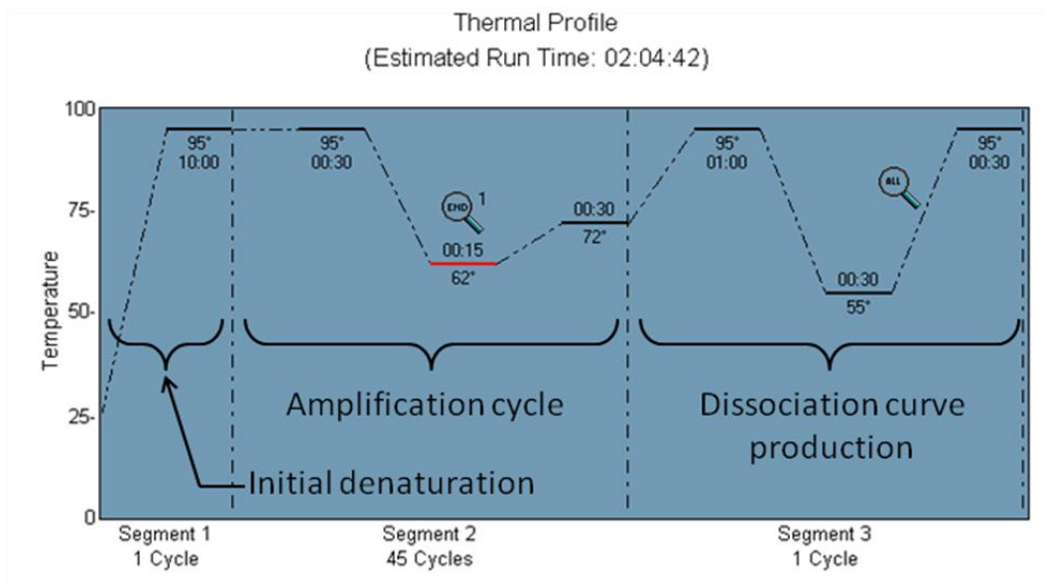
Figure 7. 5 : Thermal profile of the quantitative PCR
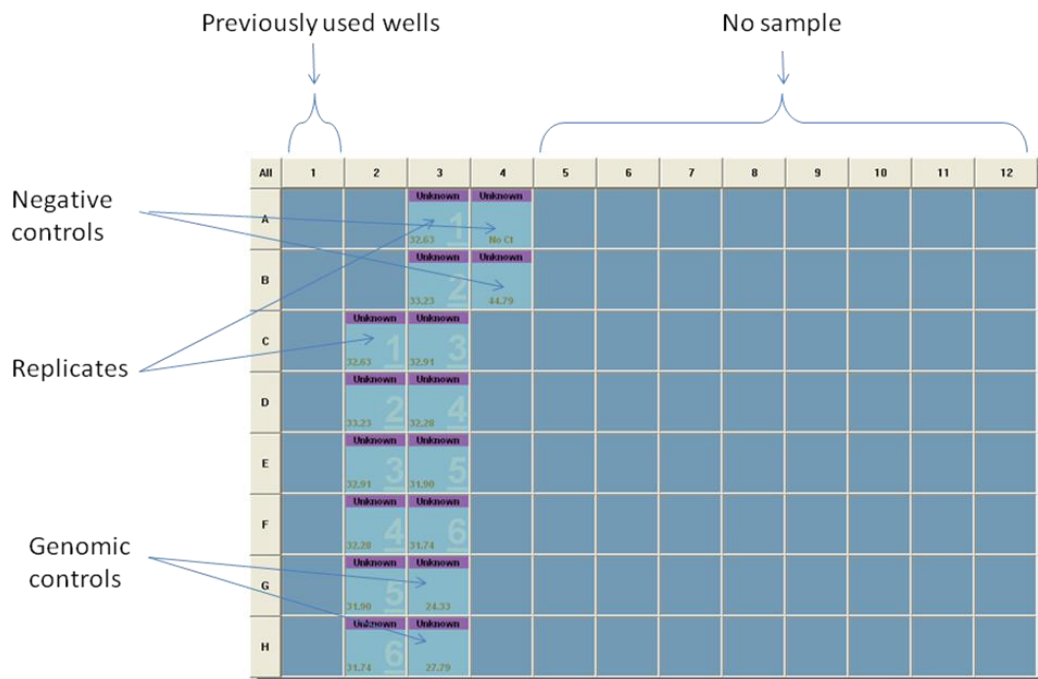
Figure 7. 6 : Plate setup for qPCR experiment

7.3.2.3. Dissociation and Standard curves

Dissociation curves are used to control the presence of primer-dimers or non-specific product formation in each well. Dissociation curves are also known as « melting curves » from the way this curve is produced. The samples are first denatured at 95°C, followed by an annealing step and a gradual increase in temperature, while the fluorescence levels are recorded. The primer-dimers exibit a lower melting

temperature than the amplified product and therefore can be easily detected on this type of curve. Figure 7.7 shows a normal dissociation curves with a single peak. The dissociation curves of the genomic controls are only present in this particular graph. Figure 7.8 shows the dissociation curves of several samples. While some of the curves have a single peak, others have two peaks, revealing the presence of primer-dimer formation. The conventional PCR method have not shown any non-specific product formation, therefore these peaks confirm the presence of primer-dimer formation.
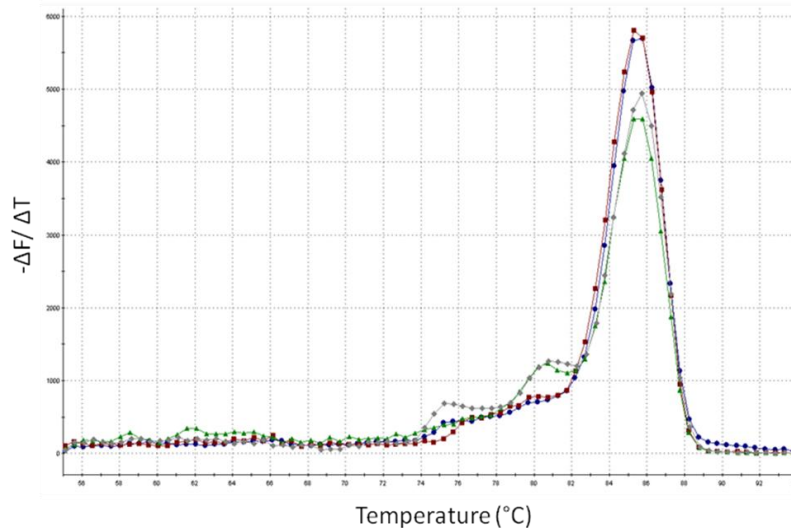

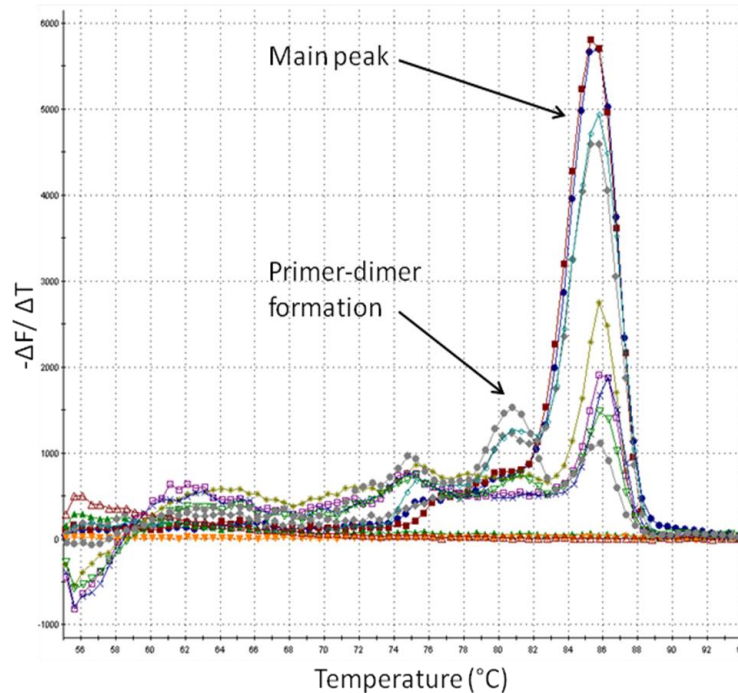*Figure 7. 7: Dissociation curves of a serial dilution of genomic controls.*

Figure 7. 8: The dissociation curve of the samples. It provides information about the presence of primer-dimers

A standard curve can also be established to obtain further information on the reaction. On a standard curve, the initial concentration of DNA in the sample is plotted against the threshold cycle value for each sample as shown in Figure 7.9. The information that can be obtained from the strandard curve, includes :

- The absolute quantification of DNA present in the solution

- The PCR efficiency : the sample points must be as close as possible from the ideal slope of -3.32 corresponding to an efficiency of 100%[3]

Standard curves for absolute quantification, are obtained using dilution series of known template [7.3]. In one experiment, four positive controls of serially diluted solutions of human genomic DNA were used to build the standard curve. The Human Genomic DNA initially comes at a concentration of 210ng/mL. The dilutions used were 1 :10, 1 :100, 1 :1000 and 1 :10,000. 5µL of solution was used in each well with 20µL of master mix solution. Therefore the theoretical quantity of DNA in the first genomic control (1 :10) can be calculated as 105ng, the second (1 :100) 10.5ng, the third (1 :1000) 1.05ng and the fourth (1 :10,000) 0.105ng. In Figure 7.9, these quantities match with the standard curves results.
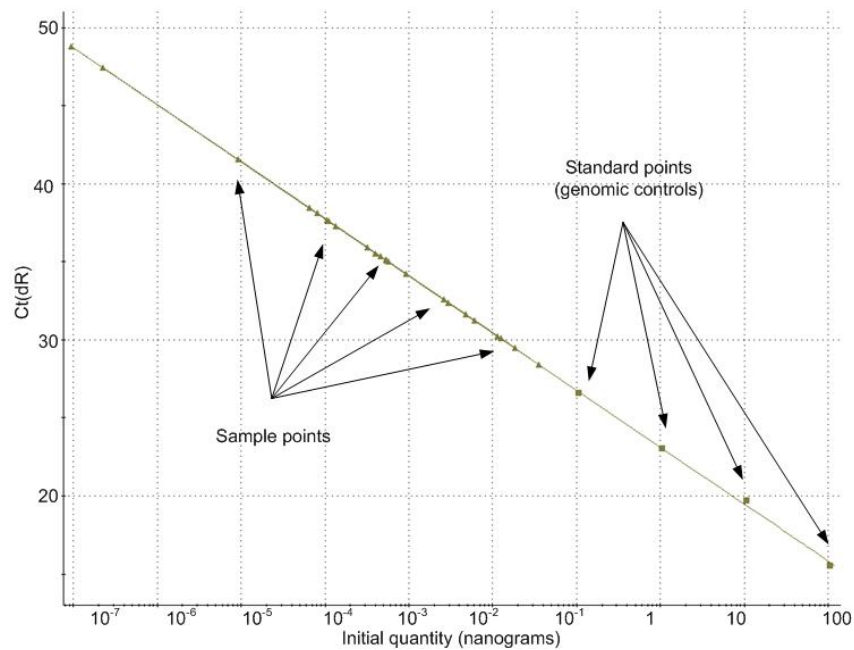

Figure 7. 9: Standard curve based on the standard points of the genomic controls.

---

[3] The concentration of DNA doubles at each PCR cycle if the efficiency is 100%, therefore the slope of the curve is $-1/\log_{10}(2)=-3.32$

7.3.3 Results

A typical amplification curve for a series of unpurified plasma and four dilutions of genomic controls is shown in Figure 7.10. The fluorescent signal level is low during the first cycles of the real-time PCR, this is called the baseline. The threshold of the reaction is set when a statistical increase in the fluorescent signal is detected. In theory the threshold can be set at any point of the exponential curve, but is usually set up automatically at "*10 times the standard deviation of the fluorescent value of the baseline*" [7.3]. The value at which a curve cross the threshold is called the threshold cycle (Ct) and corresponds to the number of cycle necessary to reach a given threshold fluorescence. The four positive controls with serial dilution values of 1:10, 1:100, 1:1000 and 1:10000 show the lowest Cts, respectively Ct(G1), Ct(G2), Ct(G3), and Ct(G4). As the Ct is inversely proportional to the initial quantity of template DNA present in the sample, it means that the genomic controls have the highest quantity of DNA, as expected.

From Figure 7.10 it can be observed that the unpurified plasma samples have high or no Cts. The whole blood control and negative control do not show any amplification at all (no Ct).
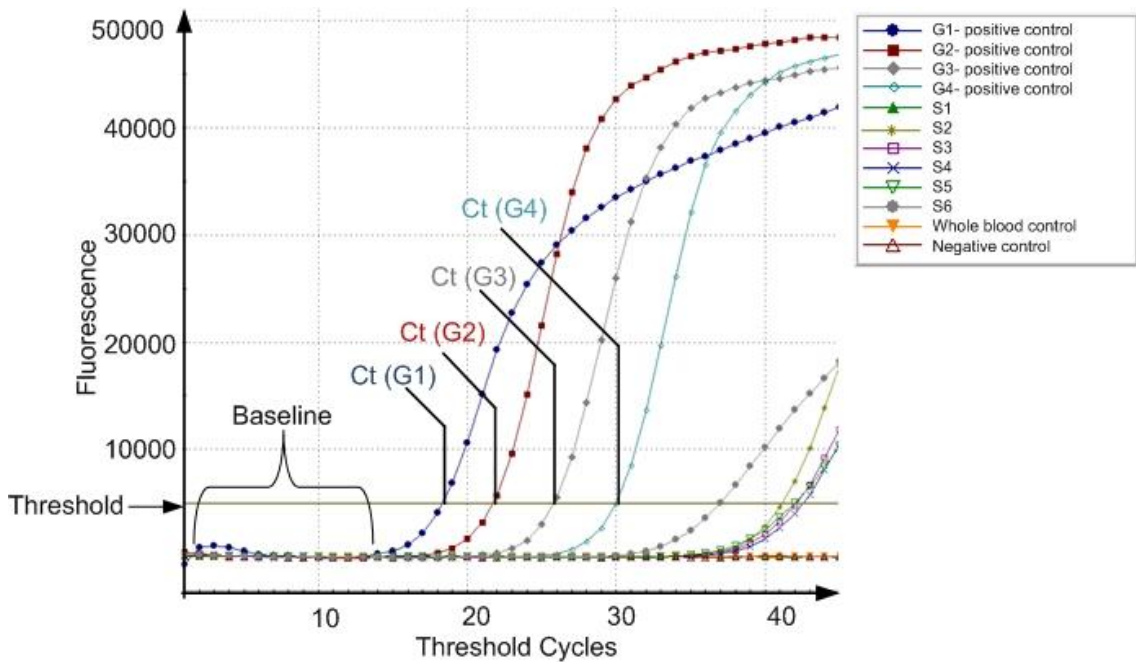

Figure 7. 10: Typical amplification curves from qPCR on B-actin gene from genomic controls and unpurified plasma samples

The amplification curve, however, cannot be analysed without verifying if primer-dimer formation have occurred from the dissociation curves. In Figure 7.11, the amplification curve and dissociation curve of four samples (unpurified plasma) show that the Cts from S3 and S4 are due to the formation of primer-dimer in the well. In conclusion, an amplification curve, does not necessarily mean a positive results: this might be due to primer-dimer formation only. Additionally, an amplification curve can be given by a non-specific product that will also have a different dissociation curve. The dissociation curve should therefore be verified for each sample, after each real-time PCR. This has to be taken into account for the operation of a future integrated qPCR device onto a lab-on-chip. Alternatively, the analysis can be based on the Cts only, given that primer-dimer formation generally do not occur before 30 or 40 cycles. This solution would be at the expense of small or difficult product amplification which necessitates a higher number of cycles.
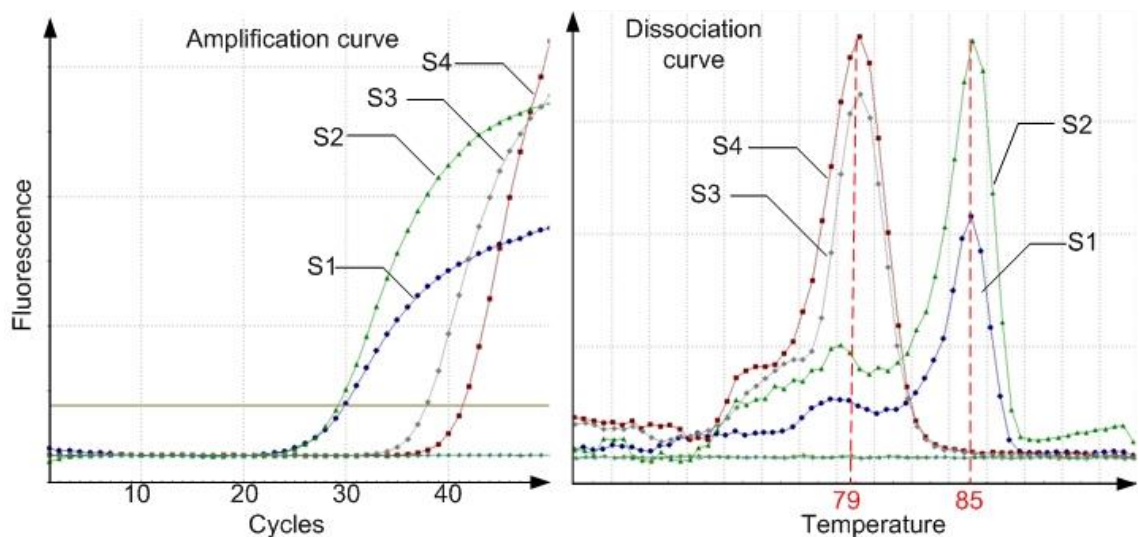
Figure 7. 11: Amplification curve and dissociation curve of four unpurified plasma samples.

In Figure 7.12, the data of six samples and two controls are analysed using the amplification and the dissociation curves.

All of these samples have 100% purity efficiency, but dilution levels are varied. S1 and S2 have a 1:20 dilution level. S3 and S4 have a 1:10 dilution level, and S5 and S6 have a 1:5 dilution level. On the amplification curve, S3, S4, S5 and S6 show relatively significant amplification with Ct values between 30 and 40. S1, S2 and the two controls show no or little amplification. However, the dissociation curve reveals that only S3

and S6 have real "product" amplification, with a distinct curve. A small peak due to primer-dimer formation can be observed on S5 dissociation curve. However, given that the product peak is more than twice the height of the the primer-dimer peak, the product can be considered to have been amplified. S4 show a dissociation curve with a primer-dimer peak higher than the product peak. Although it has been showed that cfDNA in plasma can be amplified using this technique, the presence of primer-dimer formation jeopardizes the quantification of DNA levels in each sample.
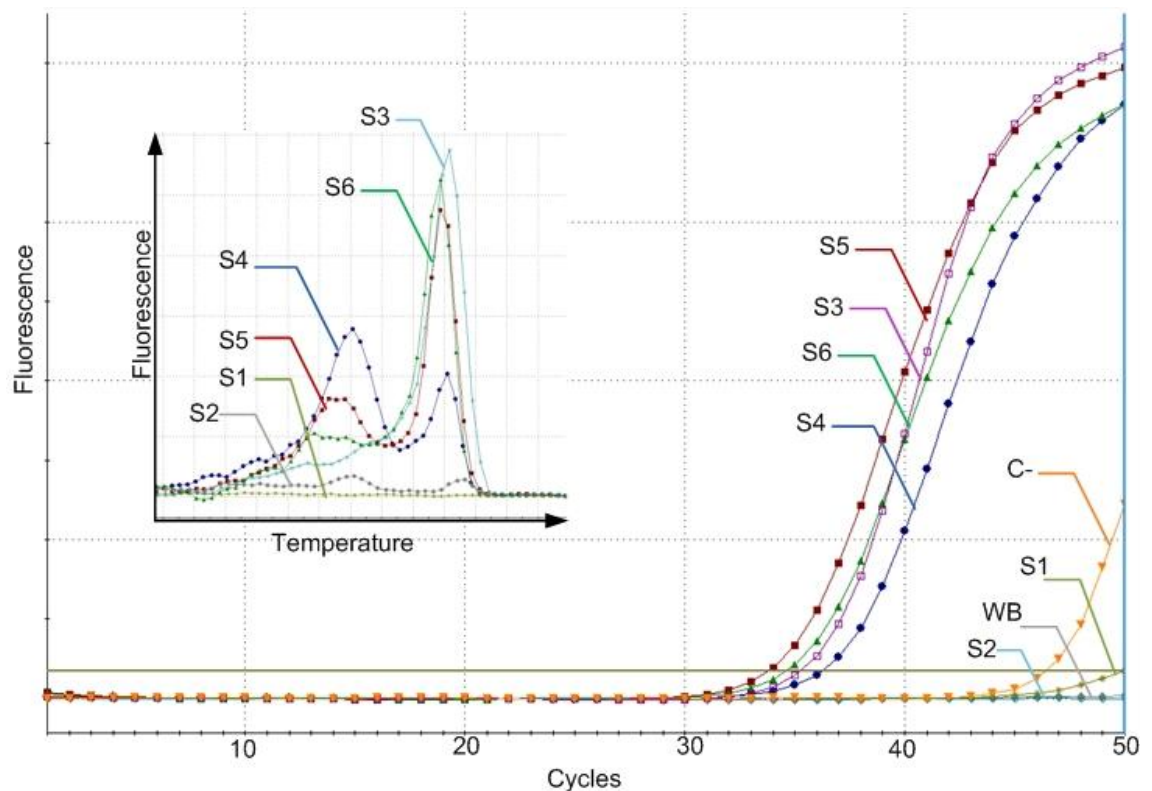
Figure 7. 12: Amplification curve of six unpurified samples. Inset: dissociations curves for the same six samples. Note: the colours between the two graphs do not match. (Data on genomic controls not shown).

In another experiment, the influence of purification on the detection of cell-free DNA via real-time PCR was studied. DNA was extracted from four plasma samples (1:9 dilution) with 100% purity efficiency using QIAGEN blood mini kit following the manufacturer instructions. A real-time PCR was carried out on the 8 samples. Figure 7.13 presents the amplification curve obtained. From Figure 7.13, it is clear that the amplification of purified sample gives high Cts (between 20 and 25), comparable to the levels of the positive controls, while unpurified samples have very low Cts. The dissociation curves were checked, and showed that only the product was amplified in the purified samples.

In conclusion, it was shown that fluorescent PCR could be performed on unpurified plasma samples obtained on-chip. From the present results, it has been difficult to repeat the amplification of unpurified sample. One explanation for this effect might be that the real-time PCR might be more sensitive to remaining inhibitors.

Nevertheless, the amplification of gene in non-purified samples might be possible with the fine tuning of reagent and temperature cycles, an optimization process which has not been carried out in this study.
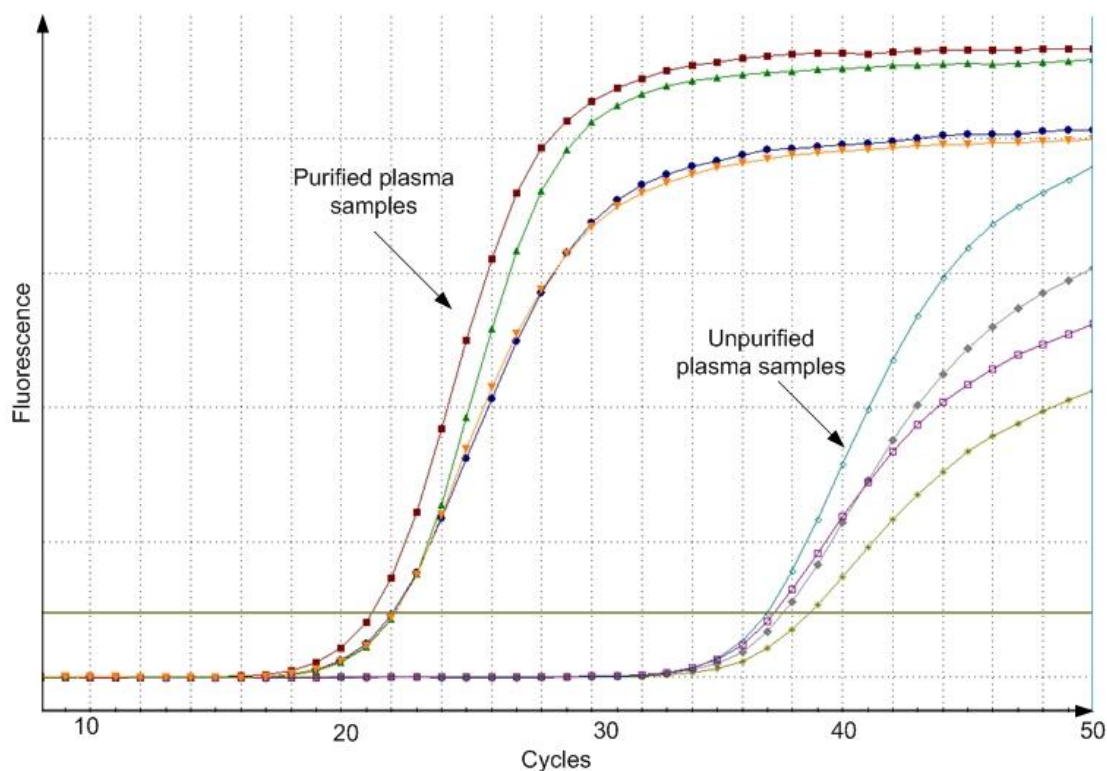
Figure 7. 13: Amplification curve of purified samples and unpurified samples

7.3.4 Conclusions

A qPCR study was carried out using the plasma samples extracted on-chip. It is envisaged that qPCR might be more sensitive to the remaining hemoglobin levels present in unpurified plasma samples. No significant data was extracted from the qPCR carried out on unpurified samples. Nevertheless, DNA template was successfully amplified from positive controls, purified samples and some unpurified samples and might be optimised.

As highlighted at the beginning of this section, real-time PCR is the best choice for on-chip integration. In this small study, it has been shown that the amplification of house-keeping gene via real-time PCR on unpurified sample is not impossible but difficult. The

usefulness of the dissociation curve to analyse if the fluorescence comes from the product amplification or primer-dimer was demonstrated. Dissociation curves should therefore be integral part of on-chip analysis as they are at the moment in macro-sized tools. Despite the difficulties of the physical integration of qPCR on-chip, as well as its operation on difficult samples, this solution will probably be used more and more in the future in LOC modules.

7.4 cffDNA extraction from maternal plasma

7.4.1 Motivations and ethical approval

One attractive application of blood plasma separation and cfDNA detection is the possibility of detecting foetal genes in the maternal blood early on during the pregnancy. Several studies have shown the possibilities of using foetal cell-free DNA levels as biomarkers for chromosomal abnormalities such as Down syndrome or pregnancy-associated diseased such as preeclampsia [7.8,9,10].

In the previous section we have shown that it is possible to detect house-keeping genes in plasma extracted on-chip. However, redundant house-keeping genes are relatively easy to detect, extracting cffDNA from maternal blood is a more challenging task. Figure 7.14 presents the typical protocol set-up for this study. The research project and proposed protocol was approved by the Lothian Research Ethics committee and the Lothian NHS Research and Management committee. The letters of approval can be read in Appendix D1 and D2.

Pregnant women in their first and third semester were recruited at the maternal unit of Edinburgh Royal Infirmary and presented with an information sheet. Signed consent forms were obtained from patients aged between 18 and 45. Information sheets and consent forms can be read in Appendix D3 and D4. All women gave a sample at a single point only.

A closed blood collection system, S-MonovetteTM (Sarstedt) as shown in Figure 7.15, was chosen to extract from 2 to 4mL of blood from patients. The S-Monovette blood collection system contains sufficient anticoagulant (Potassium EDTA), but causes
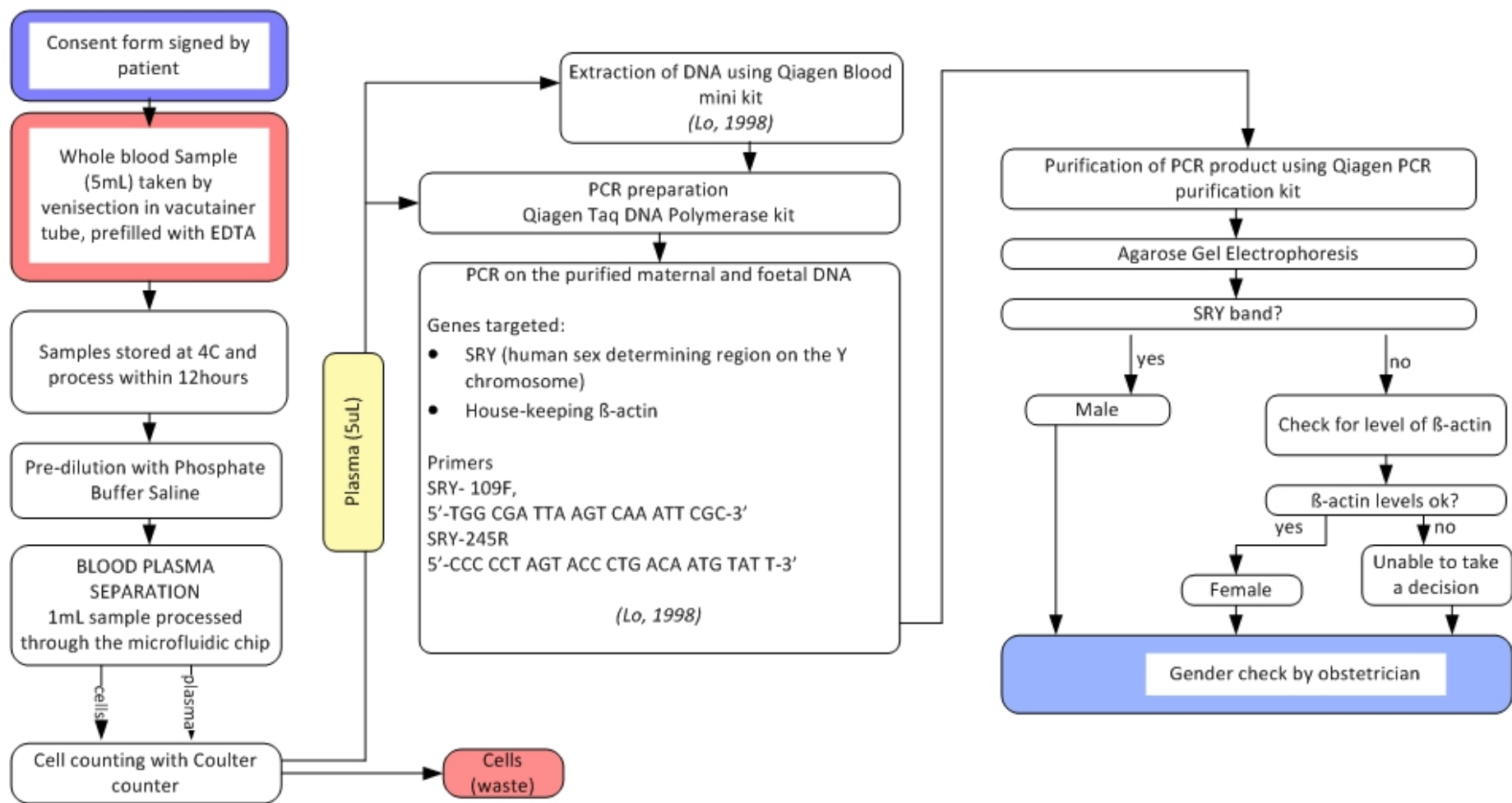
Figure 7. 14: Generic protocol for fetal sex detection via fluorescent PCR on maternal plasma samples.

minimum dilution of the sample. Samples were subsequently stored at 4°C awaiting for collection within 12 hours.

Figure 7. 15: S-Monovette (Sarstedt) blood transfusion tubes prefilled with EDTA are used for blood collection at the Simpson Institute for Reproductive Health.

7.4.2 Material and methods

Figure 7.14 presents a generic protocol for the fetal sex detection via a normal fluorescent PCR on maternal samples. The microfluidic chips used in this study have the same design as the second generation device with 15µm width plasma channel. Using this methodology, the separation will be efficient and the channel will not be clogged up by SU8 material as it could sometimes occurred in the 10µm design. Additionally, the plasma channels have been moved about 20µm upstream to fit exactly in the corner of the constriction. The chips are provided by Epigem and are solely used for this clinical study. A single microfluidic chip is used per sample to avoid cross-contamination. Furthermore, the platform is also changed and the fluid adaptors are autoclaved between each sample.

Whole blood samples were carefully diluted at 1:3, irrespectively of their intrinsic hematocrit level. Aliquots of each whole blood samples each diluted samples were placed in individual eppendorfs tubes for hematocrit level verification. A Beckmann Coulter Counter was used to obtain the hematocrit level of each whole blood and individual samples as described earlier.

2mL of 1:3 diluted blood samples was loaded in a disposable syringe (BD Plastipak) and loaded on a syringe pump (Alladin, World Precision Instruments). The samples were

loaded at a 5mL/h entrance flow rate. Once the blood samples filled the main channel, the separation occurred and the plasma was extracted through the microfluidic network. The cell-enriched mixture was collected in an eppendorf tube for disposal. The ~0.3mL of extracted plasma was collected in a 1mL eppendorf and stored on ice until the cell counting was performed within 6 hours. After the cell counting, the serum samples were stored at -20°C until further processing.

DNA Extraction from serum samples

In a previous experiment, it was shown that cell-free DNA in human serum could be detected directly in serum. In this experiment, fetal DNA is to be extracted from plasma containing maternal and fetal DNA. Without a study of the paternal genome, only genes from the Y chromosome of male foetus can be detected among the maternal plasma. Genes from the Y-chromosome such as SRY or DYS14 will be amplified and will confirm the sex of the foetus. Furthermore, a house-keeping gene will be amplified and will act as a positive control for the efficiency of the PCR for each sample.

In this experiment, the total number of DNA copies is low, and therefore to minimize the risk of negative outcome, the fetal and maternal DNA could be purified from the serum samples using the Qiagen Blood minikit. However, this was not carried out in this particular study.

Good primer design is important, especially in multiplex PCR, to avoid primer-dimer formation. As shown in Table 7.4, the melting temperatures of the primers chosen are within 5°C of each other.

Name	Sequence	Tm°C	nt	A	T	C	G
GAPDHFOR	gaaggtgaaggtcggagtca	61.45	20	6	3	2	9
GAPDHREV	gacaagcttcccgttctcag	61	20	4	5	7	4
SRYREV	cccctagtaccctgacaatgtatt	62.85	25	6	7	9	3
SRYFOR	tggcgattaagtcaaattcgc	59.2	21	6	6	4	5

Table 7. 4: Oligo concentration : 0.25µM, salt concentration: 100mM, primerdigital.com/tools

A single PCR and multiplex PCR were designed. The PCR master mix for the single PCR is shown in Table 7.5, it is in essence similar to the PCR master mix developed in the first part of this study.

	[Start]	[Finish]	Volume /rxn
Forward primer	10µM	0.4µM	1µL
Reverse primer	10µM	0.4µM	1µL
10xTaq buffer	10x	1x	2.5µL
dNTP	2.5mM	0.1mM	1µL
Polymerase	5U/mL	0.2U/mL	1µL
MgCl2	25mM	4mM	4µL
Water	N/A	N/A	8.5µL
Sample	N/A	N/A	5µL
Total reaction volume			25µL

Table 7. 5: Start concentration, final concentration and volume per reaction for the single PCR on GAPDH and SRY sequences.

Another master mix is created for the multiplex PCR as shown in Table 7.6. This time, four primers are present for the amplification of both GAPDH and SRY in the same tube. The concentrations vary slightly, for example, the GAPDH primers concentration is now divided by two and the SRY primer concentration is twice that of the GAPDH primers.

	[Start]	[Finish]	Volume /rxn
Forward primer (SRY)	10µM	0.4µM	1µL
Reverse primer (SRY)	10µM	0.4µM	1µL
Forward primer (GAPDH)	10µM	0.2µM	0.5µL
Reverse primer (GAPDH)	10µM	0.2µM	0.5µL
10xTaq buffer	10x	1x	2.5µL
dNTP	2.5mM	0.2mM	2µL
Polymerase	5U/mL	0.2U/mL	1µL
MgCl2	25mM	4mM	4µL
Water	N/A	N/A	7.5µL
Sample	N/A	N/A	5µL
Total reaction volume			25µL

Table 7. 6: Start concentration, final concentration and volume per reaction for the multiplex PCR on GAPDH and SRY sequences.

In this experiment, thermal cycling was initiated with a 15min denaturation at 95°C, followed by 40 cycles of 30s denaturation at 94°C, 20s primer annealing at 62°C, 1min extension at 72°C. The final extension step consisted of a further 10min cycle at 72°C and the samples were then kept on hold at 8°C until further processing.

The samples used in one experiment are detailed in Table 7.7. In total 7 single PCR and 5 multiplex PCR were carried out with the same temperature cycle. The aim of this experiment is to compare the efficiency of single and multiplex PCR, relative to the detection of foetal DNA.

PCR	sample	content
Normal	S1	*hgDNA(ctrl+)*
Normal	S2	*hgDNA(ctrl+)*
Normal	S3	*water(ctrl-)*
Normal	S4	Unpurified plasma from LOC5p2
Normal	S5	Unpurified plasma from LOC5p2
Normal	S6	Unpurified plasma from LOC7p2
Normal	S7	Unpurified plasma from LOC7p2
Multiplex	S8	*hgDNA(ctrl+)*
Multiplex	S9	*water(ctrl-)*
Multiplex	S10	Purified plasma LOC7
Multiplex	S11	Centrifugated and purified LOC5
Multiplex	S12	LOC7p2

Table 7. 7: Characteristics of the samples and controls used in the fetal DNA detection experiment

7.4.3 Results

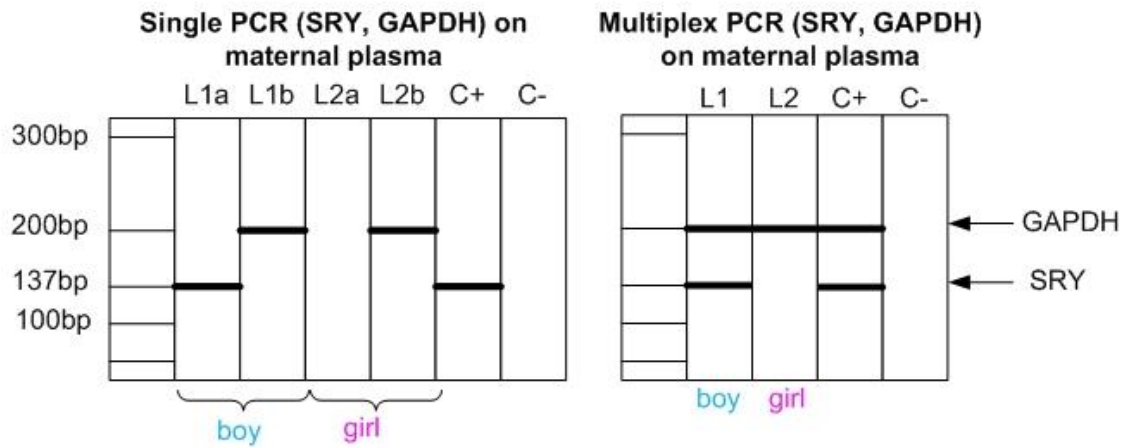Expected results for a single and multiplex PCR are presented in a schematic, Figure 7.16, for clarity.

Figure 7. 16: Expected foetal sex detection results on a single PCR and a multiplex PCR

A photograph of the resulting gel electrophoresis is presented in Figure 7.17. The detailed analysis of each lane of the gel is carried out in Table 7.8. Generally, both single and multiplex PCR have been successfully carried out. In single PCR the bands are clear while in the multiplex PCR the bands are faint, indicating that the multiplex PCR could be further optimized.
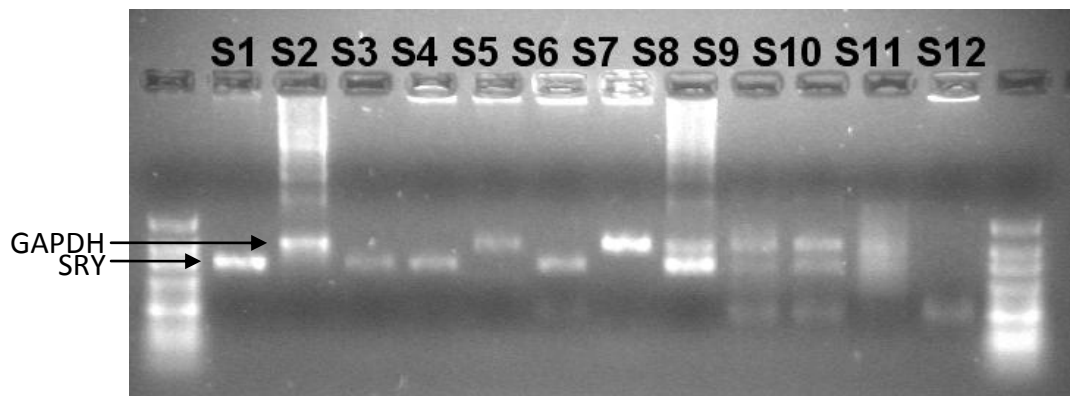

Figure 7. 17: SYBRsafe-stained 3% agarose gel of PCR products obtained with GAPDH and SRY primers and unprepared plasma samples obtained by microfluidic extraction. The first and last lanes are a molecular weight marker (Ultra-low range DNA ladder, PeqLab).

185

PCR	sample	Presence of SRY band?	Presence of GAPDH band?	Comments
Normal	S1	Yes	*n.a.*	Control ok
Normal	S2	*n.a.*	yes	Control ok
Normal	S3	Yes	*n.a.*	Contamination with SRY
Normal	S4	Yes>conta	*n.a.*	BOY?
Normal	S5	*n.a.*	yes	BOY?
Normal	S6	Yes>conta	*n.a.*	BOY?
Normal	S7	*n.a.*	Yes	BOY?
Multiplex	S8	yes	yes	Control ok
Multiplex	S9	yes	yes	contamination
Multiplex	S10	yes	yes	Confirms S6 and S7
Multiplex	S11	yes	yes	Confirms S6 and S7
Multiplex	S12	no	no	Dilution too high?

Table 7. 8: Detailed analysis of the gel electrophoresis results

The following conclusions can be drawn relatively to the PCR efficiency and the fetal sex detection from Table 7.8:

- Both the single and multiplex PCR are working (positive controls S1, S2, S8)
- Slight contamination is observed in the negative controls of the normal PCR and the multiplex PCR
- Successful amplification has been achieved on the sample LOC 5 and LOC 7 that were randomly for this experiment
- From the presence of two bands in Lanes S4, S5, S6 and S7, the foetal gender of samples LOC 5 and LOC 7 should be male, unless contamination has been greater than expected.

Furthermore, to investigate the influence of the sample purification and the dilution three controls as followed, all were amplified in the same way (multiplex PCR). The conclusions relatively to the method of extraction are presented in the Table 7.9.

In conclusion, the experiments on the extraction of cffDNA from maternal blood are on-going work. Preliminary results suggest that it is possible to amplify cffDNA from maternal plasma extracted on-chip. Eradicating contamination from the PCR experiment will confirm these results. Demonstration of cffDNA extraction from

maternal plasma will be a great achievement and will pave the way towards developing integrated tool for on-site prenatal diagnosis.

PCR Sample name	Sample reference	Protocol on the sample	Results
S10	LOC7	Microfluidic separation (dilution 1:3)	Both bands amplified Although this sample has diluted substantially, both bands can be seen very clearly
S11	LOC5	Centrifugation separation (no dilution) And Purification	Both bands amplified Bands unclear Although this sample is the ideal sample (no dilution, purified) it does not give better results, indicating that dilution should not a problem in further testing
S12	LOC7	Microfluidic separation (dilution 1:3) No purification	No band Multiplex PCR might have failed because of the lack of purification

Table 7. 9: Analysis on the extraction methods.

7.5 Conclusions

In this chapter, detection of genomic sequence from on-chip extracted plasma has been carried out with success, therefore showing the high quality of the plasma. Several PCR techniques, such as single and multiplex conventional PCR and real-time PCR have been used to analyse and quantify the presence of genomic sequence. Single conventional PCR has proven in this study to be the most reliable and robust technique to amplify genomic sequences from unpurified plasma. However, optimisation of the multiplex, conventional PCR and real-time PCR will also undoubtedly demonstrate that these methods can also be used for DNA detection for specific cases.

Other biomarkers may be also detected in the plasma such as proteins or microRNA. MicroRNA detection in plasma is relatively new and is particularly useful for cancer diagnostics. Protein detection in on-chip extracted plasma has been performed by Fan et al [7.1] and Sollier et al [7.2]. Sollier et al has shown that a passive microfluidic extraction did not reduce the number of major proteins present in the blood and furthermore verified the integrity of these proteins.

7.6 References

[7.1]   Rong Fan, Ophir Vermesh, Alok Srivastava, Brian K. H. Yen, Lidong Qin, Habib Ahmad, Gabriel A. Kwong, Chao-Chao Liu, Juliane Gould, Leroy Hood, and James R. Heath, *Integrated barcode chips for rapid, multiplexed analysis of proteins in microliter quantities of blood*, Nat Biotech **26**, 1373 - 1378 (2008).

[7.2]   M. Cubizolles E. Sollier, Y. Fouillet, J.L. Achard., *Fast and continuous extraction from whole human blood based on expanding cell-free layer devices*, biomedical microdevices (2010).

[7.3]   Invitrogen, *Real-time PCR: from theory to practice*. (undated).

[7.4]   E. Buel J.A. Nicklas, *Development of an Alu-based, Real-Time PCR Method for quantitation of Human DNA in Forensic samples*, J. Forensic. Sci **48**, 1-9 (2003).

[7.5]   Jinliang Xu Chunsun Zhang, Wenli Ma, Wenling Zheng, *PCR microfluidic devices for DNA amplification*, Biotechnology advances **24** (3), 243-284 (2006).

[7.6]   Scott Stelick Nathanial C. Cady, Madanagopal V. Kunnavakkan, Carl A. Batt, *Real-time PCR detection of Listeria monocytogenes using an integrated microfluidics platform*, Sensors and Actuators B **107**, 332-341 (2005).

[7.7]   Se Ho Park Dae-Sik Lee, Haesik Yang, Kwang-Hyo Chung, Tae Hwan Yoon, Sung-Jin Kim, Kyuwon Kim, Youn Tae Kim, *Bulk-micromachined submicroliter-volume PCR chip with very rapid thermal response and low poser consumption*, Lab On Chip **4**, 401-407 (2004).

[7.8]   P. Ernault J.M. Costa, *Automated Assay for Fetal DNA Analysis in Maternal Serum*, Clin Chem. **48**, 679 (2002).

[7.9]   Y.M.D. Lo, *Recent Advances in Fetal Nucleic Acids in Maternal Plasma* J. Histochem. Cytochem **53**, 293 (2005).

[7.10] D. W. Bianchi and J. Hanson, *Sharpening the Tools: A summary of a National Institutes of Health workshop on new technologies for detection of fetal cells in maternal blood for early prenatal diagnosis*, Journal of Maternal-Fetal & Neonatal Medicine **19** (4), 199–207 (2006).

Chapter 8 – Conclusions and Outlook

8.1 Conclusions

This thesis has described using eight chapters, the design, test and biological validation of microfluidic systems for the separation of plasma from blood.

Following on from the motivation and layout of the thesis as presented in the first chapter, an extensive literature survey on recent developments of cell separation techniques was carried out and presented in the second chapter alongside the main applications of cell separation.

The blood flow, and in particular, the flow of red blood cells was studied in the third chapter. The various physical effects associated with the morphology of the cells, the complex fluid dynamic of the blood have allowed an empirical understanding of the complexity of flow of red blood cells. Particularly, it was highlighted that both inertial and laminar forces can produce lateral forces on the cells in a laminar flow situation. Using the concepts presented, two generations of microdevices for blood plasma separation were designed.

Following on from the modelling of the microfluidic system as a network of electrical equivalent lumped elements, an analytical and numerical study presented in the fourth chapter of this thesis provided insight into the network behaviour. It was clearly shown that the separation network can be influenced by external features such as the platform channels or the capillaries plugged at the back of the system. Using the example of the blood plasma separation device, it was demonstrated that a more generic design methodology can be implemented for microfluidic network that can accommodate the influence of external fluidic circuitry onto the critical functional performance of the network. For the first time, a "design for packaging" solution was presented for microfluidic applications.

Following the design of a microfluidic chip for separation of plasma from blood, several manufacturing techniques carried out by several partners from the 3D-Mintegration project were presented. The data gathered, suggested that although it has a large turn around time from design to manufacture, a manufacturing process based on

photolithography is for the moment the most reliable technique for microfluidic manufacturing.

The separation of plasma from whole blood at different dilution levels was extensively characterised for two different designs in chapter 6. An increase of 30% in the separation efficiency was found in the second generation device. For this generation, 100% separation efficiency was achieved even with the use of relatively large channels (20μm), thereby allowing the mass-manufacturing of the device via micro-injection moulding for example. The blood flow was observed in the microchannels and the particular behaviour of the platelet aggregation described.

To characterise the extracted plasma biologically, PCRs were carried out on the cell-free DNA present in the plasma outlet. Cell-free GAPDH sequences were successfully amplify in plasma samples of varying dilution and purity, thereby demonstrating the integrity of the biomarkers during separation. For the first time, a study of the influence of the on-chip extracted plasma purity on the amplification of a house-keeping gene was presented.

8.2 Various technical issues encountered in this study

Amongst the problems encountered, cell counting has been an issue from the start. At the beginning cells were counted using disposable hemacytometer, however this method was found extremely tedious and inaccurate. This technique was found unsuitable for the repetitive measurements needed in this study. A more automated counting technique was employed that makes use of image analysis software and photos taken from the disposable cell counter. The technique, albeit better, was still too laborious and unreliable for the counting of cells in a high number of samples. An informal collaboration with the Department of Marine Science at the School of Life Science allowed the use of a flow cytometre which offers a complex and precise screening of the cells and plasma samples. When the study moved to the Division of Pathway Medecine, Edinburgh University, an automated cell coulter counter was found in the Cardio-vascular department which provided the best cell characterisation technique. This technique is fast, relatively accurate and does not require any kind of sample preparation apart from dilution if the hematocrit level is too high. Cell counting

using the Coulter counter is best when completed by an in-depth flow cytometric analysis which is picking up small discrepancies overlooked by the Coulter counter. Therefore, an additional flow cytometry study was set-up in the Flow lab of Edinburgh University, Royal Infirmary [8.1].

Micron-resolution Particle Image Velocimetry (µPIV) is a much sought after tool for the characterisation of flow in microfluidic systems [8.2]. In µPIV, fluorescent microparticles are tracked using a high-speed camera via a microscope objective and the different points are mapped to create a velocity vector field. The microfluidic system was first of all modified to allow the µPIV inverted microscopy system to be focused on the top surface of the chip. Figure 8.1 shows a cross-section view of the device before and after the modification.
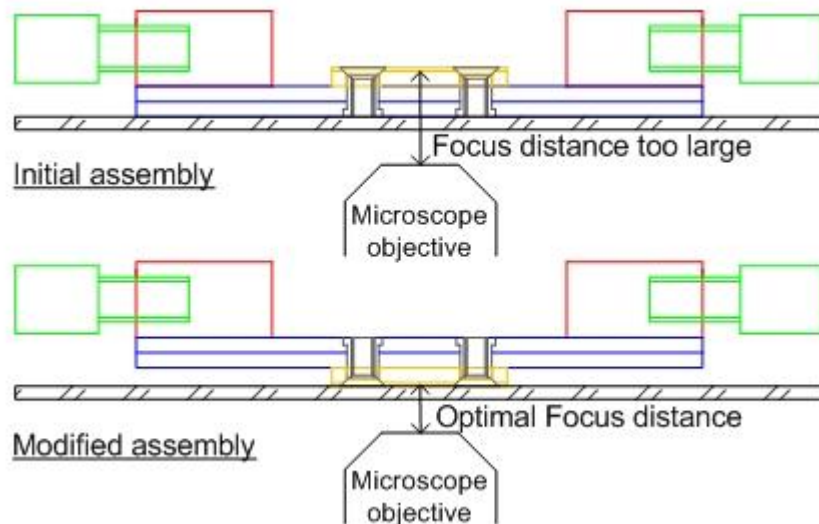

Figure 8. 1: Illustration of the chip and platform assembly for µPIV measurement. The chip is represented in orange.

Two collaborations were started to apply µPIV to characterise the flow rates in the system and provide data feed in the different simulation models. The first collaboration with Loughborough University provided vector field images of the flow in the second generation device, as shown in Figure 8.2. In this experiment the flow was seeded with 1µm fluorescent particles and the actual flow was measured using holographic µPIV. Qualitatively, the creation of a cell-free "slow" zone can be observed at the corner of the constriction and the flow escaping to the plasma channel comes from this zone. Unfortunately, no formal analysis of these images against CFD or high-level modelling data was pursued due to a lack of time. It would have been very useful

191

to extract flow rates from this data and correlate the flow rate ratios with the efficiency obtained. This could be part of some future work.
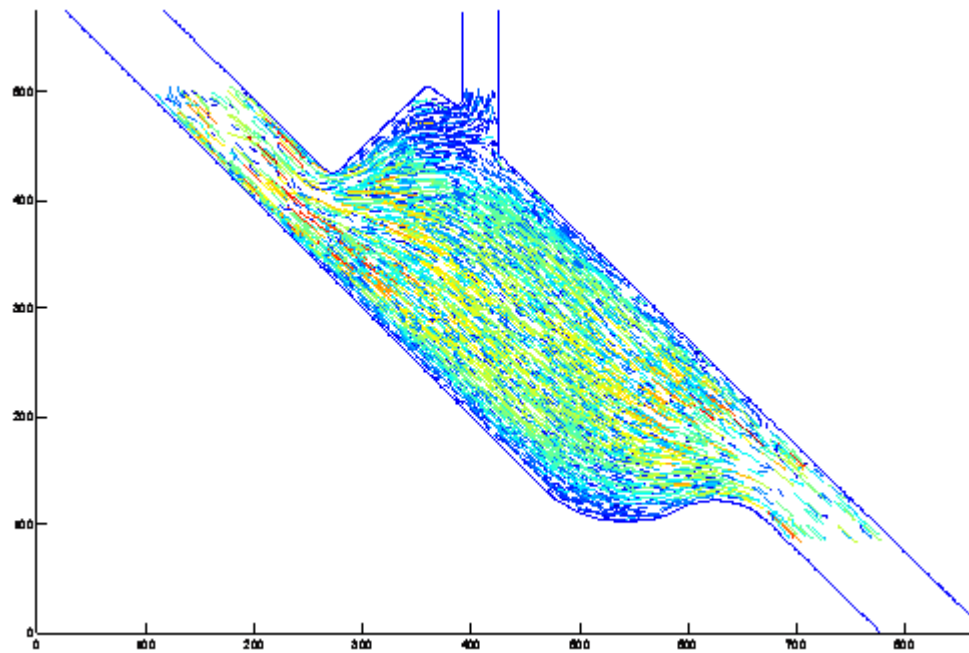
a

Figure 8. 2: PIV vector field in the blood plasma separation device. Courtesy of Andrew Wormald and Prof Jeremy Coupland, Loughborough University

In the second collaboration with Dr John Christy from Edinburgh University, the apparatus comprised a LEICA CT R4000 laser system and a Dantec Dynamic Nanosense MKII camera. The data was recorded and analysed via the Flow Manager software from Dantec. Figure 8.3 shows the area of interest in this PIV study and a photograph with raw data. In the photograph, one can see a number of 1μm fluorescent particles, some of them agglomerated. Some of the 1μm particles have entered the plasma channels, which raise the question about the type of particles to be used in this PIV study. Larger particles might be more suitable to study the flow of RBCs in this particular network.

However it was later determined that the flow speed of interest was too high for the system. Additionally, glitches on the photographs induced by a problem on the camera hindered the compilation of the vector fields. The data produced could not be used and the time for this study was very limited.
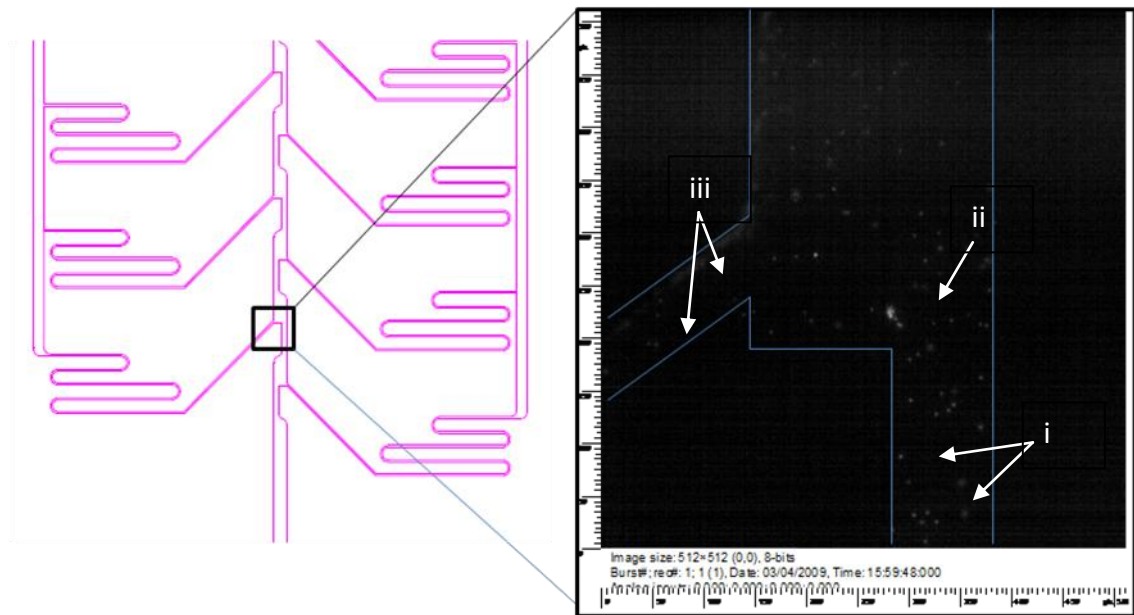
Figure 8. 3: Micron-resolution PIV experiment. Left: the second bifurcation entrance is the area of interest in the system. Right: Raw uPIV data of the area of study. (i) Fluorescent microparticles (1µm) can be observed in the main channel (ii) An agglomeration of 1µm particles (iii) Particles entering the plasma channel.

In the future, the system could greatly benefit from a full extensive uPIV analysis. As suggested elsewhere, fluorescent particles might be encapsulated in deformable vesicle that would mimic RBC behaviour.

8.3 Limitations of the system and future work

8.3.1 Processing time

The system has been shown to accommodate flow rates considerably higher compared to other research groups who studied separation of plasma from blood. The time needed for separation remains however high. For a 1mL syringe content, the separation speed can range from thirty to three minutes for dilution levels ranging from nil to 1:10, using the second generation device. At high levels of dilution levels (1:20), the separation time can be quicker and of the order of hundreds of seconds; however, this dilution level introduces another problem with the concentration of analytes for subsequent analysis. A trade-off has therefore to be found between the required minimum concentration of analytes to allow detection and the speed required for the separation process. This will depend on the application. For example

in plasma viscometry, there is no concentration of analytes to be accounted for, therefore the separation speed can be higher.

One solution to overcome the problem of the separation speed is to put two devices or more, in parallel. This introduces more complexity in the system but allows for lower process time. In this case the footprint is not necessarily larger as the devices are stacked. The geometries chosen for the blood plasma separation system allow an easy "stacking configuration", as shown in Figure 8.4.
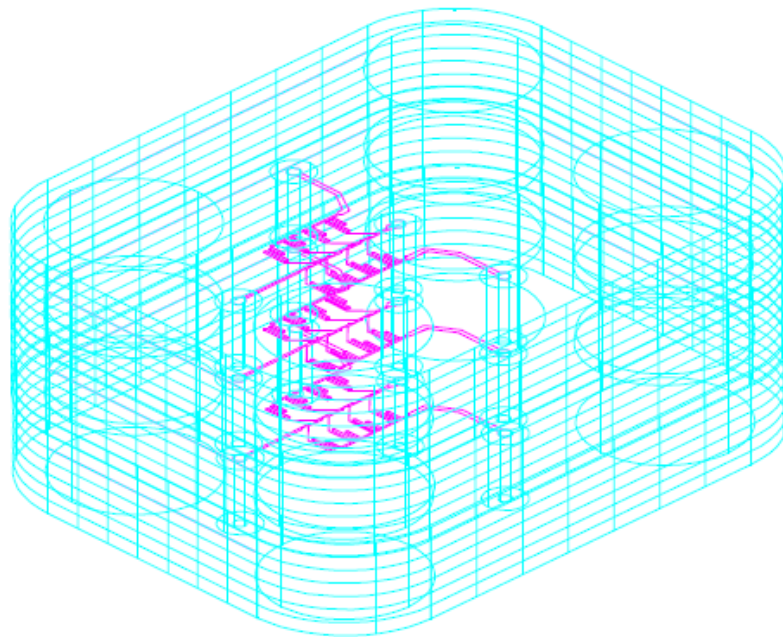

Figure 8. 4: Conceptual stacking configuration for a high-throughput blood plasma separation

8.3.2 Blockage

Blockages have sometimes been a problem for the smooth operation of the blood plasma device. Pre-filtration of the blood off-chip can be time-consuming and would defeat the idea of sample preparation on-chip. It is proposed to integrate a pre-filtration module that would be placed in the main channel of the blood plasma separation device but before the plasma channels as shown in figure 8.5. The pre-filtration module is composed of a number of posts located in columns with a lateral pitch from each other. The aim of this pre-filtration module is to capture any particle of dust or platelets-cells aggregate with an approximate diameter over 30μm. The fact that cells of interest can be trapped in this module can be a disadvantage if the some

cells need to be analysed. However, the separated plasma portion is only to be studied, then this might a simple, yet effective way to remove unwanted large particles before the fine separation. A plug of cells might form over a certain period of use, if the device is to be employed several ties. Characterisation of this filtration technique needs to be carried out.
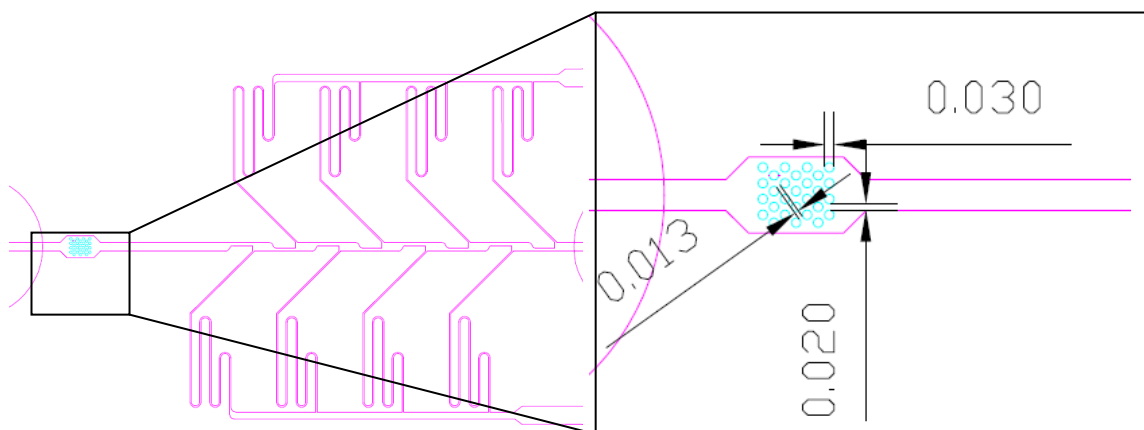
Figure 8. 5: An integrated pre-filtration module featuring arrays and columns of 30μm pillars.

8.3.3 Pumping system

In this study, a non-integrated syringe pump was used to activate the flow in the microfluidic chip. Syringe pumps have the advantage to be a common sight in hospitals, they are a familiar tool not only for the doctors but also for the nurses. However, syringe pumps are quite bulky and can have a foot print about 200% the size of the chip itself. In the future, an integrated pumping system could be envisaged. The integrated system will have to produce a continuous, high speed flow. The continuity is foreseen to be especially difficult to achieve, but could be possible using micro-sized peristaltic pump with microfluidic diodes to smooth the flow.

8.3.4 Integrability

The platform associated with the microfluidic chip developed in this study is a totally passive platform solely useful for handling the fluid.

An active type of platform could be envisaged from the present study as a useful example of future work to be carried out. This platform would allow the smart interconnection of disposable microfluidic chips. Broad microfluidic features could be built into the platform while the thin features such as the separation network could be

placed in the disposable polymeric chips. The blockages are more likely to be found in the thin features, hence the disposability of the polymeric parts featuring the thin network. Additionally, this platform could have active actuators such as heaters and sensors. This concept, presented in Figure 8.6, has several advantages: it allows the user to discard the parts more likely to be blocked (single-use) while retaining the expensive parts such as heaters and sensors for repeated usage.
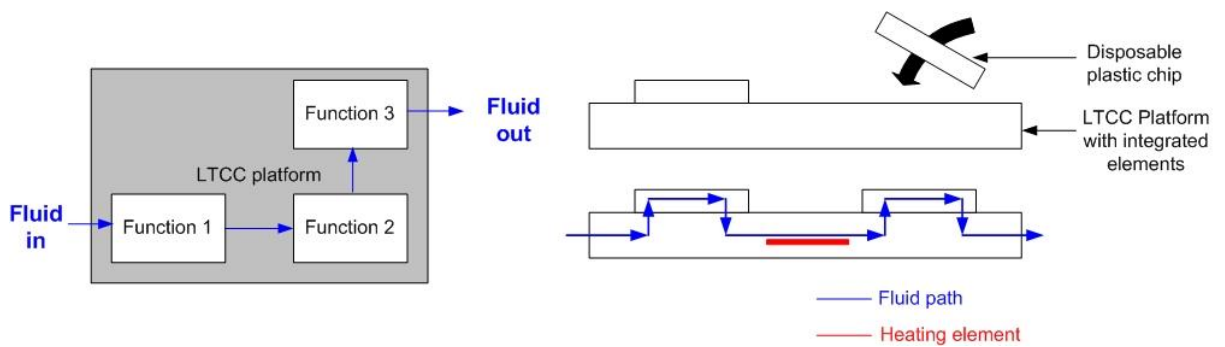

Figure 8. 6: Conceptual LTCC platform for microfluidic function integration

As a proof of concept, a LTCC platform has been manufactured using the LTTC facilities at Heriot-Watt University, as shown in Figure 8.7 (a,b). Ferrules, as in the Fluence system as describe in Chapter 5, are used to connect the fluidic path from the platform to the microfluidic chip. Different cavities have been manufactured in the LTCC stack to allow the positioning of a heater and three thermocouples to monitor the temperature inside the LTCC channel. Attempts have been made to manufacture integrated Joule heaters directly onto LTTC layers as shown in Figure 8.7 (c).

This platform could serve as a demonstrator for PCR on a LTCC substrate in connection with the use of a polymeric blood plasma separation system.
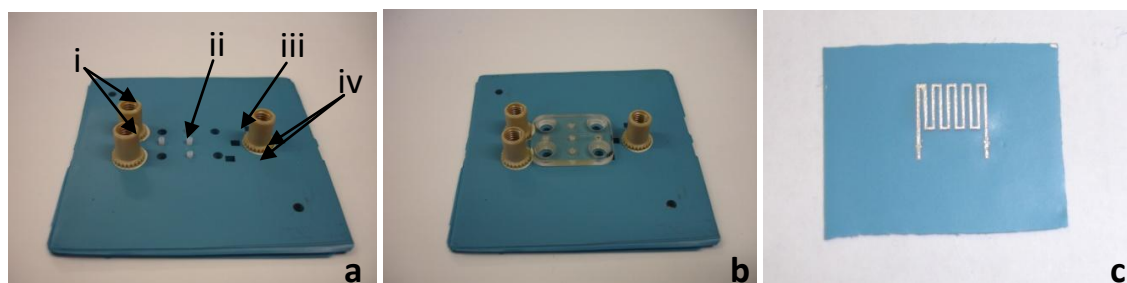

Figure 8. 7: (a) LTCC platform without plastic microfluidic chi, (i)Nanoport™ connectors for fluidic access, (ii) Ferrule to link fluidic path between the platform and the chip, (iii)Holes for screws to tighten the chip onto the platform, (iv)Cavities for thermocouples to monitor the temperature in the

LTCC channels (b) LTCC platform with plastic microfluidic chip (c) Integrated heater on LTCC, Courtesy of Yves Lacrotte, Heriot-Watt University

8.4 Future Outlook

In this study, passive continuous blood plasma separation using polymer microfluidic chip has been shown to be a valuable technique to extract cellular and plasma portion out of whole blood. Extensive characterisation has shown that this technique does not harm the cells and produces clear plasma that can be readily processed for other analysis steps.

Such a separation module could be integrated to other lab-on-chip modules such as PCR and detection analysis for the manufacturing of an entire integrated NIPD system as shown in Figure 8.8.
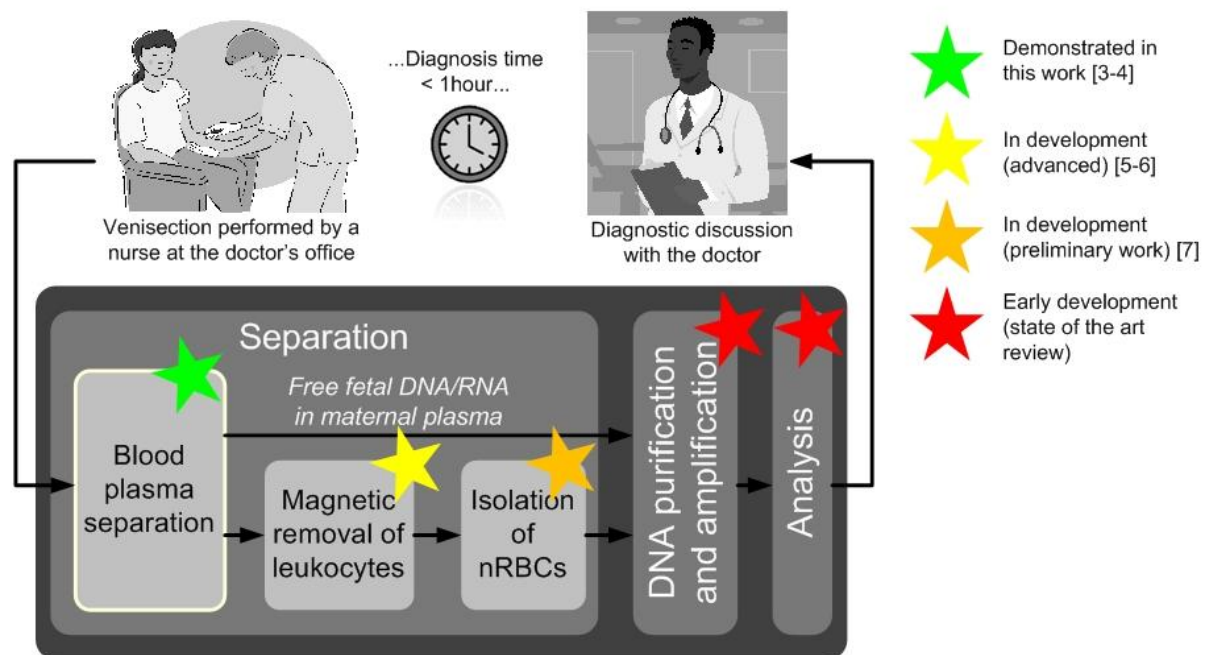
Figure 8. 8: Current development status of a portable and modular system for non-invasive prenatal diagnosis at Heriot-Watt University, May 2010.

This platform has been conceptualised as a modular entity, therefore each component might be used on its own, or part of a different system. As demonstrated throughout this thesis, applications for blood plasma separation microdevices are numerous and can be found summarised in Table 8.1. More importantly the miniaturisation of this strategic preliminary step in a clinical context is expected to help to produce more efficient and practical lab on chip systems.

Clinical context	Targeted analyte/parameter in plasma
Cancer	MicroRNA
Prenatal diagnosis	Cell-free foetal DNA
Myeloma	Plasma viscosity
Transplantation	Levels of donor cfDNA in host plasma

Table 8. 1: Summary of application where blood plasma separation is a primary step

8.5 References

[8.1] http://www.qmri-cytometry.ed.ac.uk/ , last accessed April 2010

[8.2] C. D. Meinhart, M. Sigurdson and D. Tretheway, *Analysis of Microscale Transport for BioMEMS*, The 1st International Symposium on Micro & Nano Technology, Honolulu, Hawaii, USA (2004)

[8.3] R.S. Dhariwal M. Kersaudy-Kerhoas, M.P.Y. Desmulliez and L. Jouvet,, *Hydrodynamic blood plasma separation in microfluidic channels*, Microfluidics and Nanofluidics **8**, 1613-4982 (2010).

[8.4] M. Kersaudy-Kerhoas, D. M. Kavanagh, R.S. Dhariwal, C. J. Campbell, and M. P. Y. Desmulliez, *Validation of a blood plasma separation system by biomarker detection*, Lab Chip, **10**, 1587–1595 (2010)

[8.5] D.M. Kavanagh, D.Flynn, F.Amalou, B.G. Moffat, R.Dhariwal and M.P.Y. Desmulliez, *Microsystems Technology for the Separation of foetal cells from maternal blood*, 2nd Electronics and System integration Technology conference, Greenwich, UK, (2008)

[8.6] D.M.Kavanagh, M. Kersaudy-Kerhoas, S. K.Pavuluri, R. S. Dhariwal and M.P.Y. Desmulliez, *Fabrication and Testing of Microfluidic Devices for Blood Cell Separation*, 2nd Micro and Nano Flows Conference West London, UK (2009)

[8.7]S.K. Pavuluri, R.Lopez-Villaroya, E.McKeever, G.Goussetis, M.P.Y. Desmulliez, D. Kavanagh, *Integrated Microfluidic Capillary in a waveguide Resonator for chemical and Biomedical sensing*, Journal of Physics: Conference series **178**, 1-6 (2009)